Imperial College London

DESIGN, SYNTHESIS, AND CHARACTERISATION OF NEXT-GENERATION CHOLINE KINASE INHIBITORS

Ning Wang

Imperial College London

Department of Surgery and Cancer

A dissertation submitted for the degree of

Doctor of Philosophy

Declaration of Originality

I hereby declare that this dissertation is my own original work and conducted by myself, except where otherwise clarified. This work was conducted between November 2017 and March 2021 under the supervision of Dr. Diana Brickute, Dr. Louis Allott and Prof. Eric Aboagye at Imperial College London, UK.

Copyright Declaration

The copyright of this thesis rests with the author. Unless otherwise indicated, its contents are licensed under a Creative Commons Attribution-Non Commercial 4.0 International Licence (CC BY-NC).

Under this licence, you may copy and redistribute the material in any medium or format. You may also create and distribute modified versions of the work. This is on the condition that: you credit the author and do not use it, or any derivative works, for a commercial purpose.

When reusing or sharing this work, ensure you make the licence terms clear to others by naming the licence and linking to the licence text. Where a work has been adapted, you should indicate that the work has been changed and describe those changes.

Please seek permission from the copyright holder for uses of this work that are not included in this licence or permitted under UK Copyright Law.

Abstract

Abnormal lipid metabolism is a common feature of cancers. In the clinic, elevated phosphocholine, an essential membrane lipid precursor, is revealed as a phenotype associated with malignant lipid metabolism. Overexpression of choline kinase alpha isoform (CHKA), is recognised as a predominant factor responsible for the phenotype, and, therefore, CHKA has become a novel therapeutic target for cancer. In the previous work by Trousil *et al.*, a potent CHKA inhibitor ICL-CCIC-0019 was reported, which displayed high cellular activity but undesirable pharmacological properties to be ameliorated. In this thesis, CK146, an active analogous scaffold of ICL-CCIC-0019, bearing a reactive piperazine handle, is presented. This novel scaffold opens the further possibilities for structural elaboration of the classic pharmacophore by innovatively exploiting two advanced drug development strategies. In the first strategy, selective CHKA inhibition was attempted to be achieved by prodrug CK145, *via* the incorporation of an *ε*-(Ac)Lys motif into CK146. In the second strategy, a peptide ligand targeting prostate-specific membrane antigen (PSMA) receptor was embodied in CK146 to afford CK147, aimed to realise the targeted delivery to the malignant cells with high expression of PSMA receptors on cell surface.

As expected, the precursor scaffold CK146 displayed high CHKA activity in kinase screening (CHKA activity as part of a 15 human lipid kinase screen: CK146: 69%, ICL-CCIC-0019: 53%) and good antiproliferative activity against four selected cancer cell lines (overall GI_{50} against HCT-116, A549, HepG2 and Caco-2: CK146: 2.5 ± 0.3 μM, ICL-CCIC-0019: 0.5 ± 0.02 μM). Proposed prodrug CHKA inhibitor (CK145) and PSMA-targeted CHKA inhibitor (CK147) were successfully synthesised. The pharmacological activity and pharmacokinetic profiles of the obtained compounds were evaluated *in vitro*. Although attempts to improve the pharmacological profiles of ICL-CCIC-0019 were not effective by these two modification strategies, important and informative structure-activity relationships were concluded and have been reported.

Acknowledgement

I would like to acknowledge Prof. Eric Aboagye who created this project and offered me the opportunity to perform this work in such a multidisciplinary team full of excellent experts. Your unfailing enthusiasm towards science and dedication to continuous improvement and innovation have inspired me through this 4-year work, and will always be the lighthouse of my career path.

I would also like to thank my daily supervisors Dr Louis Allott and Dr Diana Brickute. You are not only my academic supervisors, but also my mentors in life. This work can never be completed without your dedicated supervision, endless help and unceasing encouragement. Your strict attitudes towards achieving high standards and resilient life philosophies are unquestionably the models to follow in my lifetime.

My sincere thanks also go to Mr Chris Barnes, Dr Marta Braga, Dr Haonan Lu, Ms Ala Amgheib, Dr Ruisi Fu, Mr Jin Hui Teh. Your constructive suggestions, stimulating scientific conversations and kind help on this work are invaluable. Particular thanks also go to Dr Laurence Carroll and Dr Trevor Ferris who initiated this project and helped me to get into the right frame of mind for the project from the very beginning.

Mum and Dad, I love you. You are the best parents ever. You are always my strongest support in every respect of my life, and your unreserved love has always provided me with confidence against any challenges. Yuan, thank you for being such a support in helping me overcome my frustrations and seeing the bigger picture. Last but not least, I want to thank my funding bodies, Imperial College London and China Scholarship Council, for the support throughout this period.

It has been an absolute pleasure to work in the Aboagye group. The company and kindness of the whole group will be forever cherished in the years to come.

Publications

The following publication is associated with this dissertation:

[1] **Wang, N.**; Brickute, D.; Braga, M.; Barnes, C.; Lu, H.; Allott, L.; Aboagye, E. O., Novel Non-Congeneric Derivatives of the Choline Kinase Alpha Inhibitor ICL-CCIC-0019. *Pharmaceutics* 2021**,** 13 (7), 1078.

The following publications were published during this degree, but are not included in this work:

[2] Li, Y.; Inglese, M.; Dubash, S.; Barnes, C.; Brickute, D.; Braga, M. C.; **Wang, N.**; Beckley, A.; Heinzmann, K.; Allott, L.; Lu, H.; Chen, C.; Fu, R.; Carroll, L.; Aboagye, E. O., Consideration of Metabolite Efflux in Radiolabelled Choline Kinetics. Pharmaceutics 2021, 13 (8), 1246.

[3] Allott, L.; Amgheib, A.; Barnes, C.; Braga, M.; Brickute, D.; **Wang, N.**; Fu, R.; Ghaem-Maghami, S.; Aboagye, E. O., Radiolabelling an 18F biologic via facile IEDDA “click” chemistry on the GE FASTLab™ platform. Reaction Chemistry & Engineering 2021, 6 (6), 1070-1078.

[4] Allott, L.; Chen, C.; Braga, M.; Leung, S. F. J.; **Wang, N.**; Barnes, C.; Brickute, D.; Carroll, L.; Aboagye, E. O., Detecting hypoxia in vitro using 18F-pretargeted IEDDA “click” chemistry in live cells. RSC Advances 2021, 11 (33), 20335-20341.

[5] Allott, L.; Brickute, D.; Chen, C.; Braga, M.; Barnes, C.; **Wang, N.**; Aboagye, E. O., Development of a fluorine-18 radiolabelled fluorescent chalcone: evaluated for detecting glycogen. EJNMMI Radiopharmacy and Chemistry 2020, 5 (1), 17.

Table of Contents

1. Introduction 19

1.1 Abnormal choline metabolism related to upregulated CHKA activity in tumourigenesis 19

1.1.1 Kennedy pathway for phosphatidylcholine (PtdCho) biosynthesis 19

1.1.2 Choline and choline transport 21

1.1.3 Choline metabolism in cancer 25

1.1.4 Upregulated CHKA activity leads to the cholinic phenotype 28

1.2 Inhibition of CHKA as a Cancer Treatment Strategy 30

1.2.1 RNAi Studies 30

1.2.2 CHKA crystal structure 33

1.2.3 Small-molecule CHKA inhibitors 37

1.3 CHKA inhibition as novel therapeutic strategies for other pathologies 51

1.4 Innovative drug modification approaches to modulating the pharmacological properties of drug molecules 52

1.4.1 Prodrug strategy 53

1.4.2 Targeted delivery strategy 57

1.5 Research aims 60

2. Materials and Methods 62

2.1 Chemical synthesis 62

2.2 Radiosynthesis of [^{18}F]D4-FCH 62

2.3 High-performance liquid chromatography (HPLC) 62

2.4 Shake-Flask method 66

2.5 Cell culture 67

2.6 Anti-Proliferative assay (Sulforhodamine B Assay) 68

2.7 Lipid kinase screening 68

2.8 ADME study (*In vitro*) 69

2.9 Bicinchoninic acid (BCA) protein assay 69

2.10 Western blotting 69

2.11 *In vitro* uptake and metabolism study of CK145 70

2.12 Limit of detection (LOD) of CK146 70

2.13 Conjugate stability test of CK147 71

2.14 Cellular uptake and metabolism study of ICL-CCIC-0019, CK146, CK147 and CK148 in presence and absence of serum 71

2.15 [^{18}F]D4-FCH uptake study *in vitro* 72

2.16 Statistical Analysis 73

3. Design and synthesis of the novel prodrug CHKA inhibitor 74

3.1 Introduction of the prodrug strategy 74

3.2 SAR and design rationale 77

3.3 The synthesis of prodrug strategy (Results and Discussion) 80

3.3.1 Synthesis of ICL-CCIC-0019 and CK14 80

3.3.2 Synthesis of CK146 and CK144 82

3.3.3 Synthesis of CK145 85

3.3.4 Synthesis conclusions 87

4. Design and synthesis of the novel PSMA-targeted CHKA inhibitor 89

4.1 Introduction to PSMA-targeted CHKA inhibitor strategy 89

4.2 SAR and design goal rationale 90

4.3 Synthesis of CK147 (Results and Discussion) 93

4.3.1 Synthesis of CK146-SH 94

4.3.2 Synthesis of CK147 *via* thiol-maleimide conjugation 102

4.4 Synthesis conclusions 104

5. Biological evaluation 105

5.1 Introduction to biological evaluation 105

5.2 Evaluation of lipophilicity 105

5.3 Chemical stability of conjugate CK147 in serum 108

5.4 Antiproliferative activity assessment (SRB Assay) 110

5.4.1 Prodrug strategy 112

5.4.2 Drug delivery strategy 115

5.5 Cellular uptake and *in vitro* metabolism 117

5.5.1 Prodrug strategy 119

5.5.2 Drug delivery strategy 122

5.6 Lipid kinase screening 123

5.7 ADME study 127

5.7.1 Kinetic solubility and permeability 128

5.7.2 Fasted state simulated gastric fluid (FaSSGF) stability 133

5.7.3 Human Microsome Metabolic Stability 134

5.8 [^{18}F]D4-FCH uptake *in vitro* study 137

5.9 Discussion 139

5.9.1 Prodrug Strategy 140

5.9.2 Drug Delivery Strategy 143

6. Thesis conclusions & future work 146

6.1 Summary of work and achievements from this thesis 146

6.2 Future work 151

6.2.1 Short-term goals 151

6.2.2 Long-term goals 152

7. Experimental 153

Synthesis 153

8. References 163

9. HPLC chromatograms 184

10. Supplementary information 190

11. Appendix 202

Appendix A: ^{1}H NMR, ^{13}C NMR, MS spectra 202

Appendix B: Kinase Screen 225

List of Figures

Figure 1. 1: Important phospholipid structures.....19
Figure 1. 2: The Kennedy Pathway: CDP-choline pathway and CDP-ethanolamine pathway
.....21
Figure 1. 3: Transformation of choline into 4 classes of biomolecules in the body 23
Figure 1. 4: Choline metabolite analysis by ^{1}H and ^{31}P MRS: 26
Figure 1. 5: The principles of PET. 28
Figure 1. 6: The structures of CHKA2 monomer in ribbon diagram, with ADP and PCho molecules concomitantly present.....34
Figure 1. 7: The interactions of ADP with CHKA2 at the ATP-binding site 35
Figure 1. 8: The interactions of choline with CHKA2 at the choline-binding site 36
Figure 1. 9: Chemical structures and pharmacological data of corresponding CHKA inhibitors.....38
Figure 1. 10: Chemical structure of HC-3, where the molecule is divided into two fragments
.....39
Figure 1. 11: Chemical structure of MN58B.....41
Figure 1. 12: An overview of the symmetrical and nonsymmetrical CHKA inhibitors designed by Trousil *et al*.....42
Figure 1. 13: Chemical structure of CK37......47
Figure 1. 14: Chemical structure of V-11-023907 (A) and V-11-0711 (B)......48
Figure 1. 15: Schematic of targeted delivery strategy 57

Figure 3. 1: The prodrug *in vitro* conversion scheme illustrating the selective two-step drug activation in cancer cells by HDAC and CTSL 75
Figure 3. 2: A prodrug moiety sensitive to HDAC and CTSL cleavage: Boc-Lys(Ac)-R 77
Figure 3. 3: The structures of ICL-CCIC-0019, CK14 and CK146 78
Figure 3. 4: Graphical representation of the design goals to generate a novel CHKA prodrug inhibitor 79
Figure 3. 5: The compounds synthesised in the prodrug strategy 80
Figure 3. 6: The scheme of Lewis acid catalysed nucleophilic substitution on the pyridine analogue 85

Figure 4. 1: Chemical structures of [^{99m}Tc]L1 (A) and [^{18}F]AlF-Glu-Urea-Lys-(Ahx)L3 (B), where the Lys-Urea-Glu binding motif is highlighted 89
Figure 4. 2: Graphic representation of design goals of novel PSMA-targeting CHKA inhibitor
.....91
Figure 4. 3: Graphic representative of thiol-maleimide reaction with CK146-SH.....93
Figure 4. 4: Amine alkylation and acylation by amine activation.....95
Figure 4. 5: Graphic scheme of amide bond formation by NHS ester crosslinking reaction
.....95

Figure 4. 6: An unexpected reaction occurred during the coupling, which yielded a side product with the same mass as compound 12 98
Figure 4. 7: Graphic scheme of sulfhydryl group synthesis *via* disulfide reduction 100
Figure 4. 8: Graphic scheme of amide bond formation *via* EDC coupling 101
Figure 4. 9: Graphic scheme of thioether bond formation *via* thiol-maleimide conjugation 102

Figure 5. 1: The chemical stability characterisation of CK147 in RPMI 1640 medium supplemented with 10% serum at 37 ˚C 110
Figure 5. 2: Chemical structure of SRB 111
Figure 5. 3: Immunoblotting analysis of HDAC 1 in HepG2, HCT-116, A549 and Caco-2 cell lines; n = 2 112
Figure 5. 4: Growth inhibition of HCT-116, A549, HepG2 and Caco-2 cells by ICL-CCIC-0019, CK146 and CK145 113
Figure 5. 5: Antiproliferative activities of ICL-CCIC-0019, CK146 and CK145 in two colon cancer cell lines after 120-hour treatment 114
Figure 5. 6: Immunoblotting analysis of PSMA and CHKA in 22Rv1, C4-2B, LNCap, PC3, PNT1A, R1-AD1 and R1-D567 cells; n = 2 115
Figure 5. 7: Comparison of growth inhibitory activities among ICL-CCIC-0019, CK146 and CK147 in 22Rv1, C4-2B, LNCap, PC3, PNT1A, R1-AD1, R1-D567 and HCT-116 cells 116
Figure 5. 8: Spontaneous formation of bilayers by lipids 117
Figure 5. 9: Passive and active transport 118
Figure 5. 10: Calibration curves of ICL-CCIC-0019 and CK145 119
Figure 5. 11: Investigation of the fractional uptake of ICL-CCIC-0019 and CK145 in HCT-116 cells, determined by HPLC at selected time points 120
Figure 5. 12: HPLC analysis of HCT-116 cell lysates after 1 h and 2 h incubation with or without CK145 121
Figure 5. 13: Cellular uptake study of ICL-CCIC-0019, CK146, CK147 and CK148 in C4-2B using medium with or without FCS 122
Figure 5. 14: Drug uptake percentages following 4-hour incubation with ICL-CCIC-0019, CK146, CK147 and CK148 in medium with or without FCS 123
Figure 5. 15: The principle of ADP-Glo^{TM} Kinase Assay 124
Figure 5. 16: Heatmap of lipid kinase selectivity screening against 15 human lipid kinases using ICL-CCIC-0019, CK14, CK144, CK145, CK146 and CK147 126
Figure 5. 17: Biopharmaceutics Classification System (BCS) as proposed by Amidon *et al.* 129
Figure 5. 18: Schematic illustration of the Caco-2 monolayer cultured on a permeable filter support 131
Figure 5. 19: Preparation of subcellular fractions 135
Figure 5. 20: Chemical structures of typical radiotracers related to choline metabolism in current use and development 137
Figure 5. 21: [^{18}F]-D4-FCH percent uptake in C42B and HCT-116 cells (PSMA negative) following 1-hour incubation in the absence (Control group; compounds in DMSO) or presence of compounds at 1 or 10 µM (n = 6; mean ± SD) 139

Figure 5. 22: Chemical structures of reported albumin-binding moieties and a similar structural fragment in CK147 144
Figure 5. 23: Proposed (A) intramolecular and (B) intermolecular electrostatic interactions (blue dashed line) for CK147 which inhibit activity towards the PSMA receptor and CHKA 145

Figure 6. 1: Key SAR findings of this thesis 150

Figure 9. 1: Purification and chemical identity confirmation of compound 5; HPLC method used: A 184
Figure 9. 2: HPLC monitoring of compound 5 Boc deprotection (HPLC method used: A) ..185
Figure 9. 3: The HPLC chromatogram of CK144 purification by semi-preparative HPLC using HPLC method A 186
Figure 9. 4: HPLC analysis of the crude containing CK145 which was provided by Creative Chemistry Ltd 186
Figure 9. 5: HPLC chromatograms of CK145 purification 187
Figure 9. 6: The HPLC chromatogram of purified CK145 (254 nm; HPLC method C) 187
Figure 9. 7: The HPLC chromatogram of the crude containing compound 11 (HPLC method used: E) 188
Figure 9. 8: Optimisation of semi-preparative HPLC methods using dual wavelengths (254 nm and 294 nm) 188
Figure 9. 9: The NHS ester crosslinking of CK146 and compound 10 (HPLC method used: F). 189
Figure 9. 10: The stability investigations of compound 10 using TEA (HPLC method used: F) 189

Figure S10. 1: Decomposition check of compound 11 by two-dimensional thin-layer chromatography (TLC) plates 190
Figure S10. 2: ^{1}H NMR characterisation of the crude containing compound 11 191
Figure S10. 3: MS analysis of the component collected from semi-prep HPLC purification 191
Figure S10. 4: MS analysis of the coupling between CK146 and compound 10 192
Figure S10. 5: MS check of the mock EDC coupling using 1-(4-Pyridyl)piperazine hydrochloride 192
Figure S10. 6: MS analysis of EDC coupling between CK146 and dithiodiglycolic acid 193
Figure S10. 7: The semi-preparative HPLC chromatogram of the coupling between dithiodiglycolic acid and CK146 193
Figure S10. 8: HPLC analysis of the thiol-maleimide conjugation yielding compound 16 (HPLC method C) 194
Figure S10. 9: Condition investigations and monitoring of compound 16 deprotection using analytical HPLC (HPLC method F) 194
Figure S10. 10: MS analysis of the compound collected at 12.5 min:sec on HPLC (HPLC method F). 196

Figure S10. 11: The HPLC chromatograms of CK146 detection in media with or without CK145 treatment (HPLC method F); wavelength: 294 nm 196
Figure S10. 12: MS analysis of the FCS-free medium without drug treatment 197
Figure S10. 13: MS analysis of the FCS-free medium incubated with ICL-CCIC-0019 for 4 hours 197
Figure S10. 14: MS analysis of the FCS-free medium incubated with CK146 for 4 hours ... 198
Figure S10. 15: MS analysis of the FCS-free medium incubated with CK147 for 4 hours ... 198
Figure S10. 16: MS analysis of the FCS-free medium incubated with CK148 for 4 hours ... 199
Figure S10. 17: MS analysis of the FCS supplemented medium without drug treatment. 199
Figure S10. 18: MS analysis of the FCS supplemented medium incubated with ICL-CCIC-0019 for 4 hours 200
Figure S10. 19: MS analysis of the FCS supplemented medium incubated with CK146 for 4 hours 200
Figure S10. 20: MS analysis of the FCS supplemented medium incubated with CK147 for 4 hours 201
Figure S10. 21: MS analysis of the FCS supplemented medium incubated with CK148 for 4 hours 201

Figure 11. 1: ^{1}H NMR of ICL-CCIC-0019. 202
Figure 11. 2: ^{13}C NMR of ICL-CCIC-0019. 203
Figure 11. 3: MS analysis of ICL-CCIC-0019. 203
Figure 11. 4: ^{1}H NMR of CK14. 204
Figure 11. 5: ^{13}C NMR of CK14. 204
Figure 11. 6: MS analysis of CK14. 205
Figure 11. 7: ^{1}H NMR of compound 3. 205
Figure 11. 8: ^{13}C NMR of compound 3. 206
Figure 11. 9: MS analysis of compound 3. 206
Figure 11. 10: ^{1}H NMR of compound 4. 207
Figure 11. 11: ^{13}C NMR of compound 4. 207
Figure 11. 12: MS analysis of compound 4. 208
Figure 11. 13: ^{1}H NMR of compound 5. 208
Figure 11. 14: ^{13}C NMR of compound 5. 209
Figure 11. 15: MS analysis of compound 5. 209
Figure 11. 16: ^{1}H NMR of compound 6. 210
Figure 11. 17: ^{13}C NMR of compound 6. 210
Figure 11. 18: MS analysis of compound 6. 211
Figure 11. 19: ^{1}H NMR of compound 7. 211
Figure 11. 20: ^{13}C NMR of compound 7. 212
Figure 11. 21: MS analysis of compound 7. 212
Figure 11. 22: ^{1}H NMR of compound 8. 213
Figure 11. 23: MS analysis of compound 8. 213
Figure 11. 24: ^{1}H NMR of compound 9. 214
Figure 11. 25: ^{13}C NMR of compound 9. 214
Figure 11. 26: MS analysis of compound 9. 215

Figure 11. 27: ^{1}H NMR of compound 10. 216
Figure 11. 28: ^{13}C NMR of compound 10. 217
Figure 11. 29: ^{1}H NMR of compound 11. 218
Figure 11. 30: ^{13}C NMR of compound 11. 219
Figure 11. 31: MS analysis of compound 11. 219
Figure 11. 32: ^{1}H NMR of compound 14. 220
Figure 11. 33: ^{13}C NMR of compound 14. 220
Figure 11. 34: MS analysis of compound 14. 221
Figure 11. 35: ^{1}H NMR of compound 16. 221
Figure 11. 36: ^{13}C NMR of compound 16. 222
Figure 11. 37: MS analysis of compound 16. 222
Figure 11. 38: ^{1}H NMR of compound 17. 223
Figure 11. 39: ^{13}C NMR of compound 17. 223
Figure 11. 40: MS analysis of compound 17. 224

List of Tables

Table 1. 1: Recent prodrugs approved by FDA.....55

Table 3. 1: Reagents and conditions used for Boc deprotection of Compound 5......83
Table 3. 2: Boc deprotection progress of compound 5.....84
Table 3. 3: The CHKA inhibitors synthesised in this chapter 87

Table 4. 1: Reaction condition optimisation of the crosslinking yielding compound 11.....96

Table 5. 1: Log D values of choline kinase inhibitors involved in the preliminary investigations using shake-flask method.....108
Table 5. 2: The mRNA levels of four selected cell lines 112
Table 5. 3: Kinetic solubility of ICL-CCIC-0019, CK14, CK144, CK145, CK146 and CK147; n = 2, mean ± SD 130
Table 5. 4: Kinetic solubility classifications.....130
Table 5. 5: Compound permeability data (Papp) and efflux ratios 132
Table 5. 6: Permeability classifications 133
Table 5. 7: Compound half-lives of the FaSSGF stability test 134
Table 5. 8: Human microsome metabolic stability data of ICL-CCIC-0019, CK14, CK144, CK145, CK146 and CK147 using S9 fractions.....136

Table S10. 1: Growth inhibitory activities (GI_{50}) of ICL-CCIC-0019, CK146 and CK145 after 120-hour treatment in HCT-116 and Caco-2 cells 195
Table S10. 2: Growth inhibitory activities (GI_{50}) of ICL-CCIC-0019, CK146 and CK147 in 22Rv1, C4-2B, LNCap, R1AD1, R1-D567, PC3, PNT1A and HCT-116 cells 195

List of Schemes

Scheme 2. 1: Radiosynthesis of [^{18}F]-D4-FCH 62

Scheme 3. 1: Synthesis of ICL-CCIC-0019 (1) and a CK14 (2), and the *mono*-DMAP derivative compound with a tetradecyl linker (3) 81
Scheme 3. 2: Synthesis of CK146 (6) 82
Scheme 3. 3: Synthesis of CK144 (8) 84
Scheme 3. 4: Synthesis of CK145 (9) 86

Scheme 4. 1: Synthesis of CK146-SH *via* unsymmetrical DMAP derivative quarternisation 94
Scheme 4. 2: The first synthetic route of CK146-SH utilising extension of the tertiary amine end on piperazine group *via* NHS ester crosslinking chemistry. 99
Scheme 4. 3: The second synthetic route of CK146-SH utilising extension of the tertiary amine end on piperazine group *via* EDC crosslinking..... 100
Scheme 4. 4: The mock EDC coupling reaction using 1-(4-Pyridyl)piperazine hydrochloride 101
Scheme 4. 5: The thiol-maleimide conjugation between CK146-SH and $(OtBu)_3$PSMA-maleimide synthesised CK147 (17) 103

Abbreviations

Ac-	Acetylated-
ADC	Antibody-drug conjugate
ADME	Absorption, distribution, metabolism and excretion
ADP	Adenosine diphosphate
AMC	7-Amino-4-methylcoumarin
AR	Androgen receptor
ATCC	American Type Culture Collection
ATP	Adenosine triphosphate
AUC	Area under the curve
BCA	Bicinchoninic acid
BCS	Biopharmaceutics Classification System
Boc	*tert*-Butyloxycarbonyl protecting group
BSA	Bovine serum albumin
CCT	Cytidylyltransferase
CDP-choline	Cytidine diphosphocholine
CDP-ethanolamine	Cytidine diphosphoethanolamine
CHKA / *chka* (gene)	Choline kinase alpha
CHKB / *chkb* (gene)	Choline kinase beta
CHT	High-affinity choline transporter family
CK	Choline kinase
CPT	Choline phosphotransferase
CTL	Choline transporter-like family
CTP	Cytidine trisphosphate
CTSL	Cathepsin L
DCM	Dichloromethane
DIEA	*N*,*N*-diisopropylethylamine
DMAP	*N,N*-dimethylaminopyridine
DMF	Dimethylformamide
DMPK	Drug metabolism and pharmacokinetic
DNA	Deoxyribonucleic acid
dsRNA	Double-stranded RNA
DTT	Dithiothreitol

DUPA	2-(3-(1,3-Dicarboxypropyl)-ureido)pentanedioic acid
ECL	Enhanced chemiluminescence
ECT	Ethanolamine-phosphate cytidylyltransferase
EDC	1-Ethyl-3-(3-dimethylaminopropyl) carbodiimide
EGF	Epidermal growth factor
EK	Ethanolamine kinase
EPT	Ethanolamine phosphotransferase
ER	Endoplasmic reticulum
FaSSGF	Fasted state simulated gastric fluid
FCS	Fetal calf serum
FDA	US Food and Drug Administration
FLS	Fibroblast-like synoviocytes
Glu	Glutamate
GPC	Glycerophosphocholine
GRP78	Glucose-regulated protein 78
HC-3	Hemicholinium-3
HDAC	Histone deacetylases
HER2	Human epidermal growth factor receptor 2
HPLC	High-performance liquid chromatography
IS	Internal standard
IRE1a	Inositol-Requiring protein 1
IUPAC	International Union of Pure and Applied Chemistry
LDC	Ligand-drug conjugate
LDH	Lactate dehydrogenase
Lys	Lysine
LOD	Limit of detection
LOF	Loss-of-function
MeCN	Acetonitrile
MRS	Magnetic resonance spectroscopy
mRNA	Messenger RNA
MS	Mass spectrometry
MTT	3-(4,5-Dimethylthiazol-2-yl)-2–5-diphenyltetrazolium bromide
NHS ester	*N*-Hydroxysuccinimide ester
NMR	Nuclear magnetic resonance
OCT	Low-affinity polyspecific organic cation transporter

Papp	Apparent permeability coefficient
PBS	Phosphate buffered saline
PCa	Prostate cancer
PCho	Phosphocholine
PDGF	Platelet-derived growth factor
PEG	Polyethylene glycol
PET	Positron emission tomography
PEMT	*N*-Methyltransferase
PIK4CB	Phosphatidylinositol 4-kinase beta
ppm	parts per million
PSMA	prostate-specific membrane antigen
PtdCho	Phosphatidylcholine
PtdEtn	Phosphatidylethanolamine
Puro	Puromycin
QSAR	Quantitative structure–activity relationship
RA	Rheumatoid arthritis
RaI-GDS	RaI guanine nucleotide dissociation stimulator
RNA	Ribonucleic acid
RNAi	RNA interference
rRNA	Ribosomal RNA
RIPA	Radioimmunoprecipitation assay
RISC	RNA-induced silencing complex
SAR	Structure-activity relationship
SD	Standard deviation
siRNA	Short interfering RNA
SMCC	Succinimidyl 4-(*N*-malemidomethyl) cyclohexane-1-carboxylate
S_N2	Bimolecular nucleophilic substitution
S_NAr	Nucleophilic aromatic substitution
SRB	Sulforhodamine B
TCA	Trichloroacetic acid
tCho	Total choline-containing compound
TCEP	Tris(2-carboxyethyl)phosphine
TEA	Triethylamine
TFA	Trifluoroacetic acid
TLC	Thin-layer chromatography

tRNA	Transfer RNA
TSTU	*N*,*N*,*N'*,*N'*-Tetramethyl-*O*-(*N*-Succinimidyl)uranium tetrafluoroborate
UDPGA	Uridine-Diphosphate-Glucuronic acid
UGT	Uridine 5'-Diphospho-Glucuronosyltransferase
^{18}F-fluoromethylcholine	[^{18}F]-FCH
^{18}F-FEC	[^{18}F]-fluoroethylcholine
^{18}F-3'-fluoro-3'-deoxy-L-thymidine	[^{18}F]-FLT

1. Introduction

1.1 Abnormal choline metabolism related to upregulated CHKA activity in tumourigenesis

1.1.1 Kennedy pathway for phosphatidylcholine (PtdCho) biosynthesis

Phospholipids are the major molecular components of biological membranes for eukaryotes and bacteria [6]. They have a typical structure composed of fatty acids and a platform (normally glycerol or sphingosine) to which a small organic alcohol molecule is attached *via* a phosphodiester bond (Figure 1.1 A) [6]. Phospholipids built on a glycerol platform are called phosphoglycerides. Phosphatidylcholine (PtdCho, also called lecithin), serving choline as the alcohol moiety, is the predominant phosphoglyceride (> 50%) in mammalian membranes (Figure 1.1 B) [7, 8].

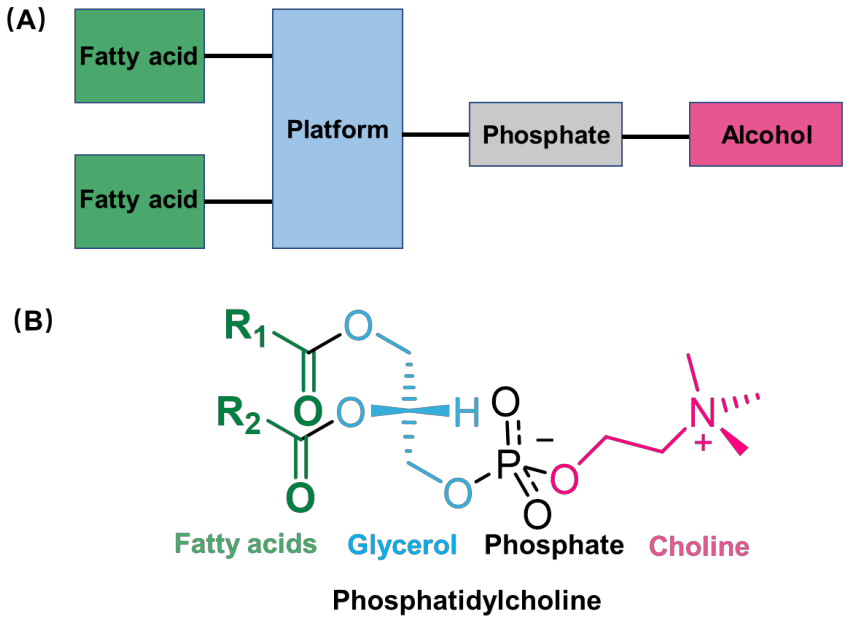


Figure 1. 1: Important phospholipid structures. (A) The schematic representation of a phospholipid (Green (R1/R2): fatty acids; Blue: glycerol or sphingosine; Black: phosphate; Magenta: choline); (B) the chemical structure of phosphatidylcholine.

PtdCho can be synthesised *de novo* by the Kennedy pathway (cytidine diphosphocholine (CDP-choline) pathway) and incorporated into mammalian cell membranes [9]. The Kennedy

pathway contains two mirroring branches named by their intermediates, Cytidine diphosphocholine (CDP-choline) pathway and cytidine diphosphoethanolamine (CDP-ethanolamine) pathway (Figure 1.2). PtdCho is synthesised predominantly through the CDP-choline pathway, whereas CDP-ethanolamine pathway can also contribute *via* *N*-methyltransferase (PEMT) at extreme demand such as starvation and pregnancy [10, 11].

CDP-choline pathway consists of three enzymatic steps, where choline is involved as a precursor (Figure 1.2). In the first step, choline kinase (CK) catalyses the phosphorylation of choline *via* adenosine triphosphate (ATP) hydrolysis in the presence of magnesium ions, which yields phosphocholine (PCho). Subsequently, PCho is converted into CDP-choline by phosphocholine cytidylyltransferase (CCT) *via* cytidine trisphosphate (CTP) hydrolysis. In the last step, PtdCho is synthesised with 1,2-diacylglycerol *via* a condensation reaction, catalysed by choline phosphotransferase (CPT). The CCT catalysis is considered as the main rate-limiting step in PtdCho synthesis in cancer cells, but in some circumstances, CK can become the rate-limiting and regulatory factor [12, 13].

The synthesis of phosphatidylethanolamine (PtdEtn) follows an analogous route involving similar reactions, except for the exploitation of ethanolamine instead of choline (Figure 1.2).

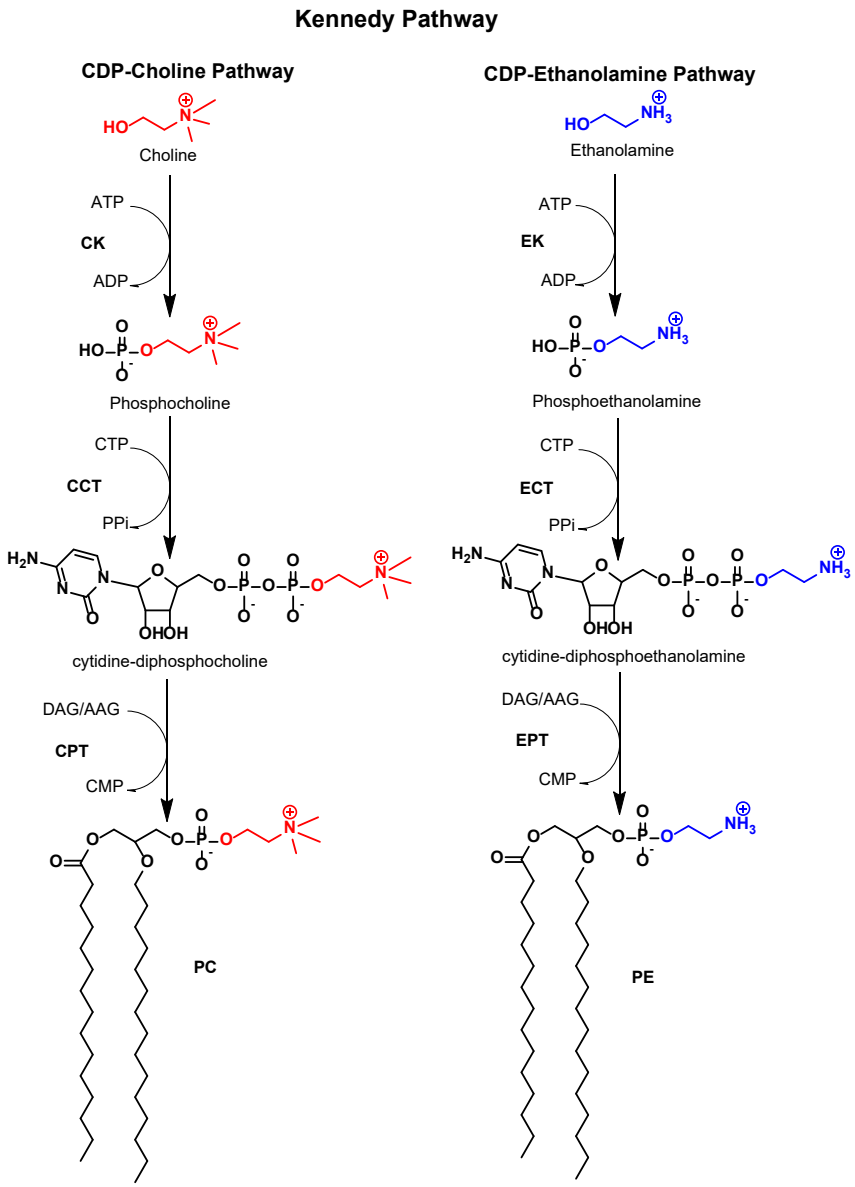


Figure 1. 2: The Kennedy Pathway: CDP-choline pathway and CDP-ethanolamine pathway. The enzymes involved in CDP-choline pathway: CK: choline kinase; CCT: CTP: phosphocholine cytidylyltransferase; CPT: 1, 2-diacylglycerol choline phosphotransferase; the enzymes involved in CDP-ethanolamine pathway: EK: ethanolamine kinase; ECT: CTP: ethanolamine-phosphate cytidylyltransferase; EPT: 1, 2-diacylglycerol ethanolamine phosphotransferase. Choline and ethanolamine are coloured in red and blue respectively.

1.1.2 Choline and choline transport

The synthesis of PtdCho stems from the ingestion of choline, a vitamin-like nutrient essential for both fetal development and adults. The dietary deficiency of choline leads to growth and

memory disorders during fetal development because of choline's multiple influences on stem cell functions; these influences can cause structural and functional alterations in brain and spinal cord, and thus increase the risk of neural defects and memory disfunction [8]. For adults, long-term choline deficiency is found related to fatty liver development [14], muscle damage and increased risk of cardiovascular diseases [15-17].

Choline has several biological functions and it undergoes different transformation processes in the body (Figure 1.3). Choline majorly serves as the precursor of membrane phospholipids such as PtdCho, PtdEtn and sphingomyelin [8]. A small fraction of choline participates in acetylation *via* choline acetyltransferase, which produces acetylcholine, an important neurotransmitter for central/peripheral nervous system and neuromuscular junctions [18]; choline also contributes to the synthesis of signaling lipids and lipid mediators such as sphingosylphosphorylcholine and platelet-activating factor [8]. Finally, choline is a major methyl group donator from the diet: the oxidation of choline, occurring in kidney and liver, produces betaine; betaine participates in the methylation process of homocysteine and generates methionine, the precursor of the methylation agent *S*-adenosylmethionine [8, 19]. In conclusion, choline and its metabolites play vital roles in maintaining the structural integrity and signaling function of cell membranes; the metabolites of choline affect neurotransmission and choline serves as a major dietary source of methyl groups [8, 20, 21].

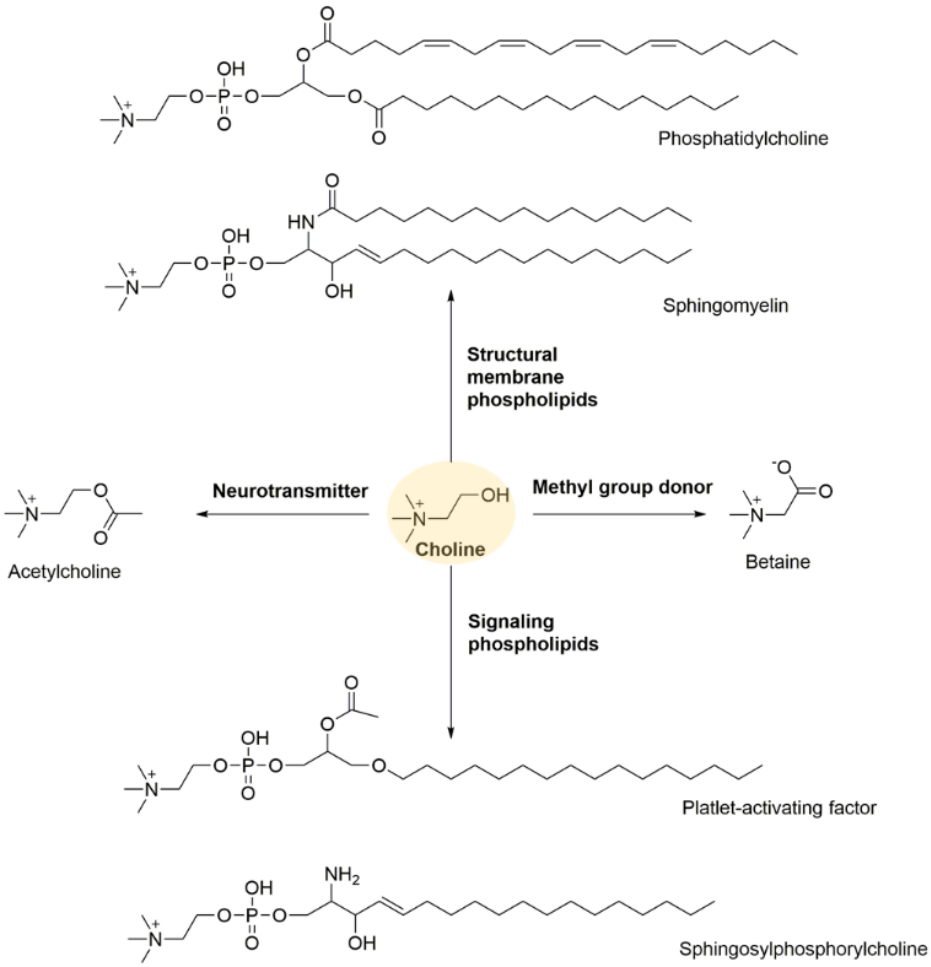


Figure 1. 3: Transformation of choline into 4 classes of biomolecules in the body: the membrane lipids phosphatidylcholine and sphingomyelin, the neurotransmitter acetylcholine, the methyl group donor betaine or the lipid mediators platelet-activating factor and sphingosylphosphorylcholine [20].

As choline bears a positively charged quaternary amine, effective uptake of choline into cells is mediated by protein transporters. Three prominent transmembrane protein systems for choline transport are well documented, revealed by kinetic studies using radiolabeled choline derivatives and inhibitors (*e.g.* hemicholinium-3, HC-3). These include, high-affinity choline transporter family (CHT), choline transporter-like family (CTL) and low-affinity polyspecific organic cation transporters (OCTs) [19].

CHT family is a class of high-affinity (K_m[1] for choline: 0.5 - 3 μM) Na^+- and energy-dependent choline transport proteins, which are sensitive to the inhibition by HC-3 at low concentrations (K_i[2]: 1 - 3 μM) [22]. This transport protein family (*e.g.* CHT1) is predominantly expressed in cholinergic neurons and mainly contributes to the choline transport for the biosynthesis of acetylcholine [19]. On the contrary, the CTL family, also recognised as an active transport system but less dependent on Na^+, bears relatively lower affinity (K_m for choline: 20 - 200 μM) and is less sensitive to HC-3 inhibition (K_i: 20 - 200 μM) [19]. The CTL family is mainly exploited to supply choline for the purpose of phospholipid synthesis, and it is ubiquitously distributed [19]. The OCT family, also called Solute Carrier 22 (SLC22), is responsible for polyspecific cationic transport, mediating the transport of various endogenous organic cations [19]. The affinity of OCTs is the lowest among the three main choline transport systems due to its intrinsic transport mechanism of reversible passive diffusion [23]. They are mainly expressed in kidney and liver [19]. It is noteworthy that one or a combination of choline transport systems with specific functions is exploited in organs so as to ensure sufficient choline uptake [19].

[1] Michaelis-Menten constant (abbreviated as K_m) represents the substrate concentration at which the rate of enzymatic reaction is at half-maximum.

[2] The inhibitor constant K_i represents the concentration of the inhibitor that produces half maximum inhibition.

1.1.3 Choline metabolism in cancer

Upregulated choline metabolism was revealed as a novel metabolic hallmark of cancer by magnetic resonance spectroscopy (MRS) in the 1980s [24]. The characterisation of this so-called cholinic phenotype observed in the clinic refers to increased levels of PCho [25, 26]. Owing to the development and improved clinical availability of non-invasive imaging techniques such as MRS and positron emission tomography (PET), the cholinic phenotype was revealed and has been widely applied in radiological diagnosis, prognosis and for monitoring drug response in cancer treatment [24].

The principle of MRS is that the nuclear magnetic resonance active atomic nuclei (*e.g.* ^{1}H, ^{31}P, ^{13}C, and ^{19}F) placed in an external electromagnetic field can be excited, and then the radiofrequency produced can be detected [27]. The electron clouds surrounding the nucleus give extra electronic shields against the magnetic field, and thus alter the resonance frequency recorded [27]. This resonance difference is reflected as chemical shift (expressed as parts per million, ppm) which is a value independent of the magnetic field strength [27]. In summary, MRS can provide information about the chemical environment of the nuclear spin including number of chemical bonds, neighbouring nuclei, and overall chemical structure [27]. Glunde *et al*. highlighted the concept of total choline-containing compounds (tCho), where tCho represents the combination of choline, PCho and glycerophosphocholine (GPC); the tCho appears as one overlapping peak in the non-invasive *in vivo* ^{1}H MR spectra due to the limited spectral resolution (Figure 1.4) [24]. The signal comes from nine chemically equivalent ^{1}H of the quaternary ammonium moiety in choline, displaying a chemical shift between 3.2 and 3.3 ppm (Figure 1.4A). This single peak can be resolved using high-resolution ^{1}H MRS [24]. ^{31}P MRS, on the other hand, detects the signals from the phosphate groups of choline metabolites from extraction (Figure 1.4B). However, clinical applications of ^{31}P MRS are limited due to its low sensitivity *in vivo* [24]. Besides the limited image resolution, inability of PET imaging to distinguish tumours from nonmalignant hypermetabolic processes emphasises the need for further understanding metabolic differences between tumor and normal tissues [28]. For the study of metabolic biomarkers in

cancer, *in vitro* cell line systems are undoubtedly useful tools that reveal the interplay between altered metabolism of tumour and gene expression. However, comparative profiling of intracellular metabolites across heterogeneous cell line panels is still a major challenge [29]. Tumour cells, in spite of similar genetic background or tissue of origin, can maintain specific metabolic profiles [30]. Normalisation of metabolite abundance and comparison of cell signatures across different cell types with different morphology and size are thus needed in the workflow to overcome the limitations [29]. Cancer cell heterogeneity and plasticity also bring metabolic diversity, and it remains challenging to assess metabolism at the single-cell level [28]. Furthermore, alterations in tumour microenvironment also contribute to cancer progression, which need to be taken into account when using *in vitro* cell line models often devoid of microenvironment factors [31]. The importance of *in vivo* conditions and clinical settings for investigating metabolic target in cancer are thus highlighted.

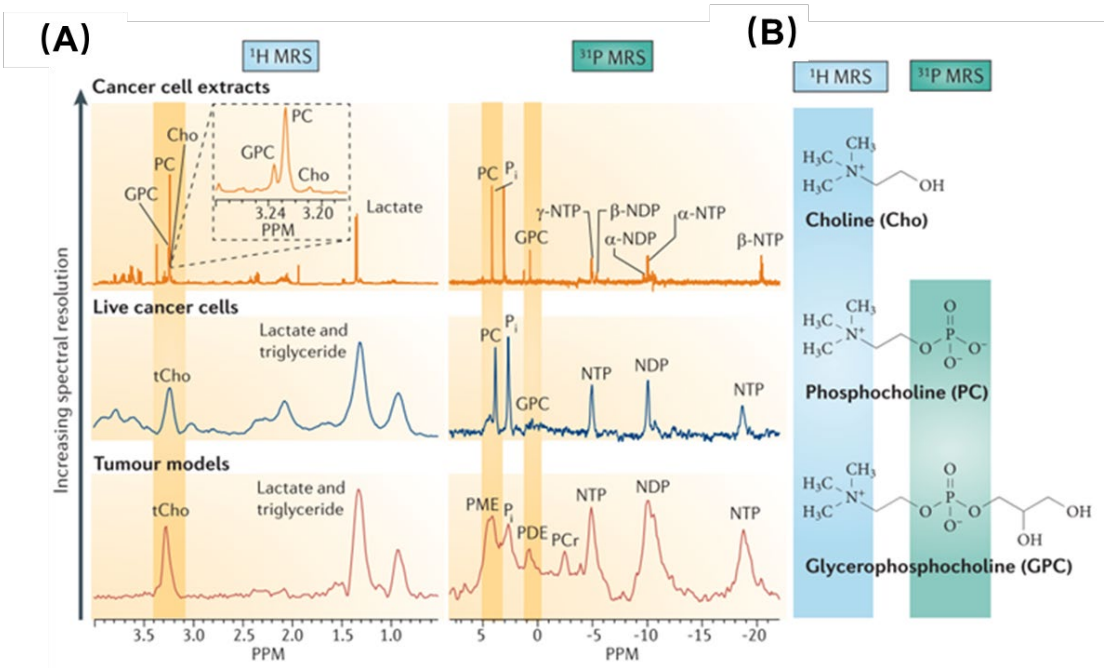


Figure 1. 4: Choline metabolite analysis by ^{1}H and ^{31}P MRS: (A) MRS spectra obtained *in vivo* (live cancer cells and tumour models) and in cancer cell extracts; (B) Chemical structures of tCho. Nine equivalent protons resonating in ^{1}H MRS are highlighted in blue, whereas the ^{31}P-containing phosphate yielding the ^{31}P MRS signal is highlighted in green. Figure extracted from Glunde *et al.* 2011, with permission of the rights holder, Springer Nature [24].

PET is a non-invasive imaging modality capable of providing real-time dynamic visualisation and measurement of *in vivo* physiological processes by tracing radioactive compounds (radiotracers) [32]. A number of radiopharmaceuticals have been developed for PET imaging to visualise various biochemical and metabolic processes in oncology, such as 2-[^{18}F]-fluorodeoxyglucose ([^{18}F]-FDG) targeting glucose metabolism, 3'-[^{18}F]fluoro-3'-deoxy-L-thymidine ([^{18}F]-FLT) targeting deoxyribonucleic acid (DNA) synthesis, and [^{18}F]-fluoromethyl-[1,2-$^{2}H_4$]-choline (D4-[^{18}F]-FCH) for choline metabolism [32-34].

The radioisotopes extensively used in PET imaging of metabolic processes have relatively short half-lives ($t_{1/2}$)[3], such as ^{11}C (half-life $t_{1/2}$ = 20.4 min) and ^{18}F ($t_{1/2}$ = 109.8 min) [35, 36]. The spontaneous decay of a radionuclide emits a positron, an antiparticle to the electron. The positron is positively charged and immediately annihilates after encountering the electron [32, 37]. The process of annihilation can generate two photons in the form of γ rays; these rays are emitted in opposite directions (nearly 180°) but carry the same energy (511 keV), and this pair of signals can be recorded by the detectors (Figure 1.5) [32, 37]. The signal pairs detected within a short-coincidence time window (1 - 10 ns) will be recognised as valid true-coincidence events [37]. By summarising the true-coincidence events, which reflect the radioactivity detected from the patient, the distribution of isotope can be obtained and visualised [37].

Several PET tracers related to choline metabolism, including [^{11}C]choline and D4-[^{18}F]-choline have been developed and investigated [34, 38]. The choline metabolic tracers, as choline mimic, are also transported into cells by choline transporters and undergo the first step of the Kennedy pathway where tracers are phosphorylated by CK. Accordingly, the trapped tracers in cells are located at the regions with high activity of CK; high accumulation of the tracers observed is associated with the hyperactivation of CK.

[3] Half-life ($t_{1/2}$) is the time taken for a radioisotope to decay to half of its initial quantity.

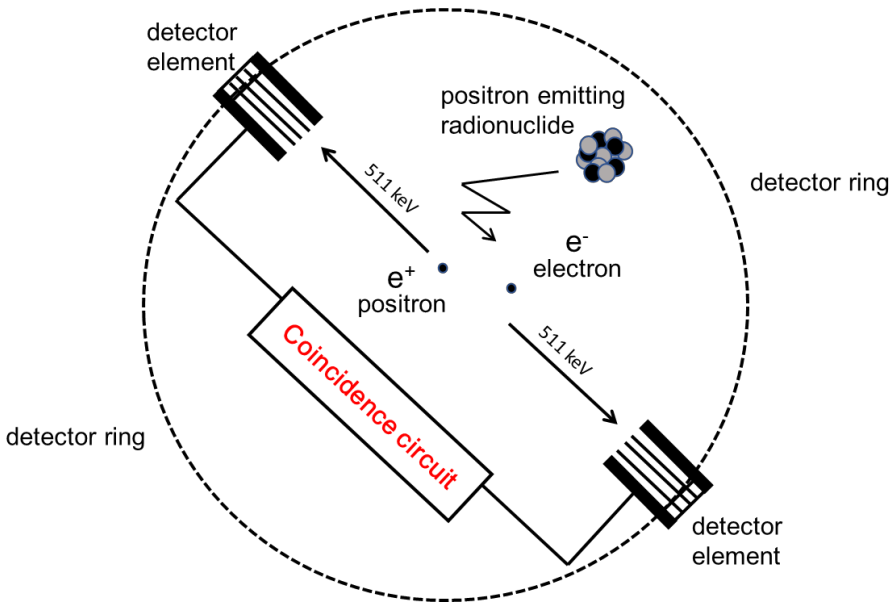


Figure 1. 5: The principles of PET.

1.1.4 Upregulated CHKA activity leads to the cholinic phenotype

In 1953, the choline kinase in yeast was discovered, and the phosphorylation product PCho was successfully isolated [39]. However, the function of CK was not revealed until 1984 owing to the successful purification of the enzyme into homogeneity from the rat kidney [40]. Then cloning and cDNA studies of CK from various species enabled a better understanding of gene structures [9, 13, 41-44]. In humans, there are three CK isoforms discovered, which are encoded by two separate genes: choline kinase alpha (*chka*: CHKA1 and CHKA2) and beta (*chkb*: CHKB) [9]. CHKA1 and CHKA2 share a high degree of homology because they come from the transcription of the same *chka* gene by differential splicing; CHKB is a product of the separate gene (*chkb*) [9]. The monomers of CK isoforms are not active; the homo- and heterodimer forms of CK display different enzymatic activities [9, 45]. CHKA homodimers are the most active [46]: CHKA1 and CHKA2 homodimers have dual choline and ethanolamine kinase activity (the affinity for choline is higher), and are found essential to PtdCho biosynthesis; CHKB homodimers are the least active: CHKB is predominantly responsible for PtdEtn synthesis, and thus cannot compensate for loss of CHKA; the heterodimers of CK exhibit intermediate specificity and mixed enzymatic functions [46, 47]. CK is largely located in the cytoplasm of the cells, although the nuclear localisation of CHKA has also been

reported in the prostatic epithelial neoplasms by our lab [9, 48]. Both CHKA and CHKB are expressed ubiquitously in the body, although the tissue distributions are different [9]. CHKA is highly expressed in key organs for lipid metabolism such as liver and kidney, while CHKB is expressed more in heart [8, 9]. CHKA and CHKB also have highly homologous domains (~60% similarity) in their putative amino acid sequences, but their functions in biological processes are different [9, 45]. The CHKA knockout study in mice showed that CHKA loss caused the embryonic lethality because of PtdCho deficiency during the fetal development [45, 49]. On the other hand, CHKB is related to muscle development: the mice with *chkb* gene deletion survived to adulthood but developed hindlimb muscular dystrophy and forelimb bone deformity [45, 50].

In recent years, the implication of CK in cancer has boosted research in the field. As introduced in Chapter 1.1.3, abnormal choline metabolism characterised by elevated levels of PCho and tCho was identified by MRS in most human cancers [24]. The increased expression of CHKA, but not of CHKB, has been recognised as the main factor leading to the upregulation of CK and the cholinic phenotype observed in the clinic [24]. The overexpression of CHKA has been reported in a broad range of tumour-derived cell lines and biopsies from patients with respect to their corresponding normal counterparts [24, 51-58]. Furthermore, the overexpression of CHKA was found to correlate with advanced histological tumour grade, poor prognosis and reduced survival in breast and non-small-cell lung cancers [55, 59]. In prostate cancer (PCa), CHKA was found as a co-chaperone for the androgen receptor (AR) to maintain AR downstream signaling which causes resistance to therapy and therefore brings challenges to treatment [60].

CHKA is found activated by growth factors such as epidermal growth factor (EGF) and platelet-derived growth factor (PDGF), as well as oncogenes including Ras, Raf, Mos and c-Src [24]. Elevated levels of PCho, implying the hyperactivation of CHKA, can be associated with the expression of Ras oncogenes [61]. The transformation of Ras oncogenes increased the CHKA activity in NIH3T3 cells, and therefore the cell sensitivity to CHKA inhibition by CHKA inhibitors was increased 2 – 3 fold after transformation, compared to the parental cells [61]

However, the exact mechanisms underlying this phenotype remain unclear. Ramírez de Molina *et al.* have demonstrated that Ral guanine nucleotide dissociation stimulator (RaI-GDS) and Ras effector PI3 kinase played vital roles in CHKA activation [62]. The cells that overexpressed wild-type Ras displayed significant CHKA activation, and the activation was accordingly decreased when the cells were transfected with mutant Ras isoforms that only interact with the two downstream targets GDS or PI3K [62] Although Ral-GDS and PI3K were recognised as two efficient stimulators for CHKA activation, sufficient activation of CHKA turned out to require other Ras downstream pathways [62] Further investigations on elucidating the mechanistic link between CHKA activation and the downstream target modulation are still missing. Upregulated RhoA signaling mediated *via* ROCK was also reported to cause increased CHKA activation by the same authors, but the study did not demonstrate direct interaction between ROCK and CHKA [63]. It could be concluded that besides its upregulation in human malignancies, CHKA may have oncogenic properties *in vitro* and *in vivo*. However, it is noted that the hyperactivation of CHKA could be inferred as the result of interplay among various oncogenes related to abnormal cell growth, and the direct regulatory mechanisms remain to be fully understood.

CHKA has been validated as a potential target for cancer therapeutics, due to its upregulation in various malignancies, interaction with key oncogenic signaling and involvement in oncogenic transformation [64]. Existing pharmacological approaches aimed at CHKA inhibitor development have challenges to improve inhibitor specificity/selectivity. The off-target effects of CHKA inhibitors beyond the CDP-choline pathway are undesirable. Novel strategies targeting CHKA inhibition with high specificity and selectivity are therefore required to provide the cancer patients with suitable therapeutic index.

1.2 Inhibition of CHKA as a Cancer Treatment Strategy

1.2.1 RNAi Studies

There is a growing interest in exploiting CHKA inhibition as a therapeutic strategy for cancers.

The feasibility of cancer treatment by targeting CHKA with therapeutics was first studied and supported by RNA interference (RNAi).

Ribonucleic acids (RNA) are a class of essential biological macromolecules to various cellular processes including gene expression, protein synthesis and regulation in living organisms. Most RNA molecules are single-stranded with a similar helix skeletal structure as DNA. Double-stranded RNA (dsRNA) is often seen in virus and RNAi studies [65, 66]. RNA molecules can be thought as biopolymers as they are also assembled from nucleotide units, like DNA. There are three main types of RNA playing different roles in protein synthesis, namely messenger RNA (mRNA), transfer RNA (tRNA), and ribosomal RNA (rRNA). mRNA is the transcription product from DNA which carries the genetic blueprint and guides the synthesis of proteins; tRNA is responsible for the translation of mRNA into proteins; rRNA forms ribosome that performs protein synthesis [67].

In recent years, the techniques inducing loss-of-function (LOF) of genes have been widely used in biological process analysis to deepen the understanding on genetic mechanisms. These techniques include gene mutagenesis, CRISPR, RNAi and pharmacological inhibition [68]. RNAi is advantageous over other approaches in investigating the function loss of CHKA in several aspects: RNAi can achieve specific RNA targeting and thus allows the knockdown of specific isoforms such as CHKA; RNAi can generate partial loss of gene function, which can be used in the identification and validation of potential drug targets with low cost but high throughput [69, 70].

RNAi is a biological process where RNA molecules inhibit gene expression or translation by neutralising mRNA. In 1991, RNAi was discovered and described as a biological response to the dsRNA [66]. In the studies of nematode (*Caenorhabditis elegans*), the injection of dsRNA was found to evoke the silencing of the genes whose sequences were complementary to those of the introduced dsRNAs [66]. It is now understood that those dsRNAs were processed into single-stranded short interfering RNA (siRNA) fragments (~22 nucleotides) by

the RNase enzyme called Dicer [71]. The siRNAs were incorporated into the RNA-induced silencing complex (RISC), which identifies and silences complementary mRNAs to specifically suppress the target protein [71]. The biological pathways supporting dsRNA-induced gene silencing exist in most eukaryotes [72].

RNAi is a useful tool in validating CHKA as a promising therapeutic target of cancer. A large-scale RNAi screening against 650 known and putative kinases revealed a two-fold increase of apoptosis in the HeLa cervical carcinoma cells with CHKA knockdown [73]. Yalcin *et al.* found that RNA-mediated CHKA inhibition disrupted the essential pathways for transformed cell survival by inhibiting AKT and ERK phosphorylation; the growth inhibition of xenografts in athymic mice was also observed in the study [74]. Glunde *et al.* investigated the RNAi-mediated suppression of CK using a panel of breast cancer cell lines including a non-malignant cell line MCF-12A and three malignant cell lines MCF-7, MDA-MB-231 and MDA-MB-435 [53]. A significant reduction in cell proliferation and accelerated differentiation were caused by the down-regulation of CHKA expression, which was likely due to the inhibition on DNA synthesis and cell cycle regulation [53, 75]. The effects of decreased CHKA expression on CK, PCho and tCho were not evident in the non-malignant cell line MCF-12A, which could be related to the low basal CK expression in these cells [53]. A further study was performed by Krishnamachary *et al.* in which a RNAi-based gene therapy targeting CK was delivered to the athymic mice bearing MDA-MB-231 xenografts *via* a lentiviral vector [76]. The mRNA and protein levels were inhibited by 80% after the injection of short-hairpin RNA; the mRNA levels of CK were reduced by ~35% on the tumour site, and it thus inhibited the CK activity and tumour growth [76].

In summary, the effects of CHKA down-regulation mediated by RNAi were less pronounced in non-malignant models, inferring that small-molecule inhibition of CHKA would selectively target malignant cells without affecting their normal counterparts. All these findings together have highlighted the crucial role of CHKA in tumour survival and progression, as well as its potential in cancer therapeutic intervention.

1.2.2 CHKA crystal structure

The crystal structures of human CHKA2 in its apo (substrate-free), ATP- and PCho-bound forms were elucidated by Malito and his colleagues (protein data bank code: 2CKO, 2CKP and 2CKQ respectively) [77]. The protein sequences and CHKA crystal structures of other species have also been studied [78, 79]. CHKA isoforms were found to share highly-conserved protein sequence regions which mainly contain two clusters of residues: the Brenner's motif (frequently seen in the phosphotransferase family) and the choline kinase motif (specific to the choline kinase family) [79]. As a result, the two main binding sites of CHKA were revealed.

CHKA is identified as 'atypical kinase' because it adopts a typical catalytic core of the eukaryotic protein kinase but does not conserve all the usual kinase motifs [77, 79, 80]. Each monomer of the heterodimers is composed of two domains (N and C-terminal domains) connected by a short β-strand (Figure 1.6) [77]. The highly-specific nucleotide (ADP: adenosine diphosphate / ATP) binding site of CHKA is located at a large cavity formed by N and C-terminal lobes (Figure 1.6) [77]. The adenine ring of the nucleotide molecule produces H-bond interactions with Ile209 and Gln207; Leu144 and Leu313 are two conserved hydrophobic residues positioned on both sides of the adenine ring, contributing to the suitable positioning and binding of the nucleotide molecule (Figure 1.7) [77].

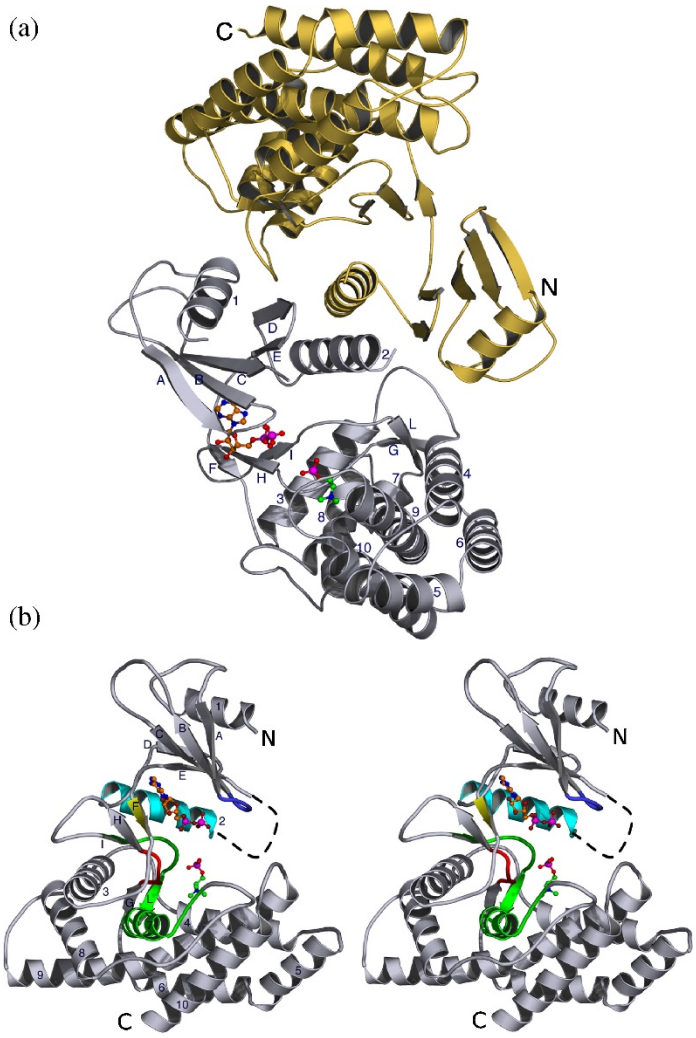


Figure 1. 6: The structures of CHKA2 monomer in ribbon diagram, with ADP and PCho molecules concomitantly present. (a) CHKA2 dimer (grey/yellow ribbon) oriented perpendicular to the plane of the page; (b) A stereo diagram of a CHKA2 monomer drawn after a vertical rotation of 90° with respect to the orientation in (a). The key elements are coloured: the ATP-binding loop in blue, the short β-strand connecting the N and C-terminal domains in yellow, the Brenner's motif in red, and the choline kinase motif in green. In this and the following figures, ball-and-stick representation of ADP and PCho molecules are displayed with their carbon atoms coloured in orange and green, respectively. Oxygen, nitrogen and phosphate atoms are coloured in red, blue and magenta, respectively. Figure extracted from Malito *et al.* 2006, with permission of the rights holder, Elsevier [77].

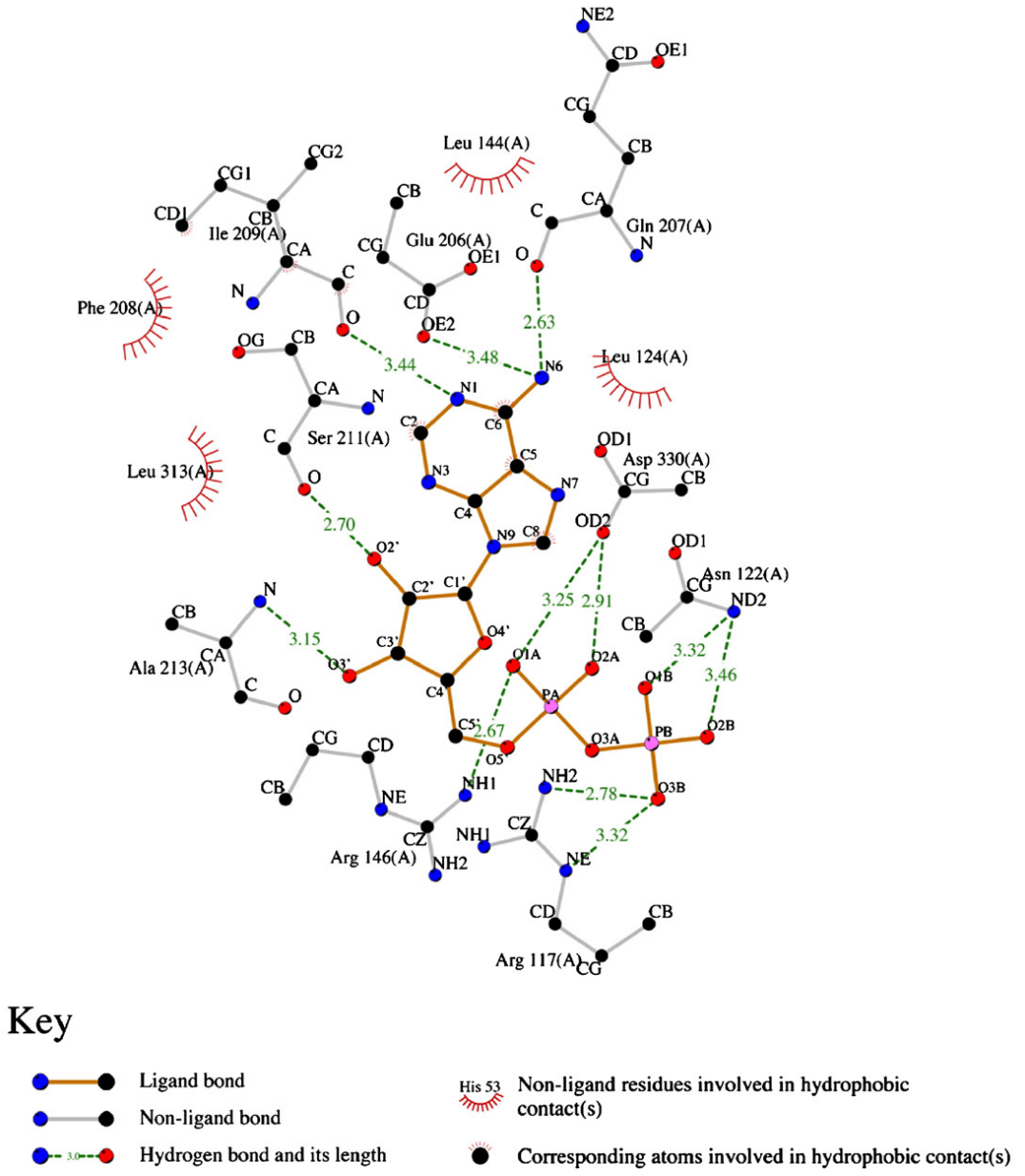


Figure 1. 7: The interactions of ADP with CHKA2 at the ATP-binding site. The key elements have been enclosed below the figure; ligand bonds, carbon, oxygen, nitrogen and phosphorous atoms are coloured in orange, black, red, blue and purple, respectively. Figure extracted from Malito *et al.* 2006, with permission of the rights holder, Elsevier [77].

The choline binding site is a deep hydrophobic groove located near the C-terminal with negatively charged residues (Glu215, 217, 218, 309, 349, 357, 434 and Asp353) on the rim and at the deep end of the groove (Asp306, Asp330 and Glu349; Figure 1.8A) [77]. Both hydrophobic and electrostatic forces are two main factors leading to the interactions between CHKA and choline [81]. Although the rim surface of the choline binding site is

composed of abundant negatively charged residues, the base of the choline pocket where choline actually binds to is surrounded by conserved aromatic residues (Tyr333, 354, 440, and Trp420, 423; Figure 1.8B) [77]. When choline molecule docks into the active choline binding site, its positively charged quaternary amine is stabilised by the interactions with the aromatic residues on the site. The whole CHKA enzyme undergoes a conformational change when choline docks into the negative pocket, which subsequently affects the ATP binding loop [77].

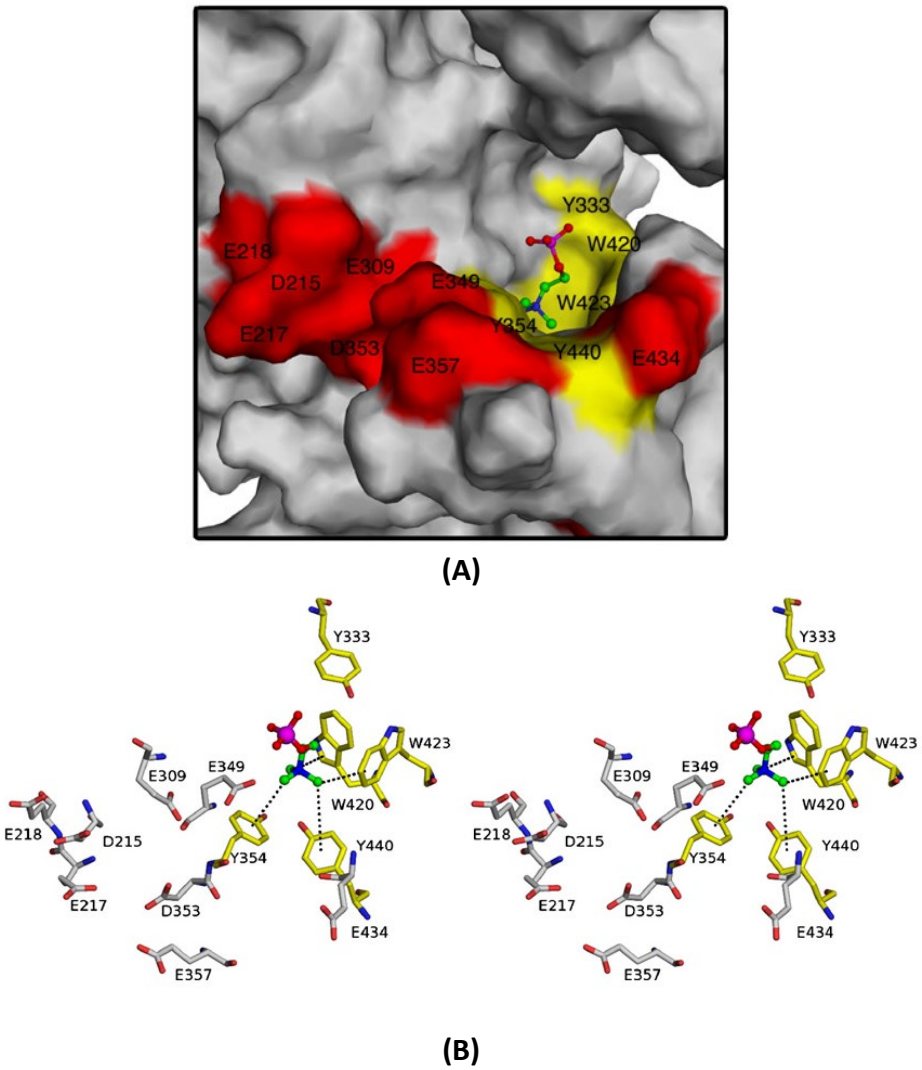


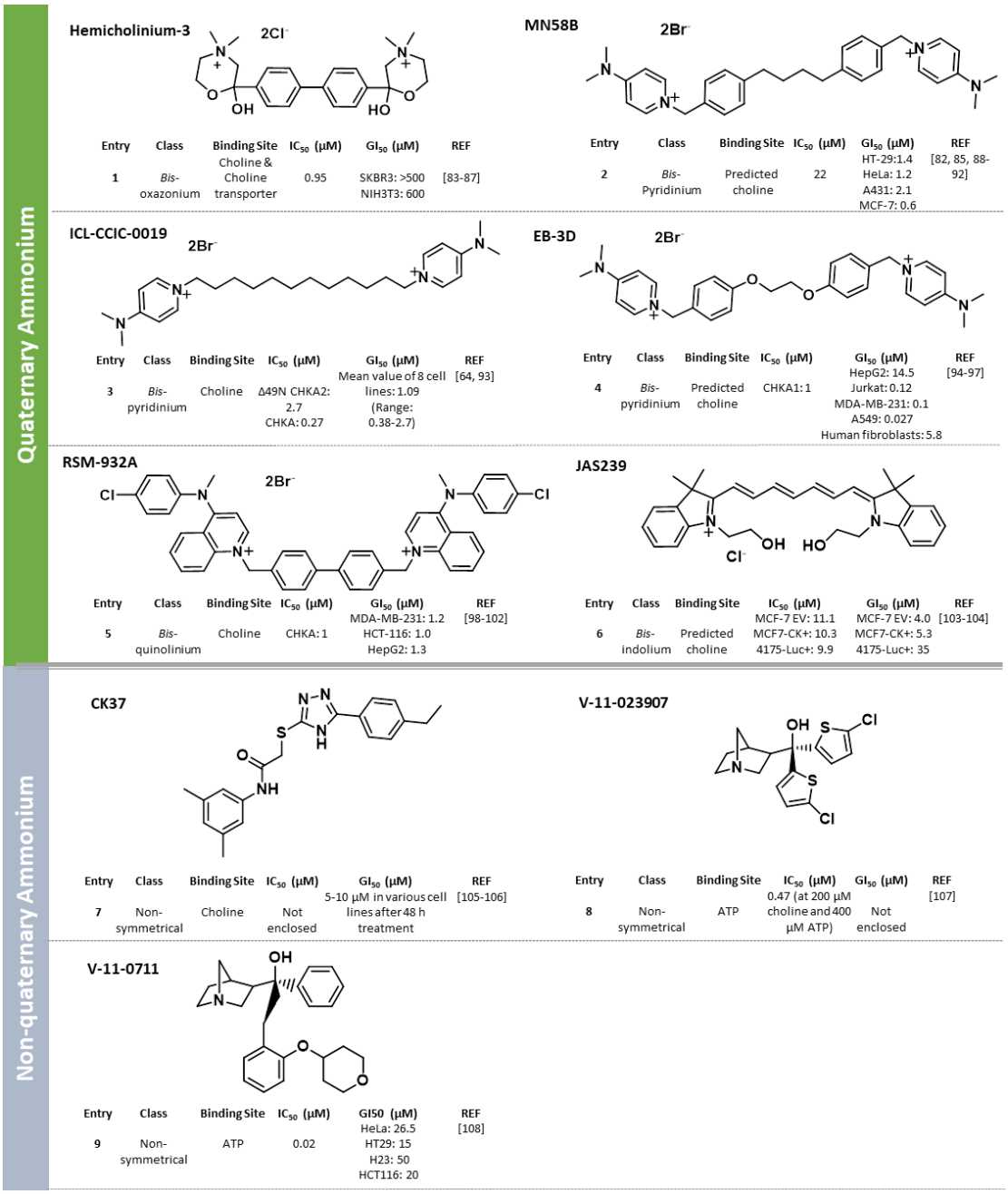
Figure 1. 8: The interactions of choline with CHKA2 at the choline-binding site. (A) Zoom of the choline-binding groove; the hydrophobic and negative residues are coloured as yellow and red surface, respectively; (B) The stereo view which shows the interactions between the quaternary ammonium moiety of choline and the hydrophobic conserved residues (yellow sticks). Solvent-accessible negatively charged residues are coloured as grey sticks. Oxygen,

nitrogen and phosphorous atoms are coloured in red, blue and magenta, respectively. Figure extracted from Malito *et al.* 2006, with permission of the rights holder, Elsevier [77].

1.2.3 Small-molecule CHKA inhibitors

The structure information of CHKA substrate binding sites provides the insights of essential pharmacophore for the rational design of CHKA inhibitors. In consideration of hydrophobic effects and electrostatic properties adopted by the choline binding site, the structures offering strong electrostatic interactions with the choline binding site can translate into high affinities of CHKA inhibitors. The features of potential structures can include but not be limited to: (1) a permanent positively charged quaternary amine that mimics choline; (2) an aromatic moiety adjacent to the amine, which allows the π-π interaction with the hydrophobic groove.

Since CHKA was proposed as a druggable therapeutic target for cancer [82], to date, a number of lead compounds with inhibitory activity against CHKA have been designed and synthesised. These inhibitors are unquestionably novel cancer therapeutic intervention strategies by interfering with malignant metabolism. Several reported CHKA inhibitors with different structural characteristics are listed and introduced in this section (Figure 1.9).



Entry	Class	Binding Site	IC_{50} (μM)	GI_{50} (μM)	REF
1	*Bis*-oxazonium	Choline & Choline transporter	0.95	SKBR3: >500 NIH3T3: 600	[83-87]
2	*Bis*-Pyridinium	Predicted choline	22	HT-29:1.4 HeLa: 1.2 A431: 2.1 MCF-7: 0.6	[82, 85, 88-92]
3	*Bis*-pyridinium	Choline	Δ49N CHKA2: 2.7 CHKA: 0.27	Mean value of 8 cell lines: 1.09 (Range: 0.38-2.7)	[64, 93]
4	*Bis*-pyridinium	Predicted choline	CHKA1: 1	HepG2: 14.5 Jurkat: 0.12 MDA-MB-231: 0.1 A549: 0.027 Human fibroblasts: 5.8	[94-97]
5	*Bis*-quinolinium	Choline	CHKA: 1	MDA-MB-231: 1.2 HCT-116: 1.0 HepG2: 1.3	[98-102]
6	*Bis*-indolium	Predicted choline	MCF-7 EV: 11.1 MCF7-CK+: 10.3 4175-Luc+: 9.9	MCF-7 EV: 4.0 MCF7-CK+: 5.3 4175-Luc+: 35	[103-104]
7	Non-symmetrical	Choline	Not enclosed	5-10 μM in various cell lines after 48 h treatment	[105-106]
8	Non-symmetrical	ATP	0.47 (at 200 μM choline and 400 μM ATP)	Not enclosed	[107]
9	Non-symmetrical	ATP	0.02	HeLa: 26.5 HT29: 15 H23: 50 HCT116: 20	[108]

Figure 1. 9: Chemical structures and pharmacological data of corresponding CHKA inhibitors: HC-3 [83-87], MN58B [82, 85, 88-92], ICL-CCIC-0019 [64, 93], EB-3D [94-97], RSM-932A [98-102], JAS239 [103, 104], CK37 [105, 106], V-11-023907 [107], V-11-0711 [108].

1.2.3.1 Quaternary ammoniums

1. Hemicholinium-3 (HC-3)

HC-3 was designed and developed around a *bis*-oxazonium pharmacophore in 1950s. Although it was recognised as the most potent CHKA inhibitor at this time, HC-3 was also found as a competitive inhibitor of high-affinity choline transporters due to its structural similarity to choline [83]. Before its role as a CHKA inhibitor, HC-3 was exploited as a research tool due to its ability to inhibit acetylcholine synthesis in the nervous system [83]. HC-3 was observed to cause respiratory paralysis in many animal models because of its inhibition of choline uptake which leads to a rapid depletion of acetylcholine pool in the nerve terminal [83]. In terms of CHKA inhibition, HC-3 has a low micromolar affinity against purified human CHKA (IC_{50}: 0.95 μM) and a relatively poor cell growth inhibition when tested in SKBR-3 and NIH3T3 cells (GI_{50} > 500 μM) [84-86]. Although in many studies HC-3 was revealed capable of inhibiting choline uptake and reducing PtdCho levels *in vitro*, administering HC-3 at doses necessary for *in vivo* CHKA inhibition caused serious off-target effects on the neuronal high-affinity choline transporters, acetyltransferase, as well as acetylcholinesterase [87]. These findings greatly limited the therapeutic use of HC-3 in cancer treatment.

Continuous work had been carried out in different labs attempting to improve the antiproliferative profiles of HC-3 by investigating the structure-activity relationships (SAR) of HC-3 and its congeners. The modifications on the symmetrical structure of HC-3 can be mainly divided into two fragments, labelled as A and B, respectively in Figure 1.10. The SAR of the two fragments is addressed separately in the next paragraph.

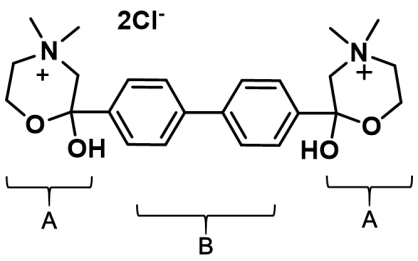


Figure 1. 10: Chemical structure of HC-3, where the molecule is divided into two fragments: (A) the two oxazinium rings and (B) the biphenyl portion.

A large number of analogous compounds to HC-3 have been synthesised, with modifications at fragment A [83]. The results emphasised the following SAR: (1) the quaternary amine is recognised as the pharmacophore essential for maintaining the so-called HC-3-like activity, which is related to choline transport inhibition, as most tertiary ammonium derivatives are inactive; (2) it is noteworthy that the substitution of the oxazinium rings using pyridinium, quinolinium, isoquinolinium, or quinuclidinium rings offered less or little HC-3-like activity, but elicited novel pharmacological actions, such as acetylcholinesterase inhibition [83]. Assessment of the pharmacological data using the moieties of varying lengths and lipophilicity drew the conclusion that replacement of the central biphenyl portion in HC-3 by aryl, alkyl, or cycloalkyl moieties did not significantly compromise the hemicholinium-like activity and potency [83]. The biphenyl fragment in HC-3 is, thus, identified as a space linker responsible for establishing an optimal distance (14-15 Å) between the nitrogen atoms [83].

2. MN58B

To improve the selectivity and activity of HC-3 against CHKA, a series of compounds were developed on the structural basis of HC-3 by Juan Carlos Lacal and his colleagues [88]. This class of *bis*-pyridinium compounds demonstrated significantly improved CHKA inhibitory and antiproliferative activities by the following modifications: (1) the oxazonium rings in HC-3 were replaced by aromatic heterocycles; (2) 1,2-ethylene(*bis*-benzyl) moiety was used as the space linker in the molecules instead of the biphenyl fragment; (3) according to the quantitative structure-activity relationship (QSAR) investigations, the electron-donating groups (*e.g. N,N*-dimethyl moiety) at the C4-position of the pyridinium head-groups could elicit the best *ex vivo* CHKA inhibition [85].

Among all the molecules synthesised and tested, MN58B, as a *bis*-pyridinium salt, showed satisfactory *in vitro* pharmacological profiles and good lipophilicity (Figure 1.11): MN58B exhibited selective CHKA inhibitory activity (IC_{50}: CHKA1: 5 μM, CHKB: 107.5 μM); it also exhibited good *in vitro* and *in vivo* potencies against tumour proliferation and reduced PCho production in a variety of carcinoma cell lines and tumour models (*e.g.* GI_{50} of 1.4 μM in HT-

29 cell line and 70% tumour reduction in HT-29 mouse xenograft) [82, 85]. MN58B treatment can cause enhanced ceramide levels and endoplasmic reticulum (ER) stress in cells, which are related to cellular apoptosis and disrupted lipid metabolism induced by CHKA inhibition [89, 90]. Notably, both effects were pronounced, and promoted apoptosis in tumour cells, while normal cells under the same treatment stayed in a reversible cell cycle arrest and remained less affected [89, 90]. However, MN58B was not able to completely inhibit the CHKA activity at pharmacologically relevant concentrations (60% CHKA activity inhibition was observed using 20 µM MN58b in MDA-MB-468 and 6 µM in MDA-MB231 cells) [91, 92].

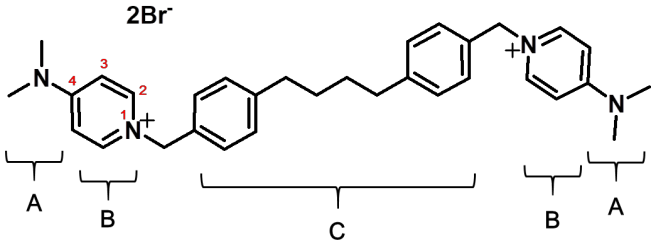


Figure 1. 11: Chemical structure of MN58B. The key modifications compared to HC-3 are divided into three fragments: (A) the *N,N*-dimethyl moiety at the C4-position, (B) the pyridinium ring and (C) 1,2-ethylene(*bis*-benzyl) moiety.

3. ICL-CCIC-0019

A series of novel symmetrical and asymmetrical *N,N*-dimethylaminopyridine (DMAP) derivatives have been designed and synthesised as potent CHKA inhibitors by Trousil *et al*, where DMAP mimicked the cationic choline moiety [93]. The design of this class of inhibitors exploited DMAP as pharmacophore for two reasons: (1) the nitrogen atom in DMAP can form a permanent positively charged quaternary amine that mimics choline; (2) the aromatic moiety of DMAP adjacent to the amine allows the π-π interaction with the hydrophobic groove of the choline binding site to facilitate binding; (3) DMAP was a cationic choline-mimicking group in the previous study where the inhibitors showed good CHKA activities and lipophilicity [85].

The symmetry of compounds and the lengths of spacer linkers were investigated in this work

(Figure 1.12, left). In symmetrical DMAP derivatives as CHKA inhibitors, alkyl chains with different numbers of carbon atoms (C8 to C14) connect two cationic DMAP rings as choline-mimicking moieties [93]. The increase of carbon atoms successively improved the CHKA activity of the symmetrical compounds [93]. The nonsymmetrical DMAP derivatives, in which the cationic DMAP moiety on one side was substituted with adenine analogues, were also designed and synthesised, aiming to achieve the dual binding of choline and ATP pockets (Figure 1.12, right) [93]. The dodecyl linker was selected in this study because a distance of about 14 Å was ideal to bridge both choline and ATP pockets [93]. Although a mixed type of inhibition was validated by the enzymatic kinetic study, the introduction of adenine moieties caused loss of CHKA activity in the nonsymmetrical compounds [93].

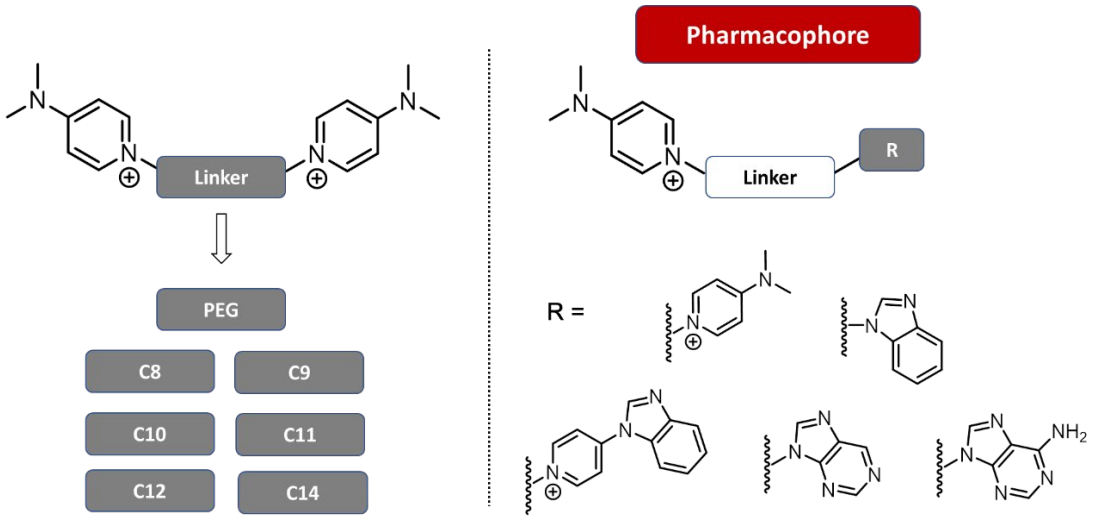


Figure 1. 12: An overview of the symmetrical and nonsymmetrical CHKA inhibitors designed by Trousil *et al*. Symmetrical inhibitors (left) with different linker lengths were designed to target the choline pocket; in the nonsymmetrical inhibitors (right), one side of the cationic DMAP moiety was replaced by adenine analogues, attempting to target both choline and ATP pockets.

Among all the DMAP derived CHKA inhibitors, ICL-CCIC-0019 (IC_{50}: 0.27 µM), a symmetrical compound with a dodecyl linker, is the most studied. ICL-CCIC-0019 displayed selective antiproliferative activity *in vitro* (mean IC_{50} against 8 cancer cell lines: 1.09 µM, range: 0.38 - 2.7 µM; GI_{50} range against normal cell lines: 30 - 120 µM) [64, 93]. Additionally, it has a similar CHKA inhibitory activity to MN58B, but the synthesis of ICL-CCIC-0019 is much

simpler [93]. In [^{3}H]-choline uptake studies, ICL-CCIC-0019 successfully reduced intracellular PCho concentration and simultaneously inhibited the synthesis of phospholipids such as PtdCho [64]. Satisfactory kinase selectivity of ICL-CCIC-0019 was confirmed by screening against a panel of 131 human kinases [64]. Induction of G1 arrest and apoptosis activated by caspase 3/7 in several cancer cell lines were also seen in assays with ICL-CCIC-0019 [64]. In the *in vivo* study using the HCT-116 xenograft model, ICL-CCIC-0019 showed metabolic stability in plasma and was found to accumulate extensively in liver and kidney, but the oral bioavailability was limited [64]. A relatively stable concentration at the tumour site (1 μM) was maintained throughout the study [64]. The treatment with ICL-CCIC-0019 resulted in potent antitumour activity *in vivo* by CHKA inhibition, which was further associated mechanistically with CHKA inhibition using [^{18}F]-D4-FCH [64].

ER stress and mitochondrial toxicity were two phenotypes observed in ICL-CCIC-0019 treatment, and were thought as the main mechanism of action of cell death, relatively specific to cancer cells, with normal cells less affected [64]. However, the reduced cell survival induced by ICL-CCIC-0019 could also be due to the molecular interactions with the other enzymes in CDP-choline pathway such as CPT [64]. This finding, together with the slight weight loss observed in the *in vivo* model (< 20%) by ICL-CCIC-0019 treatment, urge the development of a novel candidate with optimised selectivity over the target [64].

4. EB-3D

EB-3D and its derivatives are recently reported as *bis*-pyridiniums, which contain a novel 1,2-dioxoethane linker [94]. This series of compounds was designed by interchanging the substitution pattern of their linkers with the corresponding novel linker where two oxygen atoms were introduced; the successful cationic choline-mimicking moieties described in the previous work were maintained in these molecules for further development: as the most representative compound from the series, EB-3D adopted a symmetrical structure where quaternary DMAP was the choline-mimicking moiety [94]. The introduction of the novel linker was expected to improve compound polarity and solubility due to a classical

bioisosteric exchange between carbon and oxygen atoms [94]. Additionally, according to docking studies, the synclinal conformation of the linker could also improve compound affinity to CHKA: by allowing the insertion of EB-3D into the choline binding site and enhancing the antiproliferative effects [94].

Several sets of preclinical evaluations were carried out using different cancer models. In general, EB-3D offered a better CHKA activity than MN58B, and it exhibited good antiproliferative profiles against a panel of human cancer cell lines and in primary cultures [94-97]. Higher antiproliferative activity of EB-3D was observed in rapidly proliferating cells such as mitogen-stimulated lymphocytes compared to quiescent cells [94]. Moreover, EB-3D increased sensitivity to chemotherapies in leukemia T-cells; it also induced senescence in breast cancer cell lines and strongly synergised with the common breast cancer therapies [95, 96]. EB-3D treatment *in vivo* reduced the tumour size of the breast cancer mouse model at low doses and showed an antimetastatic effect in metastasis models [95]. It was revealed that EB-3D affected PtdCho biosynthesis *via* both CDP-choline pathway and cellular choline uptake [97]. Importantly, EB-3D lowered the CHKA protein levels probably *via* the effects on the AMP-activated protein kinase signaling pathway [97]. However, similar to ICL-CCIC-0019, mitochondrial toxicity and ER stress were also seen with EB-3D treatment, implying similar mechanism of action and toxicity profiles despite the diverse chemical structures [97].

5. RSM-932A (TCD-717)

QSAR studies on HC-3 analogues had highlighted not only the potency of pyridine derivatives, but also compound lipophilicity; low compound lipophilicity would impede the antiproliferative efficacy of CHKA inhibitors in cells [98]. With more investigations on steric and electrostatic interactions at the choline binding site, quinolinium or isoquinolinium were used to substitute pyridinium moieties in compounds so as to improve the cell permeability [99]. The *bis*-quinoliniums exhibited better antiproliferative profiles compared to the *bis*-pyridiniums because of their increased lipophilicity, but the alternative cell death mechanism besides CHKA inhibition was postulated as a concern [100].

The most representative CHKA inhibitor derived from this class is RSM-932A, which was the first CHKA inhibitor to enter Phase I clinical trial for advanced solid tumour treatment (clinical trials number: NCT01215864) [99, 101]. In its preclinical characterisation, RSM-932A displayed high specificity to CHKA (CHKA IC_{50}: 1 μM, CHKB: IC_{50}: 33 μM) and broad-spectrum antiproliferative activities at the submicromolar range [99, 101]. Under *in vivo* conditions, RSM-932A exhibited a LD_{50}[4] of 12 mg/mL in the immunocompetent mouse model and an effective dose[5] of 7.5 mg/mL in the HT-29 mouse xenograft model with 70% tumour inhibition by the end of treatment [99, 101]. The use of RSM-932A also synergised with the standard antineoplastic agents (*e.g.* 5-FU) for colorectal tumour treatment in the *in vivo* combination studies [102]. Notably, RSM-932A induced ER stress by the same mechanism as observed in MN58B, where the levels of inositol-requiring protein 1 (IRE1a) and glucose-regulated protein 78 (GRP78) are elevated to recover the misfolded proteins [90]. Interestingly, protein destabilisation was not a sign observed in the cell apoptosis induced by ICL-CCIC-0019, implying alternative mechanisms of antiproliferative activity [64].

6. JAS239

JAS239 is a near infrared fluorescent HC-3 mimetic which was developed as a potential optical imaging agent for tumour diagnosis and staging [103]. JAS239 is derived from the

[4] LD_{50} represents the concentration of the dose that induced 50% death in mice (Indicated in mg/mL).
[5] The effective dose used in the *in vivo* experiments (Indicated in mg/mL).

carbocyanine dye and bears a *bis*-indolium structure; the aliphatic space linker of JAS239 offers the molecule fluorescence within the near-infrared window ideal for *in vivo* optical imaging [103]. Fluorimetry and confocal microscopy showed that JAS239 entered breast cancer cells independent of choline transporters and accumulated in cytosol rich in choline kinase [103]. Compared to MRS and PET imaging, its improved selectivity of CHKA over choline transporters and other pathway enzymes makes JAS239 a useful tool for monitoring pharmacological CHKA inhibition [103, 104]. *In vitro* study using breast cancer cell lines showed that JAS239 has a comparable antiproliferative and CHKA inhibitory potency to MN58B [104]. ^{1}H MRS studies validated the competitive binding of JAS239 to choline site and its induced reduction of choline phosphorylation [103]. The biodistribution and growth inhibition of 4175-Luc+ tumour xenografts were investigated using JAS239 optical imaging [104]. A significantly higher accumulation of JAS239 was observed in the CHKA-overexpressed tumour models compared to its normal counterparts; the tumour growth rate and tCho metabolite levels were also lowered by JAS239 to the same degree as MN58B without noticing obvious toxic effects [104]. Of note, since JAS239 does not affect choline transporters, the observed decrease of PCho and cell viability suggests that the cell viability loss in malignant cells is mechanistically linked to the PCho reduction. It should be kept in mind that, however, the transport of JAS239 into cells is mainly driven by lipophilicity, the accumulation of JAS239 could, thus, not be organ-selective: the infrared fluorescence of JAS239 was also detected in major organs besides the tumour sites [104]. The whole-body near-infrared imaging by JAS239 is inferred not directly instructive, and the differentiation of the tissue malignancy from the background noise may be problematic.

7. CK37

Despite most CHKA inhibitors bearing the quaternary ammonium moiety, which was deemed essential for receptor binding by mimicking choline, a few non-charged compounds have been indentified by an *in silico* screening of the ZINC chemical library using the x-ray structure of CHKA2 [105, 106]. From the 50 potential candidates, 16 best-score compounds with high affinity to CHKA choline site were selected for further evaluation, where CK37 was

the only compound significantly inhibiting the CHKA activity in HeLa cell lysates and was, thus, further investigated [105]. CK37 is a structually distinct, non-charged CHKA inhibitor (Figure 1.13) [105]. Despite being uncharged, CK37 is choline-competitive but not effective enough to inhibit the recombinant CHKA: PCho production was decreased by 60% with CK37 (25 µM) [105]. The exposure to high concentrations of CK37 attenuated MAPK and PI3K/AKT signaling by decreasing AKT and ERK phosphorylation [105]. In a lung tumour xenograft of the mouse model, CK37 also significantly decreased the tumour growth and tumour PCho levels by 48% and 51% relative to vehicle, respectively [105].

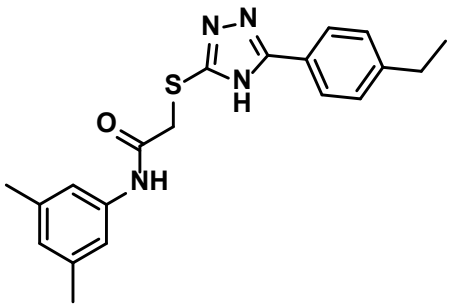
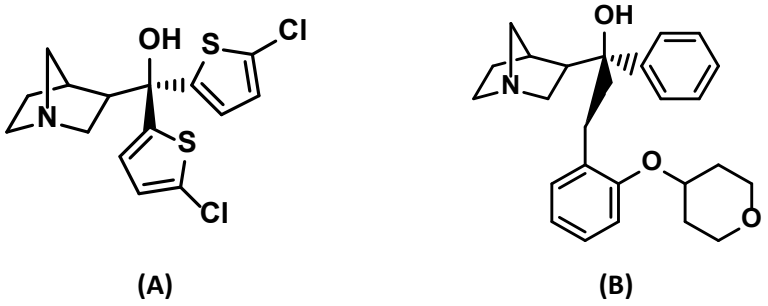


Figure 1. 13: Chemical structure of CK37.

8. V-11-023907 and V-11-0711

V-11-023907 and V-11-0711 are two ATP competitive CHKA inhibitors discovered using high-throughput screening of the Vertex compound library (Figure 1.14) [107]. V-11-023907 displayed high activity against CHKA (IC_{50}: 500 nM) in the enzymatic kinetic studies using the spectrophotometric assay [107]. However, the compound was revealed capable of binding to CHKA in different enzyme states, which urged development of more potent and selective CHKA inhibitors [107]. Discovered by a structure-directed lead optimisation programme of the same company (Vertex Pharmaceuticals), V-11-0711 was the only compound from the series that has been reported to have been tested in cells [108]. It exhibited higher activity and selectivity towards CHKA (IC_{50}: CHKA: 20 nM, CHKB: 220 nM; although absolute CHKB activity is high compared to MN58B) and satisfactory selectivity against a panel of 50 kinases [108]. Intriguingly, despite of its outstanding CHKA selectivity, V-11-0711 was found insufficient to induce apoptosis and cause cancer cell death compared to the cell death observed in the parallel siRNA knockdown of CHKA in HeLa cells [108]. The reversible growth

of cancer cells after the withdraw of V-11-0711 from media, was inferred by the authors as reflecting either the necessity of choline pocket inhibition or that CHKA may possess scaffolding properties independent of its catalytic activity [108]. While the scaffolding properties of CHKA are known, the need for choline pocket inhibition is supported by work using JAS239 [103].



(A) (B)

Figure 1. 14: Chemical structure of V-11-023907 (A) and V-11-0711 (B).

Summary of CHKA inhibitor structure-activity relationship (SAR)

Extensive molecular modelling on *bis*-pyridinium salts combined with the crystal structure information of CHKA have highlighted the importance of linker moiety, distance between quaternary ammoniums, delocalisation of positive charges by electron-donating groups, and steric hindrance when designing novel CHKA inhibitors [109]. Some key points of the SAR learned from the data of existing CHKA inhibitors are summarised below.

Charge. The positive charge in the molecules is a typical choline-mimicking property of most CHKA inhibitors. Cyclic or aromatic quaternary ammoniums, as the most representative cationic choline mimetics, have been exploited in the most CHKA inhibitors. The quaternary ammonium is identified essential to maintain the compound affinity towards choline pocket (CHKA inhibitory activity), and is further related to the compound antiproliferative activity against cancer cells. Most non-charged or single-charged CHKA inhibitors exhibit partial or complete loss of CHKA activity [105]: most tertiary ammonium derivatives were CHKA-inactive [110, 111]; the partial activity loss was frequently seen in the non-symmetrical CHKA inhibitors pursuing the dual binding of choline and ATP sites, and this loss was less severe when both charges were maintained [93]; for the non-charged molecules with high CHKA affinity and selectivity such as V-11-0711, their limited potency to cause cancer cell death largely prevents clinical translation [108].

The successful cationic heads described mainly include pyridinium and quinolinium (and their derivatives), of which the latter has a higher lipophilicity and could, thus, improve the antiproliferative profiles of compounds [84, 85, 93, 99, 112, 113]. However, off-target effects on choline transporters or other key enzymes in CDP-choline pathway were also seen in pyridinium and quinolinium derivatives, which bring challenges to compound modification [64, 99, 100]. Alternative cell death mechanism besides CHKA inhibition have also been observed in those molecules, which needs to be further studied and clarified [64, 99, 100]. Mitochondria are double-membrane-bound organelles, highly dynamic in nature from their network structures. In cancer, mitochondria regulate many altered processes, from metabolism to oxidative stress to apoptosis of cancer cells [114, 115]. The prominence of

mitochondria's role in cancer provides a rationale to design anti-cancer agents targeting mitochondria. Dequalinium and pyridinium head groups, recognised as delocalised lipophilic cations, have been exploited in mitochondria-targeting ligands [116]. These highly hydrophobic compounds with positive charges would preferentially accumulate in the mitochondria of cancer cells which have highly negatively-charged microenvironment within the mitochondrial matrix [117]. The observed structural similarity thus implies the concerns on mitochondrial toxin of the CHKA inhibitors with pyridinium head groups. For instance, the loss of mitochondria membrane potential and mitochondrial respiration were seen in the ICL-CCIC-0019 treatment, and could be a distinct mechanism of anti-proliferation besides CDP-choline pathway inhibition [64]. Similarly, MN58B, containing pyridinium head groups, also decreased mitochondrial respiration and mitochondrial potential [64]. It is intriguing to note, however, that the toxic effects of MN58B on tumour cells could be proceeded the mitochondrial mechanism [118]. A loss of mitochondrial potential was seen after caspase 3 activation, indicating that the apoptosis of cancer cells is induced *via* a mitochondrial independent mechanism [118].

Linker. The linker is important to pharmacological profiles of CHKA inhibitors from several aspects. The linker provides an optimised distance between two quaternary ammonium moieties (normally 14 - 15 Å), although a considerable degree of variation of inter-nitrogen distance may seem allowed [64, 83, 111]. In addition, linker lipophilicity can affect CHKA affinity, antiproliferative activity and even compound stability [64, 83, 111]. For example, the DMAP-derived CHKA inhibitor with a polyethylene glycol (PEG) chain was found unstable despite of an improved aqueous solubility [64]. The effects of linker length on CHKA inhibition can be more important than those on antiproliferative activity in quinolinium derivatives [100]. The docking study of EB-3D revealed that the introduction of the 1,2-dioxoethane linker not only increased compound solubility, but also improved its CHKA affinity by forming a new conformation [94].

Lipophilicity. Lipophilicity is key for not only choline pocket binding affinity, but more importantly for antiproliferative activity when designing CHKA inhibitors. CHKA inhibitors with high choline pocket affinity usually bear cationic head groups which nevertheless reduce the total compound lipophilicity. In the development of RSM-932A, trispyridinium compounds exhibited higher CHKA inhibitory activity than bispyridinium counterparts [99]. However, the trispyridinium structures were less antiproliferative against cancer cells due to their reduced lipophilicity to cross cell membrane [99]. The transmembrane mechanism of CHKA inhibitors involves active choline transport and passive diffusion, of which the latter could play a predominant role when CHKA inhibitor structures are less recognised by choline transporters. JAS239, for example, is a reported choline transporter-independent CHKA inhibitor; its special structure potentiates its application in monitoring compound response which excludes the effects from choline transporters [103].

1.3 CHKA inhibition as novel therapeutic strategies for other pathologies

In recent years, new roles of choline kinase in other pathologies have been reported, and the exploitation of choline kinase inhibitors as novel therapeutics against malaria, Gram-positive bacteria and rheumatoid arthritis (RA) has received growing attention [100, 119-122]. The similarities between the choline binding site of human choline kinase and those of some parasite species (*e.g. Plasmodium falciparum (P.f.*)) elicit the rationale to apply CHKA inhibition as novel anti-parasite strategies [123-125]. Several human CHKA inhibitors have been reported to inhibit the growth of parasite species *P.f.* through multiple mechanism, including the inhibition of *P.f.* choline kinase and *P.f.* ethanolamine kinase [123, 124]. Following this rationale, Zimmerman *et al.* revealed the homology of the *Streptococcus pneumoniae* choline kinase active site to human CHKA1 [122]. MN58B and RSM-932A inhibited the bacteria growth at both enzymatic and cellular levels where RSM-932A displayed higher potency (RSM-932A: IC_{50}: 10 µM, EC_{50}: 0.4 µM; MN58B: IC_{50}: 197 µM, EC_{50}: 0.5 µM) [122]. In a recent study, high CHKA expression was found in the synovium of the patients with RA and also in *ex vivo* cultured fibroblast-like synoviocytes (FLS), which are the non-immune cells found in synovial tissues [120, 121]. The aggressive behaviour of FLS

modulated by mitogen activated protein kinase and PI3K/AKT signalling could be suppressed by MN58B [120, 121]. Compared to the vehicle, the clinical scores of the mouse model with established severity of inflammatory arthritis were reduced after MN58B administration [120, 121].

Taken together, all the findings potentiate the benefits of repurposing CHKA inhibitors to the treatment of other prevalent diseases such as infection and RA.

1.4 Innovative drug modification approaches to modulating the pharmacological properties of drug molecules

Following the target identification and validation, discovery and optimisation of lead compounds are the main themes of drug design. In the past hundred years, versatile molecular modification strategies have been exemplified in drug discovery and development to ameliorate the physiochemical, pharmacological and pharmacokinetic profiles of the lead candidates with high biological activity. Traditional modification strategies emphasise structural homology. Congeners or analogues with higher activity or improved physiochemical/metabolic properties are usually obtained in lead optimisation using classical modification methods such as bioisosterism and *in silico*-based structural recognition [126-128]. In these methods, similar valence electron structures, lipophilicity and steric effects are considered to maintain compound biological activity based on profound understanding on receptors and compound SAR [126]. However, for those cytotoxic agents with high efficacy in cells but so-caused limited therapeutic window, traditional drug modification methods are not feasible to meet the demand of maximising their therapeutic activity while minimising the undesirable side effects. Novel innovative drug modification strategies are needed to realise the specific activation, controlled release or targeted delivery of these drug molecules in the target cells and tissues, in an attempt to elicit their best potential benefits for patients. Two innovative drug modification approaches, which exploit the specific metabolic conversion and targeted delivery of drug molecules, respectively, are introduced in this section.

1.4.1 Prodrug strategy

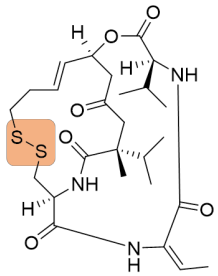
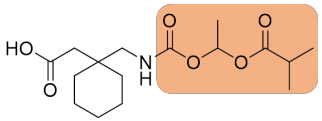
Prodrugs refer to the bioreversible derivatives of active drug molecules, usually with little or no pharmacological activity [129, 130]. The design of bioactive molecules into prodrugs enables the *in vitro* or *in vivo* release of the active parent molecules, which will exert their desired activity after undergoing enzymatic and/or chemical transformation [129, 130]. Since formally raised in 1960s, prodrug strategy has served as a useful tool in current drug development, by which physicochemical, biological and organoleptic barriers of pharmacologically active agents suffering low bioavailability and poor patient compliance can be overcome [131, 132]. More than 30 prodrugs have been approved by the US Food and Drug Administration (FDA) over the past decade, which accounts for approximately 10% of worldwide marketed drugs [130, 132]. The high rate of success witnessed in prodrug approach has encouraged the development of novel therapeutic entities with better clinical profiles than their parent molecules, and the percentage of prodrugs on the market is expected to exceed 20% in the coming few years [130, 132].

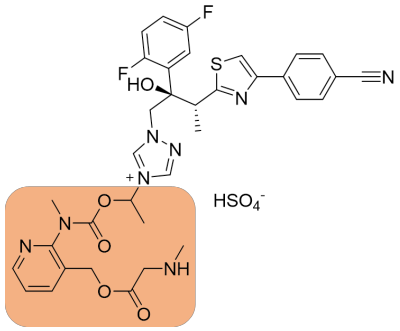
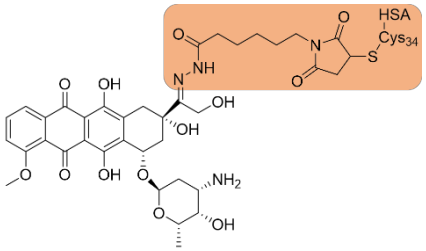
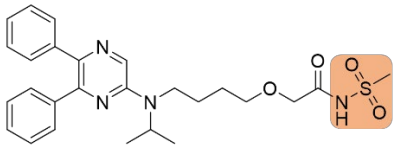
A few representative prodrug strategies reported or approved by FDA in recent years are listed in Table 1.1. Ideal profiles of prodrugs include at least one of the following: proper aqueous solubility and good membrane permeability to achieve sufficient oral bioavailability, high stability to reach the expected site(s) for prodrug conversion, efficient recovery rate and release of the active parent drugs, and satisfactory safety properties of both prodrug and the non-drug moieties, which do not have unfavourable pharmacological effects [129, 133, 134]. Accordingly, common prodrug modifications make the parent molecules into esters (to improve permeability and prolong drug action duration), phosphate esters (to increase aqueous solubility) and amino-acid derivatives (to facilitate carrier-mediated absorption) [129, 130].

Specific and complex prodrug modifications targeting site-specific overexpressed enzymes or altered physiological conditions are frequently exploited in developing anticancer therapies; the prodrug strategy optimises the undesired pharmacological profiles of active parent

molecules by its selective activation [130]. In these cases, prodrugs can be distributed ubiquitously, but will be dominantly activated and turn into cytotoxic at the desired site(s) with altered properties in malignant tissue.

Table 1. 1: Recent prodrugs approved by FDA. The table is reproduced from Rautio, *et al*. Nature Reviews Drug Discovery 2018, 17 (8), 559-587. The prodrug moiety is highlighted in orange [130].

Prodrug name (therapeutic area)	Functional group structure	Structure	Prodrug Strategy
Romidepsin (Istodax) Cutaneous T cell lymphoma (zinc-dependent HDAC inhibitor, 2009) [135]	Disulfide bond		➢ Reduction of the disulfide bond by glutathione produces an active monocyclic dithiol
Gabapentin enacarbil (Horizant) Restless leg syndrome or postherpetic neuralgia (GABA and calcium-channel modulator, 2011) [136, 137]	*N*-[1-(isobutyryloxy)ethoxy] carbonyl		➢ Increased permeation *via* gastrointestinal transporters

Isavuconazonium (Cresemba) Invasive aspergillosis or mucormycosis (azole antifungal; inhibits synthesis of ergosterol, a cell wall component, 2015) [138]	Sarcosine ester		➢ Sarcosine ester is cleaved to release an alcohol that self-immolates to release isavuconazole ➢ Improved solubility
Aldoxorubicin (INNO-206) (anticancer drug, 2002) [139]	maleimide moiety		➢ The maleimide moiety reacts with cysteine 34 of human serum albumin; doxorubicin is released after cleavage of the hydrazone bond
Selexipag (Uptravi) Pulmonary hypertension (non-prostanoid prostacyclin receptor agonist, 2015) [140, 141]	*N*-Acylsulfonamid		➢ Prolonged duration of action and reduced side effects because of the reduction in peak-to-trough fluctuations

1.4.2 Targeted delivery strategy

Targeted drug delivery has largely propelled the development of anticancer therapies from the perspective of tackling pharmacological issues such as toxicity, drug resistance and tissue heterogeneity [142, 143]. Novel targeted drug delivery approaches involving different nano-systems and bioconjugates enable the successful modulation of anticancer drugs and result in wider therapeutic windows and better bioavailability [142].

In a targeted delivery strategy, the small-molecule therapeutic agent is conjugated to a targeting moiety in order to improve its toxicologic or pharmacokinetic profiles by being delivered to a specific target (Figure 1.15). Different from prodrug strategy, the activity of the parent drug is not necessary to be masked by the targeting moiety in drug delivery strategy. The targeting moiety can be a macromolecule (*e.g.* synthetic polymer, glycoprotein, lipoprotein and DNA) [144-147], a monoclonal antibody (*e.g.* antibody-drug conjugate (ADC)) [148, 149] or low-molecular weight ligands and peptides [150, 151]. A linker between the therapeutic agent and the targeting moiety is often used to increase the mobility of ligands and, thus, improves drug binding efficiency with receptors [143]. In drug uptake *via* endocytosis, the use of linkers can control drug release from its carrier, which could realise not only effective targeting but also intracellular internalisation of the whole drug-carrier complexes [143, 152].

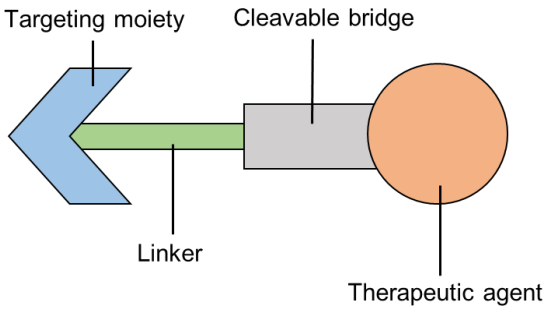


Figure 1. 15: Schematic of targeted delivery strategy. The design of a targeted therapeutic agent generally involves: a targeting moiety, a linker connected to a cleavable bridge that is stable in body circulation but allows drug release following endocytosis into a target cell, and

a cytotoxic therapeutic agent [151].

A huge success exploiting targeted drug delivery strategy is witnessed in Kadcyla® (trastuzumab emtansine), a clinically used ADC targeting human epidermal growth factor receptor 2 (HER2) positive breast cancer [153]. To deliver the therapeutic agent specifically to malignant cells with HER2 overexpression, the cytotoxic agent, antitubulin drug DM1, is linked to a humanised anti-HER2 IgG1 antibody (Trastuzumab) *via* a heterobifunctional linker [154, 155]. Trastuzumab emtansine is internalised into cells after binding to the HER2 antigen on the cell surface; the antibody component of the conjugate undergoes lysosomal degradation and releases DM1-containing catabolites which bind tubulin and cause mitotic arrest and cell death [156]. Trastuzumab alone inhibits malignant cell antiproliferation by binding to HER2 receptor, preventing HER2 dimerisation and eventually inhibiting the activation of MAPK and PI3K/AKT signalling pathways [156]. The combination, on the other hand, takes advantage of monoclonal antibody specifically targeting cancer-related antigens, which largely improves the therapeutic window of the drugs with unmodifiable systemic toxicity [157].

Small-molecule ligands and peptides are also alternatives to antibodies for targeting cancer-specific antigens, such as folate derivatives [151, 158]. Folate derivatives target folate receptor, a protein overexpressed in epithelial cancers [158]. The relevant conjugate in development is vintafolide: a folic acid, as the targeting moiety, is linked to cytotoxic desacetyl vinblastine *via* a peptide linker composed of a reducible disulphide bond and a self-immolative spacer for drug release [151, 159].

Prostate-specific membrane antigen (PSMA) is another promising receptor over-expressed in PCa cells and neovasculature of most solid tumours [130, 160, 161]. The important role of PSMA in prostate carcinogenesis and progression, together with its unique expression difference (100 - 1000 fold higher overexpression in malignancies) and endocytic function make it an imaging biomarker and a therapeutic target for PCa [160, 161]. PSMA acts as a glutamate-preferring carboxypeptidase and this enzymatic activity allows the selective

targeting of PSMA using urea-based derivatives of glutamic acid [162-165]. In the Phase III VISION study, ^{177}Lu-PSMA-617, a molecular radiotherapy using glutamate-urea-lysine (Glu-Urea-Lys) as the PSMA targeting ligand, significantly improved overall survival in patients with metastatic castration-resistant PCa [165-167].

The advantages of small-molecule drug conjugates over ADCs mainly lie in their small size, so they could have faster and better penetration into solid tumours, and their synthesis is simpler [130]. However, most characterised small ligands to date have demonstrated a certain level of kidney uptake and undesired accumulation in normal organs, which may be radiometal-mediated [130].

1.5 Research aims

The derivatisation of ICL-CCIC-0019 using traditional modification methods is challenging. The quaternary amine structures that mimic choline are essential to CHKA activity and could not be modified structurally. In addition, off-target effects on choline transporters and relevant enzymes in CDP-choline pathway were usually observed in potent CHKA inhibitors with quaternary amines [64, 99, 101]. For this situation, advanced drug modification strategies are needed to reduce the off-target accumulation and toxicity in target tissue, turning to controlled release or selective delivery of CHKA inhibitors. Targeted drug action can be achieved by either site-specific bioactivation of a prodrug (prodrug strategy) or site-directed drug delivery (drug delivery strategy) [130]. Herein, two innovative drug modification strategies (prodrug strategy and drug delivery strategy) that could be used for developing CHKA inhibitors are investigated. Based on the profound understanding of the structural activity rationale of ICL-CCIC-0019, the main aim of this project is to develop novel generation ICL-CCIC-0019 congeners by using innovative drug modification strategies.

The following milestones were set:

1. Design and synthesis of an active ICL-CCIC-0019 derivative scaffold (**CK146**) with a 'synthetic handle' (functional group) for further drug modifications using prodrug approach and targeted delivery strategy;

2. Design and synthesis of the CK146-based prodrug (**CK145**) as a novel CHKA inhibitor using -(Ac)Lys peptide motif [168];

3. Design and synthesis of the PSMA-targeted CHKA inhibitor (**CK147**), where CK146 is linked to a small peptide ligand (Glu-Urea-Lys) specifically targeting PSMA using thiol-maleimide chemistry [154, 169];

4. Comprehensive *in vitro* pharmacological and preliminary pharmacokinetic evaluation of

the novel CHKA inhibitors, including the data on drug stability and cellular uptake, kinase selectivity, antiproliferative activity, 'Absorption, Distribution, Metabolism and Excretion' (ADME) studies;

5. Elucidation of the SAR of novel CHKA inhibitors synthesised in this project.

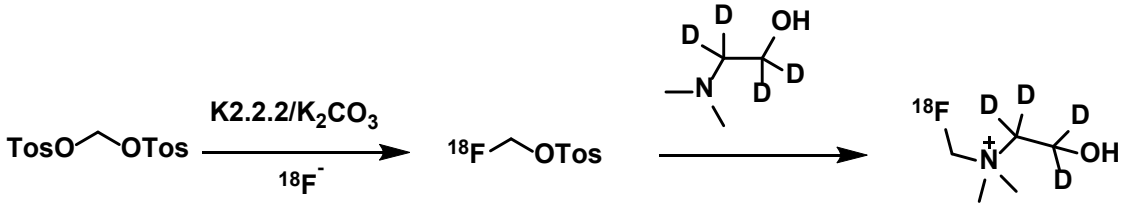
2. Materials and Methods

2.1 Chemical synthesis

The chemical synthesis of ICL-CCIC-0019, CK14, CK145, CK146, CK147 and CK148 are described in the Experimental. The structures of compounds were confirmed by nuclear magnetic resonance (NMR) spectroscopy and mass spectrometry (MS) (see Chapter 11, Appendix A).

2.2 Radiosynthesis of [^{18}F]D4-FCH

The radiosynthesis procedure of [^{18}F]D4-FCH has been described elsewhere [38, 170]. The [^{18}F]-D4-FCH (200 MBq in 1 mL 0.09% NaCl solution) used in this work was radiolabelled on a FASTlab synthesiser (GE Healthcare, Amersham, UK) by Mr Chris Barnes, Imperial College London (Scheme 2.1).



Scheme 2. 1: Radiosynthesis of [^{18}F]-D4-FCH.

2.3 High-performance liquid chromatography (HPLC)

The HPLC chromatograms obtained in this work were analysed using Waters™ Empower (Hertfordshire, UK) and Laura software (LabLogic, Sheffield, UK).

HPLC Method A

Instrument: Waters™ 600 pump (Hertfordshire, UK) equipped with a DG 604 vacuum degasser (Alexandria, Minnesota, USA) and a Waters™ 2487 dual λ absorbance detector (Hertfordshire, UK);

Stationary phase: Phenomenex® Luna 5µ C18 (2) 100Å 250 × 4.6 mm;

Gradient: mobile phase: A) water (0.2% formic acid), B) methanol; gradient: B (v/v): 5% to

40% in 20 min, 40% to 80% in 25 min, 80% to 95% in 15 min, 95% to 5% in 2 min;

Wavelengths: 254 nm and 294 nm;

Flow rate: 5 mL/min;

Injection volume: 2 mL;

Temperature: room temperature;

HPLC Method B

Instrument: Waters™ 600 pump (Hertfordshire, UK) equipped with a DG 604 vacuum degasser (Alexandria, Minnesota, USA) and a Waters™ 2487 dual λ absorbance detector (Hertfordshire, UK);

Stationary phase: Phenomenex® Gemini 5µ C18 100 × 10 mm;

Gradient: mobile phase: A) water (0.2% formic acid), B) methanol (0.2% formic acid); gradient: B (v/v): 20% to 70% in 30 min, 70% to 20% in 15 min;

Wavelengths: 254 nm;

Flow rate: 1 mL/min;

Injection volume: 20 µL;

Temperature: room temperature;

HPLC Method C

Instrument: Waters™ 600 pump (Hertfordshire, UK) equipped with a DG 604 vacuum degasser (Alexandria, Minnesota, USA) and a Waters™ 2487 dual λ absorbance detector (Hertfordshire, UK);

Stationary phase: Phenomenex® Luna 5µ C18 (2) 100Å 250 × 4.6 mm;

Gradient: mobile phase: A) water (0.2% formic acid), B) methanol; gradient: B (v/v): 20% to 45% in 15 min, 45% to 70% in 25 min, 70% to 20% in 5 min;

Wavelengths: 254 nm and 318 nm;

Flow rate: 5 mL/min;

Injection volume: 2 mL;

Temperature: room temperature;

HPLC Method D

Instrument: Waters™ 600 pump (Hertfordshire, UK) equipped with a DG 604 vacuum degasser (Alexandria, Minnesota, USA) and a Waters™ 2487 dual λ absorbance detector (Hertfordshire, UK);

Stationary phase: Phenomenex® Luna 5µ C18 (2) 100Å 250 × 4.6 mm;

Gradient: mobile phase: A) water (0.2% formic acid), B) methanol; gradient: B (v/v): 5% to 40% in 5 min, 40% to 60% in 15 min, 60% to 80% in 10 min, 80% to 95% in 5 min, 95% to 5% in 2 min;

Wavelengths: 254 nm and 294 nm;

Flow rate: 4 mL/min;

Injection volume: 1 mL;

Temperature: room temperature;

HPLC Method E

Instrument: Waters™ 600 pump (Hertfordshire, UK) equipped with a DG 604 vacuum degasser (Alexandria, Minnesota, USA) and a Waters™ 2487 dual λ absorbance detector (Hertfordshire, UK);

Stationary phase: Phenomenex® Luna 5µ C18 (2) 100Å 250 × 4.6 mm;

Gradient: mobile phase: A) water (0.2% formic acid), B) acetonitrile; gradient: B (v/v): 30% to 41% in 30 min, 41% to 95% in 5 min, 95% to 30% in 5 min, 30% for 5 min;

Wavelengths: 254 nm and 294 nm;

Flow rate: 4 mL/min;

Injection volume: 2 mL;

Temperature: room temperature;

HPLC Method F

Instrument: Waters™ 600 pump (Hertfordshire, UK) equipped with a DG 604 vacuum degasser (Alexandria, Minnesota, USA) and a Waters™ 2487 dual λ absorbance detector (Hertfordshire, UK);

Stationary phase: Phenomenex® Gemini 5µ C18 150 × 4.6 mm;

Gradient: mobile phase: A) water (0.2% formic acid), B) acetonitrile (0.2% formic acid); gradient: B (v/v): 5% to 95% in 16 min; 95% to 5% in 1 min; 5% for 3 min;

Wavelengths: 254 nm and 294 nm;

Flow rate: 1 mL/min;

Injection volume: 100 µL;

Temperature: room temperature.

To evaluate the *in vitro* uptake of ICL-CCIC-00019 and CK145 by HPLC analysis, external calibration curves were established using ICL-CCIC-0019 and CK145 (the concentration range: 0.05, 0.1, 1, 5 and 7 µM in HPLC mobile phase, water:acetonitrile:formic acid, 95:5:0.2 v/v/v). The corresponding peak was integrated to determine the area under the curve (AUC), which was plotted against the sample concentration. Linear regression was applied to the data (R^2 = 0.999), and the equation of the line was used to calculate the unknown concentrations of ICL-CCIC-0019 and CK145.

HPLC Method G

Instrument: Agilent 1100 series (G1312A Pump, G1322A Degasser, G1314A Variable Wavelength Detector) (Stockport, UK);

Stationary phase: Phenomenex® Gemini 5µ C18 150 × 4.6 mm;

Gradient: mobile phase: A) was water (0.2% formic acid), B) acetonitrile; gradient: B (v/v): 5% to 95% in 15 min; 95% to 5% in 1 min; 5% for 3 min;

Wavelengths: 254 nm;

Flow rate: 1 mL/min;

Injection volume: 100 µL;

Temperature: room temperature.

To determine the unknown concentrations of CK147 in the *in vitro* studies by HPLC analysis, internal calibration curves were established, where ICL-CCIC-0019 served as the internal

standard (IS). An internal standard is referred as to a compound added to a sample in a known concentration to facilitate the qualitative identification and/or quantitative determination of the sample components [171]. Chromatograms were analysed using Laura software to integrate peaks and determine the AUC. The IS ratio was calculated for each sample by dividing the peak area of CK147 by that of IS, and the concentration of CK147 was determined by comparing the IS ratio to a concomitantly performed standard curve. Standard curves, containing CK147 concentrations of 7.5, 15, 30, 60 and 120 µg/mL and a fixed concentration of ICL-CCIC-0019 (20 µg/mL) in water:acetonitrile:formic acid (95:5:0.2, v/v/v), were constructed by plotting the IS ratio versus the known concentration of CK147 in each sample. Linear regression was applied to the data (R^2 = 0.9999), and the equation of the line was used to calculate unknown concentrations of CK147.

2.4 Shake-Flask method

The Log D values of compounds were evaluated using shake-flask method. Compound phosphate buffered saline (PBS) solutions were prepared (10 µM, 500 µL) in Eppendorf tubes before adding another 500 µL of 1-octanol into each tube. The Eppendorf tubes were then fixed on an IKA® KS 130 basic shaker (IKA® Werke GmbH & Co. KG, Staufen, Germany) and shaken for 1 h at ambient temperature (21 ˚C). The 1-octanol layer (upper organic phase) was carefully aspirated and discarded by pipettes. Ten microlitres from the PBS phase were taken to be analysed by NanoDrop® ND-1000 spectrophotometer (NanoDrop Technologies, Wilmington, USA). The Log D values were calculated by the formula below (Equation 2.1):

$$\text{Log D} = \text{Log}\ \frac{C_{\text{Octanol}}}{C_{\text{PBS}}} = \text{Log}\ \frac{C_{10\ \mu\text{M PBS}} - C_{\text{PBS after shaking}}}{C_{\text{PBS after shaking}}}$$

Equation 2.1: Log D calculation of the synthesised CHKA inhibitors, where $C_{Octanol}$: the concentration of the compound in the 1-octanol phase at equilibrium; C_{PBS}: the concentration of the compound in the PBS phase at equilibrium; $C_{10\mu M\ PBS}$: the concentration of the compound stock solution in PBS (10 µM) and $C_{PBS\ after\ shaking}$: the concentration of the compound in the PBS phase after shaking.

Three repetitions were performed for each sample under the same conditions.

2.5 Cell culture

HCT-116 (colorectal carcinoma; American Type Culture Collection (ATCC)), A549 (lung carcinoma; ATCC), 22Rv1 (prostate carcinoma; ATCC), C4-2B (prostate cancer; ATCC), LNCap (prostate carcinoma; ATCC), R1-AD1 and R1-D567 (prostate carcinoma; these two cell lines were obtained *via* a material transfer agreement with Prof Scott Dehm, University of Minnesota) [172], PC3 (prostate adenocarcinoma; ATCC) and PNT1A (prostate epithelial cell line; this cell line is a gift from Prof Charlotte Bevan, Imperial College London) were maintained in RPMI 1640 (Sigma Life Science, Gillingham, UK). HepG2 (liver carcinoma, ATCC) and Caco-2 (colorectal adenocarcinoma, ATCC) were maintained in DMEM (BioWhittaker®, Lonza, Basel, Switzerland). The RPMI was supplemented with 10% FCS (Fetal Calf Serum, First Link UK Ltd., Wolverhampton, UK) and 10% L-glutamine (gibco®, Life Technologies, Paisley, UK; 200 mmol, 100 mL). Caco-2 cell line was maintained in DMEM media (BioWhittaker®, Lonza, Paisley, UK) containing 20% FCS and 10% L-glutamine. Cells were cultured at 37 ˚C in a humidified atmosphere with 5% CO_2 (CO_2 air-jacketed incubator, NUAIRE DH Autoflow, Plymouth, USA). Cell lines were authenticated by provider (ATCC). No additional authentication of cells was performed. The cell handling and medium preparation were carried out using aseptic techniques in the class II safety cabinet (BioMAT2, Class 2 microbiological safety cabinet complies with BS EN 12469: 2000, Manchester, UK). All the reagents used for cell culture were incubated in Grant GD100 water bath (Grant Instruments, Cambridge, UK) in advance.

Sub-culturing was carried out using trypsin-EDTA (gibco® by Life Technologies, Paisley, UK; 1X, 100 mL). Trypisinisation was performed along with cell counting and seeding. The cell pellets obtained from trypsinisation were transferred to a 50 mL falcon tube and collected by centrifugation at 1930 RPM (Hettich® Universal 32R Benchtop Centrifuge, Tuttlingen, Germany). Appropriate amount of medium was added into the tube before a full mixing. Twenty microlitres of the cell suspension were taken and then mixed with 20 µL Trypan Blue (Sigma Life Science, Gillingham, UK) in a 1.5 mL Eppendorf tube by pipetting (Dilution factor = 2). Ten microlitres of the stained cell sample were loaded into a hemocytometer (Bright-Line, Hausser Scientific, , Horsham, USA) for cell counting by Countess II FL cell counter (Life

technologies, Thermo Fisher Scientific, Loughborough, UK).

2.6 Anti-Proliferative assay (Sulforhodamine B Assay)

Half-maximal growth inhibitory concentrations (GI_{50}) were determined in clear 96-well plates (Corning Costar, Flintshire, UK) using sulforhodamine B (SRB) assay as described elsewhere [173]. Cells were seeded in 96-wells at respective cell densities determined by their cell growth curves (HCT-116: 1000 cells/well; A549: 3000 cells/well; Caco-2: 2000 cells/well; HepG2: 2000 cells/well; 22Rv1: 5000 cells/well; C4-2B: 5000 cells/well; LNCap: 6000 cells/well; R1-AD1: 20,000 cells/well; R1-D567: 6000 cells/well; PC3: 5000 cells/well; PNT1A: 6000 cells/well). After 24 h, the cells were treated in six replicates with medium or different concentrations of compounds in medium, and incubated for selected hours (a standard SRB assay uses 72 hours). The cells were fixed with 10% trichloroacetic acid (TCA) and stained with 0.4% SRB in 1% acetic acid after incubation. The stained protein was solubilised with 10 mM Tris-base and optical density values were measured at 540 nm using a Multiskan® Microplate photometer (Thermo Scientific, Loughborough, UK). Growth inhibition curves were plotted as percentages of the control groups and GI_{50}s were determined by the least squares fitting method using GraphPad Prism 7.0. All the chemicals used in this experiment were from Sigma-Aldrich (Gillingham, UK).

2.7 Lipid kinase screening

The lipid kinase screening for ICL-CCIC-0019, CK14, CK145, CK146 and CK147 (the compound testing concentration used for the screening: 10 μM) was carried out by MRC PPU International Centre for Kinase Profiling (Dundee, UK) (See Appendix B). The lipid kinase screening panel consists of 15 human recombinant lipid kinases, and Promega ADP Glo™ High Throughput Assay kits (Promega, Southampton, UK) were used for kinase screening. In each test, reference compounds were included for quality control. Mean percentage activity inhibited by compounds and standard deviation (SD) for all the repeats were calculated.

2.8 ADME study (*In vitro*)

The *in vitro* ADME study of ICL-CCIC-0019, CK14, CK145, CK146 and CK147 was carried out by Charles River Drug Discovery Services (Essex, UK).

2.9 Bicinchoninic acid (BCA) protein assay

Bovine serum albumin (BSA) standards (Thermo Fisher Scientific, Loughborough, UK) with a concentration range of 0 - 1.35 mg/mL were freshly prepared in advance to establish a calibration curve. The cell lysate samples were diluted in PBS. Twenty microlitres of the diluted cell lysates were added into a clear 96-well plate. The BCA working reagent was prepared by mixing BCA assay reagent A with B (A:B, 50:1, v/v; Pierce™, Thermo Fisher Scientific, Loughborough, UK), which afforded a clear, green solution. Two hundred microlitres of the BCA working reagent were added into each well containing the cell lysates. The plate was then incubated at 37 °C (Sanyo®, Osaka, Japan) for 30 min and placed into a microplate reader (Multiskan® EX Micro plate photometer, Thermo Scientific, Loughborough, UK) for optical density measurement at 560 nm. The protein concentration of the cell lysates was finally calculated using the standard curve plotted by GraphPad Prism 7.0 software.

2.10 Western blotting

The cell pellets were collected from trypsinisation and then lysed in radioimmunoprecipitation assay (RIPA) buffer (R0278, Sigma-Aldrich) containing protease and phosphatase inhibitors (Thermo Fisher, Loughborough, UK) on ice for 30 minutes. The protein concentrations of the cell lysates were determined using BCA assay described above. According to the calculation, equal amounts of protein (10 μg) were resolved on 4 - 15% mini-protein TGX gels (456-1086 Bio-Rad, Watford, UK) and transferred to PVDF membranes (Trans-Blot Turbo Transfer Packs, Bio-Rad, Watford, UK). Membranes were blocked in 5% milk in PBS containing 0.1% v/v tween-20, and subsequently incubated with the following primary antibodies at 4 ˚C overnight: HDAC1(10E2), 1:8000, #5356s, Cell Signalling Technology, London, UK; Calnexin, 1:5000, #ADI-SPA-860-D, ENZO life sciences, Exeter, UK; CHKA, 1:1000,

#HPA024153, Sigma-Aldrich, Gillingham, UK; PSMA (D78E), 1:1000, #12815, Cell Signalling Technology, London, UK; GAPDH (D16H11), 1:10000, #5174, Cell Signalling Technology, London, UK. Secondary HRP-conjugated mouse and rabbit antibodies (1:8000 and 1:5000; #7076P2 and #sc-2005; Cell Signalling, London, UK and Santa Cruz Biotechnology Cell Signalling, California, USA, respectively) were applied for an hour at room temperature. Signals were visualised by chemiluminescence detection (Amersham, RPN 2016) using enhanced chemiluminescence (ECL) Western Blotting Detection Reagent (GE Healthcare, Amersham, UK) and Amersham Hyperfilm (GE Healthcare, Amersham, UK).

2.11 *In vitro* uptake and metabolism study of CK145

HCT-116 cells were seeded into cell culture dishes (Corning Costar, Flintshire, UK; 150×25 mm) with a cell density of 7×10^6 per dish. The cells were allowed to settle and grow to achieve 80% confluency. On the treatment day, the cells were incubated with/without ICL-CCIC-0019 or CK145 (50 µM of 5 mL RPMI with 10% FCS and 1% L-glutamine) for 1 hour and 2 hours in the incubator. The medium was aspirated off and the cells were carefully scraped, washed three times in ice-cold PBS and collected by centrifugation (4 ˚C, 4000×g). The cell pellets were resuspended in 1 mL water:acetonitrile:formic acid (95:5:0.2, v/v/v) and disrupted by an ultrasonic cell disruptor (Soniprep 150, MSE Ltd., London, UK) for a minute on ice. One hundred microlitres of the filtered supernatant from centrifuge (4 ˚C, 15,000×g) were analysed by HPLC. Three injections were carried out for each sample. Intracellular drug amount was normalised to cellular protein of each plate using BCA assay. The HPLC method used in this study is described in HPLC method F.

2.12 Limit of detection (LOD) of CK146

Using the HPLC system described in HPLC method G, LOD of the active form of CK145 (CK146) was tested and calculated by the equation below (Equation 2.2):

$$\text{LOD} = \frac{3 \times \text{Baseline noise} \times \text{Standard amount}}{\text{Sample signal height}}$$

Equation 2.2: LOD calculation.

The baseline noise of the HPLC system was measured. After verifying the response of several dilutions, a standard CK146 solution with a concentration close to the detection limit was prepared and injected for at least three times. Then the average signal height of CK146 standard samples and baseline were calculated.

2.13 Conjugate stability test of CK147

The conjugate stability of CK147 in medium was assessed. To 6-well plates were added, in a sterile-manner, vehicle-containing DMSO (control group) or CK147 (treatment group); vehicle was RMPI medium (50 μM of 5 mL RMPI supplemented with 10% FCS and 1% L-glutamine in each well). The plates were gently shaken for 5 seconds and then incubated at 37 ˚C in a humidified atmosphere containing 5% CO_2. At 0, 2, 4, 6, 24, 48 and 72 hours, 200-μL aliquots of medium from each well were taken and transferred into a 1.5-mL Eppendorf tube with 198.4 μL acetonitrile and 1.6 μL of 2.5 mg/mL ICL-CCIC-0019 as the IS (the final concentration of ICL-CCIC-0019: 20 μg/mL). After a brief vortex, the Eppendorf tube was placed at 4 ˚C for 30 min to facilitate protein precipitation. Fifty microliters of the resulting supernatant from centrifuge (4 ˚C, 15,000×g) was taken to supplement with 70 μL of water:acetonitrile:formic acid (95:5:0.2, v/v/v) and sonicated for a min. One hundred microliters of the solution were injected into the HPLC system described as HPLC method G. Three repeats were performed for each sample.

2.14 Cellular uptake and metabolism study of ICL-CCIC-0019, CK146, CK147 and CK148 in presence and absence of serum

Cell lysate sample preparation

C4-2B prostate cancer cells were seeded into cell culture dishes (Corning Costar, Flintshire, UK; 150×25 mm) with a cell density of 7×10^6 per dish. The cells were allowed to settle and grow to achieve 80% confluency. On the treatment day, the cells were incubated with ICL-CCIC-0019, CK146, CK147 and CK148 (50 μM of 7 mL RPMI medium with or without 10% FCS) for 4 hours in the incubator. After the incubation, the aliquots of medium were taken out for further preparation before HPLC analysis (see the medium sample preparation section). The

medium was aspirated off and cells were carefully scraped, washed with ice-cold PBS three times and collected by centrifugation (4 ˚C, 4000×g). The cell pellets were resuspended in 500 µL of ice-cold acetonitrile:PBS (50:50, v/v) for cell disruption. The cell disruption was performed by a Precellys® 24 homogeniser (Bertin Technologies, Montignyle-Bretonneux, France) at 4 ˚C. After acetonitrile evaporation at ambient temperature, 50 µL of cell lysis was taken for protein analysis. Another 100 µL of the supernatant obtained after centrifuge (4 ˚C, 15,000×g) was resuspended in 100 µL formic acid:water (0.2%, v/v). Next, 100 µL of the filtered solution was analysed using the HPLC system described in HPLC method G. Three injections were carried out for each sample. Intracellular drug amount was normalised to cellular protein of each plate using BCA assay.

Medium sample preparation for HPLC analysis

250-µL aliquots of medium (with or without 10% FCS) were transferred into 1.5 mL tube containing 250 µL acetonitrile. After a brief vortex, the tube was placed at 4 ˚C for 30 min for protein precipitation. One hundred microliters of the resulting supernatant from centrifuge (4 ˚C, 15,000×g) were resuspended in 100 µL formic acid:water (0.2%, v/v). One hundred microliters of the filtered sample were analysed by HPLC system described in HPLC method G. Three injections were performed for each sample.

2.15 [^{18}F]D4-FCH uptake study *in vitro*

HCT-116 and C4-2B cells were seeded at a density of 5×10^5 cells per well into 6-well plates (Corning Costar, Flintshire, UK) and incubated overnight. Cells were treated with compounds (CK14, CK145, CK146 and CK147; 1 or 10 µM) for 1 hour.

Without cell wash by PBS after treatment

The cells were pulsed with [^{18}F]D4-FCH (740 kBq) in presence of the tested compounds in 1 mL for an additional hour at 37 ˚C. Cells were washed three times in ice-cold PBS and lysed in 1 mL RIPA buffer. The radioactivity of 800 µL lysate from each well was counted on a gamma counter (Perkin Elmer, Beaconsfield, UK) and normalised to protein content as determined by

BCA assay.

2.16 Statistical Analysis

Data were represented as mean values $\pm$ SD in figures. Unpaired two-tailed t-tests from GraphPad Prism 7.0 were used to determine the significance in the experiments. Statistic differences were recognised significant at $0.01 < p < 0.05$, very significant at $0.001 < p < 0.01$ and extremely significant at $0.0001 \leq p < 0.001$ and $p < 0.0001$.

3. Design and synthesis of the novel prodrug CHKA inhibitor

3.1 Introduction of the prodrug strategy

In this work, derivatisation of ICL-CCIC-0019 was first investigated using the prodrug strategy originally described by Ueki *et al* [168]. Noticing the upregulation of HDAC and CTSL in malignant cells, Ueki and his colleagues successfully developed a prodrug moiety which can be cleaved in a step-wise manner on the basis of the enzymatic activity of these two families [168].

The mammalian HDAC family is composed of 4 classes (I, II, III, and IV) containing 18 enzymes, mainly responsible for removing acetyl groups from ε-*N*-acetyl lysine (Lys) residues on histone and thus facilitating DNA binding [174]. HDAC isoforms have various specific functions in tissues. An important role in cell survival and proliferation was found for HDAC class I [175]. Tumour cells need upregulated HDACs to proliferate under stress conditions [176]. Based on unique functions and disease relevance revealed in HDACs, several inhibitors targeting HDAC class I and II have been designed and undergoing pre-clinical or clinical trials as anti-cancer therapeutics [175].

CTSL, as one of cysteine protease isoforms, is recognised as a lysosomal proteolytic enzyme catalysing protein degradation by peptide bond cleavage [177]. During the past few years, more specific functions of CTSL related to cell death and cancer cell invasion were confirmed; upregulation of CTSL is also deemed as a hallmark of metastatic cancer [177-180].

The successful release of the active molecule *via* prodrug strategy was preliminarily validated by attaching the prodrug moiety to a fluorescent moiety named 7-amino-4-methylcoumarin (AMC) [181]. The released AMC from Boc-Lys(Ac)-AMC was successfully detected after the two-step conversion by endogenous HDAC and CTSL activities in malignant cells [168].

Furthermore, the release of AMC was inhibited specifically either in the presence of pan-HDAC inhibitors or CTSL inhibitors [182, 183]. This confirmed the dependency of both HDAC and CTSL activity to process the prodrug strategy in live cells. By specific small-molecule inhibition, the HDAC subtypes responsible for activating the Boc-Lys(Ac) moiety were also investigated, and it was revealed that class I HDACs, instead of the class II, played a major role in the process [168].

Having validated the utility of the prodrug strategy, Ueki and his colleagues attempted to incorporate a cytotoxic drug into the prodrug by conjugating the prodrug moiety Boc-Lys(Ac) to the drug molecule. Puromycin (Puro) is an antibiotic that inhibits protein synthesis by causing premature chain termination on ribosome and thus kills cells [184]. Puromycin was selected to evaluate the HDAC- and CTSL-dependent prodrug activation since its free amino group was reasoned essential to cytotoxicity; this amino group also serves as an available handle for prodrug moiety attachment [168]. The Boc-Lys(Ac)-Puro was accordingly synthesised by conjugating Boc-Lys(Ac)-OH to the amino group of Puromycin (Figure 3.1) [168].

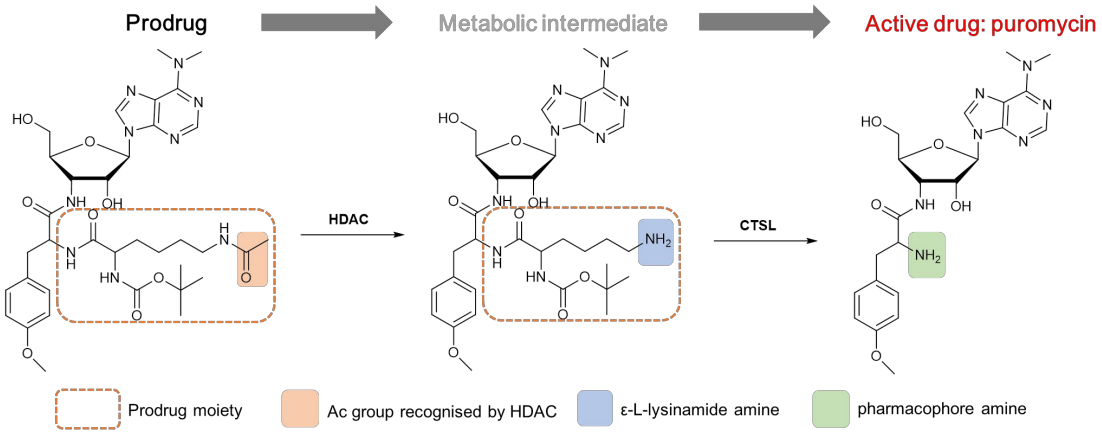


Figure 3. 1: The prodrug *in vitro* conversion scheme illustrating the selective two-step drug activation in cancer cells by HDAC and CTSL [168].

To preliminarily evaluate the antiproliferative selectivity of Boc-Lys(Ac)-Puro *in vitro*, a series of colon cell lines exhibiting different HDAC and CTSL activities were used [168]. Boc-Lys(Ac)-Puro displayed comparable antiproliferative profiles (GI_{50} values are in the 10 µM range) in

malignant colon cells with high HDAC and CTSL activities [168]. On the other hand, non-malignant colon cells such as Caco-2 grew to confluency after the treatment and the GI_{50} values were not measurable, which revealed the cytotoxic selectivity of Boc-Lys(Ac)-Puro [168]. Malignant cell lines of other cancer types such as pancreatic, liver and cervical cancers could also be killed by Boc-Lys(Ac)-Puro with a similar dose-response pattern observed in malignant colon cells [168]. The mechanism of the cell death induced by Boc-Lys(Ac)-Puro was elucidated by immunological detection: Boc-Lys(Ac)-Puro was converted into parental Puromycin in malignant cancer cells and caused cell death by a Puro-dependent mode of action [168]. In the subsequent animal study where mouse xenograft models bearing HCT-116 and HT-29 cells were established, Boc-Lys(Ac)-Puro dose-dependently inhibited tumour growth, and the daily administration of Boc-Lys(Ac)-Puro up to 150 mg kg^{-1} per dose was tolerated as determined by weight loss of mice [168].

In summary, the success of Boc-Lys(Ac)-Puro provides a new approach to improve the pharmacological profiles of the cytotoxic agents by modifying their amino groups using a small-molecule masking moiety.

In this work, abnormal elevated levels of HDACs and CTSL, essential to malignant proliferation, are exploited for the enzymatic transformation of ICL-CCIC-0019 prodrug into the active parent molecule [168]. The design of a proposed ICL-CCIC-0019 prodrug molecule requires an ε-acetylated-Lys group to be coupled to the active molecule. A slight variation on ICL-CCIC-0019 structure is, thus, required to facilitate the addition of the prodrug moiety. In brief, the prodrug Lys (Ac)-active ICL-CCIC-0019 derivative will be activated under increased levels of both HDACs and CTSL by two steps: The acetyl group (highlighted in orange, Figure 3.2) in the prodrug moiety can be removed by HDAC in the first step which liberates the free ε-amine end (highlighted in blue, Figure 3.2); in the second step, CTSL cleaves the peptide bond connecting the *tert*-Butyloxycarbonyl (Boc)-protected lysine residue to the active drug, which therefore 'unlocks' the active drug molecule (Figure 3.2) [168].

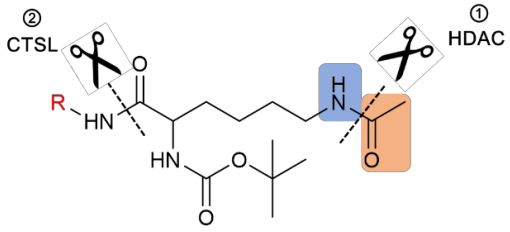


Figure 3. 2: A prodrug moiety sensitive to HDAC and CTSL cleavage: Boc-Lys(Ac)-R. The amine end in drug molecules can be modified using the Boc-Lys(Ac) moiety. The acetyl group and the free ε-amine moiety were highlighted in orange and blue, respectively [168].

3.2 SAR and design rationale

The incorporation of ICL-CCIC-0019 into Boc-Lys(Ac) prodrug moiety was attempted with the aim of ameliorating its toxicity. As the structural diversity of ICL-CCIC-0019 is very limited, the direct modification of the molecule is not feasible (Figure 3.3A). Designing a precursor molecule for ICL-CCIC-0019 derivatisation is thus needed to allow further structural modifications. Ideally, the precursor is an ICL-CCIC-0019-derivative, but more importantly it is expected to contain a 'reactive handle' and to maintain CHKA activity. The DMAP moiety is an essential pharmacophore of ICL-CCIC-0019 and is therefore to be retained in the precursor molecule [85]. Our previous investigations on SAR of the symmetrical CHKA inhibitors revealed that the length of the alkyl linker chain between the DMAP moieties

impacted compound activity [93]. The symmetrical DMAP derivative CHKA inhibitor adopting a tetradecyl linker (CK14) exhibited the highest CHKA activity (IC_{50} against recombinant CHKA2: ICL-CCIC-0019: 270 nM, CK14: 150 nM) (Figure 3.3B) [93]. A tetradecyl linker was thus considered for incorporation into the precursor molecule so as to elicit the best potency within the prodrug context.

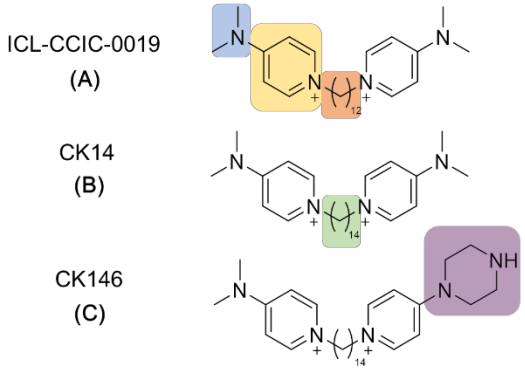


Figure 3. 3: The structures of ICL-CCIC-0019, CK14 and CK146. The key structural components in the molecules are highlighted: the *N,N*-dimethyl moiety, quaternary pyridinium, dodecyl linker and tetradecyl linker, and the piperazine 'reactive handle' are coloured in blue, yellow, orange, green and purple, respectively [93].

As previously introduced, the exploration of the SAR of *bis*-pyridinium CHKA inhibitors emphasises not only the linker moiety, but also the delocalisation of positive charges by electron-donating groups [98]. The *N,N*-dimethyl moieties in ICL-CCIC-0019 are strong electron-donating substituents, which enhance the delocalisation of the positive charges, stabilise the quaternary ammonium rings and increase CHKA activity of the molecule [85]. Here a piperazine group was innovatively introduced to substitute the *N,N*-dimethyl moiety on one side of the symmetrical structure, giving rise to a precursor molecule (CK146) which permits further modifications whilst maintaining the configuration of ICL-CCIC-0019 (Figure 3.3C). The piperazine group has a free secondary amine end which can serve as a chemistry handle facilitating the conjugation of the prodrug moiety.

The SAR of the novel prodrug molecule CK145 derived from CK146 is illustrated in Figure 3.4. In brief, a non-symmetrical ICL-CCIC-0019 prodrug derivative that adopts a tetradecyl linker

was designed, using the prodrug strategy whereby an acetylated lysine linkage was conjugated to its piperazine handle *via* amide formation. It was hypothesised in this project that the CHKA activity of CK146 could be reduced by masking one of its pharmacophore using the prodrug moiety. This could be achieved because the steric effects of the prodrug bulk may disrupt the molecular binding of CK145 to the choline pocket. The steric hindrance was desired to mask one of the quaternary ammonium moieties and thus to impair CHKA activity, resulting in reduced CHKA activity similarly observed in nonsymmetrical 'half'-linker structures [93]. Accordingly, CK145 was designed to be selectively cleaved in order to release CK146 in a stepwise manner within cancer cells with aberrant upregulation of HDAC and CTSL enzymes.

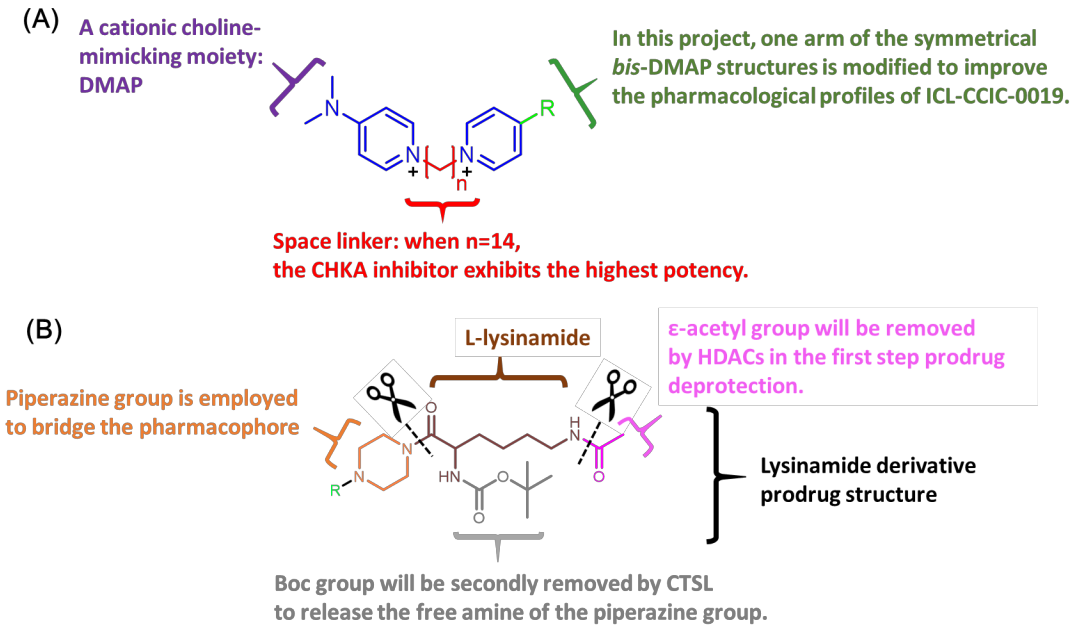


Figure 3. 4: Graphical representation of the design goals to generate a novel CHKA prodrug inhibitor: (A) the *bis*-DMAP CHKA inhibitor structure and (B) the derivative prodrug structure.

In this project, we aimed to improve the pharmacological profiles of ICL-CCIC-0019 by investigating a prodrug strategy. By this, the drug candidate was expected to meet the criteria for high tumour therapeutic index and to retain good inhibitory activity against CHKA and good selectivity of CHKA inhibition both *in vitro* and *vivo* while displaying improved distribution (less to liver tissue) and toxicity profiles (reduced body weight loss observed in mice). It was hypothesised that, the prodrug, CK145, as a derivative of ICL-CCIC-019, would

maintain inhibitory activity with reduced side effects.

3.3 The synthesis of prodrug strategy (Results and Discussion)

This project aims to verify the prodrug strategy by synthesis of a series of compounds in three categories (Figure 3.5): the reference molecules ICL-CCIC-0019 (**1**) and CK14 (**2**), the precursor molecule CK146 (**6**) and the desired prodrug molecule CK145 (**9**). ICL-CCIC-0019 and CK14 are symmetrical DMAP derivatives reported as potent CHKA inhibitors bearing space linkers of different lengths. CK144 (**8**), as a derivative of CK146, is designed by addition of the methylated piperazine steric bulk; through this structural alternation, the effects of the introduced piperazine moiety on compound pharmacological activity can be investigated in parallel. CK146 is the active parent molecule, which is hypothesised to be the terminal metabolic product of its prodrug CK145.

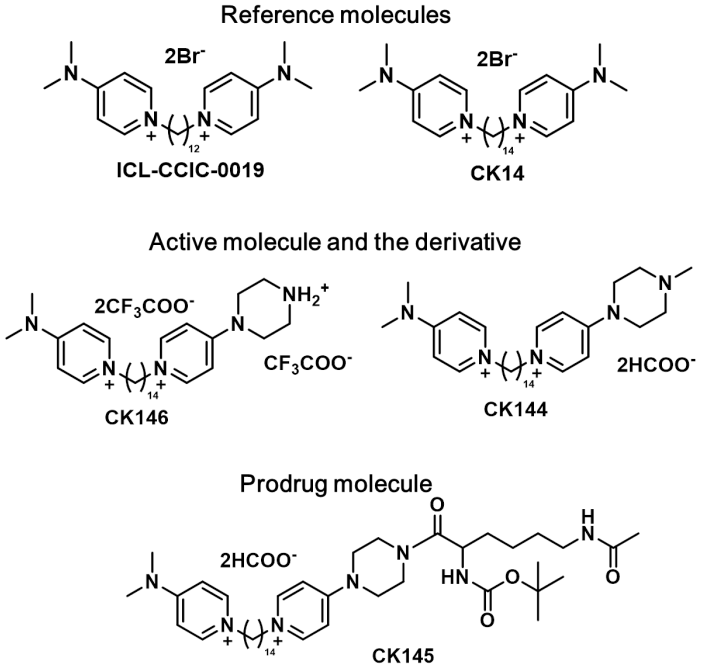


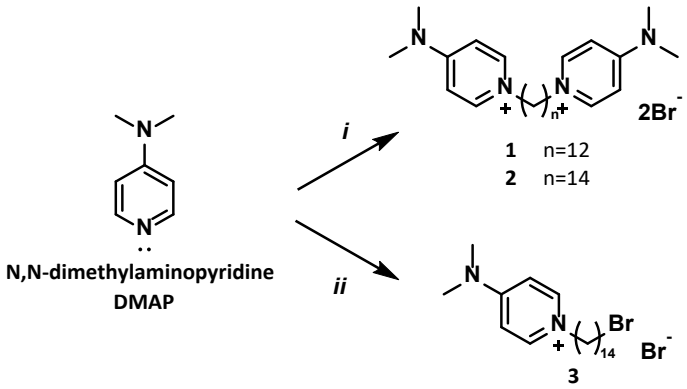
Figure 3. 5: The compounds synthesised in the prodrug strategy.

3.3.1 Synthesis of ICL-CCIC-0019 and CK14

The synthesis of ICL-CCIC-0019 (**1**), CK14 (**2**) and the 'half-structure' mono-DMAP derivative with a tetradecyl linker (**3**) was carried out using reported procedures (Scheme 3.1) [93].

Similar reaction conditions with varied molar ratios of starting materials were employed to avoid the formation of side products. For the synthesis of *bis*-DMAP compounds, the ratio of DMAP to spacer linkers (1,12-dibromododecane/1,14-bromotetradecane) used in the reaction was in accord with the stoichiometric ratio (DMAP:linker = 2:1). For the synthesis of compound **3**, 1,14-bromotetradecane was used in excess (DMAP:linker = 1:2) so as to avoid the formation of *bis*-DMAP compounds [93].

The quarternisation of the heterocycle nitrogen in DMAP *via* bimolecular nucleophilic substitution (S_N2) was successfully carried out at 110 ˚C, where DMAP served as a nucleophile. The species in the reaction transition state are more polar than starting materials, and the lone pair of the endocyclic nitrogen in the DMAP ring needs to be free for attacking the electrophile. 2-Butanone, as a polar aprotic solvent, was therefore selected since it can stabilise the transition state and not interact with the N-lone pair by forming hydrogen bond [113]. In the reaction, 2-butanone facilitated the precipitation of charged quaternary pyridinium salts that were less soluble, which pushed the reaction towards the formation of the product.



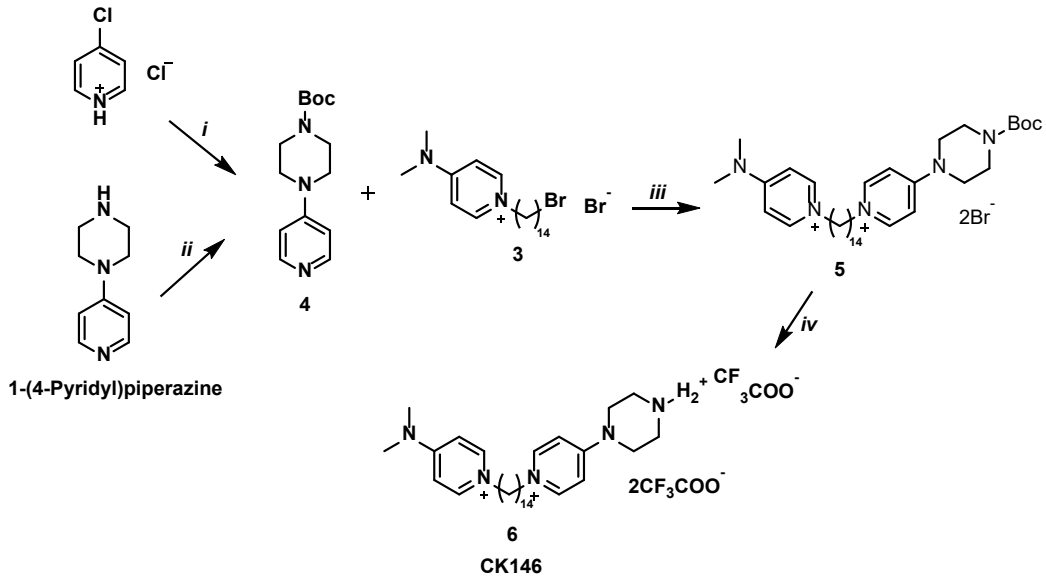
Scheme 3. 1: Synthesis of ICL-CCIC-0019 (1) and a CK14 (2), and the *mono*-DMAP derivative compound with a tetradecyl linker (3). Reagents and reaction conditions: i) 1,12-dibromododecane/1,14-bromotetradecane, 2-butanone, 110 ˚C, 3 hours; ii) 1,14-bromotetradecane, 2-butanone, 110 ˚C, 3 hours.

After the reaction, the addition of diethyl ether in large excess accelerated product precipitation. A wash of the precipitates using 2-butanone could remove unreacted, soluble

starting materials. The precipitates were further purified by recrystallisation from ethanol and 2-butanone. The recrystallisation using methanol was not successful as it largely solubilised the products. Compound **1**, **2**, and **3** were all obtained as fine white powders in good yields when filtered under gravity filtration (yields respectively: 84%, 80% and 64%, respectively); filtration under vacuum was avoided as it resulted in obvious compound loss.

3.3.2 Synthesis of CK146 and CK144

The synthesis of CK146 consists of three steps (Scheme 3.2). Synthesis of compound **4** was initially attempted using 4-chloropyridine hydrochloride *via* nucleophilic aromatic substitution (S_NAr) at 135 ˚C, in which case K_2CO_3 was used to promote the S_NAr reaction and to neutralise the acid produced as side-product [93]. However, 4-chloropyridine hydrochloride is hazardous and the yield was low (28%). An optimised method to synthesise compound **4** was established using commercially available 1-(4-pyridyl) piperazine. The secondary amine in 1-(4-pyridyl) piperazine was Boc-protected with DMAP catalysis in dichloromethane (DCM). By this method, compound **4** was successfully obtained in an excellent yield (94%).



Scheme 3. 2: Synthesis of CK146 (6). Reagents and reaction conditions: i) 1-Boc-piperazine, K_2CO_3, DMF, 135 ˚C, overnight, N_2; ii) Di-*tert*-butyl decarbonate, DMAP, DCM, RT, overnight; iii) MeCN, 110 ˚C, 72 hours, N_2; iv) TFA, MeCN, RT, overnight.

The coupling between compound **3** and **4** was attempted following the conditions used by Trousil *et al.*, where a S_N2 reaction was performed using K_2CO_3 in dimethylformamide (DMF) [93]. Despite the synthesis of compound **5**, this procedure was not efficient as there were unreacted compound **3** remaining in the reaction, which needed to be removed in the subsequent purification step. Compound **5** had to be purified by semi-preparative reversed-phase HPLC using a C18 column at a high concentration of 10 mg/mL, and the yield was largely compromised (24%). Good resolution of compound **5** was obtained by gradient elution (see HPLC method A). The peak at 29.3 min was confirmed to be the desired compound **5** by MS analysis (Figure 9.1). The purity of the combined fractions (> 98%) was confirmed (Figure 9.1). To simplify the purification process, other synthetic methodologies were tested to improve the conversion efficiency of the reaction. A sealed tube method was introduced this time by means of refluxing of compound **3** and **4** in acetonitrile (MeCN) under nitrogen atmosphere for 72 hours [94, 185]. This method afforded compound **5** with an excellent yield (97%) and high purity (91%), and therefore the purification step was not needed.

CK146 was synthesised by Boc-deprotection of compound **5** using trifluoroacetic acid (TFA) in acetonitrile. Several conditions involving different solvents and temperatures were tested to get optimised yields (Table 3.1).

Table 3. 1: Reagents and conditions used for Boc deprotection of Compound 5.

Entry	Solvent	Mol Eq of TFA	Temp. & Time	Yield
1	MeOH	15	RT, 2 hours	14%
2	MeOH	15	60 ˚C, 2 hours	14%
3	H_2O	15	RT, 2 hours	14%
4	H_2O	15	60 ˚C, 2 hours	30%
5	MeCN	15	RT, 2 hours	35%

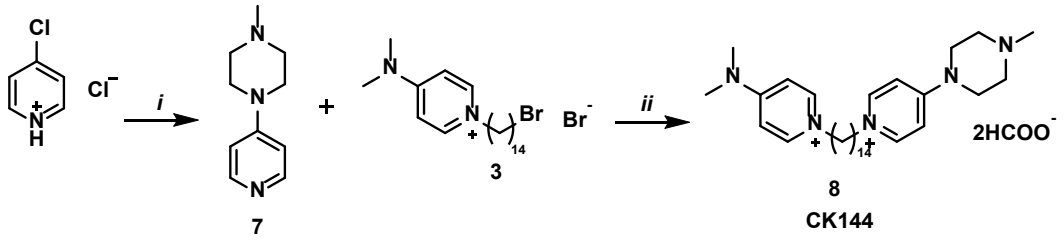
A set of small-scale deprotection experiments using the conditions of entry five was performed before scaling up. The reaction progress over 16 hours was monitored by HPLC (Table 3.2, Figure 9.2). It was inferred that the deprotection could be completed in 24 hours with a yield of 85%. The final scale-up reaction was conducted by using 1:1 (v/v) TFA and MeCN, in which case the yield obtained was increased to 93%.

Table 3. 2: Boc deprotection progress of compound 5. Five different time points (0-hour, 5-hour, 6-hour, 9-hour and 16-hour) were selected to monitor conversion rate of **5** using 15X TFA in acetonitrile at room temperature.

Time	Integrated peak area% under the HPLC curve *
0 h	14%
5 h	73%
6 h	78%
9 h	85%
16 h	85%

* Determined by HPLC analysis of an aliquot of the reaction mixture at each time point.

CK144 was synthesised using similar synthetic routes as introduced for CK146, but involving 1-methylpiperazine as a starting material (Scheme 3.3).



Scheme 3. 3: Synthesis of CK144 (8). Reagents and reaction conditions: i) 1-methylpiperazine, ZnI_2 2.5 mol% , MeCN, 75 ˚C, 24 hours, N_2; ii) K_2CO_3, DMF, 130 ˚C, overnight, N_2.

Compound **7** was produced using the method established by Abou-Shehada *et al.* [186]. Zinc iodide, as a Lewis acid, was used to activate the pyridine ring for the S_NAr reaction. The catalysis mechanism was supported by the fact that pyridine *N*-oxides were orders of magnitude more reactive in nucleophilic substitution than pyridines due to the formation of stable intermediates (Figure 3.6) [187]. It was, thus, hypothesised that Lewis acids, such as zinc iodide, could also activate the pyridine ring in a similar pattern as the oxygen in pyridine *N*-oxides [186].

After the reaction, distillation under vacuum was initially carried out in order to obtain compound **7** as an oil; the boiling point of compound **7** was predicted to be 290 ˚C. However, distillation proved inefficient as the crude was partly carbonised when the temperature was

set over 150 ˚C under reduced pressure. The purification of compound **7** was finally achieved by flash chromatography on silica, which was successful and afforded the compound as a yellow oil (yield: 53%).

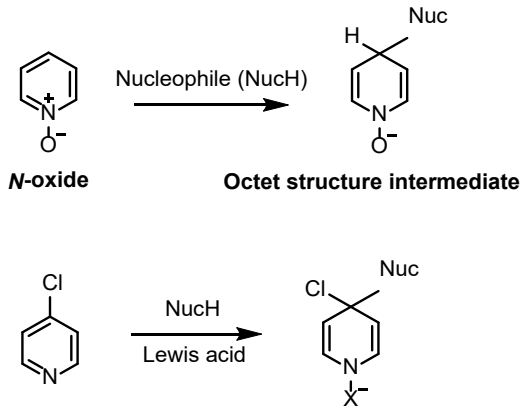
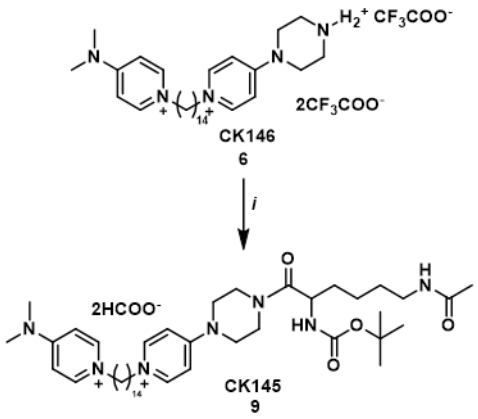


Figure 3. 6: The scheme of Lewis acid catalysed nucleophilic substitution on the pyridine analogue.

With compound **7** in hand, CK144 (**8**) was subsequently synthesised adopting the same reaction conditions initially tested with CK146, where the S_N2 reaction was carried out in DMF with the addition of K_2CO_3 as a base. CK144 was purified by semi-preparative HPLC. The signal at 12.3 min:sec in the HPLC chromatogram was identified as CK144 by MS analysis (Figure 9.3). Optimised synthetic routes for CK144 involving sealed tubes, metal catalysts or more basic conditions might be investigated in future for a larger scale synthesis.

3.3.3 Synthesis of CK145

The synthesis of CK145 (**9**) was performed by contract synthesis (Creative Chemistry Ltd., Hampton, UK) following a reported procedure [168]. In brief, CK146 was coupled with commercially available α-Boc-Lys(ε-Ac)-OH in the presence of 1-ethyl-3-(3-dimethylaminopropyl) carbodiimide hydrochloride (EDC·HCl), 1-hydroxybenzotriazole (HOBt·H_2O) and *N*,*N*-diisopropylethylamine (DIEA) in DMF at room temperature (Scheme 3.4).



Scheme 3. 4: Synthesis of CK145 (9). Reagents and reaction conditions: i) α-Boc-Lys(ε-Ac)-OH, EDC·HCl, HOBt· H_2O,DIEA, DMF, RT, overnight.

The product identity was confirmed by liquid chromatography-mass spectrometry (LC-MS). The isolation of CK145 was then established by developing efficient HPLC methods to achieve a reliable separation of the components in the crude sample provided by the company. The sample was initially analysed by HPLC (HPLC method B), and the signal at 21.9 min:sec was confirmed to be CK145 according to the MS analysis (Figure 9.4).

The scaling up of the sample purification was then investigated. The binary mobile phase composed of water and methanol supplemented with appropriate acid agents was used to provide high solubility of the sample. Instead of using 0.1% TFA in mobile phase, 0.2% formic acid was selected to offer a pH of 3, so as to improve the peak shapes on the reversed-phased semi-preparative column without deprotecting the Boc group in CK145.

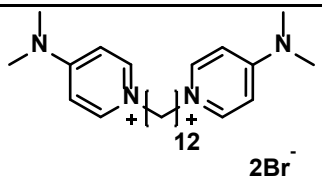
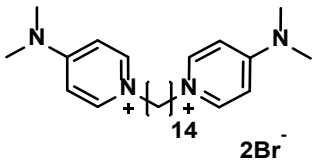
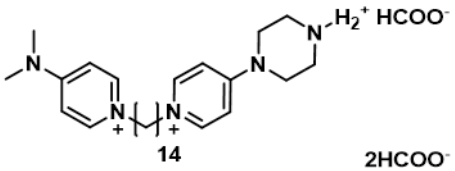
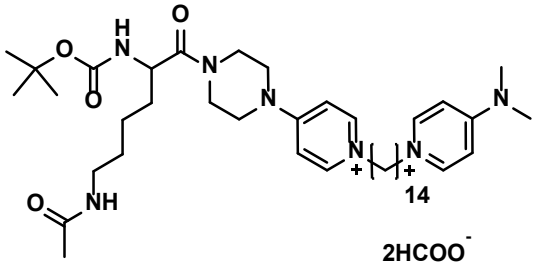
To test the maximal sample loading amount, the loading limit was investigated by dual wavelength monitoring. The wavelength at 318 nm offered a minimal absorbance of CK145 during the full wavelength scanning and was, thus, selected for the subsequent HPLC purification of CK145 to allow the scale-up loading of the crude. The maximal sample loading amount was tested by slowly increasing 6-fold under signal monitoring at 318 nm. The maximal loading limit turned out to be 30 mg/mL, over which the resolution of the targeted peak was poorer (HPLC method C, Figure 9.5).

CK145 was finally recovered by evaporation under *vacuo*, followed by lyophilisation with a combined yield of 37.5%. The dry CK145 with a purity of 98% was ready for biological evaluation (Figure 9.6).

3.3.4 Synthesis conclusions

The synthesis of a small library of CHKA inhibitors, including ICL-CCIC-0019, CK14, CK144, CK145 and CK146, has been successfully achieved (Table 3.3).

Table 3. 3: The CHKA inhibitors synthesised in this chapter.

CHKA inhibitors	Structure	Overall yield
ICL-CCIC-0019		84%
CK14		80%
CK146		53%
CK145		38%

All the compounds obtained displayed high solubility in water and DMSO, and were all taken forward for biological evaluation. The synthesis of ICL-CCIC-0019, CK14 and compound **3** followed the literature methodology which was straightforward and afforded good yields (mean yield: ~80%) [93]. Several synthetic routes were adapted in order to improve the yields of DMAP derivative head compounds (compound **4** and **7**). Compound **4** was obtained

in a lower yield compared to compound **7**, its *N*-methyl piperazine counterpart, *via* S_NAr reaction under the same synthetic conditions. This could have resulted from the reduced nucleophilicity of the *N*-Boc-piperazine, so it was less reactive. Boc bulk addition was, thus, exploited to synthesise compound **4** in a simplified way.

Sealed-tube reaction turned out to be the most efficient method for the S_N2 coupling between the 'half-structure' and the DMAP derivative head bulks with an excellent yield. HPLC purification was also avoided in this step.

One of the most challenging part in this project was to purify the target compounds by semi-preparative HPLC. Besides the time and efforts required, the main limitation of HPLC purification was the low recovery rate of the positively charged molecules analysed under the HPLC conditions chosen at the time, probably due to the high polarity of the aromatic amine structures of these compounds. To obtain satisfactory peak shapes, acidified mobile phases were used, which could prevent the secondary interaction of the silanol groups with chemicals on the stationary phase surface. Novel synthetic and purification methods that provide better reaction conversion and isolation efficiency need to be explored in future work. Improvements of current HPLC systems by introduction of suitable ion-pair reagents should also be considered .

4. Design and synthesis of the novel PSMA-targeted CHKA inhibitor

4.1 Introduction to PSMA-targeted CHKA inhibitor strategy

PSMA is significantly overexpressed on the cell membrane of most prostate cancer (PCa) cells (100 – 1000 fold higher expression than that in normal cells), and its expression levels increase with the cancer aggressiveness [188, 189]. These biological characteristics make PSMA an attractive therapeutic and prognostic target. The enzymatic properties of PSMA as a glutamate-preferring carboxypeptidase and its internalisation characteristics enable peptide-based targeted therapeutics and prognosis of PCa [190]. Using *in silico* screening, a glutamate urea ligand 2-(3-(1,3-dicarboxypropyl)-ureido) pentanedioic acid (DUPA) was recognised, which exhibited high specificity and binding affinity to PSMA receptor [191-193]. A series of Urea-based DUPA analogues have been subsequently developed, including the Glu-Urea-Lys ligand (Figure 4.1A), which has boosted the clinical potential of novel targeting tools for diagnostics, therapeutics and prognostics of PCa [194-197].

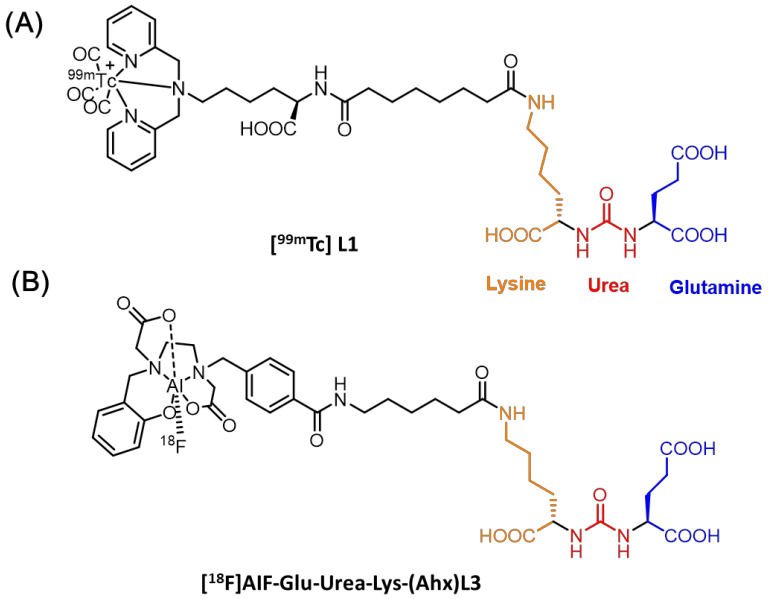


Figure 4. 1: Chemical structures of [^{99m}Tc]L1 (A) and [^{18}F]AlF-Glu-Urea-Lys-(Ahx)L3 (B), where the Lys-Urea-Glu binding motif is highlighted.

A number of radiopharmaceuticals and small-molecule drug conjugates have been designed around the Glu-Urea-Lys binding motif, such as [^{99m}Tc]L1 and [^{18}F]AIF-Glu-Urea-Lys-(Ahx)L3 (Figure 4.1B) [169, 190, 194, 198]. A Glu-Urea-Lys Ligand-conjugated siRNA system was developed by Lee *et al*, which successfully suppressed the expression of androgen receptor *in vivo* [169]. The PSMA-targeting Glu-Urea-Lys motif was exploited in a lipid nanoparticle formula that contained the siRNA able to inhibit the expression of androgen receptor [169].

PSMA internalisation takes place once the Glu-Urea-Lys conjugate binds to PSMA, followed by the lysosomal degradation and efficient release of payload in the cytoplasm during endosomal recycling [190, 199]. The payload can be a radiopharmaceutical or a cytotoxic agent for imaging and therapeutic purposes.

4.2 SAR and design goal rationale

CHKA is a therapeutic target of PCa, and plays a crucial role in the signalling maintenance of androgen receptor that leads to therapy resistance [24, 60]. CHKA inhibitors like ICL-CCIC-0019 also displayed antiproliferative activity against PCa cells [64]. The cytotoxic ICL-CCIC-0019 can be conjugated to PSMA-targeting bulk, which results in a ligand-drug conjugate (LDC) for PCa treatment.

In this work, a peptide-based targeted drug delivery strategy was designed to optimise the pharmacological profiles of ICL-CCIC-0019 by achieving specific PSMA targeting. The small-molecule Glu-Urea-Lys ligand was utilised in this strategy owing to its high-affinity, and specific binding to PSMA [160, 169]. To facilitate the LDC, CK146 was similarly utilised in this strategy as a starting scaffold that provides a reactive piperazine handle for the conjugation of Glu-Urea-Lys PSMA binding motif. The SAR of the PSMA-targeted CHKA inhibitor CK147 derived from CK146 are illustrated in Figure 4.2.

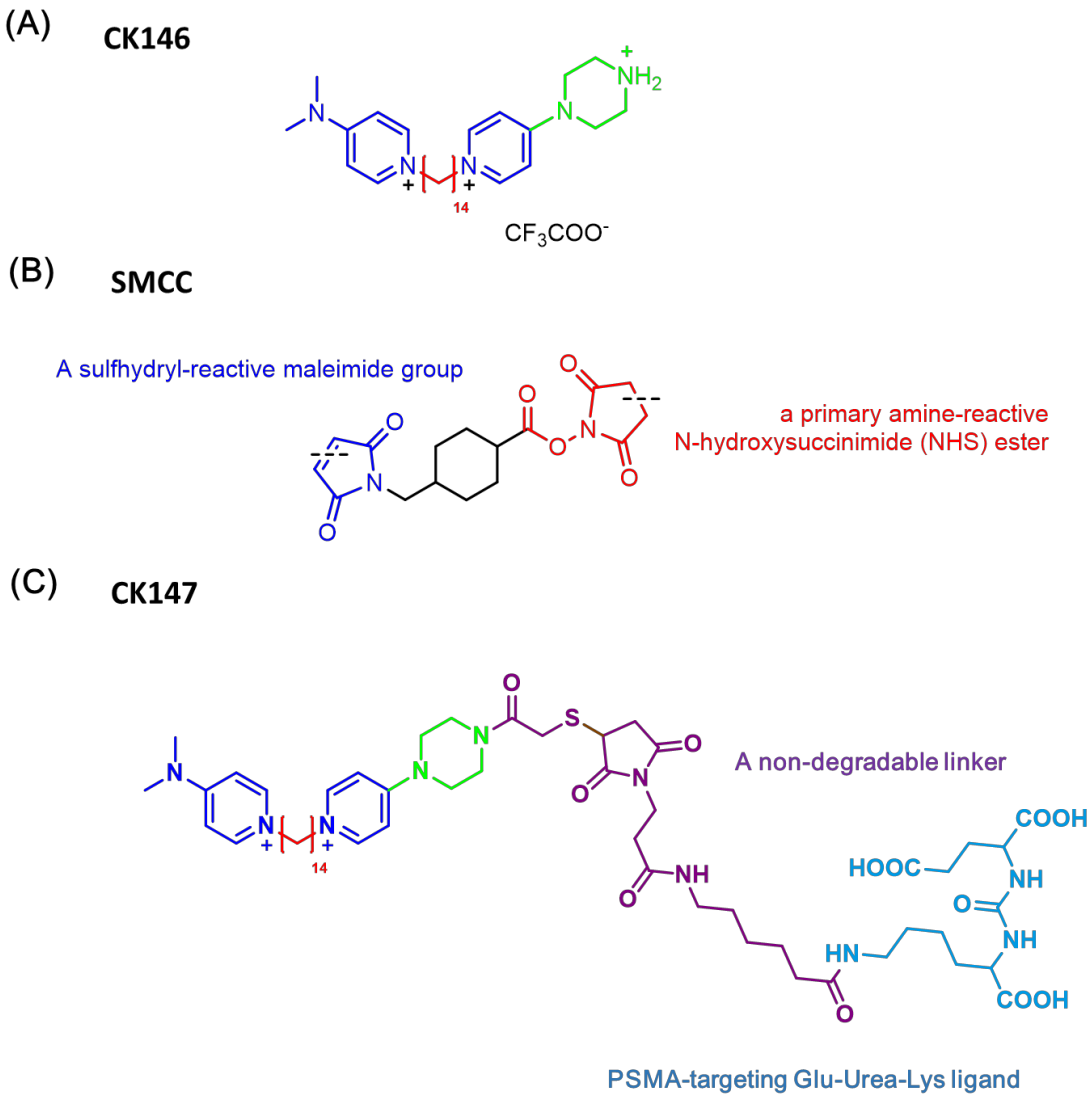


Figure 4. 2: Graphic representation of design goals of novel PSMA-targeting CHKA inhibitor. (A) chemical structure of CK146; (B) chemical structure of the cross-linked species used in Kadcyla®: succinimidyl 4-(*N*-malemidomethyl) cyclohexane-1-carboxylate (SMCC) [154]; two reactive ends are highlighted in red and blue respectively with the reactive positions labelled with dash lines; (C) chemical structure of PSMA-targeting CHKA inhibitor CK147.

This novel LDC CK147 contained the ICL-CCIC-0019 derivative scaffold CK146 (Figure 4.2A) and the Glu-Urea-Lys ligand conjugated *via* a linker mimicking the link pattern of Kadcyla®: similar to the cross-linking pattern of Kadcyla® (Figure 4.2B), the free sulfhydryl group of a designed ICL-CCIC-0019 derivative was to be conjugated to a maleimide group of a linker which connected the Glu-urea-Lys ligand (Figure 4.2C). The maleimide alkane linker used in

this strategy was non-cleavable and could thus provide good plasma stability compared to the cleavable linkers [149]. However, effective degradation of LDCs may be a requirement for using non-cleavable linkers to ensure the release of the active drug molecules. The Glu-urea-Lys ligand specifically targeting PSMA was hypothesised to deliver the drug conjugate to the cell surface with overexpressed PSMA. After binding to PSMA, the ICL-CCIC-0019 conjugate would be translocated through endocytosis and accumulate in the cells, exerting its antiproliferative function after the potential lysosomal degradation to release CK146 [149, 200].

In this chapter, improvements in the pharmacological profiles of ICL-CCIC-0019 was attempted by exploiting PSMA-targeting delivery strategy. By the incorporation of Glu-Urea-Lys ligand, high expression levels of PSMA in PCa cells was hypothesised permitting specific delivery of the ICL-CCIC-0019 derivative, thus reducing its toxicity by selective drug uptake. The aim of this strategy is to synthesise CK147, the conjugate of the ICL-CCIC-0019 derivative scaffold (CK146) with the PSMA binding motif Glu-Urea-Lys ligand *via* thiol-maleimide chemistry.

4.3 Synthesis of CK147 (Results and Discussion)

As introduced, the conjugation reaction that produced CK147 relied on thiol-maleimide chemistry: the sulfhydryl group in CK147 precursor (CK146-SH) could efficiently react with the maleimide group under reducing biorthogonal conditions (Figure 4.3); the Glu-Urea-Lys ligand attached to maleimide was commercially available and ready for use without further process; the efforts were, thus, focused on the efficient synthesis of CK146-SH.

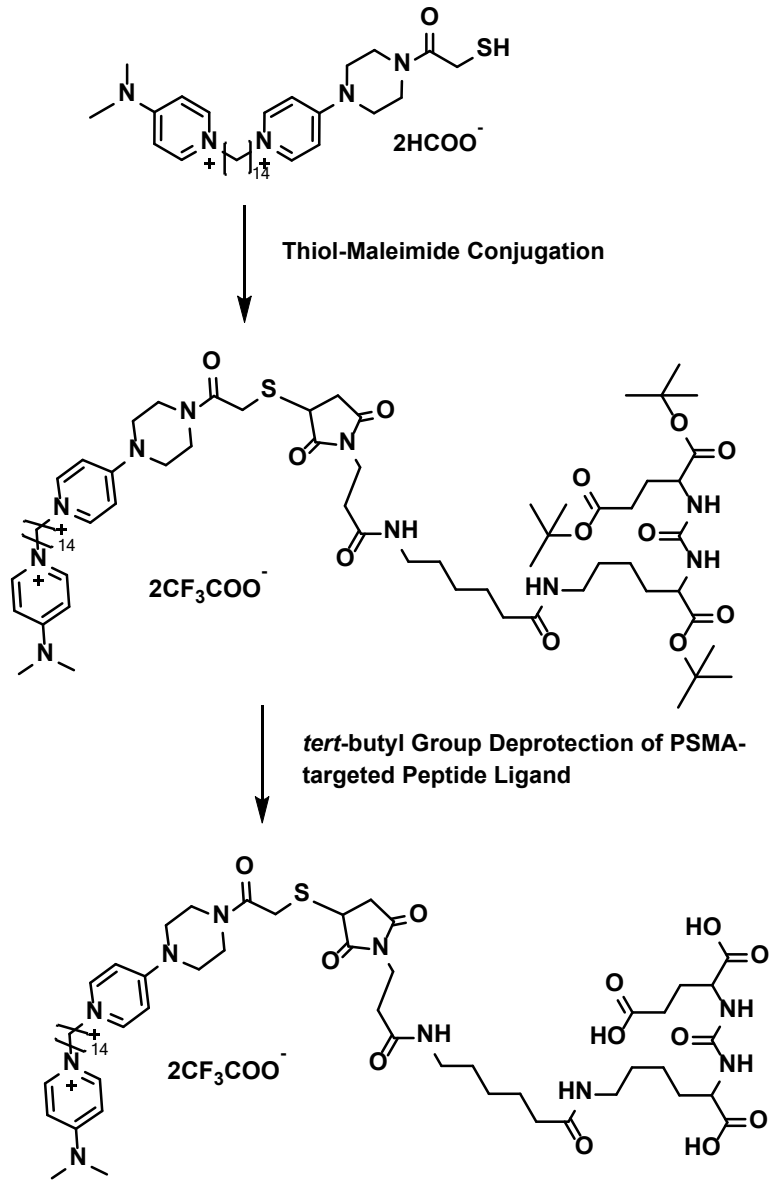
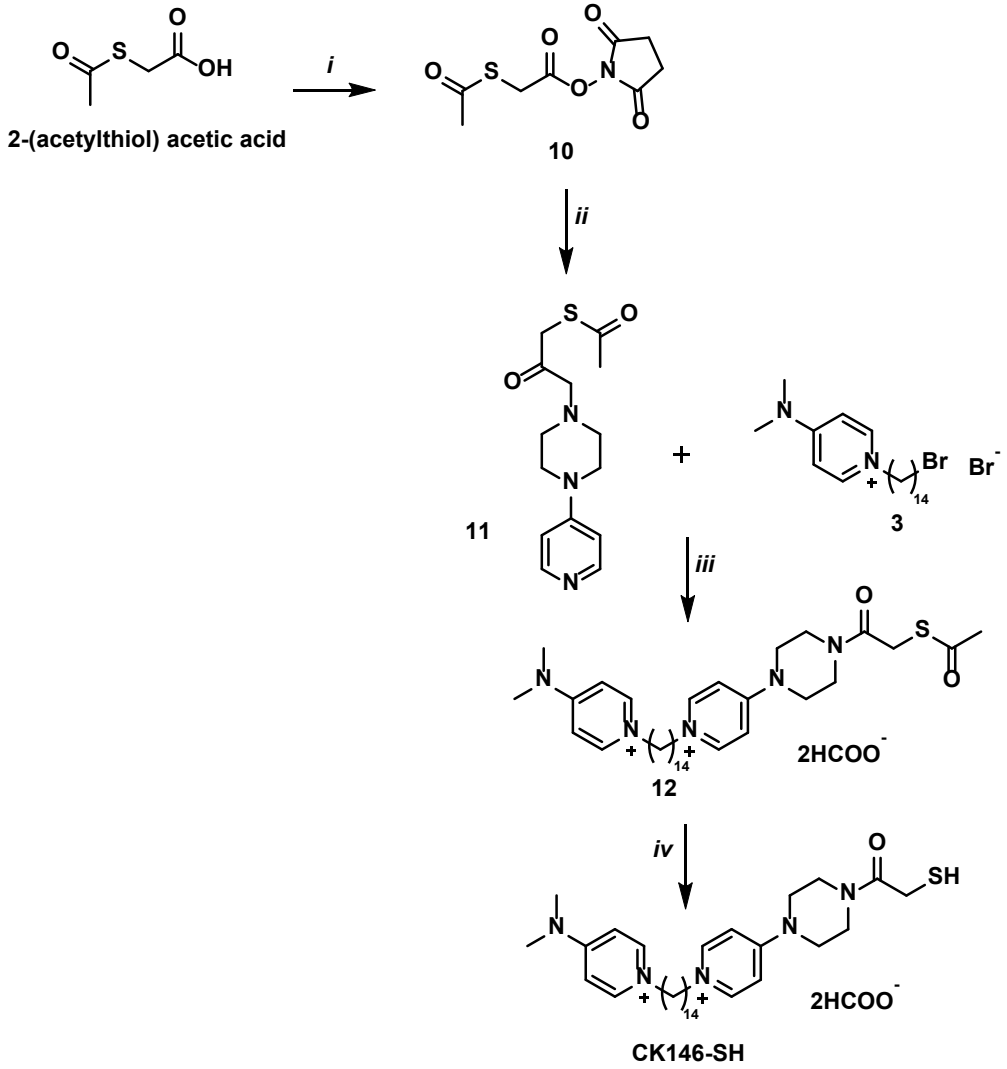


Figure 4. 3: Graphic representative of thiol-maleimide reaction with CK146-SH.

4.3.1 Synthesis of CK146-SH

In this section, two routes were attempted to offer CK146-SH *via* different bioconjugation reactions of amines. The first synthesis plan exploited unsymmetrical DMAP derivative quarternisation. The proposed route is shown in Scheme 4.1. CK146-SH was hypothesised to be obtained from the coupling between the asymmetric tetradecane 'half-linker' compound (**3**) and compound **11**. The deacetylation of the sulfhydryl group in compound **12** would finally offer CK146-SH which is ready for thiol-maleimide conjugation introduced in next section.



Scheme 4. 1: Synthesis of CK146-SH *via* unsymmetrical DMAP derivative quarternisation. Reagents and reaction conditions: i) TSTU, Anhydrous MeCN, anhydrous Pyridine, RT, overnight, N_2; ii) 1-(Pyridin-4-yl)piperazine, anhydrous MeCN, TEA, RT, overnight, N_2; iii)

K_2CO_3, DMF, 130 °C, overnight.

The synthesis of compound **11** involved amine activation by *N*-hydroxysuccinimide (NHS) ester. Amine-coupling process is one of the most important reactions in bioconjugation since it is extensively employed in the modification of peptide molecules, proteins or the host of other macromolecules [201]. The primary amine modifications include amine alkylation and acylation (Figure 4.4).

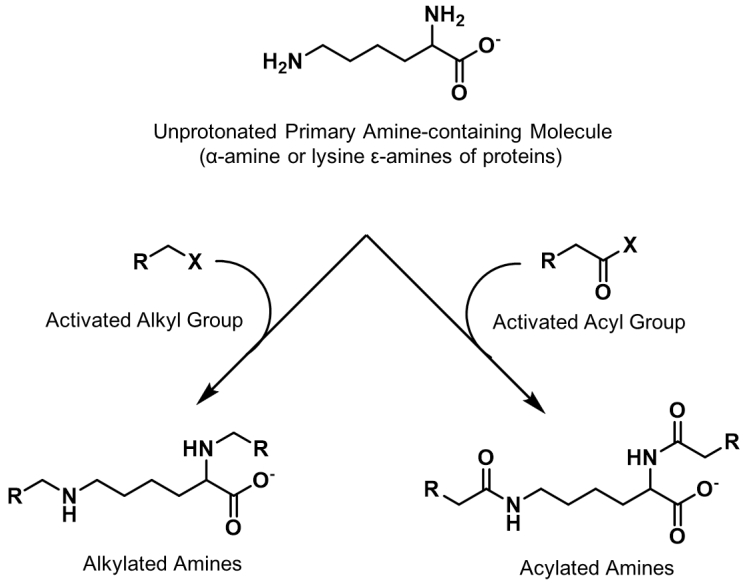


Figure 4. 4: Amine alkylation and acylation by amine activation.

NHS esters are one of the most common crosslinkers for amine acylation. An NHS ester derivative undergoes an S_N2 reaction with nucleophiles and forms an acylated product, in which case an NHS leaving group is released [202]. Compared to sulfhydryl or hydroxyl groups, the reactions of NHS esters with primary or secondary amines offer more stable linkages (Figure 4.5) [202]. Thioesters and ester linkages are susceptible to hydrolysis in aqueous environment [202].

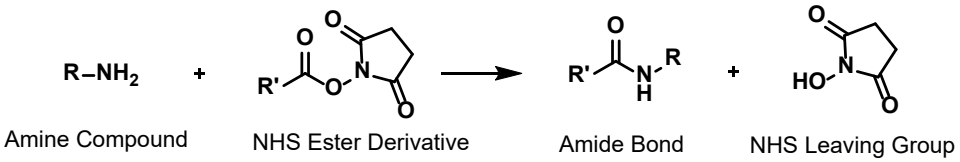
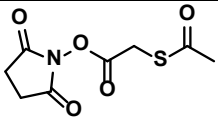
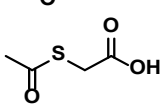
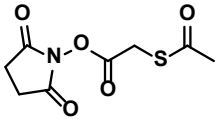


Figure 4. 5: Graphic scheme of amide bond formation by NHS ester crosslinking reaction.

In the first step of CK146-SH synthesis (Scheme 4.1), the precursor molecule 2-(acetylthiol) acetic acid, containing an acetylated sulfhydryl group, was first activated by an uranium-based activation agent *N*,*N*,*N*',*N*'-Tetramethyl-O-(*N*-succinimidyl)uranium tetrafluoroborate (TSTU), which yielded compound **10** as an amine-reactive NHS ester at ambient temperature. According to NMR spectra analysis, the hydrolysis of compound **10** was noted as a side reaction in which case the side-product NHS was released. This hydrolysis side reaction was eliminated by using absolute dry organic solvent acetonitrile. DMAP was also added as a proton acceptor to improve the reaction efficiency.

Compound **11** was then conjugated *via* amide bond formation between 1-(pyridin-4-yl) piperazine and compound **10** under basic anhydrous conditions by using triethylamine (TEA). The reaction conditions were optimised as shown in Table 4.1. The purification of compound **11** was challenging because of its high solubility in water and susceptibility to decomposition on silica: compound decomposition was observed during thin-layer chromatography (Figure S10.1); compound **11** was successfully purified by crystalisation despite poor product recovery (25%). The purity of the crude containing compound **11** after the reaction was investigated by analytical HPLC and found high (90%). It was confirmed by ^{1}H NMR that the impurities were mainly upfield with chemical shifts between 2 and 3 ppm, while the downfield aromatic region looked clean (Figure 9.7 and S10.2). Compound **11** was therefore used in its crude form without further purification for the next-step reaction yielding compound **12**.

Table 4. 1: Reaction condition optimisation of the crosslinking yielding compound 11.

Entry	Starting material	Reagents and conditions	Work-up	Yield
1		DMF, TEA, N_2, overnight, RT	Not applicable	< 40%
2		HOBt, EDC·HCl DMF, TEA, N_2, overnight, RT	Extraction (EtOAc: brine)	< 10%
3		MeCN, TEA, N_2, overnight, RT	Column chromatography and crystalisation	25%

The coupling reaction to synthesise compound **12** was conducted using compound **11** and the asymmetric tetradecane 'half-linker' compound **3** in the presence of K_2CO_3 in DMF at 130 °C. Semi-preparative reverse phase HPLC was used to scale up the purification of compound **12** (Figure 9.8). The identity of the compound was then confirmed by MS and NMR analysis from fractions collected from HPLC purification. According to the NMR spectra, a side reaction had occurred simultaneously during coupling, which yielded an unexpected product with the same mass as compound **12** (Figure 4.6 and S10.3). The protons of the methylene groups attached to the quaternary amine (Figure 4.6A, coloured in magenta) were integrated to two instead of four in ^{1}H NMR, confirming that a side product had been synthesised (Figure 4.6A). It was inferred that the sulfhydryl group of compound **12** was liberated under the harsh reaction conditions. These conditions also facilitated the coupling of the sulfhydryl group to compound **3** (Figure 4.6B). Accurate MS confirmed this hypothesis (Figure S10.3).

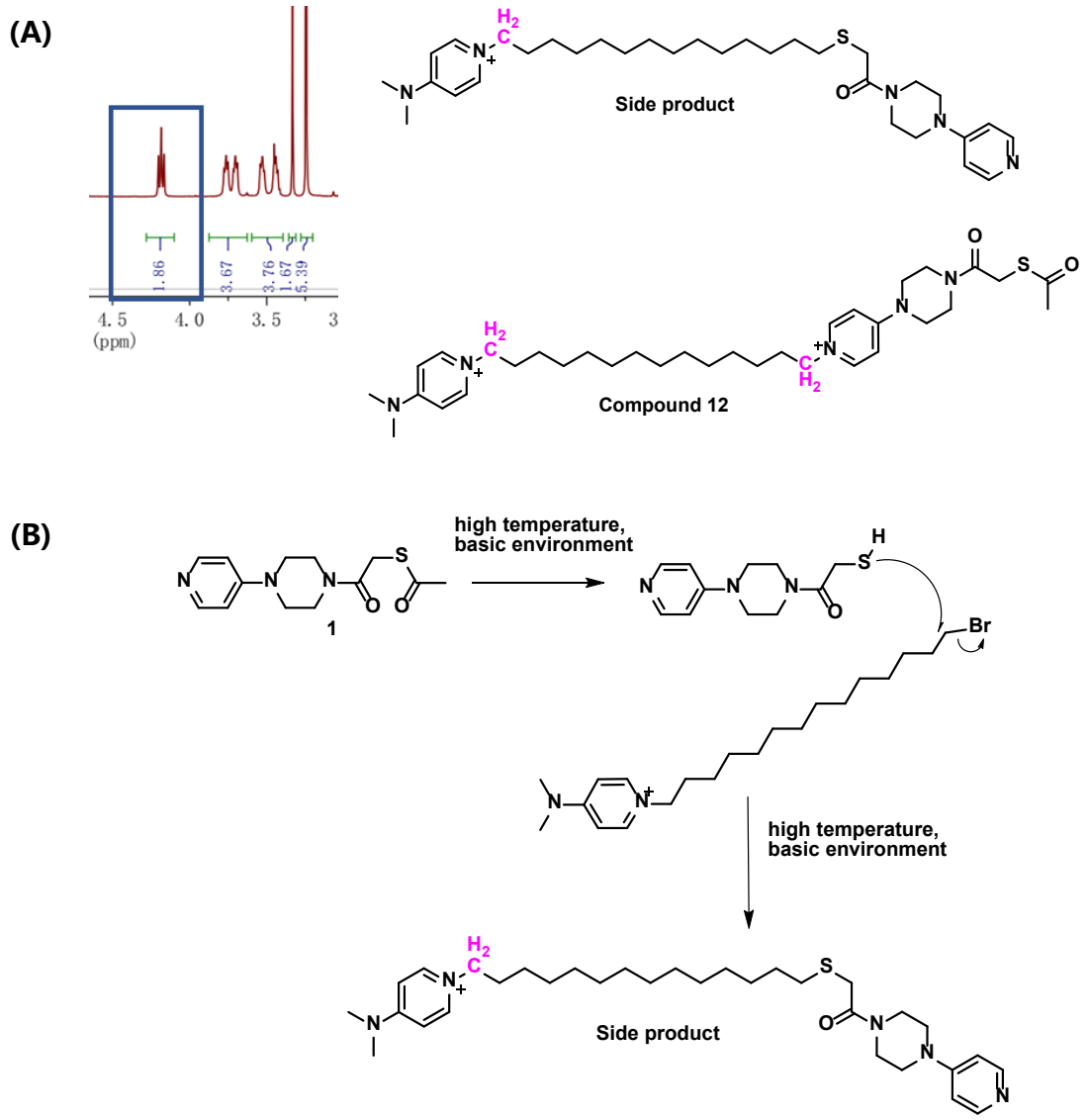
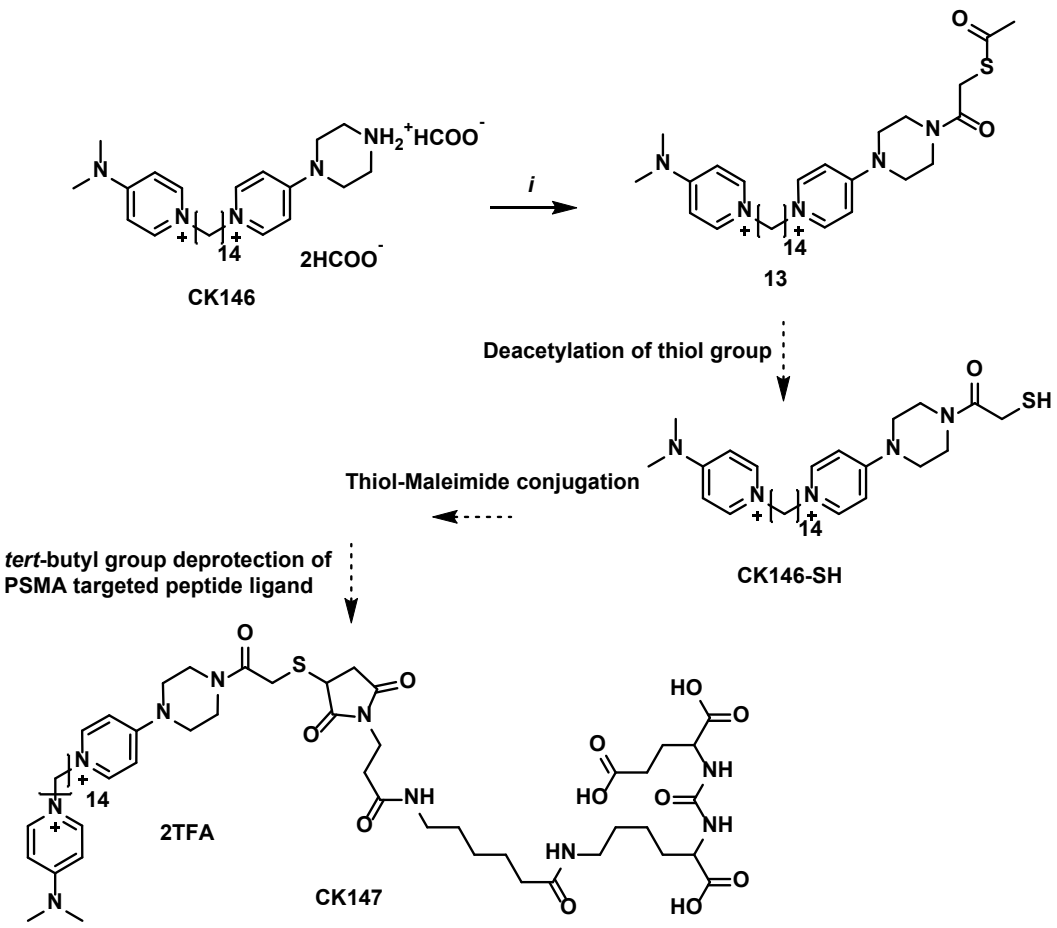


Figure 4. 6: An unexpected reaction occurred during the coupling, which yielded a side product with the same mass as compound 12. (A) deduction on the chemical structure of the side product according to ^{1}H NMR; (B) mechanism demonstrations of the side reaction.

Alternative synthetic routes were, thus, developed to avoid the harsh conditions needed for the formation of the second quaternary amine and to avoid the formation of side products. An ideal way to obtain CK146-SH was to extend the tertiary amine end on piperazine group of CK146 *via* amide synthesis, which usually requires milder reaction conditions. CK146 could be derivatised to bear a sulfhydryl group for conjugation to the PSMA-targeting moiety *via* a maleimide moiety. Two methods were explored to access CK146-SH. As shown in the first route (Scheme 4.2), NHS ester crosslinking was used to yield the stable amide bond.



Scheme 4. 2: The first synthetic route of CK146-SH utilising extension of the tertiary amine end on piperazine group *via* NHS ester crosslinking chemistry. Reagents and conditions: i) compound **10** made in-house, TEA, anhydrous MeCN, RT, overnight.

Compound **10**, as an NHS ester, was stirred with CK146, and the reaction was monitored by HPLC (Figure 9.9). Unfortunately, only singly charged ions were detected in MS analysis, suggesting that the starting material may have decomposed (Figure S10.4). Reaction optimisation also proved unsuccessful due to the sensitivity of compound **10** to TEA (Figure 9.10).

The second synthetic route that successfully yielded the desired CK146-SH utilised carbodiimide crosslinking chemistry and disulfide reduction. The sulfhydryl group in CK146-SH is highly reductive and is, thus, not stable for storage. Reduction of the disulfide bond can be an effective method to introduce sulfhydryl groups for the thiol-maleimide reaction [202].

Disulfide reduction with low concentrations of reducing agents such as tris(2-carboxyethyl)phosphine (TCEP) and dithiothreitol (DTT) will cleave disulfide bonds; two sulfhydryl groups can be obtained from the cleavage of each disulfide bond (Figure 4.7).

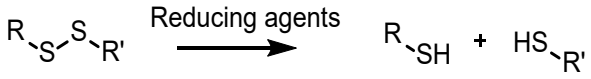
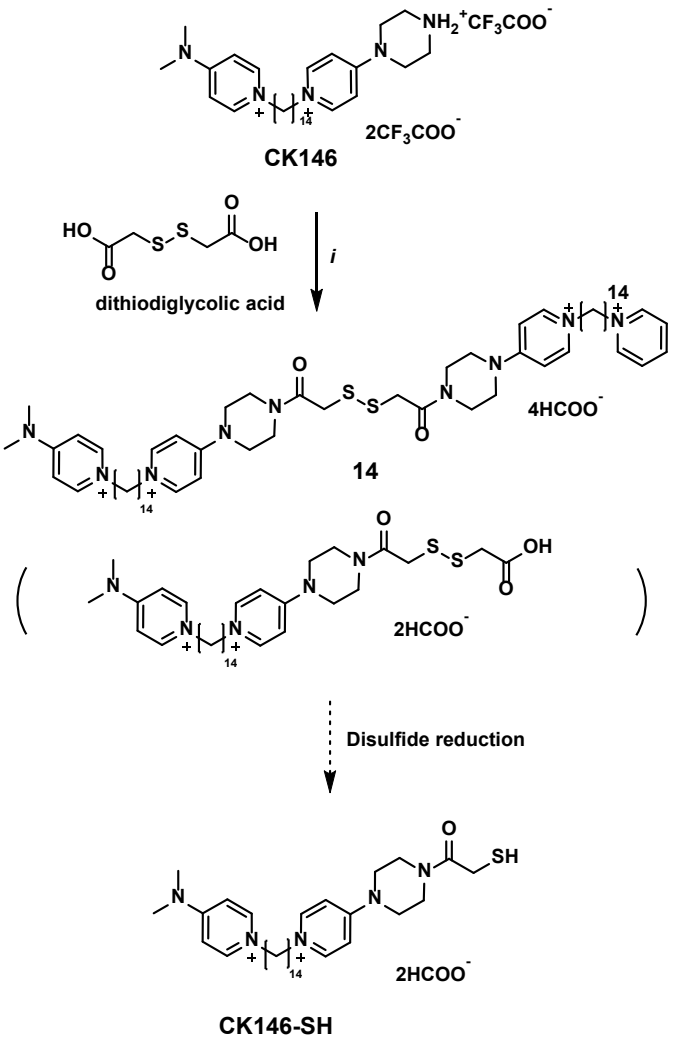


Figure 4. 7: Graphic scheme of sulfhydryl group synthesis *via* disulfide reduction.

The amide formation between CK146 and dithiodiglycolic acid could yield precursor molecules of CK146-SH as monomer and dimer (compound **14**) disulfide conjugates; by disulfide reduction of the precursor molecules, CK146-SH can be immediately produced for thiol-maleimide conjugation (Scheme 4.3).



Scheme 4. 3: The second synthetic route of CK146-SH utilising extension of the tertiary

amine end on piperazine group *via* EDC crosslinking. Reagents and conditions: i) EDC hydrochloride, HoBt, DIPEA, anhydrous DMF, N_2, 72 hours, RT.

To achieve the amide formation of the secondary amine end on piperazine group, carbodiimide crosslinking was considered. Carbodiimides are zero-length crosslinking reagents commonly used for amide formation between a carboxylate group and an amine [202]. They mediate amide formation without introducing additional chemical structures between the conjugating molecules and are, thus, called zero-length reagents. In a carbodiimide-mediated crosslinking reaction, *e.g.* EDC coupling, *N*-substituted carbodiimides react with carboxylic acids, which form highly-reactive intermediate *O*-acylisourea derivatives (Figure 4.8) [202]. Although these intermediates are very short-lived, they can efficiently react with a nucleophile such as an amine and form a stable amide bond [202].

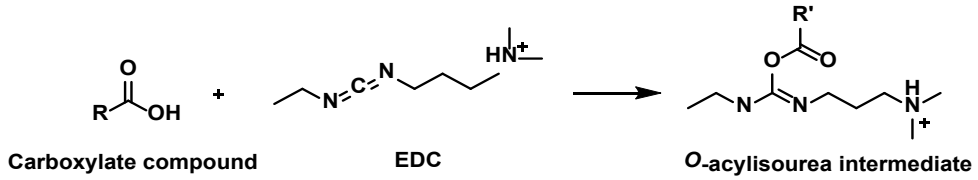
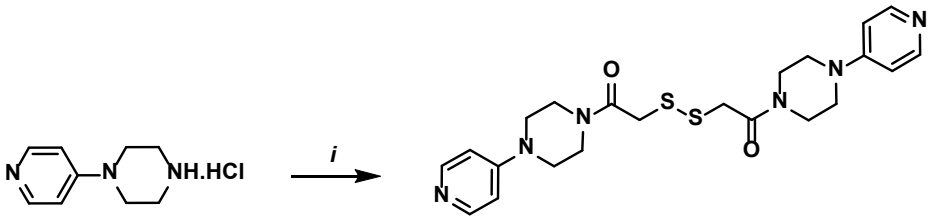


Figure 4. 8: Graphic scheme of amide bond formation *via* EDC coupling.

Reaction conditions of amide formation *via* EDC crosslinking were first tested using 1-(4-Pyridyl)piperazine hydrochloride and EDC hydrochloride (Scheme 4.4); the reaction conditions yielded the desired monomer and dimer disulfide conjugates (Figure S10.5).



Scheme 4. 4: The mock EDC coupling reaction using 1-(4-Pyridyl)piperazine hydrochloride. Reactions and conditions: i) Dithiodiglycolic acid, EDC hydrochloride, HoBt, DIPEA, anhydrous DMF, RT, N_2, overnight.

The similar reaction between CK146 and dithioldiglycolic acid was then performed under the same conditions. Both monomer and dimer disulfide conjugates were separated and collected by semi-preparative HPLC purification for the next-step disulfide reduction (Figure S10.6 and S10.7).

4.3.2 Synthesis of CK147 *via* thiol-maleimide conjugation

With the monomer and dimer CK146-disulfide conjugates in hand, CK146-SH could be produced by disulfide reduction and participate in the subsequent thiol-maleimide reaction to synthesise CK147.

Maleimides, also called maleic acid imides, are a category of useful crosslinking agents for thiol reactions. Thiol-maleimide conjugation is recognised as a specific type of Michael addition reaction. In brief, the double bond of maleimides can be attacked by thiolate anion as a nucleophile and form stable thioether bonds at a specific pH range of 6.5 to 7.5 (Figure 4.9) [202]. At higher pH values, the side reactions between maleimides and amino groups will take place [203]. Therefore, a successful thiol-maleimide conjugation emphasises both reaction pH values and a reductive reaction environment to produce CK146-SH from its disulfide bond forms.

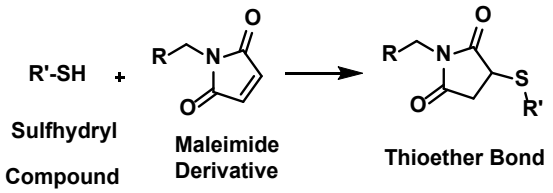
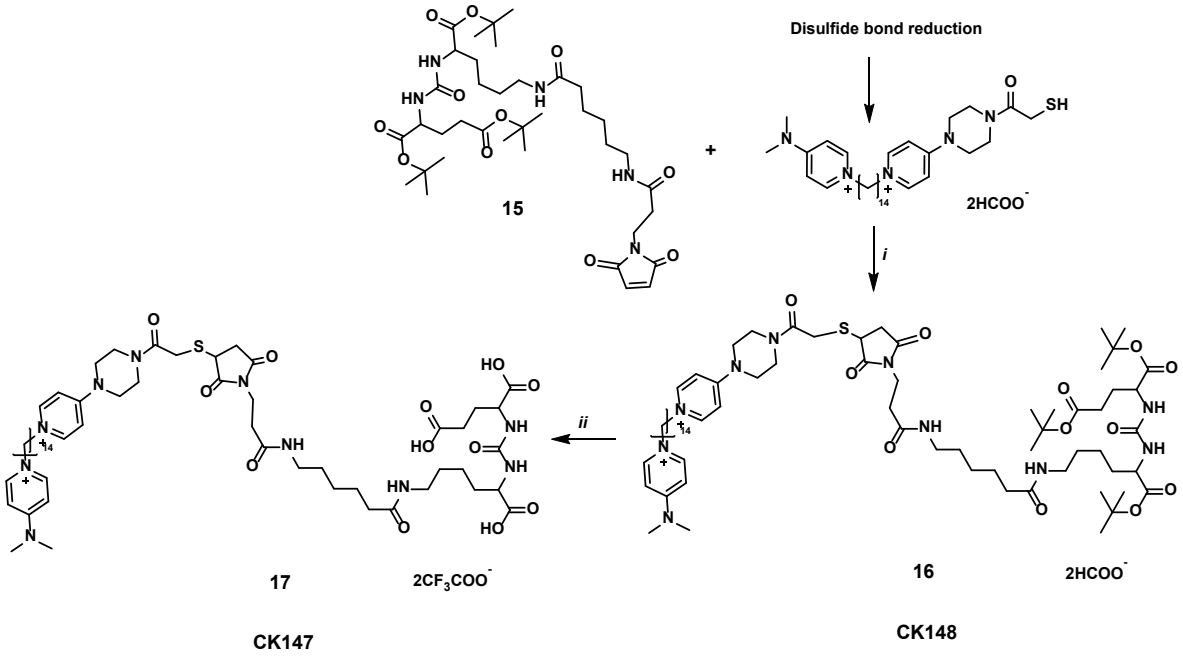


Figure 4. 9: Graphic scheme of thioether bond formation *via* thiol-maleimide conjugation.

In this experiment, compound **14** was reduced with TCEP hydrochloride in Tris-HCl buffer (pH = 7) followed by the dropwise addition of compound **15** ($(OtBu)_3$PSMA-maleimide) in a degassed mixture solution of DMF and Tris-HCl buffer. This procedure successfully gave the desired CK148 (compound **16**) in a high yield of 85% (Figure S10.8). The last-step deprotection of CK148 using TFA was monitored by HPLC, which yielded the final product

CK147 (**17**) ready for use without further purification (purity: 95%, determined by HPLC, Figure S10.9).



Scheme 4. 5: The thiol-maleimide conjugation between CK146-SH and $(OtBu)_3$PSMA-maleimide synthesised CK147 (17). Reagents and conditions: i) TCEP, PSMA-Maleimide, Tris-HCl buffer (pH 7.3, degassed), DMF, RT, overnight, N_2; ii) TFA, DCM, RT, overnight.

4.4 Synthesis conclusions

In this chapter, a series of synthetic routes utilising different bioconjugation techniques have been explored to achieve the efficient synthesis of the desired PSMA-targeted CHKA inhibitor CK147 (**17**). The whole process of the synthesis could be divided into two parts, the synthesis of CK146-SH and the subsequent synthesis of CK147 *via* maleimide-thiol reaction. In this case, the synthesis of CK146-SH was seen as a main challenge due to the reactivity and reducibility of the sulfhydryl group. The unsymmetrical quaternisation of the DMAP derivative used in the synthesis of CK144 and CK146 was not feasible for CK146-SH since the acetyl protection group in the molecule was hydrolysed under the coupling conditions with a high temperature and a basic environment. The sulfhydryl group was liberated under these conditions and offered only the side-product from the undesired coupling pattern.

To avoid the harsh conditions in the synthesis of CK146-SH, we turned to bioconjugation methods involving milder conditions for the conjugation of the molecules with biological origin or fragments/derivatives of biomolecules [202]. The amide synthesis *via* carbodiimide activation and disulfide bond reduction followed by thiol-maleimide conjugation were performed successfully and offered the final product CK147 in an acceptable yield (25%).

The compound CK147 synthesised at this stage together with the molecules synthesised in Chapter 3 will allow for preclinical drug evaluation in the next chapter, by which the prodrug and PSMA-targeted drug delivery strategy raised in this project would be verified from different drug discovery aspects and inspire its future development.

5. Biological evaluation

This work is associated with [1], and the permission of reuse of all the figures and tables are not required according to the publisher (https://www.mdpi.com/openaccess).

Wang, N.; Brickute, D.; Braga, M.; Barnes, C.; Lu, H.; Allott, L.; Aboagye, E. O., Novel Non-Congeneric Derivatives of the Choline Kinase Alpha Inhibitor ICL-CCIC-0019. Pharmaceutics 2021, 13 (7), 1078.

5.1 Introduction to biological evaluation

The aim of this chapter was to assess the effects of the prodrug and PSMA-targeted drug modifications *in vitro*. The pharmacological activity of the compounds were evaluated by kinase screening and antiproliferative assay. The drug selectivity and ADME profiles of the prodrug molecule CK145 and PSMA-targeted molecule CK147 were studied. The *in vitro* conversion investigation of CK145 and CK147 by HPLC, MS and [^{18}F]D4-FCH uptake studies were also carried out to understand the results obtained.

5.2 Evaluation of lipophilicity

Lipophilicity is a crucial physicochemical property in drug discovery and development [204]. According to the International Union of Pure and Applied Chemistry (IUPAC) 'gold book', lipophilicity refers to the affinity of a molecule or a moiety for a lipophilic environment [171]. In medicinal chemistry, this index reflects the capability of drug molecules transporting across the lipid structures (*e.g.* most biological membranes), as well as drugs' interactions with target proteins [204]. Therefore, the investigation of lipophilicity is essential to the preliminary evaluation of novel drug candidates, and it helps medicinal chemists to estimate their pharmacological, pharmacokinetic and pharmacodynamic profiles in biological systems [205].

It is generally accepted that lipophilicity contains two major structural contributions: (1)

hydrophobicity: the term reflects cavity formation, hydrophobic and dispersive forces; (2) polarity: the term reflects more directional electrostatic interactions and hydrogen bonds [206]. Lipophilicity is the concept describing the equilibrium between these two contributions. To determine the lipophilicity of a compound, its distribution behaviour in a biphasic system is measured in either liquid-liquid (a non-polar/organic phase and a polar/normally aqueous phase) or solid-liquid phase (compound retention is analysed on reversed-phase HPLC or thin layer chromatography) [171, 204].

Lipophilicity is mathematically characterised as partition coefficient **P** which is defined as the ratio of the concentrations of a neutral molecule in organic (C_{org}) and aqueous (C_{aq}) phases at equilibrium (Equation 5.1):

$$\mathbf{P} = \frac{C_{org}}{C_{aq}}$$

Equation 5.1: Partition coefficient P calculation. C_{org} and C_{aq} represent the concentrations of a neutral molecule in organic and aqueous phases, respectively.

To facilitate interpretation, lipophilicity is usually expressed in a logarithmic scale, and log P is used to describe the partitioning of unionised species in biphases. For ionisable compounds, distribution coefficient (Log D) is introduced, which takes both neutral and ionised species of the compounds into account at given pH. Log D can be calculated using the equation below (Equation 5.2):

$$\text{Log } \mathbf{D} = \text{Log } \left(\frac{C_{org}}{C_{ionised\ aq} + C_{neutral\ aq}}\right)$$

Equation 5.2: Log D calculation. C_{org} represents the concentration of the neutral fraction of the ionisable compound in organic phase; $C_{ionised\ aq}$ represents the concentration of the ionised fraction of the ionisable compound in aqueous phases, and $C_{neutral\ aq}$ represents the concentration of the neutral fraction of the ionisable compound in aqueous phase.

As previously mentioned, lipophilicity can be measured in either a liquid-liquid system or by

chromatography. The systematic study measuring lipophilicity was first carried out by Hansch and Fujita, who initiated octanol and water as an optimal liquid-liquid system that well mimics compounds' partitioning across cell membrane [207]. In the further research, Hansch established correlation between physicochemical properties of compounds and their biological activities by QSAR modelling based on this system [207, 208]. The shake-flask methodology was accordingly coined and has remained the most classical method for the measurement of lipophilicity. In brief, the Log P values of compounds can be calculated by measuring the compound concentration in two phases using UV spectrophotometry. Key to this method is to ensure that the distribution of the tested compound in two phases reaches equilibrium by sufficient shaking or stirring.

Compared to using reversed-phase HPLC method, shake-flask method is relatively time-consuming and requires larger amounts of compounds with high purity. In addition, it is not applicable to hydrophobic compounds (Log P > 4) [209]. However, shake-flask method is still recognised as the most reliable and accurate method for the compounds with Log P values in the range of -2 to 4 [210, 211].

The Log D values of the synthesised compounds (ICL-CCIC-0019, CK14, CK145, CK146 and CK147) were evaluated using the shake-flask method. The 1-octanol layer was carefully removed and the concentrations of the compounds in the PBS layer (pH: 7.4) was determined. The Log D values were calculated using the formula below (Equation 5.3):

$$\text{Log D} = \text{Log}\frac{C_{\text{Octanol}}}{C_{\text{PBS}}} = \text{Log}\frac{C_{10\ \mu\text{M PBS}} - C_{\text{PBS after shaking}}}{C_{\text{PBS after shaking}}}$$

Equation 5.3: Determination of Log D for ICL-CCIC-0019, CK14, CK145, CK146 and CK147. $C_{Octanol}$ represents the concentration of the compound in the 1-octanol phase; C_{PBS} represents the concentration of the compound in the PBS phase; $C_{10\mu M\ PBS}$ represents the concentration of the compound stock solution in PBS (10 μM), and $C_{PBS\ shaking}$ represents the concentration of the compound in the PBS phase after shaking.

According to the calculation, it can be inferred that a negative value of Log D means the tested compound has a higher affinity to the aqueous phase; namely it is more hydrophilic. As shown in Table 5.1, all the compounds involved, except CK145 displayed negative values of Log D, which means they are highly hydrophilic compounds, due to the quaternary amine in the structures. ICL-CCIC-0019, CK146 and CK147 are three most hydrophilic compounds which had Log D values of about -1. CK145 was more lipophilic among all the compounds since its prodrug bulk group contains Boc group which increased the overall lipophilicity of the molecule. The linker lengths of compounds also had an impact on lipophilicity as the Log D value of ICL-CCIC-0019 was 10 times lower than that of CK14, its counterpart with a longer alkyl linker.

Table 5. 1: Log D values of choline kinase inhibitors involved in the preliminary investigations using shake-flask method. Three repeats of flask shaking were performed for each molecule. Data were presented as mean ± SD.

Compound name	ICL-CCIC-0019	CK14	CK146	CK145	CK147
Log D	-1.12 ± 0.06	-0.14 ± 0.02	-1.13 ± 0.01	0.34 ± 0.01	-0.79 ± 0.02

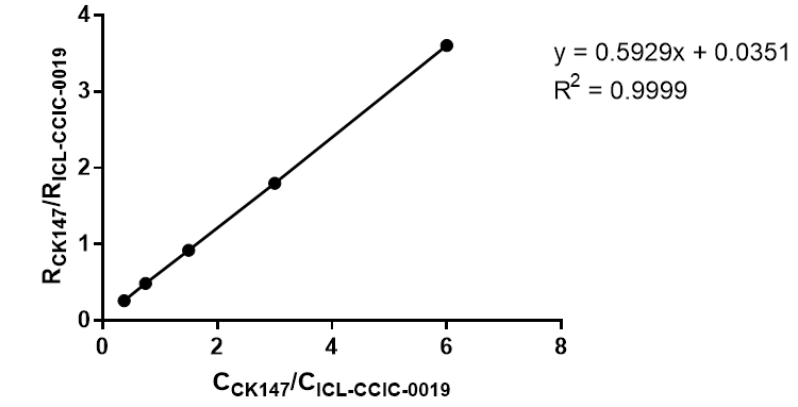
5.3 Chemical stability of conjugate CK147 in serum

As previously introduced, a ligand-drug conjugate (LDC) with targeted delivery function is always substantially complex, and it has to undergo lysosomal degradation to release the toxin part when being delivered specifically to the desired site. To understand the actual mechanism of action of LDCs, it is critical to characterise the stability profiles and explore the possible degradation pathways. The chemical reactions such as solvolysis, hydrolysis, oxidation and racemization could not only cause the loss of the expected activity of the parent drug molecules, but could also lead to the formation of degradation products with side-effects [212].

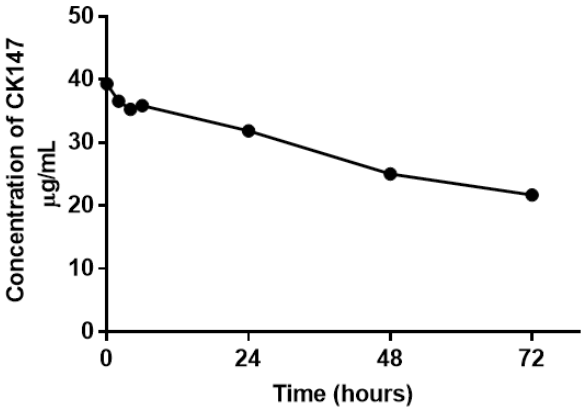
The conjugate stability of CK147 in serum was investigated by analytical HPLC using internal standard methodology. As any loss of sample during sample treatment can be compensated

by the loss of the equivalent degree of the internal standard (*i.e.* the ratio of concentration between the internal standard and the analyte should remain constant, and the ratio of two responses should remain constant), the accuracy of the chromatography analysis is, thus, thought to be improved. To achieve this, the internal standard should often be chemically similar to the analyte and should display a differential response in the analysis.

In this study, the chemical stability of CK147 was investigated in the presence of serum. As a peptide conjugate, the interaction between CK147 and serum albumin could also be checked. ICL-CCIC-0019 served as internal standard because of its structural similarity to CK146, the parent molecule of CK147. The internal standard calibration curve was plotted, where the response ratio between CK147 and ICL-CCIC-0019 was against their concentration ratio (Figure 5.1A). By applying the calibration curve to the response ratio of the samples, the concentrations of CK147 in serum could, thus, be determined. Following 72 hours' incubation, the concentrations of CK147 in the RPMI 1640 medium containing 10% FCS were respectively determined at 0, 2, 4, 6, 24, 48 and 72 hours accordingly (Figure 5.1B). CK147 remained stable in the medium at early time points (93.0 ± 0.8% intact parent at 2 hours and 89.7 ± 0.3% intact parent at 4 hours). After 72 hours' incubation at 37 ˚C, the concentration of CK147 in the medium reduced to 60.0 ± 0.3% (21.7 ± 0.2 μg/mL). However, HPLC/MS analysis confirmed existence of no chemical degradation product of CK147 during the process.



(A)



(B)

Figure 5. 1: The chemical stability characterisation of CK147 in RPMI 1640 medium supplemented with 10% serum at 37 ˚C. (A) the internal standard calibration curve of CK147, where the concentration ratios between the analyte (CK147) and the internal standard (ICL-CCIC-0019) against their response ratios was plotted; (B) CK147 concentration change trend within 72 hours; n=3, mean±SD.

5.4 Antiproliferative activity assessment (SRB Assay)

Antiproliferative activity is one of the most important indicators for biological evaluation of anti-cancer agents *in vitro*. There is a broad spectrum of assays reported in the literature for evaluating drug cytotoxicity and antiproliferative activity in oncological research. The cell death caused by various cytotoxicity mechanisms on cell functioning (*e.g.* cell membrane permeability, ATP production and enzymatic activity) can be determined using these assays

[213]. Common antiproliferative assays can be classified into four categories according to their measurement types at the end points, including: dye exclusion (*e.g.* Trypan blue), colourimetric assays (*e.g.* SRB assay, (3-(4,5-dimethylthiazol-2-yl)-2–5-diphenyltetrazolium bromide (MTT) assay and lactate dehydrogenase (LDH) assay), fluorometric assays (*e.g.* alamarBlue assay) and luminometric assays (*e.g.* ATP assay) [214].

As one of the most commonly used colourimetric assays measuring drug-induced cytotoxicity, SRB assay was used in this project to assess the antiproliferative activity of the synthesised compounds in different cancer/normal cell lines. SRB is a fluorescent dye with a bright pink colour. Structurally, it is an aminoxanthene derivative with two sulfonic groups (Figure 5.1) [173].

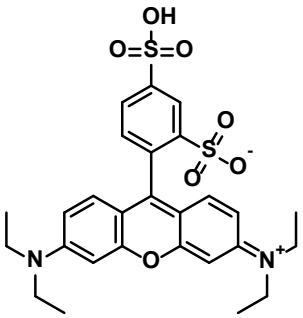


Figure 5. 2: Chemical structure of SRB.

Under mildly acidic environments, SRB molecules bind to the basic amino residues of the cells, and dissociate under basic conditions. The live cells can be stained using SRB after being fixed by TCA. The intensity of the colour from solubilised SRB dye in 10 mM Tris-base (pH = 10) is in response to the viability of cell colony, which permits the colorimetric measurement of cell viability *via* spectrophotometer [214, 215]. Compared to other most used colourimetric assays in the literature, MTT assay, SRB assay is a total protein assay that is less sensitive to condition fluctuations (*e.g.* dye solubility and time) and independent of intermediary metabolism. Therefore, the results obtained from SRB assay have less well-to-well error [214].

5.4.1 Prodrug strategy

To evaluate the antiproliferative activity of prodrug CK145, appropriate cell lines for the test were initially studied using Cancer Cell Line Encyclopaedia RNA sequencing data base. Four cancer cell lines from different origins were selected according to the mRNA levels of HDAC I class and CTSL, including HCT-116, A549, HepG2 and Caco-2 (Table 5.2). The protein expression of the HDAC 1 subtype in the cell lines was then determined using immunoblotting. HDAC 1 was found highly expressed in all selected cell lines, among which HCT-116 and HepG2 displayed highest HDAC 1 protein levels (Figure 5.3).

Table 5. 2: The mRNA levels of four selected cell lines (namely HCT-116, HepG2, A549 and Caco-2) involved in the antiproliferative studies; the data were extracted from Cancer Cell Line Encyclopedia RNA sequencing database).

Cell name / Type	HDAC1	HDAC2	HDAC3	HDAC8	CTSL
HCT116_LARGE_INTESTINE	134.13	23.44	53.53	3.12	26.88
HEPG2_LIVER	58.27	12.10	31.14	2.60	27.77
A549_LUNG	49.61	13.37	27.13	4.64	167.20
CACO2_LARGE_INTESTINE	54.92	21.74	30.81	2.94	42.10

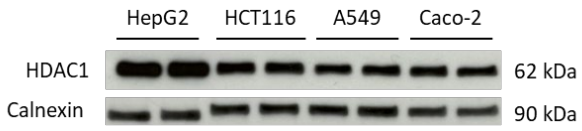


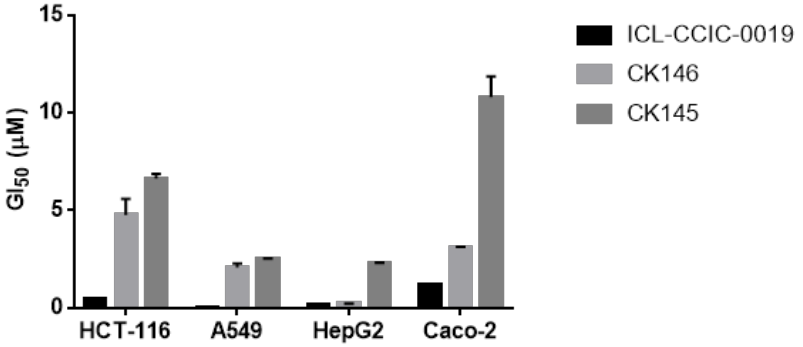
Figure 5. 3: Immunoblotting analysis of HDAC 1 in HepG2, HCT-116, A549 and Caco-2 cell lines; n = 2.

The antiproliferative activities of ICL-CCIC-0019, CK146 and CK145 were first evaluated in these four cell lines by SRB assay to investigate the effects of prodrug modifications (Figure 5.4). All the three tested compounds exhibited good antiproliferative activities against the selected cancer cell lines at low sub-micromolar or micromolar concentrations: ICL-CCIC-0019 turned out to be the most potent (mean GI_{50} in the four cell lines: 0.50 ± 0.02 μM); CK146 also showed lower but effective antiproliferative activity (mean GI_{50} against four cancer cell lines: 2.5 ± 0.3 μM) with HepG2 being most sensitive to the treatment (0.21 ±

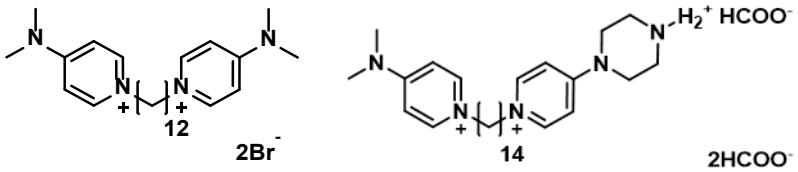
0.01 µM); the overall antiproliferative activity of CK145 (mean GI_{50} against the cell lines: 5.0 ± 0.3 µM) was similar to CK146, but it caused less cell viability loss in HepG2 and Caco-2 cells. Notably, ICL-CCIC-0019 displayed about 10-fold more growth inhibition compared to CK145 in Caco-2 cells, a less tumourigenic colon cancer cell line relative to HCT-116 cells.

	$GI_{50} \pm$ SD (µM)		
Cell lines	**ICL-CCIC-0019**	**CK146**	**CK145**
HCT-116	0.42 ± 0.03	4.76 ± 0.80	6.63 ± 0.20
A549	0.05 ± 0.00	2.07 ± 0.20	2.47 ± 0.06
HepG2	0.18 ± 0.01	0.21 ± 0.01	2.25 ± 0.06
Caco-2	1.19 ± 0.04	3.09 ± 0.05	10.80 ± 1.00

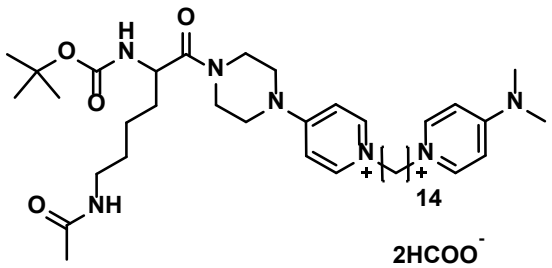
(A)



(B)



ICL-CCIC-0019 **CK146**



CK145

(C)

Figure 5. 4: Growth inhibition of HCT-116, A549, HepG2 and Caco-2 cells by ICL-CCIC-0019,

CK146 and CK145. (A) GI_{50} values were determined by SRB assay; (B) comparison of growth inhibitory activities among ICL-CCIC-0019, CK146 and CK145; n = 6, mean ± SD. (C) chemical structures of ICL-CCIC-0019, CK145 and CK146.

In the following experiments, treatment time was increased from standard 72 hours to 120 hours as has been reported in some prodrug studies (Figure 5.5 and Table S10.1) [168]. Two colon cancer cell lines HCT-116 and Caco-2 cells were involved in this study. Similar to the 72-hour treatment data, all the compounds were less antiproliferative in Caco-2 cells. An increase of GI_{50} in prodrug treatment after 120 hours was seen while those of CK146 remained the same (about 3.20 μM).

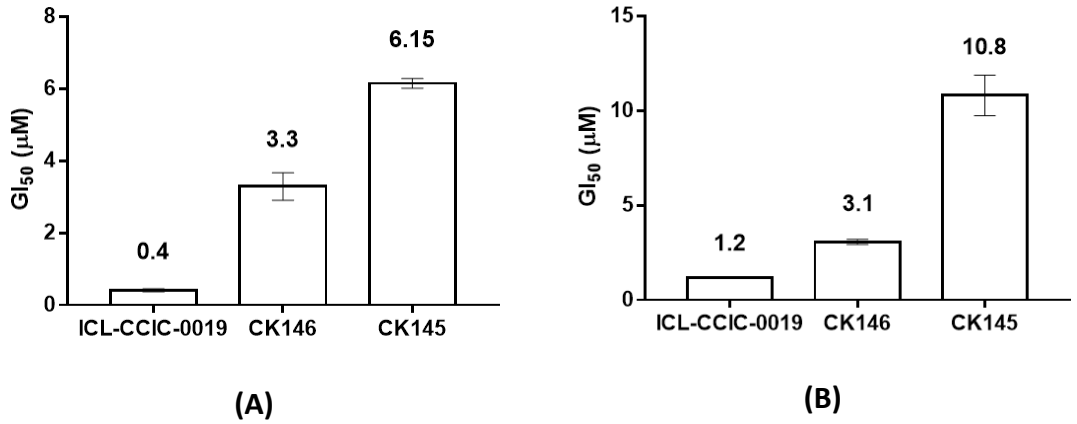


Figure 5. 5: Antiproliferative activities of ICL-CCIC-0019, CK146 and CK145 in two colon cancer cell lines after 120-hour treatment. (A) in HCT-116 cells; (B) in Caco-2 cells; n=6, mean ± SD.

5.4.2 Drug delivery strategy

The antiproliferative activities of the PSMA-targeted CHKA inhibitor CK147, ICL-CCIC-0019 and CK146 were evaluated using the prostatic cell lines with differential expression of PSMA. PSMA-positive cancer cells (22Rv1, C4-2B, LNCap), PSMA-negative cancer cell lines (PC3, R1-AD1, R1-D567 and HCT-116), and a PSMA-negative normal prostatic cell line (PNT1A) were used and checked by immunoblotting (Figure 5.6). As expected, PSMA was found expressed in 22Rv1, C4-2B, LNCap, and all the involved cell lines showed high expression of CHKA.

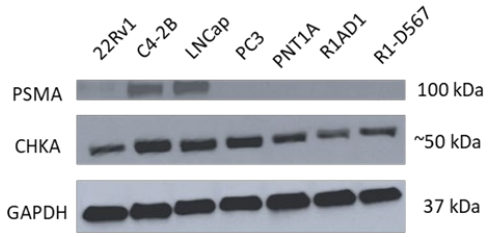


Figure 5. 6: Immunoblotting analysis of PSMA and CHKA in 22Rv1, C4-2B, LNCap, PC3, PNT1A, R1-AD1 and R1-D567 cells; n = 2.

Similarly, ICL-CCIC-0019 and CK146 effectively inhibited the growth of all the selected cell lines with a mean GI_{50} across eight cell lines of 0.6 ± 0.1 μM and 3.8 ± 0.9 μM respectively (Figure 5.7 and Table S10.2). However, all the cell lines involved in the experiment did not show obvious sensitivity towards CK147 and the mean GI_{50} across eight cell lines was up to 66.7 ± 7.2 μM. Furthermore, no correlation was found between compound antiproliferative activities and PSMA expression.

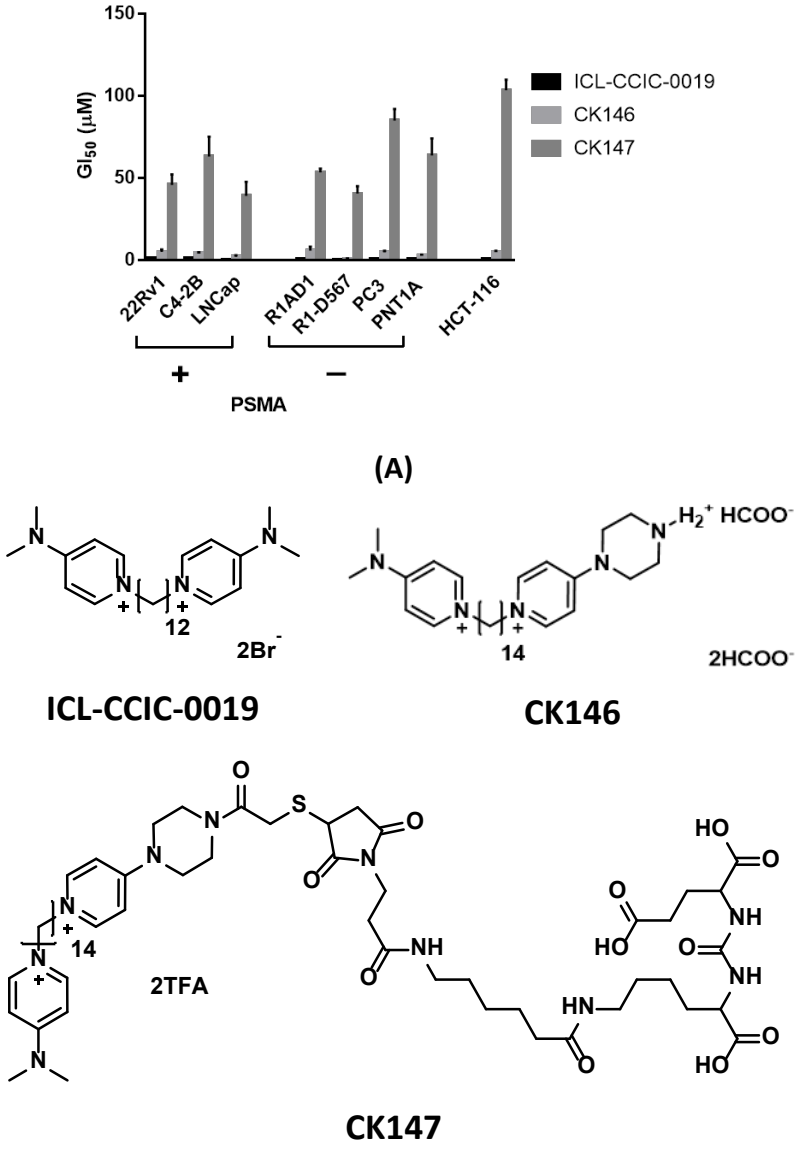


Figure 5. 7: Comparison of growth inhibitory activities among ICL-CCIC-0019, CK146 and CK147 in 22Rv1, C4-2B, LNCap, PC3, PNT1A, R1-AD1, R1-D567 and HCT-116 cells; (A) n = 6, mean ± SD; (B) chemical structures of ICL-CCIC-0019, CK146 and CK147.

5.5 Cellular uptake and *in vitro* metabolism

Cell membrane is a vital component of cells with a very complex composition and spatial structure [216]. Functionally, it not only maintains the structural integrity of cells, but also provides a stable intracellular environment for substance exchange and signalling communication [216, 217]. Cell membrane is selectively permeable, which means the passages of molecules into cells are regulated, and molecules of varying types exploit different transport mechanisms to enter cells [218]. The structure of cell membrane consists of lipid bilayer (three major lipid species are involved: glycerophospholipids, sphingolipids and cholesterol), membrane proteins and sugars [216]. As the most abundant component in membrane, lipids, as amphipathic molecules, spontaneously form bilayers as the most preferable configuration in which the hydrophilic heads of lipids are oriented towards the aqueous environment while their hydrophobic tails are oriented inward towards each other (Figure 5.8). This special configuration entitles the continuous motility of the membrane, and more importantly, it makes lipid bilayer a natural barrier to the passage of molecules and ions in and out of the cell [216].

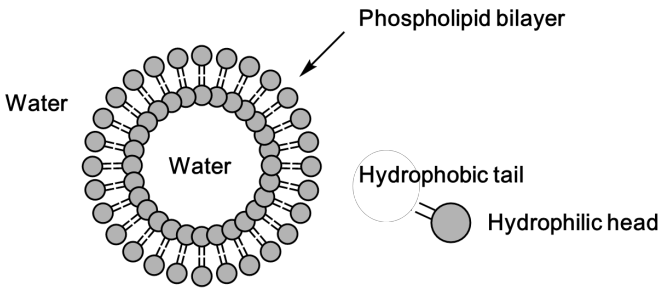


Figure 5. 8: Spontaneous formation of bilayers by lipids. The hydrophilic heads of lipids point towards the aqueous environment in bilayers; the hydrophobic tails point inward away from the water.

The selective passage function of phospholipid bilayer requires the involvement of membrane proteins [217]. As the most important components of the cell membrane, various proteins, such as channels, carriers and ion pumps, play critical roles in mediating the transport of molecules [217]. The existence of phospholipid bilayer prevents the non-

membrane transport-mediated transfer of large or charged molecules [216]. Unlike small molecules such as water, large or charged molecules are not able to cross the membrane by simple diffusion. In the presence of electrochemical gradients, ions can passively travel from a high concentration area to a low concentration area *via* channel proteins [216]. The process requires membrane proteins but no energy input and is thus called passive transport. The transport of some amino acids into cells utilises this mechanism [216]. In contrast, active transport, responsible for the transport of most large or charged exotic molecules, moves the species against the concentration gradients. This process always requires the energy compensated from ATP, light or even the gradient travel of the other molecules *via* the same transporter (Figure 5.9).

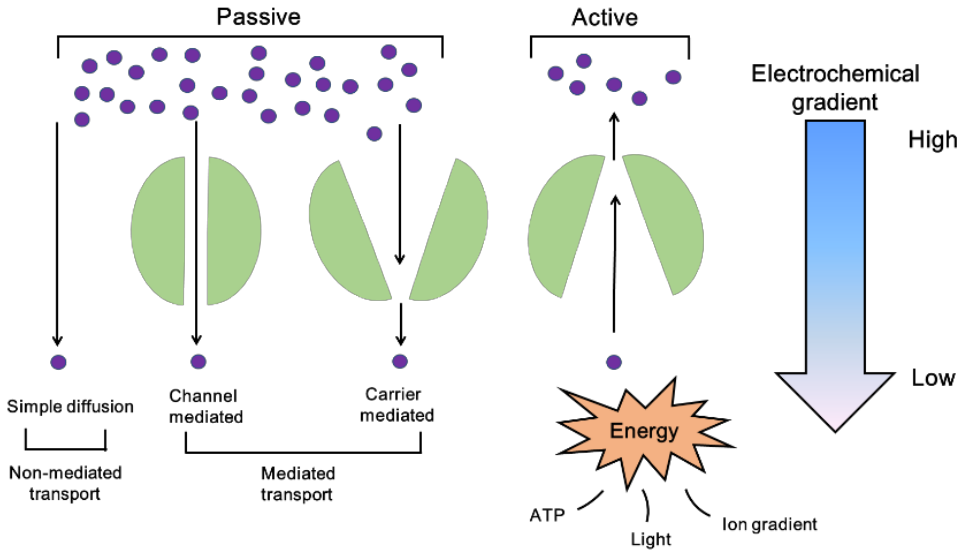


Figure 5. 9: Passive and active transport. Different types of membrane proteins involved in the processes are shown.

The cellular uptake efficiency of therapeutic molecules is key for exerting their pharmacological functions by acting on the intracellular targets. The evaluation of cellular uptake is instructive in the early-stage development of drug candidates. As previously introduced, the transport of choline and choline derivatives requires the involvement of transmembrane proteins including CHT, CTL and OCT families [19]. The cellular uptake of ICL-CCIC-0019 was hypothesised to be also mediated by these protein species. In this section, the cellular uptake efficiency and the possible metabolic mechanisms of novel ICL-CCIC-0019

derivatives CK145 and CK147 were investigated by analytical HPLC and MS.

5.5.1 Prodrug strategy

The cellular uptake studies of ICL-CCIC-0019 and CK145 were conducted in colorectal cancer HCT-116 cells. The external standard calibration curves of ICL-CCIC-0019 and CK145 were first established (Figure 5.10). Instead of being added to the unknown sample (internal standard method), the external standard is normally the analyte itself and is run alone at different concentrations [219]. The amount of the unknown sample can be predicted by calibration curve interpolation using the response of the analyte (*e.g.* peak area). External standard method is usually used when there is no need to correct the sample losses caused by complex sample preparation such as extraction and evaporation [219].

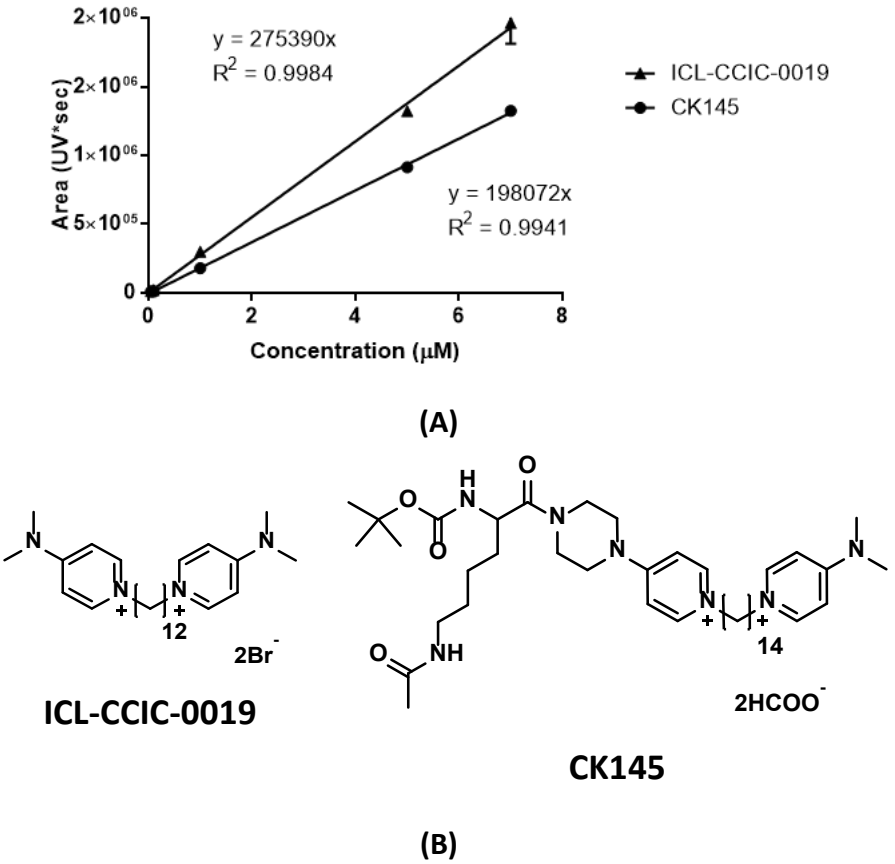
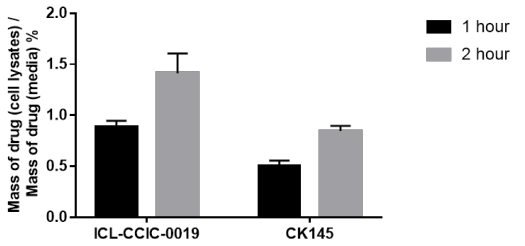


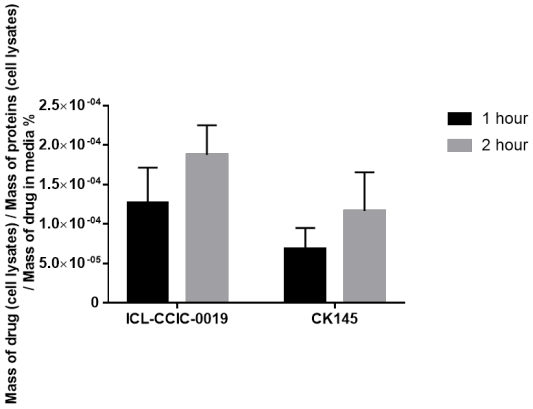
Figure 5. 10: Calibration curves of ICL-CCIC-0019 and CK145 (HPLC method F; wavelengths used: 254 nm) (A) the concentration range used for both compounds: 50 nM, 100 nM, 1 μM, 5 μM and 7 μM). For each concentration, at least three injections were performed; (B)

chemical structures of ICL-CCIC-0019 and CK145.

The concentrations of ICL-CCIC-0019 and CK145 in the HCT-116 cell lysates after incubation were determined by their external calibration curves. The compound amount in cells were calculated using the volumes of the lysate supernatant and were eventually normalised to cell protein amount in each plate by BCA assay. It was seen that both cellular uptake of ICL-CCIC-0019 and CK145 increased along with the incubation time (at 1 hour and 2 hours) (Figure 5.11). The cellular uptake in ICL-CCIC-0019 was approximately two-fold higher than CK145 at 1 hour and 2 hours' post incubation (ICL-CCIC-0019: 0.89 ± 0.06% at 1 hour and 1.41 ± 0.19% at 2 hours; CK145: 0.51 ± 0.05% at 1 hour and 0.85 ± 0.05% at 2 hours).



(A)



(B)

Figure 5. 11: Investigation of the fractional uptake of ICL-CCIC-0019 and CK145 in HCT-116 cells, determined by HPLC at selected time points (1-hour and 2-hour) (HPLC method F; wavelengths used: 254 nm). (A) percentages of compound amount in cell lysates versus the initial compound amount in media; (B) percentages of compound amount in cell lysates versus in media per unit protein; n = 3, mean ± SD.

The *in vitro* conversion of CK145 to other analytes in HCT-116 cells was also investigated at different incubation times; no conversion was observed (Figure 5.12 and S10.10). CK146 or other relevant intermediate species that could arise from cellular active efflux were also examined but were not detected in the media solution (Figure S10.11). The LOD of the HPLC method used was, thus, determined and it was confirmed that the intracellular concentration of CK145 metabolites, if any, was lower than the LOD value 1.382 µg/L.

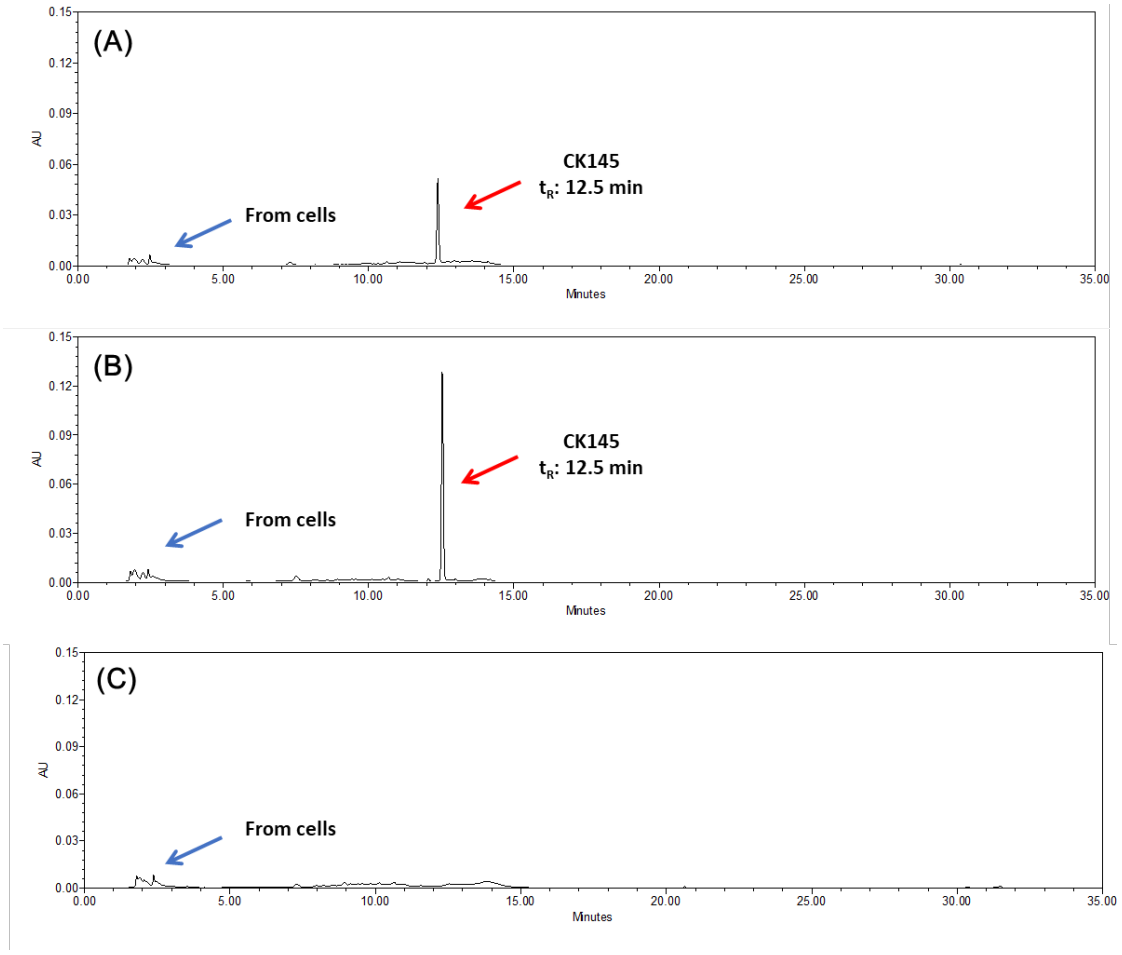
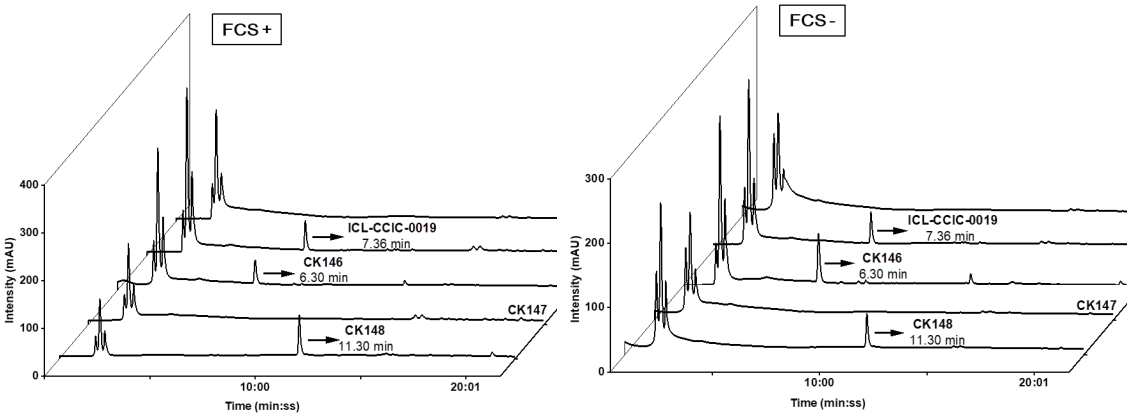


Figure 5. 12: HPLC analysis of HCT-116 cell lysates after 1 h and 2 h incubation with or without CK145 (50 µM in 5 mL RPMI medium) (HPLC method F; wavelengths used: 254 nm). The signals of cells and the signal of CK145 were labelled with blue and red arrows, respectively. (A) the HPLC chromatogram of HCT-116 cell lysates after 1-hour incubation with CK145 treatment; (B) the HPLC chromatogram of HCT-116 cell lysates after 2-hour incubation with CK145 treatment; (C) the HPLC chromatogram of HCT-116 cell lysates after 2-hour incubation without CK145 treatment (the vehicle group). Similar results were observed in three independent experiments.

5.5.2 Drug delivery strategy

The cellular uptake study of CK147 was also conducted in PCa C4-2B cells. In this study, two experimental conditions were investigated so as to evaluate the effects of serum on the compound uptake. Media supplemented with 10% FCS (the FCS positive group) or FCS-free medium (the FCS negative group) was used. Four synthesised compounds, ICL-CCIC-0019, CK146, CK147 and CK148 (the $(OtBu)_3$-protected form of CK147), were investigated in the experiment for comparison. The peak areas of compound signals from the HPLC chromatograms were integrated and calibrated using background noise from the cells. The intracellular concentrations of the compounds were eventually normalised to cell protein amount in each plate by BCA assay. It was seen in both experimental groups that ICL-CCIC-0019 (retention time (t_R): 7.36 min:sec), CK146 (t_R: 6.30 min:sec) and CK148 (t_R: 11.30 min:sec) were detected in the cell lysates by HPLC following 4-hour incubation; the cellular uptake of CK147, however, was not observed (Figure 5.13).



(A) **(B)**

Figure 5. 13: Cellular uptake study of ICL-CCIC-0019, CK146, CK147 and CK148 in C4-2B using medium with or without FCS (HPLC method G; wavelengths used: 254 nm)**.** (A) HPLC chromatograms of compound uptake analysis in medium supplemented with 10% FCS; (B) HPLC chromatograms of compound uptake analysis in FCS-free medium. The detected compounds were arrowed with their retention times (t_R, min:sec).

In detail, ICL-CCIC-0019 and CK146 had similar mean uptake of 24.9 ± 1.4 % μg^{-1} protein and

34.1 ± 0.6 % μg^{-1} protein for FCS positive and negative groups, respectively (Figure 5.14). Significantly higher cellular uptake in both experimental groups was seen for CK148 (mean ± SD in two experiment groups: 42.5 ± 11.5 % μg^{-1} protein) compared to its deprotected form CK147 (Figure 5.14). All compound uptake was found statistically to be independent of the presence of FCS. All the tested compounds were to be confirmed stable in the cells and medium according to the HPLC/MS analysis results of the cell lysates and the medium after 4-hour incubation: compound decomposition or interconversion was not observed (Figure S10.12 - 10.21).

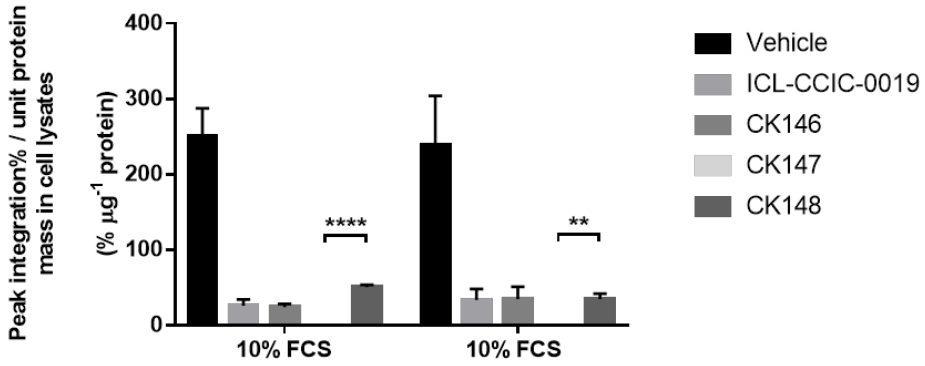


Figure 5. 14: Drug uptake percentages following 4-hour incubation with ICL-CCIC-0019, CK146, CK147 and CK148 in medium with or without FCS (HPLC method G; wavelengths used: 254 nm)**.** The data were calculated from chromatographic peak integration normalized to protein amount in cell lysates; n = 3, mean ± SD; *P* values *via* unpaired two-tailed *T*-test: ****$P < 0.0001$, **$P < 0.01$.

5.6 Lipid kinase screening

As proposed CHKA inhibitors, the kinase specificity of ICL-CCIC-0019, CK14, CK144, CK145, CK146 and CK147 against other important human lipid kinases were investigated to examine selectivity. The compounds of interest were tested against a panel of 15 human lipid kinases by Dundee University (Medical Research Council Protein Phosphorylation and Ubiquitylation Unit, International Centre for Kinase Profiling) using the ADP-Glo™ Kinase Assay.

Of the 500 protein kinases identified in the human kinome, there are approximately 20 lipid kinases [220]. The test panel involved 15 purified recombinant human lipid kinases, and the

ADP-Glo™ assay measures generated ADP as a function of the kinase reaction *via* a luciferase reaction (Figure 5.15). In brief, the kinase reaction was performed in a 96-well plate; the addition of the ADP-Glo™ Reagent into each well stops the reaction and deplete the unreacted ATP molecules. In the second step using Kinase Detection Reagent, the ADP molecules formed in the kinase reaction, on the other hand, is converted to ATP responsible for producing luminescence to be recorded. The luminescence intensity, therefore, correlates to the amount of ADP generated in the kinase reaction, which is indicative of kinase activity.

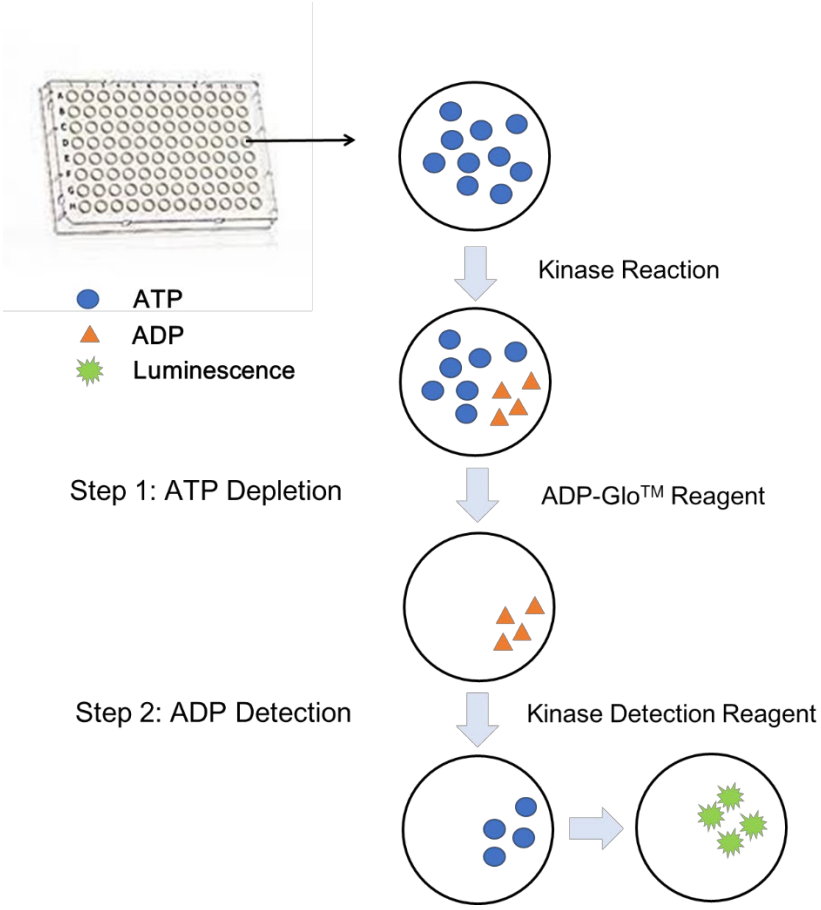
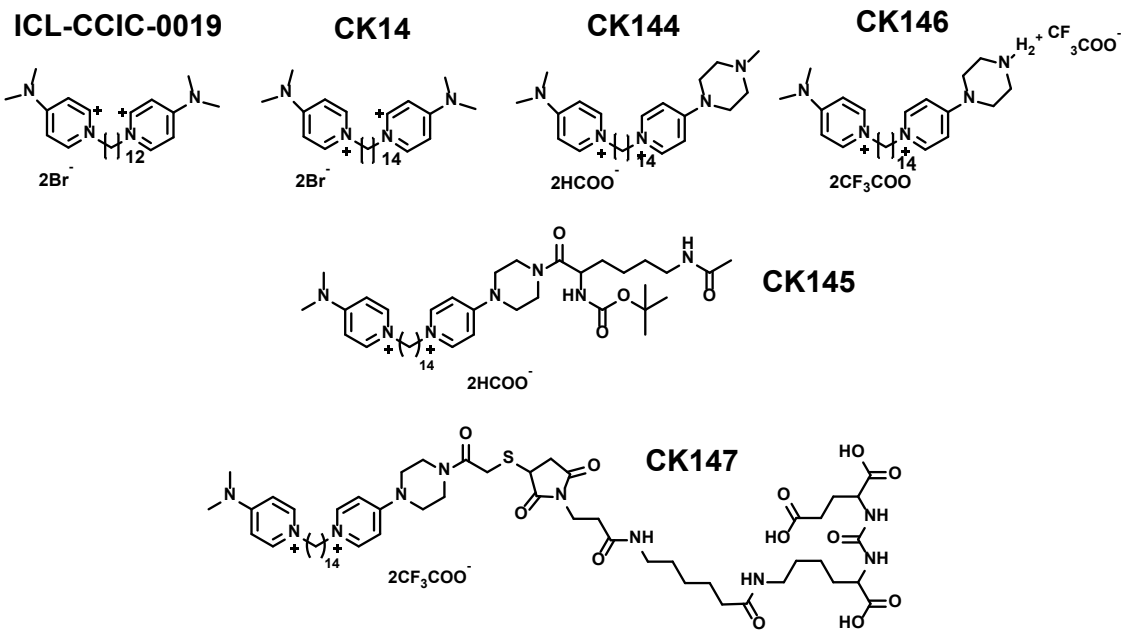
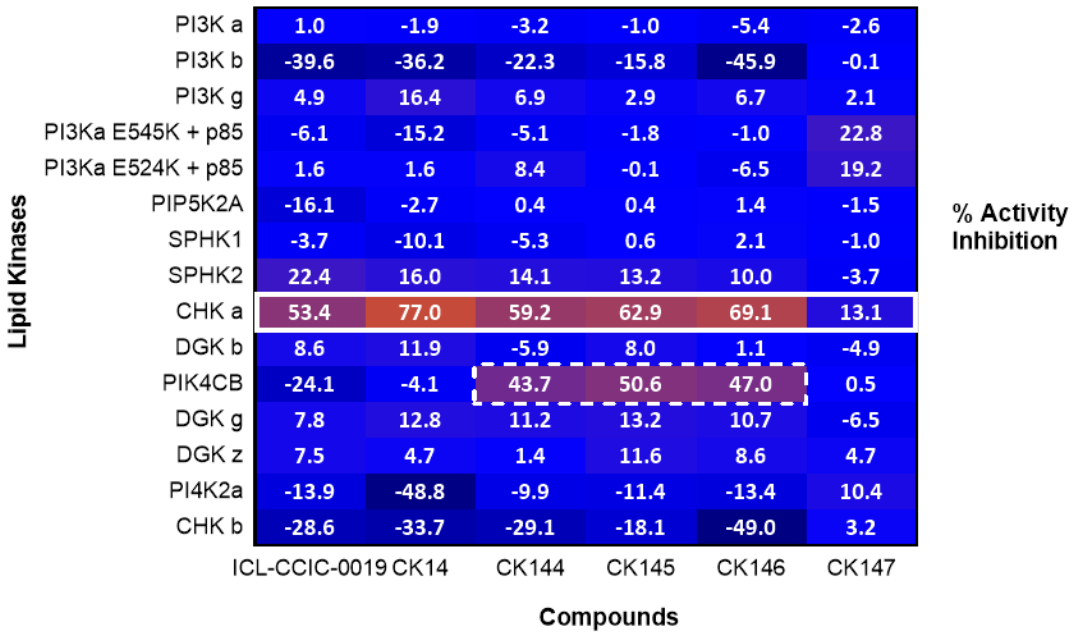


Figure 5. 15: The principle of ADP-Glo™ Kinase Assay. The assay involves two steps. In the first step, the ADP-Glo™ Reagent is used to terminate the kinase reaction and deplete the unreacted ATP, which interferes with subsequent luminescence production; in the second step, the Kinase Detection Reagent is used to convert the ADP generated in the kinase reaction into ATP, permitting the measurement *via* a luciferase reaction. The luminescence correlates with kinase activity.

In this experiment, the lipid kinase reaction was incubated in 96-well plates with the synthesised CHKA inhibitors. The inhibitory effects of the compounds on CHKA and the potential off-target effects on the other important human lipid kinases were evaluated (Figure 5.16, Dundee Lipid Kinase Screening service, for full data table see Appendix B). ICL-CCIC-0019, CK14, CK144, CK145 and CK146 showed low off-target effects and exhibited good inhibitory activities against CHKA (53.4 - 77.0% inhibition) at the tested concentration of 10 μM. As expected, the tetradecyl linker used in CK14 led to superior CHKA affinity compared to the dodecyl linker used in ICL-CCIC-0019 (the CHKA activity inhibited: ICL-CCIC-0019: 53.4 ± 2.4% and CK14: 77.0 ± 10.2%). Among all the tested compounds, CK14 was the most active and inhibited about 77% of the CHKA activity. CK146, as an adaptable structure of ICL-CCIC-0019 suitable for further modification, exhibited higher CHKA activity compared to ICL-CCIC-0019 (69.1 ± 11.2% and 53.0 ± 2.4%, respectively). CK145, the proposed prodrug molecule, also displayed good CHKA activity (62.9 ± 3.6%), while CK147, the proposed PSMA-targeted peptide conjugate was proved inactive in the test panel. An interesting finding in this experiment was to see the effective inhibition against phosphatidylinositol 4-kinase beta (PIK4CB) enzyme by CK144, CK145 and CK146, with 43.7 ± 1.9%, 50.6 ± 4.5%, 47.0 ± 0.6% inhibition, respectively.



(A)



(B)

Figure 5. 16: Heatmap of lipid kinase selectivity screening against 15 human lipid kinases using ICL-CCIC-0019, CK14, CK144, CK145, CK146 and CK147. (A) the chemical structures of ICL-CCIC-0019, CK14, CK144, CK145, CK146 and CK147; (B) the inhibition% of CHKA and PIK4CB are boxed in white and dash-line rectangles respectively. The data in percent represent the mean kinase activity inhibited by drug molecules. Tested concentration of the

CHKA inhibitors in the assay: 10 μM.

5.7 ADME study

The pharmacokinetic profiles of a compound are normally defined as its ADME properties, namely absorption, distribution, metabolism and excretion, which describe the overall deposition of the compound by interacting with organisms [208]. Once a drug is administered, it will move from the site of administration into bloodstream, which is defined as absorption process. After that, the differential distribution of the drug from the blood to tissues will be seen due to its physicochemical properties and transportation mechanisms. The drug taken into tissues, normally recognised as a xenobiotic, will be chemically processed by enzymatic systems (mostly in liver) to increase its polarity and water solubility, which facilitates the excretion of the drug from the body. This process is called metabolism. In the last phase, the drug molecule and its metabolites will be eliminated from the body *via* different routes of excretion such as urine, feces and sweat.

The ADME profiles of drug candidates are instructive throughout the whole drug discovery and development pipeline, from the early drug discovery and *in vivo* efficacy evaluation, to preclinical and final clinical studies. The vast majority of drug candidates fail in clinical trials because of the lack of efficacy or unacceptable side effects, manifested by poor bioavailability as a result of ineffective intestinal absorption or undesirable metabolic stability [221]. The effectiveness of drugs can be seen as a crucial balance among pharmacokinetics, toxicity and potency. In the early stage of drug discovery, the potency of drug candidates is a main driving factor. However, the pharmacokinetic behaviour of drug candidates can predict whether they can achieve success in the clinic [222]. *In vitro*/*in vivo* drug metabolism and pharmacokinetic (DMPK) studies are important tools to establish if a lead compound can be selected as a drug candidate at the early stage and lead optimisation phase (‘hit to lead’) of drug discovery.

In this section, the *in vitro* ADME studies of ICL-CCIC-0019, CK14, CK144, CK145, CK146 and CK147 were performed by Charles River Drug Discovery Services (Essex, UK) using developed

protocols based on the FDA draft guidance for industry: In vitro Metabolism and Transporter-Mediated Drug-Drug Interaction studies.

5.7.1 Kinetic solubility and permeability

The solubility and permeability (intestinal) of drug molecules, interrelated with other physicochemical properties, are the major factors affecting the absorption rate and extent [223]. In IUPAC gold book, solubility is defined as the analytical composition of a saturated solution expressed as a proportion of a designated solute in a designated solvent [171]. At the molecular level, solubility represents the degree to which solute molecules/ions are solvated by the solvent and diffuse freely throughout the solution. Solubility is a critical physicochemical property as dissolution of drug molecules has long been identified as a limiting factor of absorption process because only the compounds in solution form are available for permeation across the gastrointestinal membrane [223].

Permeability is another important physicochemical property to achieve desirable absorption and distribution; it is a parameter demonstrating the ability of molecules traveling through the biological membranes, and can be assessed from different aspects of molecules, including lipophilicity, hydrophilicity (hydrogen bonding ability), molecular size and flexibility [223].

The Biopharmaceutics Classification System (BCS) classifies drug substances into four categories according to their solubility and permeability, which substantially guides the selection and approval process for a large number of drug candidates (Figure 5. 17) [224]. Drug molecules from Class I and II are recognised with high permeability and thus can undergo extensive metabolism as elimination routes, while the major elimination routes of the compounds categorised in Class III and IV (low permeability compounds) are mainly excreted *via* renal and biliary systems [225].

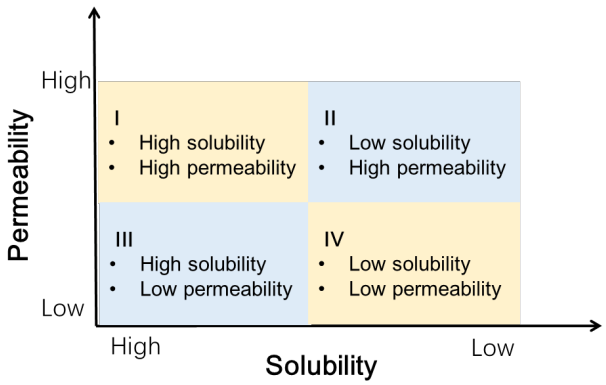


Figure 5. 17: Biopharmaceutics Classification System (BCS) as proposed by Amidon *et al.* [224].

5.7.1.1 Kinetic solubility

The normal reported solubility determination methods can be divided into the methods for determining thermodynamic solubility and methods for determining kinetic solubility [226]. The main difference between two methodologies lies in the use of the tested compound in its solid state (thermodynamic) or in a pre-dissolved solution (kinetic); accordingly, the investigations on thermodynamic solubility attempts to examine the extent to which the compound dissolves, while the kinetic solubility assays reveal the extent to which the compound precipitates [226]. Thermodynamic solubility is the gold standard for optimisation of drug candidates in terms of solubility targeting [226]. By contrast, kinetic solubility determination is less labour-intensive and more available for process automation because the drug samples are pre-dissolved as a stock solution, typically prepared in DMSO (10 mM) [226].

In this study, the kinetic solubility of the CHKA inhibitors synthesised were determined and presented in molarity (µM) (Table 5.3).

Table 5. 3: Kinetic solubility of ICL-CCIC-0019, CK14, CK144, CK145, CK146 and CK147; n = 2, mean ± SD.

Compounds	Kinetic Solubility (μM)
ICL-CCIC-0019	160.5 ± 6.4
CK14	154.0 ± 5.6
CK144	148 ± 2.8
CK145	177.5 ± 10.6
CK146	158 ± 2.8
CK147	184 ± 9.9

The top concentration used in the assay was 200 μM and the solubility classifications in 0.1 M PBS (2% DMSO, pH: 7.4) are as follows (Table 5.4):

Table 5. 4: Kinetic solubility classifications.

Solubility Class	Determined concentration (μM)
High	≥ 150 μM
Moderate	50 - 150 μM
Low	≤ 50 μM
Very low	< 5 μM

All the submitted compounds displayed high solubility in the performed kinetic solubility assay, and their determined concentrations were over 150 μM in 0.1 M PBS buffer.

5.7.1.2 Permeability and efflux assay

Caco-2, a human colon carcinoma cell line, is a common model used for intestinal permeability prediction and efflux evaluation of drug molecules [227]. The sigmoidal relationships between the drug fractions absorbed by humans and their apparent permeability coefficient (Papp) across Caco-2 monolayers have been revealed [228]. When cultured, Caco-2 cells differentiate into a monolayer with similar functions to the small intestinal villus epithelial cells, which form an intestinal monolayer wall as a rate-limiting barrier to absorption of dissolved drug molecules [227]. The reconstitution of Caco-2 cells allows the investigation of passive diffusion, uptake and efflux of drug molecules across the monolayer, and thus serves as the gold standard for the prediction of intestinal drug

permeability and absorption *in vitro* [229, 230].

Practically, Caco-2 cells are grown on permeable filter supports in a monolayer which divides the system into two chambers (Figure 5.18) [227, 228]. The drug transport is assessed in these two directions, namely the apical to basolateral (A - B) direction and the basolateral to apical (B - A) direction across the Caco-2 monolayer (Figure 5.18) [227].

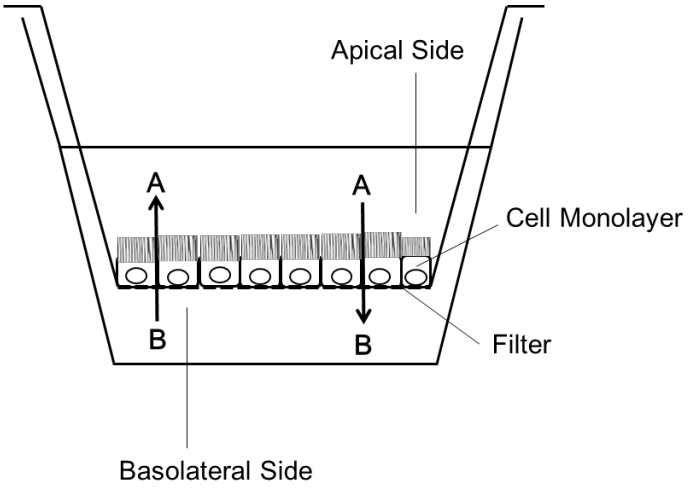


Figure 5. 18: Schematic illustration of the Caco-2 monolayer cultured on a permeable filter support.

Papp values of both directions can be calculated by the steady-state appearance rate of the drug molecule on the receiver side, divided by the initial concentration on the donor side and the surface area of the monolayer (Equation 5.4) [228, 231].

$$\text{Papp (cm/s)} = \frac{dQ/dt}{C_0 \times A}$$

Equation 5.4: Calculation of the Papp value. dQ/dt represents the appearance rate of the compound in the receiver compartment (steady-state flux); C_0 represents the initial concentration of the compound in the donor compartment and A represents the surface area of the Caco-2 monolayer.

As many brush border enzymes and transport proteins responsible for the mediation of active uptake or efflux of drugs in intestine also exist in Caco-2 cells, the Caco-2 cell

monolayer can also be used to understand the transport mechanism of drug molecules [227]. The drug concentrations in both sides are quantified by LC-MS *via* the calibration methods established. The efflux ratio (Papp B - A/ app A - B) of the drug molecules across the monolayer can be calculated to assess the bidirectional permeability of drugs. It indicates whether drug molecules undergo active efflux, namely being actively pumped out of the cells [229]. A drug molecule is suggested subject to active efflux if its efflux ratio is greater than 2 [232].

However, it should also be noted that there are limits to use Caco-2 cell models in predicting *in vivo* drug absorption: not all the important intestinal drug-metabolising enzymes are expressed in Caco-2 cells, such as CYP3A4, although it was confirmed that this enzyme can be induced by dihydroxy-vitamin D3 [233]. In addition, the buffer (*e.g.* HEPES) and the drug molecules that have inhibitory effects on uptake transporters are not suitable for this model.

The drug permeability of ICL-CCIC-0019, CK14, CK144, CK145, CK146 and CK147 was evaluated using the Caco-2 cell model, and the data were presented as Papp in A to B and B to A in Table 5.5. The recovery rates of both directions were also calculated and were recognised appreciable. All the tested compounds displayed low intestinal permeability classification (< 5×10^{-6} cm/s) according to the predictor of intestinal permeability (Table 5.6).

Table 5. 5: Compound permeability data (Papp) and efflux ratios. All the data were presented as mean values, n = 2.

Compounds	Papp A-B ($\times10^{-6}$ cm/s)	Papp B-A ($\times10^{-6}$ cm/s)	Recovery A-B %	Recovery B-A %	Efflux ratio $\frac{Papp\ B-A}{Papp\ A-B}$
ICL-CCIC-0019	< 0.1	0.9	86	85	> 8.6
CK14	< 0.1	8.7	87	80	> 87
CK144	< 0.1	0.5	98	64	> 5.2
CK145	< 0.1	0.3	107	101	> 2.8
CK146	< 0.1	0.3	114	93	> 2.6
CK147	< 0.1	< 0.1	89	78	no data*

*Poorly permeable compound which prevented the calculation of an efflux ratio.

Table 5. 6: Permeability classifications.

Permeability Classification	Papp A-B ($\times 10^{-6}$ cm/s)
Low	< 5
Moderate	5 - 20
High	> 20

All the tested compounds are suggested subject to drug efflux as the efflux ratios are all over 2. Interestingly, CK14 was proved strikingly subject to efflux effects with an efflux ratio up to 87; permeability of CK147 was too poor to permit the calculation of the efflux ratio. All the other compounds exhibited low efflux.

5.7.2 Fasted state simulated gastric fluid (FaSSGF) stability

To improve the efficiency, it is advantageous to predict the oral behaviour of drugs *in vivo* by investigating drug dissolution and stability *in vitro* using simulation of gastrointestinal conditions [234]. Over the past two decades, biorelevant media that resemble the key parameters of human gastrointestinal physiology have been developed [234]. Fasted state simulated gastric fluid (FaSSGF) is one of the biorelevant dissolution media used for the *in vitro* simulation of the fasted conditions. The medium is normally a mixed buffer of hydrochloric acid, sodium chloride, pepsin and water, and has an extremely low pH lying in the range of 1.5 - 1.9 [234]. The stability of drug molecules for oral administration under the fasted state can be evaluated using the FaSSGF buffer. The drug remaining concentrations and their half-lives are calculated using LC-MS *via* the calibration methods established.

The FaSSGF stability of ICL-CCIC-0019, CK14, CK144, CK145, CK146 and CK147 was tested using the FaSSGF buffer (pH: 1.6) (Table 5.7). It was seen that all the tested compounds, except for CK145, were stable in the FaSSGF buffer, and all the half-lives were over 10 h. The half-life of CK145 was 9.2 h.

Table 5. 7: Compound half-lives of the FaSSGF stability test. All the data were presented as mean values, n = 2.

Compounds	Half-life (Hrs)	Percent remaining %
ICL-CCIC-0019	> 10	117
CK14	> 10	95
CK144	> 10	99
CK145	9.2	74
CK146	> 10	92
CK147	> 10	97

5.7.3 Human Microsome Metabolic Stability

Liver is the primary drug metabolism site in the body. Most marketed compounds (> 60%) are reported to be cleared under the metabolism mediated by cytochrome P450 enzymes, a super monooxygenase family mostly found in liver [235]. At the early stage of drug discovery, the metabolic stability screening *in vitro* using different liver systems is often used to assess the potential first-pass clearance effect of drug candidates and to predict their hepatic metabolism *in vivo* [235]. These studies are routinely involved in the early drug discovery processes since they reveal *in-vitro* and *in-vivo* correlations. Using these approaches, drug candidates can be selected based on the metabolic stability or can be accordingly optimised with the knowledge of the metabolism mechanisms undergone [235].

There is a variety of test systems to assess drug metabolism *in vitro*, including recombinant enzymes, liver microsomes, liver S9 fractions (microsomes and cytosol), hepatocytes and isolated liver slices (Figure 5.19) [236]. Microsomes are the vesicles of hepatocytes that only contain the endoplasmic reticulum subcellular fraction [236]. The major enzymes located in the endoplasmic reticulum membrane include cytochrome P450s (Phase I enzymes), a super enzyme family with mixed oxidase functions, and Uridine 5'-diphospho-glucuronosyltransferase (UGTs) (Phase II enzymes), an enzyme family that conjugates the sugar molecule uridine-diphosphate-glucuronic acid (UDPGA) to the exotic substrates or Phase I enzyme products and facilitates their further metabolism [237, 238].

Although microsomes are one of the mostly used systems for metabolic stability assay due to several benefits such as low cost, robustness and suitability for high throughput screening or automation, the utility of human S9 fractions was preferred in this test. For early drug discovery stage, S9 fractions are inexpensive compared to hepatocytes, and they further contain the cytosolic enzymes compared to microsomes, which therefore can provide more metabolic information for certain chemotypes [236].

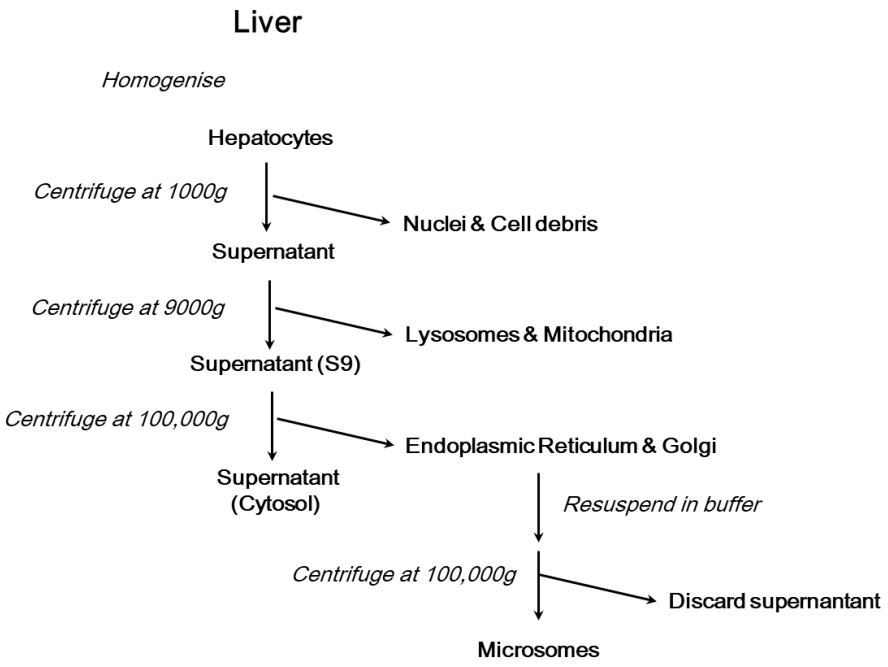


Figure 5. 19: Preparation of subcellular fractions.

The metabolic stability of compounds is typically determined by measuring their depletion over time using the S9 fraction system. The test compounds in samples are quantified using LC-MS methodology, and the metabolic half-lives of the compounds can be derived from the data of percent remaining versus time. Intrinsic clearance (Cl_{int}) can also be calculated once the microsomal protein content in the assay is determined. The *in vitro* Cl_{int} can be then scaled up to a predicted *in vivo* clearance which takes physiologically based parameters into account, including hepatocellularity (microsomes per liver), liver weight and liver blood flow. The *in vivo* clearance is an important metabolic parameter which predicts the actual clearance of the drug candidates in humans.

All the tested compounds except for CK145 seemed stable in the study (Table 5.8). ICL-CCIC-0019, CK14, CK144 and CK146 exhibited long metabolic half-lives (> 100 min), which therefore gave low clearance values (Cl_{int} < 14 µL/min/mg; predicted *in vivo* clearance < 10 mL/min/kg). By contrast, CK145 had a short metabolic half-life of 7.4 min.

The percentage of compound removed compared to liver blood flow (PCT_LBF) was also calculated (Table 5.8). The short metabolic half-life of CK145 gave not only a high predicted *in vivo* clearance value (19 mL/min/kg), but also a PCT_LBF up to 92%. As human hepatic blood flow is approximately 20 mL/min/kg, having a predicted *in vivo* clearance to close to that of human hepatic blood flow means that CK145 will leave the body very quickly [239]. All the other tested compounds had long metabolic half-lives and therefore lower PCT_LBF% (< 45%).

Table 5. 8: Human microsome metabolic stability data of ICL-CCIC-0019, CK14, CK144, CK145, CK146 and CK147 using S9 fractions. All the data were presented as mean values, n = 2.

Compounds	Half life (min)	Cl_{int} (µL/min/mg) (mg of protein in the assay)	Predicted *in vivo* clearance (mL/min/kg)	PCT_LBF %	Percent remaining %
ICL-CCIC-0019	> 100	< 14	< 10	< 45	92
CK14	> 100	< 14	< 10	< 45	101
CK144	> 100	< 14	< 10	< 45	115
CK145	7.4	188	19	92	2
CK146	> 100	< 14	< 10	< 45	127
CK147	> 100	< 14	< 10	< 45	105

5.8 [^{18}F]D4-FCH uptake *in vitro* study

Several PET tracers have been developed to visualise abnormal choline metabolism in certain malignancies with the cholinic phenotype. These radiotracers that are normally positron-labeled choline analogues, have been applied widely in the noninvasive detection of cancer by PET imaging (Figure 5.20) [240].

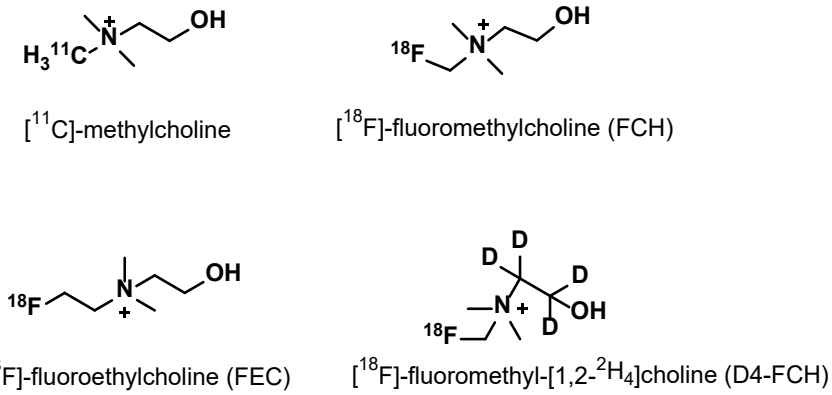


Figure 5. 20: Chemical structures of typical radiotracers related to choline metabolism in current use and development [240].

[^{11}C]-methylcholine was designed as a [^{11}C]-labelled choline analogue, and has been widely used in tumour metabolic study *in vivo* [240]. The clinical potential of [^{11}C]-methylcholine is mainly in the imaging of brain tumours and prostate carcinoma [241-243], in which cases the standard PET tracer [^{18}F]-FDG exhibits inadequate specificity and sensitivity, respectively [244, 245].

[^{18}F]-FCH, as a ^{18}F-labelled choline analogue, was developed by DeGrado *et al.* to overcome the limit of the short half-life of ^{11}C ($t_{1/2}$: 20.4 min) in [^{11}C]-methylcholine [246]. The longer half-life of ^{18}F ($t_{1/2}$: 109.8 min) is advantageous for clinical application since it enables the late imaging of tumours when the parent tracer in systemic circulation is cleared [240]. [^{18}F]-FCH had similar distributions to choline in the prostate cancer imaging study *in vivo*, which suggested that the electronegativity of the α-fluorine in the radiotracer can be well tolerated: [^{18}F]-FCH, as a choline mimic, is phosphorylated by CK and trapped in cancer cells as expected [246]. [^{18}F]-FEC has one more single methylene group in the structure relative to

[^{18}F]-FCH [246]. Both [^{18}F]-FCH and [^{18}F]-FEC exhibit higher urinary clearance compared to choline [246].

As [^{11}C]-methylcholine and the ^{18}F analogue are easily oxidised to betaine by choline oxidase localised in kidney and liver, the radioactive betaine metabolites exported into circulation can complicate PET imaging data when using a late imaging protocol [34]. A novel FCH analogue radiotracer, [^{18}F]-fluoromethyl-[1,2-$^{2}H_4$] choline ([^{18}F]-D4-FCH) was thus developed with improved metabolic stability [34]. Based on the deuterium isotope effect, the substitution of deuterium (^{2}D) for hydrogen (^{1}H) with the presence of ^{18}F together increased the stability of the tracer [34]. Lower betaine levels in liver/kidney and higher levels of parent tracer in plasma were observed, implying the improved stability of [^{18}F]-D4-FCH over FCH [34].

By using the [^{18}F]-D4-FCH made in-house, the inhibition on choline uptake by CK14, CK144, CK145, CK146 and CK147 was evaluated in the selected cell lines. In PSMA expressing C42B cells, all the compounds of interest inhibited the [^{18}F]-D4-FCH uptake dose-dependently (Figure 5.21). At the dose given at 1 μM, CK14, CK145 and CK146 inhibited the uptake of [^{18}F]-D4-FCH by approximately half (mean inhibition% by CK14, CK145 and CK146: 46 ± 1%). Among all the tested compounds, CK14 displayed the best inhibitory potency of the radiotracer; the uptake of [^{18}F]-D4-FCH was strikingly inhibited (93 ± 5%) when the dose was increased up to 10 μM. In HCT-116 cells (PSMA negative), a similar inhibition trend by tested compounds (10 μM) was seen (Figure 5.21). The mean radiotracer uptake inhibition by CK147 at a high dose (10 μM) was 59 ± 7% across the C4-2B and HCT-116 cells.

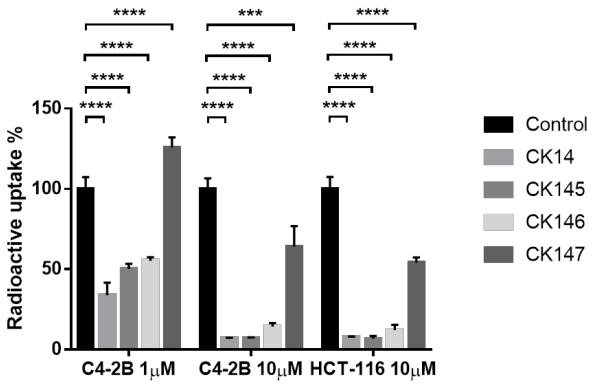


Figure 5. 21: [^{18}F]-D4-FCH percent uptake in C42B and HCT-116 cells (PSMA negative) following 1-hour incubation in the absence (Control group; compounds in DMSO) or presence of compounds at 1 or 10 μM (n = 6; mean ± SD); *P* values *via* unpaired two-tailed *T*-test: ***$P = 0.0001$, ****$P < 0.0001$.

5.9 Discussion

The physicochemical properties of drug molecules, resulting from their chemotypes, determine their pharmacokinetic parameters which directly influence the drug therapeutic efficacy by affecting how the drug molecules or their metabolites reach the site of action. In this chapter, the two innovative drug modification strategies that offered novel small-molecule CHKA inhibitors CK145 and CK147 have been evaluated comprehensively *in vitro*. The pharmacological activities of CK145 and CK147 have been investigated in terms of antiproliferation against cancer cells and their potential off-target effects by human lipid kinase screening. The relevant drug permeability and intracellular metabolism were checked by HPLC/MS to further understand the obtained pharmacological results. The informative pharmacokinetic profiles of all the CHKA inhibitors synthesised in-house were first-time characterised by ADME studies *in vitro*. At last, a target-competitive radiotracer [^{18}F]-D4-FCH was utilised to predict the *in vitro* choline uptake inhibition by the synthesised compounds.

5.9.1 Prodrug Strategy

The prodrug strategy utilised in this project, whereby an ε-acetylated lysine linkage in the prodrug (CK145) is selectively cleaved to release the active scaffold (CK146) in a stepwise manner, is highly dependent on the upregulation of HDAC and CTSL enzymes [168]. The high expression of HDAC I class, consisting of HDAC 1, 2, 3 and 8 subtypes, is hypothesised to be key to convert the prodrug CK145 into its active form; the subtype 1 of HDAC I class may contribute the most to the first-step deacetylation, activating the complete conversion of CK145 [168]. Therefore, the cancer cell lines with varying origins but high expression of HDAC 1 were selected to evaluate the antiproliferative activity of CK145. Notably, HCT-116 (colon) and A549 (lung) were two sensitive malignant cell lines to ICL-CCIC-0019 treatment, and they have high mRNA levels of HDAC1 and CTSL, respectively [64]. HepG2 (liver) cell line was used to investigate the antiproliferative potency of CK145 against malignant liver cells since extensive accumulation of ICL-CCIC-0019 in liver was previously observed in the pharmacokinetic and PET studies [247]. Caco-2 cell line, a less tumourigenic colon cell line, was used as a comparison to evaluate the potential off-target toxic effects.

All the four selected cell lines demonstrate high CHKA expression levels according to Cancer Cell Line Encyclopedia RNA sequencing database (Log2 (TPM+1) values of four selected cell lines: HCT-116: 4.66, A549: 3.78, HepG2: 5.91 and Caco-2: 6.18; TPM represents transcript per million, reflecting a relative protein expression level) [248]. Among the four cell lines, HepG2, which has the second highest CHKA expression, displayed the best sensitivity in SRB assay; in contrast, the Caco-2 cell line, despite having the highest CHKA expression level predicted, was the least sensitive to CHKA inhibitors. This could be either due to the lack of expression of choline transporter families (SLC families) in Caco-2, or due to the less tumorigenic properties of this cell line, which could imply lower CHKA enzyme activity [249]. The active scaffold of CK145, CK146 displayed lower but acceptable overall antiproliferative activity (mean GI_{50} against four cancer cell lines: 2.5 ± 0.3 μM) compared to ICL-CCIC-0019 (mean GI_{50} in the four cell lines: 0.50 ± 0.02 μM). The overall antiproliferative activity of CK145 in the four cancer cell lines (mean GI_{50} against the cell lines: 5.0 ± 0.3 μM) was similar

to CK146, but 10-fold less than ICL-CCIC-0019. The antiproliferative activity reduction in CK145 was not expected in these cancer lines with high expression of HDACs and CTSL. According to the subsequent enzymatic conversion analysis of CK145 in HCT-116 cells, it was confirmed that the conversion of CK145 *in vitro* was not successful: despite the high HDAC1 expression observed in HCT-116 cells, CK146 and any other corresponding intermediates of CK145 were not detected, indicating that the intracellular conversion of CK145 into CK146 was not triggered. This could somehow explain the difference observed in GI_{50} between CK146 versus CK145, but another unneglectable factor is the cellular uptake efficiency of the compounds. Although CK145 (Log P: 0.34 ± 0.01) was more lipophilic than ICL-CCIC-0019 (Log P: -1.12 ± 0.06) and CK146 (Log P: -1.13 ± 0.01) due to its Boc protecting group, it is not guaranteed that the cellular uptake of CK145 is efficient. The HPLC analysis on cell lysates after drug treatment indicated that the cellular uptake efficiency of the compounds was not completely dependent on compound lipophilicity: ICL-CCIC-0019 displayed approximately 2-fold higher cellular uptake than CK145 in 2 hours' post incubation in HCT-116 cells. The differential cellular uptake of compounds could be the result of multiple factors, for example mediation by choline transporters.

Despite the uptake of ICL-CCIC-0019 and CK145 into cells, likely *via* active transport by choline transporters, the low permeability of all these positively charged molecules was revealed in the ADME studies. Compared to other tested compounds, rapid decomposition of CK145 was observed in FaSSGF assay and metabolic stability assay likely due to metabolic instability of the Boc group at low pH (1.6) and peptide degradation mediated by liver microsomes, respectively. This suggests that administration *via* injection would be ideal for prodrug strategy. For the other compounds that have long half-lives and therefore lower clearance rates, intravenous administration may also be considered since the intestinal absorption of these compounds seemed poor.

In lipid kinase screening, high CHKA activity but low off-target effects were seen in CK144, CK145 and CK146 besides the classic CHKA inhibitors ICL-CCIC-0019 and CK14 (53 - 77%

inhibition at 10 μM). As desired, the tetradecyl linker introduced superior CHKA affinity observed in CK14 relative to the dodecyl linker used in ICL-CCIC-0019 (the CHKA activity inhibited: ICL-CCIC-0019: 53.4 ± 2.4%; CK14: 77.0 ± 10.2%). CK14 displayed the most CHKA potency among the tested compounds, in which case about 77% of the CHKA activity was inhibited. CK146, as an adaptable structure of ICL-CCIC-0019 suitable for further modification, promisingly exhibited higher CHKA activity compared to ICL-CCIC-0019 (the CHKA activity inhibited: CK146: 69.1 ± 11.2%; ICL-CCIC-0019: 53.4 ± 2.4%). However, the CHKA inhibition by the proposed prodrug molecule CK145 was similar to CK146 (the CHKA activity inhibited: CK145: 62.9 ± 3.6%; CK146: 69.1 ± 11.2%). This suggested that the prodrug strategy, whereby a bulky ε-(Ac)Lys structural modification had been made, was not able to mask the intrinsic activity of CK146. In the prodrug strategy introduced by Ueki *et al.*, the free amino group in Puromycin is essential to cellular toxicity, and the mask of this group by acetylation has also been proved to completely inactivate the molecule, which causes Puromycin resistance [168]. Unlike the amino group in Puromycin, the free secondary amine from the piperazine group provides the molecule with modification flexibility, but is not essential to CHKA activity. The quaternary ammoniums, as the main pharmacophore, are not completely masked by the prodrug bulk in this case: for the unsymmetrical structure of CK145, one quaternary ammonium is totally exposed, and the steric effects of the prodrug bulk attached to the other side is unlikely to completely block the binding of the molecule to the pockets of interest.

Another interesting observation in this study was that modification of the compounds with a piperazine moiety seen in CK144, CK145 and CK146 lead to additional kinase activity towards PIK4CB (at 10 μM), a potential antimalarial and antiviral target [250, 251]. In this regard, several CHKA inhibitors have been reported as capable of inhibiting the growth of parasite species *P. falciparum* (*P.f.*) through multiple mechanisms, mainly *via* the inhibition of *P.f.* choline kinase and *P.f.* ethanolamine kinase [119, 123]. The structure of CK146 presented here, as a basic scaffold, may have potential to be further modified into anti-parasite or antiviral drugs with a dual target-hitting PIK4CB and CHKA alike.

In the [^{18}F]-D4-FCH uptake study using C42B and HCT-116 cells, CK145 dose-dependently inhibited the uptake of choline analogue radiotracer [^{18}F]-D4-FCH in a similar trend to CK146. This finding suggested that the intact CK145 could possess CHKA activity, because CHKA inhibition caused by drug treatment could result in the elevated levels of choline and therefore a reduction in [^{18}F]-D4-FCH uptake. However, future investigations on CHKA inhibitory activity would better be performed using a combination of radio-HPLC analysis and purified CHKA enzymes, so as to eliminate the effects from choline transport in whole cell assays. The CHKA inhibitory activities of the tested compounds can be obtained by normalising the radioactivity to protein content and ratios of [^{18}F]-D4-FCH to its phosphorylated form.

5.9.2 Drug Delivery Strategy

In the drug delivery strategy, a small-molecule peptide (Glu-Urea-Lys) with high affinity towards PSMA was selected for conjugation with CK146 *via* a non-degradable linker, which gave rise to CK147 as a proposed ligand-drug conjugate for targeted PCa treatment [169]. The special internalisation property of PSMA receptor was expected to realise the differential uptake of CK147 in PSMA-expressing cells from the other cells [160]. CK147 that once binds to the PSMA receptor was hypothesised to be internalised into cells, followed by intracellular lysosomal degradation and release of CK146 [154].

The conjugate stability of CK147 in serum-containing media was firstly investigated by HPLC analysis over a period of 72 hours, in line with the incubation time used in the SRB proliferation assay. Although no chemical decomposition was detected, 60% intact parent at 72 hours was observed, which could result from the drug binding to serum albumin in medium. Several affinity-binding moieties such as 4-(p-iodophenyl) have been used to improve tissue distribution profiles of PSMA-targeted radiopharmaceuticals (Figure 5.22) [252, 253]. A similar structural fragment observed in CK147 may cause a similar drug interaction with serum in medium.

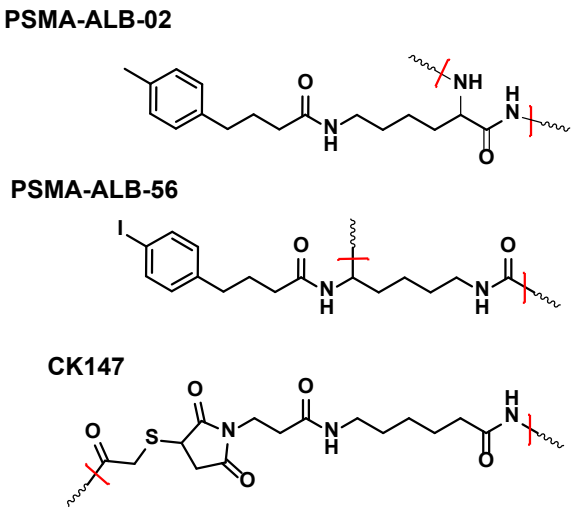


Figure 5. 22: Chemical structures of reported albumin-binding moieties and a similar structural fragment in CK147.

The antiproliferative activity (GI_{50}) of CK147 was investigated in a colon cancer cell line and seven prostate cell lines with differential PSMA expression by SRB assay. All the tested cell lines were found not sensitive to CK147 treatment, and the antiproliferative activity achieved seemed unrelated to PSMA expression according to statistics. CK147 was hydrophilic (Log P: -0.79 ± 0.02) and the permeability was extremely low. The poor antiproliferative activity of CK147 compared to CK146 under the same conditions was first thought to be related to the inefficient cellular uptake, either *via* the PSMA-driven internalisation or *via* the choline transporter-driven active transport. Therefore, experiments to investigate the cellular uptake and the *in vitro* metabolism of CK147 were performed by HPLC analysis on cell lysates and ^{18}F-D4-FCH competitive study in whole cells.

The poor cellular uptake of CK147 together with the loss of CHKA activity observed in lipid kinase screening further offered insights into the function loss of the PSMA-targeted molecule. At physiological pH, CK147 contains two positive charges from the quaternary ammonium moieties, and three negative charges from the carboxylates of the Glu-Urea-Lys peptide. Although not zwitterionic, due to the charge imbalance, a putative mechanism has been proposed combining all the findings in hand, where the positive quaternary ammonium charges may have been masked by inter- or intramolecular electrostatic interactions which

neutralise the charges and form unfavourable structural configurations capable of inhibiting both PSMA-binding and CHKA activity (Figure 5.23) [254].

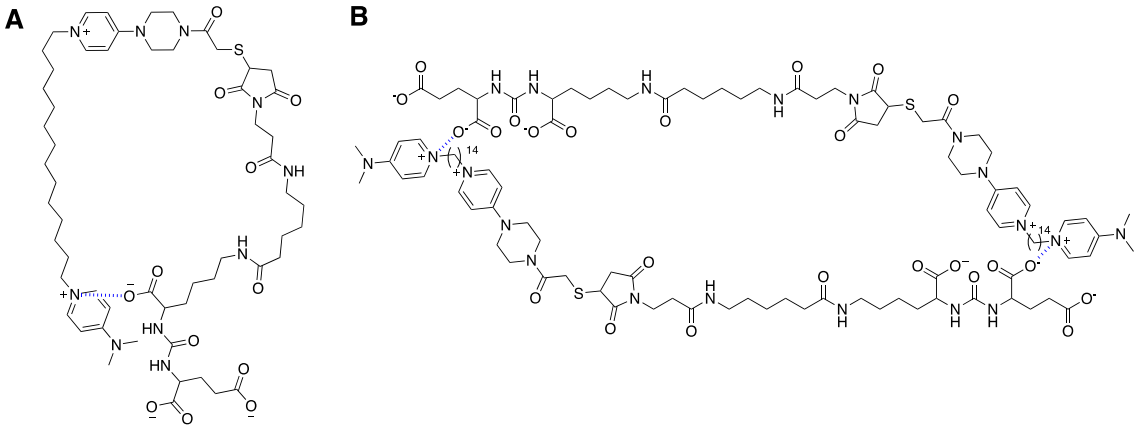


Figure 5. 23: Proposed (A) intramolecular and (B) intermolecular electrostatic interactions (blue dashed line) for CK147 which inhibit activity towards the PSMA receptor and CHKA.

This hypothesis was supported by the significant increase in cellular uptake observed in the *in vitro* uptake study with CK148, the $(OtBu)_3$-protected form of CK147. Electrostatic interactions may also contribute to the lower concentration of CK147 observed in the stability study whilst no chemical decomposition was detected. The compound may have formed complexes with serum albumin over time and then have been removed in the next protein precipitation step before MS analysis. In the subsequent work, this could be further validated by developing an HPLC methodology at physiological pH, in order to detect the intermolecular and intramolecular species as hypothesised. The molar conductivity of CK147 at different pH could also be investigated to better understand the HPLC results obtained.

6. Thesis conclusions & future work

6.1 Summary of work and achievements from this thesis

Abnormal choline metabolism associated with upregulation of CHKA is a novel cancer hallmark [24]. CHKA inhibition has been exploited as a promising cancer therapeutic strategy, and a number of small-molecule CHKA inhibitors have, therefore, been developed [119]. In the previous studies by Trousil *et al*, the efforts in medicinal chemistry were focused to realise the dual binding of choline and ATP sites [93]. This turned out feasible by using different head moieties in the molecule (DMAP moiety for choline pocket targeting and ATP-mimicking moiety for ATP pocket targeting), but the potency of these unsymmetrical CHKA inhibitors was significantly diminished [93]. Detailed pharmacological characterisation using biochemical assays and PET imaging was then applied for the symmetrical choline-competitive lead compound ICL-CCIC-0019 which displayed high antiproliferative activity and the potential to compete with choline at high concentrations in whole cells [93]. Compared to the other reported CHKA inhibitors, ICL-CCIC-0019 is superior for its high potency in cancer cells and CHKA selectivity over CHKB [247]. The selective CHKA inhibition by ICL-CCIC-0019 caused ER stress, G1 arrest and cancer cell apoptosis by the deactivation of the Kennedy pathway and decreased PtdCho [64]. Despite the merits, the dose-limiting toxicity of ICL-CCIC-0019 indicated by dose-dependent decrease of body weight in mice was observed, probably related to the intrinsic toxicity/the high liver and kidney accumulation of the compound [64].

The finding by Trousil *et al.* highlighted the selective CHKA inhibition by which the decrease in cancer cell viability was observed; combined CHKA and CHKB inhibition, however, failed to induce cell death, probably mediated *via* mitophagy or autophagy [247, 255, 256]. Similarly, the uncharged, ATP-competitive CHKA inhibitor V-11-0711 was reported ineffective in cell-based assays [108]. All these evidences suggest the necessity of novel CHKA-specific, choline-competitive scaffolds to be designed for successful clinical translation. The direct modification on ICL-CCIC-0019 is perhaps challenging for two reasons: firstly, the intrinsic

toxicity of the compound related to its quaternary ammonium structure is difficult to overcome while maintaining high CHKA selectivity [64]; secondly, the structural diversity of ICL-CCIC-0019 is very limited for direct modifications.

In this work, advanced drug development strategies were first innovatively exploited to offer novel small-molecule CHKA inhibitors on the basis of ICL-CCIC-0019 structure; the central aim of this work was to develop novel-generation CHKA inhibitors with ameliorated pharmacological profiles *in vitro*/*in vivo* but remaining satisfactory CHKA activity in targeted tissues. A novel ICL-CCIC-0019 derivative scaffold bearing a reactive piperazine handle (CK146) was first designed and successfully synthesised, which harbored potent CHKA activity similar to ICL-CCIC-0019. By using this scaffold, the quaternary ammonium moieties and the tetradecyl space linker were retained to confer the best antiproliferative potency, while the release or delivery of the cytotoxic scaffold in target tissue was proposed to be controlled by advanced modification strategies (prodrug strategy and drug delivery strategy), therefore improving the potential off-target accumulation and toxicity observed in ICL-CCIC-0019.

The challenges encountered in the synthesis of the desired prodrug CHKA inhibitor CK145 and PSMA-targeted CHKA inhibitor CK147 mainly lay in: (1) the lack of an efficient purification methodology for positively charged quaternary ammonium derivatives with high polarity and retention on C18 reverse phase columns; (2) the block building and condition optimisation of orthogonal bioconjugation to customise the thiol-maleimide crosslinking. To overcome those limits, we established a set of standardised procedures which combined analytical and semi-preparative HPLC, enabling a high-resolution fractional separation methodology for both aims of purification and *in vitro* drug metabolism studies; the structural modifications of CK146 *via* thiol and bioconjugation chemistry has also been explored, finally presented with high feasibility and good yields.

The biological evaluation of CK145 and CK147, relative to their active scaffold CK146, was

performed, whereby the CHKA activity/selectivity and potency of these two compounds were first characterised by biochemical and cell-based assays. The lipid kinase screening and cell-based antiproliferative assays could be the most critical experiments for characterising novel CHKA inhibitors, because they provided the overall behaviour information of compounds, offering insight as a sum of pharmacokinetic profiles, cell permeability and target affinity/off-target effects. Cellular uptake and metabolism studies further helped us to understand the obtained results; ADME studies predicted the *in vivo* performance of all the compounds in hand.

Despite acceptable antiproliferative activity, CK145 was seen as an atypical prodrug molecule since it possessed CHKA activity without enzymatic conversion in the cells. The CHKA activity retained in the molecule suggested that it was not feasible to mask the intrinsic activity from its quaternary ammonium moiety by prodrug bulk protection at one side. It remains to be understood, why the intracellular conversion of CK145 did not occur as expected in the cells with high expression of HDAC and CTSL. Subsequent molecular modeling studies may be required to investigate the possible reason for this observation. As the intracellular conversion was not initiated, the antiproliferative effects of CK145 were directly related to the compound level in cells. Although the lipophilicity of CK145 was increased compared to ICL-CCIC-0019, the cell permeability of CK145 was more limited as found in HCT-116 cells. Given the intrinsic cationic nature of this class of molecules, the future CHKA inhibitor scaffolds would be considered to either adopt uncharged structures (bearing with the risk of losing CHKA activity/selectivity) or would preferably be equipped with receptor-targeted moieties that could increase the uptake efficiency, *e.g. via* receptor-mediated endocytosis process.

The second part of this work was, thus, aimed to develop receptor-specific CHKA inhibitors with advances of increasing compound uptake in specific cells *via* internalisation. By applying the PSMA-targeted drug delivery strategy, however, unexpected dual loss of cellular potency and CHKA activity in CK147 was unexpected, and indicated that the conjugation of the PMSA-

targeted moiety could have impaired the compound activity *via* electrostatic interactions. The cellular uptake study *in vitro* further supported the speculation as the complexity of CK147's charge nature could increase the possibility of compound interaction the serum albumin in medium and could, thus, affect uptake efficiency. In future studies, the charge nature of CK147 under different pH environment can be further investigated so as to confirm this speculation.

Although exploitation of CK146 in those two strategies did not deliver the expected results, important and informative structure-activity relationships were observed and concluded for the first time. The key findings of this work are summarised in Figure 6.1. In conclusion, our work opens up the possibility for further structural elaboration of CK146, exploring the chemical space around this moiety and building up SAR to modulate biological and pharmacokinetic properties. An interesting and promising finding of this work is to notice that the introduction of the piperazine structure to the scaffold seems to offer CHKA inhibitors additional activities towards PIK4CB, a potential antimalarial and antiviral target. In this work, we presented the successful transformation of CK146 into two drug development processes to produce targeted cancer therapies *via* prodrug strategy (CK145) and drug delivery strategy (CK147), although conversion to active components or targeted delivery was not achieved. Regardless, we have demonstrated the feasibility and potential for modulating CHKA activity *via* piperazine functionalisation.

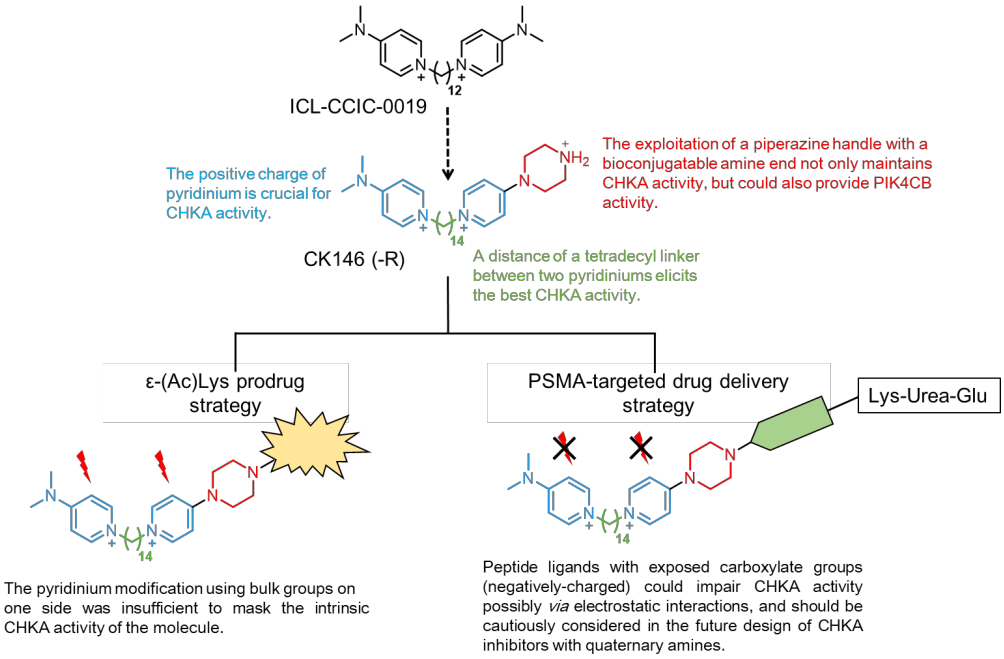


Figure 6. 1: Key SAR findings of this thesis. (A) ε-(Ac)Lys prodrug strategy; (B) PSMA-targeted drug delivery strategy.

6.2 Future work

6.2.1 Short-term goals

Short-term future study could be set to validate the obtained findings and elucidate the mechanisms, which would deepen our current understanding on SAR and inspire the further optimisation of the CHKA inhibitors synthesised:

CHKA activities of CK146 and CK145

Similar CHKA activity was seen in CK146 and its prodrug form CK145 from kinase screening, where CK146 exhibited even slightly higher CHKA activity compared to ICL-CCIC-0019. In parallel with the previous research on ICL-CCIC-0019, the molecular modelling study of CK146 can be performed to understand its possible binding modes using the crystal structure of human CHKA (pdb code: 2CKO) [77]. The remaining CHKA activity of CK145 after prodrug bulk modification also merits docking analysis to understand the mechanism so as to guide the further development of the molecule. It would also be interesting to understand the interactions of both compounds with the binding sites of interest (CHKA and ATP sites), relative to the previous binding modes observed in ICL-CCIC-0019.

PIK4CB activity of CK146

To further the utilisation of CK146 scaffold in future exploration, the observed PIK4CB activity stemming from the piperazine handle needs to be confirmed. In the kinase screening, the promiscuity of kinases could also cause off-target effects which affect the compound activity against the target of interest and produce 'false-positive' results. Although CK146 displayed PIK4CBA activity in the kinase screening, additional computational approaches such as molecular docking against PIK4CB/CHKA of *P. falciparum* would be considered for SAR purpose and to support this claim.

Charge nature of CK147

The charge nature of the amines in CK146 and its derivatives is undoubtedly worth further investigation since the exposed positive charges on pyridinium are proven essential to CHKA activity. The piperazine handle introduced in CK146 could also be protonated at physiological pH and bring additional biological activities. The CHKA activity of CK147 was masked in the kinase screening, very likely due to the electrostatic neutralisation *via* the ionisation of three carboxylate anions and two quaternary ammonium moieties (kinase screening buffer pH: 7.5). In future studies, the charge effects of different amine moieties under a wider range of pH environments on CHKA activity and uptake efficiency could be investigated by HPLC detection and conductivity analysis; docking analysis *in silico* should also be considered to validate the hypothesis.

6.2.2 Long-term goals

For long-term projects, the derivatisation of ICL-CCIC-0019 could be continued to offer a suitable candidate for clinical translation. The long-term directions for the derivatisation of ICL-CCIC-0019 may need to turn to more effective modification strategies. The main challenge is to achieve the compound selectivity while maintaining its CHKA activity and antiproliferative profiles. Advanced bio-activation strategies that allow temporary but effective mask of the permanent positive charge in quaternary ammonium are required in the future projects. Using redox and pH activation, for example, the bio-oxidisable/pH sensitive amine derivative structures could be transformed into positive quaternary charges under oxidative stress/specific pH microenvironment *in vitro*. However, proper strategy evaluation would require the establishment/selection of suitable models because of tumour heterogeneity. To realise targeted delivery of CHKA inhibitors, in addition, direct functional bulk conjugation to the active scaffold needs to be elaborated. The delivery moieties that have the potential to be ionised and charged under certain pH environment should be investigated before actual synthesis. Molecular modeling would be a very valuable tool for this perspective, which could predict the behaviours of the compounds, including the possible charge/binding modes at the sites of interest.

7. Experimental

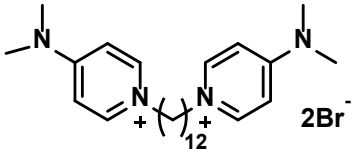
This work is associated with [1]:

Wang, N.; Brickute, D.; Braga, M.; Barnes, C.; Lu, H.; Allott, L.; Aboagye, E. O., Novel Non-Congeneric Derivatives of the Choline Kinase Alpha Inhibitor ICL-CCIC-0019. Pharmaceutics 2021, 13 (7), 1078.

Synthesis

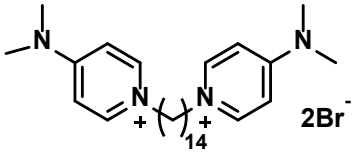
The 1,14-bromotetradecane linker used in this project was purchased from Apollo Science Limited (Cheshire, UK). The small-molecule peptide ligand targeting PSMA attached to a maleimide group ($(OtBu)_3$ PSMA-maleimide)) (**15**) was provided by Creative Chemistry (Hampton, UK). All the other reagents and solvents were purchased from Sigma-Aldrich Chemical Co. (Gil-lingham, UK) and VWR Chemicals Co. (Lutterworth, UK), and used without further purification. Silica gel (230 - 400 mesh) for column chromatography was from Aldrich Chemical Co. (Dorset, UK). TLC was performed using silica gel on Al foils (254 nm) from Sigma-Aldrich (Gillingham, UK). All TLC plates were visualized by UV lamp (UVP, Upland, CA 91786, USA). Rotary evaporation was performed by BUCHI V-850 vacuum controllers (Suffolk, UK). BioChromato® spiral plug smart evaporator (Fujisawa, Japan) was used for compound drying and to remove DMF. NMR spectra were obtained using a Bruker Avance-400 spectrometer (Coventry, UK) and all the NMR data were analysed by MestReNova software. ^{1}H NMR were recorded at 400 MHz, and ^{13}C NMR were recorded at 101 MHz. MS (ES-ToF) were all obtained in the mass spectrometry centre in the chemistry department of Imperial College London (London, UK).

1,1'-(dodecane-1,12-diyl)bis(4-(dimethylamino)pyridin-1-ium) bromide (ICL-CCIC-0019) (1)



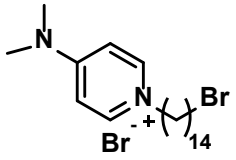
To a round bottom flask was added 4-dimethylaminopyridine (1 mmol, 122 mg) and 1,12-dibromododecane (0.5 mmol, 164 mg) in 2-butanone (10 mL). The reaction was stirred at 110 ˚ C for 3 hours and a white precipitate formed. The precipitate was filtered, washed with 2-butanone (3 × 10 mL), diethyl ether (2 × 10 mL) and subsequently dried *in vacuo*. The title compound was purified by recrystallisation with ethanol and 2-butanone to give a white solid (189 mg, yield = 84%). ^{1}H NMR (400 MHz, DMSO-d_6) δ 1.14 - 1.29 (16H, m), 1.69 - 1.78 (4H, m), 3.18 (12H, s), 4.14 (4H, t, *J* = 8.0 Hz), 7.03 (4H, d, *J* = 8.0 Hz), 8.30 (4H, d, *J* = 8.0 Hz); ^{13}C NMR (101 MHz, $CDCl_3$) δ 26.20, 28.90, 29.20, 31.40, 31.50, 40.90, 58.70, 108.90, 143.10, 156.70; HRMS (ES-ToF) m/z ($[M\text{-}Br^-]^{2+}$): calcd: 206.1778, found: 206.1767.

1,1'-(tetradecane-1,14-diyl)bis(4-(dimethylamino)pyridin-1-ium) bromide (CK14) (2)



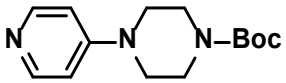
To a round bottom flask was added 4-dimethylaminopyridine (2 mmol, 244 mg) and 1,14-bromotetradecane (1 mmol, 356 mg) in 2-butanone (20 mL). The reaction was stirred at 110 ˚ C for 3 hours and a white precipitate formed. The precipitate was filtered, washed with 2-butanone (3×20 mL) and diethyl ether (2×20 mL) and subsequently dried *in vacuo*. The title compound was purified by recrystallisation with ethanol and 2-butanone to give a white solid (381 mg, yield = 80%).^{1}H NMR (400 MHz, DMSO- d_6) δ 1.14 - 1.31 (20H, m), 1.69 - 1.79 (4H, m), 3.19 (12H, s), 4.14 (4H, t, *J* = 4.0), 7.03 (4H, d, *J* = 8.0 Hz), 8.30 (4H, d, *J* = 8.0 Hz); ^{13}C NMR (101 MHz, $CDCl_3$) δ 26.30, 28.10, 28.80, 28.90, 29.50, 31.10, 40.90, 58.80, 108.90, 143.00, 156.70; MS (ES-ToF) m/z ($[M\text{-}Br^-]^{2+}$): calcd: 220.2, found: 220.2.

1-(bromomethyl)-4-(dimethylamino)pyridin-1-ium bromide (3)



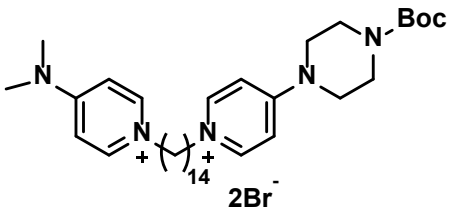
To a round bottom flask was added 4-dimethylaminopyridine (0.5 mmol, 61 mg) and 1,14-bromotetradecane (1 mmol, 356 mg) in 2-butanone (10 mL). The reaction was stirred at 110 ˚ C for 3 hours and a white precipitate formed. The reaction mixture was poured into diethyl ether (200 mL) and the precipitate was filtered and washed with 2-butanone (3×10 mL), diethyl ether (2×10 mL) and subsequently dried *in vacuo* to give the title compound as a white solid (152 mg, yield = 64%). ^{1}H NMR (400 MHz, $CDCl_3$) δ 1.17 - 1.50 (20H, m), 1.81 - 1.95 (4H, m), 3.28 (6H, s), 3.40 (2H, t, *J* = 8.0 Hz), 4.35 (2H, t, *J* = 8.0 Hz), 7.03 (2H, d, *J* = 8.0 Hz), 8.48 (2H, d, *J* = 8.0 Hz); ^{13}C NMR (101 MHz, $CDCl_3$) δ 26.20, 28.30, 28.90, 29.20, 29.51, 29.56, 29.60, 29.64, 29.70, 31.30, 32.90, 34.10, 40.60, 58.70, 108.50, 142.50, 156.40; MS (ES-ToF) m/z($[M\text{-}Br^-]^+$): calcd: 399.2192, found: 399.2208.

tert-butyl 4-(pyridin-4-yl)piperazine-1-carboxylate (4)



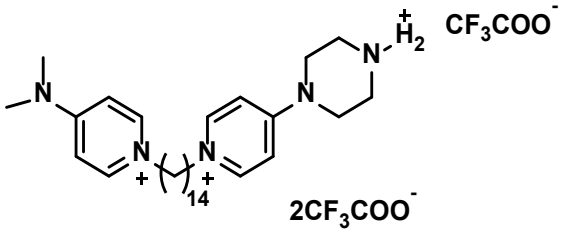
To a round bottom flask was added 4-piperazinopyridine (1 mmol, 163 mg), di-tert-butyl dicarbonate (1.5 mmol, 327 mg) and a catalytical amount of DMAP in anhydrous DMF (10 mL) and TEA (107 µL) before being purged with nitrogen. The reaction was stirred at room temperature for 16 hours before concentration *in vacuo*. The title compound was purified by flash chromatography (silica; ethyl acetate (0.3% TEA, v/v); RF value: 0.18) to give a white solid (247 mg, yield = 94%). ^{1}H NMR (400 MHz, $CDCl_3$) δ 1.39 (9H, s), 3.20 (4H, t, *J* = 4.8 Hz), 3.46 (4H, t, *J* = 4.8 Hz), 6.55 (2H, d, *J* = 6.8 Hz), 8.18 (2H, d, *J* = 6.4 Hz); ^{13}C NMR (101 MHz, $CDCl_3$) δ 28.30, 45.60, 54.50, 79.99, 108.38, 150.15, 154.40, 154.57; MS (ES-ToF) m/z ($[M+H]^+$): calcd: 264.1707, found 264.1725.

4-(4-(tert-butoxycarbonyl)piperazin-1-yl)-1-(14-(4-(dimethylamino)pyridin-1-ium-1-yl)tetradecyl)pyridin-1-ium bromide (5)



To a sealed tube **4** (0.25 mmol, 66 mg) and **3** (0.25 mmol, 120 mg) were added in dry MeCN (6 mL). The reaction was stirred at 110 ˚ C for 72 hours. The reaction mixture was cooled down to the ambient temperature and concentrated *in vacuo* to give product as a pale yellow solid (180 mg, yield = 97%). ^{1}H NMR (400 MHz, MeOD-d_4) δ 1.13 - 1.33 (20H, m), 1.37 - 1.44 (9H, s), 1.72 - 1.84 (4H, m), 3.17 (6H, s), 3.50 - 3.60 (4H, m), 3.63 - 3.70 (4H, m), 4 - 4.15 (4H, m), 6.91 (2H, d, *J* = 7.6 Hz), 7.08 (2H, d, *J* = 7.6 Hz), 8.07 (2H, d, *J* = 7.6 Hz), 8.13 (2H, d, *J* = 7.6 Hz), 8.46 (2H, s); ^{13}C NMR (101 MHz, MeOD-d_4) δ 27.20, 28.59, 30.20, 30.60, 30.68, 30.76, 31.93, 40.25, 46.92, 58.94, 59.10, 81.90, 108.90, 109.48, 143.03, 143.72, 156.15, 157.54, 157.90; MS (ES-ToF) m/z ($[M-Br^-]^{2+}$): calcd: 290.7329, found 290.7342.

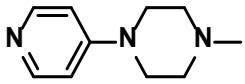
4-(dimethylamino)-1-(14-(4-(piperazin-1-yl)pyridin-1-ium-1-yl)tetradecyl)pyridin-1-ium hydrogen 2,2,2-trifluoroacetate (CK146) (6)



To a dry round bottom flask was added **5** (0.34 mmol, 253 mg) in dry MeCN (3 mL) with addition of TFA (3 mL). The reaction was stirred at room temperature for 16 hours before being concentrated to dryness *in vacuo* (265 mg, yield = 93%). ^{1}H NMR (400 MHz, MeOD-d_4) δ 1.16 - 1.32 (20H, m), 1.73 - 1.85 (4H, m), 3.17 (6H, s), 3.50 - 3.60 (4H, m), 3.26 - 3.35 (4H, m), 3.83 - 3.92 (4H, m), 4.04 - 4.18 (4H, m), 6.91 (2H, d, *J* = 7.6 Hz), 7.19 (2H, d, *J* = 7.6 Hz), 8.07 (2H, d, *J* = 7.6 Hz), 8.00 - 8.15 (2H, s), 8.23 (2H, d, *J* = 7.6 Hz); ^{13}C NMR (101 MHz, MeOD-d_4) δ 27.28, 30.28, 30.67, 30.75, 30.83, 32.01, 40.34, 44.33, 45.26, 59.05, 59.43, 108.99,

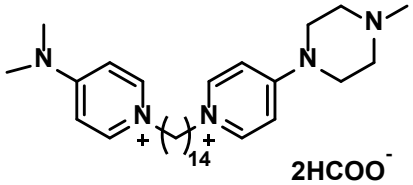
110.03, 143.11, 144.20, 157.76, 157.99. MS (ES-ToF) m/z ([M-CF_3COO^-]$^{2+}$): calcd: 240.7067, found 240.7062.

1-methyl-4-(4-pyridinyl)-piperazine (7)



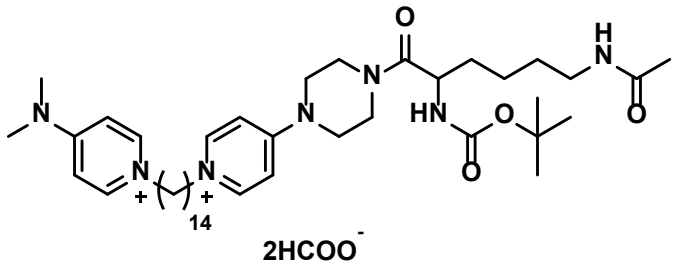
4-chloropyridine hydrochloride (20 mmol, 3 g), 1-methylpiperazine (60mmol, 6.7 mL), zinc iodide (2.5 mol% = 0.5 mmol, 8 mg) and dry MeCN (3 mL) were added into a drug round-bottom flask. The reaction was purged with nitrogen and heated to 75 ˚C for 16 hours. The reaction mixture was cooled to the room temperature and concentrated *in vacuo* before being purified by flash chromatography on silica (methanol: ethyl acetate: triethylamine, 64:27:9, RF value: 0.26). The desired product was obtained as a yellow oil of 1.88 g (yield: 53%). ^{1}H NMR (400 MHz, $CDCl_3$) δH: 2.33 (3H, s), 2.52 (4H, t, *J* = 4 Hz), 3.37 (4H, t, *J* = 4 Hz), 6.68 (2H, d, *J* = 4 Hz), 8.24 (2H, d, *J* = 4 Hz); ^{13}C NMR (101 MHz, $CDCl_3$) δ 45.9, 46.1, 54.5, 108.3, 149.7, 155; MS (ES-ToF) m/z ([M+H]$^+$): calcd: 178.1, found 178.1.

4-(dimethylamino)-1-(14-(4-(4-methylpiperazin-1-yl)pyridin-1-ium-1-yl)tetradecyl)pyridin-1-formate (CK144) (8)



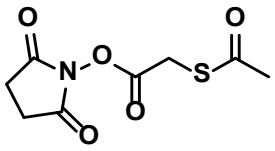
Compound **5** (3 mmol, 152 mg) was dissolved in the DMF (5 mL) containing compound **7** (3 mmol, 56.4 mg) and K_2CO_3 (0.38 mmol, 52.7 mg) before being heated to 130 ˚C for 16 hours. After the reaction, the mixture was cooled down to the room temperature and concentrated *in vacuo*. The crude was purified by preparative HPLC (HPLC method A), affording CK144 with a yield of 10.5%. ^{1}H NMR (400 MHz, $CDCl_3$) δH: 1.13 - 1.37 (20H, m), 1.75 - 1.95 (4H, m), 2.34 (3H, s), 2.55 (4H, t, *J* = 4 Hz), 3.26 (6H, s), 3.69 (4H, t, *J* = 4 Hz), 4.23 (4H, t, *J* = 8 Hz), 6.98 (2H, s), 7.18 (2H,s), 8.32 (4H, s), 8.7 (2H, s); MS (ES-ToF) m/z ([M-HCOO-]$^{2+}$): calcd: 247.7, found 247.7.

4-(4-(N^6-acetyl-N^2-(tert-butoxycarbonyl)lysyl)piperazin-1-yl)-1-(14-(4-(dimethylamino)pyridin-1-ium-1-yl)tetradecyl)pyridin-1-ium formate (CK145) (9)



The crude of **9** was provided by Creative Chemistry (Hampton, UK). The compound was synthesized from the starting materials of α-Boc-Lys(Ɛ-Ac)-OH and EDC, HOBt·H_2O, DIEA, DMF. The crude was then analysed by HPLC and MS to confirm the identity of the product. The title compound was purified by semi-preparative HPLC from the crude (HPLC method C, 307 mg, Yield = 37.5%). ^{1}H NMR (400 MHz, MeOD-d_4) δ 1.2 - 1.41 (24H, m), 1.44 (9H, s), 1.49 - 1.57 (2H, m), 1.59 - 1.76 (2H, m), 1.78 - 1.90 (4H, m), 1.93 (3H, s), 3.05 - 3.22 (2H, m), 3.25 (6H, s), 3.64 - 4.05 (4H, m), 4.12 - 4.26 (4H, m), 4.45 - 4.56 (1H, m), 6.99 (2H, d, *J* = 7.6 Hz), 7.18 (2H, d, *J* = 7.2 Hz), 8.16 (2H, d, *J* = 7.6 Hz), 8.24 (2H, d, *J* = 7.2 Hz), 8.56 (2H, s); ^{13}C NMR (101 MHz, MeOD-d_4) δ 22.61, 23.97, 27.18, 28.71, 30.00, 30.18, 30.58, 30.66, 30.73, 31.91, 32.44, 40.00, 40.26, 42.24, 45.09, 46.51, 46.92, 51.76, 58.93, 59.16, 80.63, 108.89, 109.49, 143.01, 143.73, 157.53, 157.87, 170.17, 173.21, 173.69; MS (ES-ToF) m/z ($[M\text{-}HCOO^-]^{2+}$): calcd: 375.7857, found 375.7766.

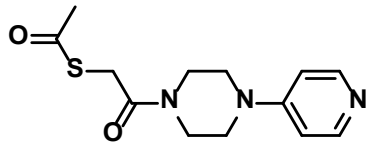
Acetylsulfanyl-acetic acid 2,5-dioxo-pyrrolidin-1-yl ester (SATA) (10)



To a round bottom flask was added 2-(Acetylthio) acetic acid (2 mmol, 280 mg) and *N,N,N,N'*-Tetramethyl-O-(N-succinimidyl)uronium tetrafluoroborate (TSTU) (3.32 mmol, 1 g) in anhydrous pyridine (7.5 mL) and acetonitrile (7.5 mL). The reaction was stirred at room temperature for 5 hours under nitrogen. The reaction mixture was then evaporated to dryness, dissolved in chloroform (15 mL) and filtered. The filtrate was washed twice with 15 mL (1:1) mixed 0.1 M phosphoric acid and brine, then one more wash with 10 mL brine. The

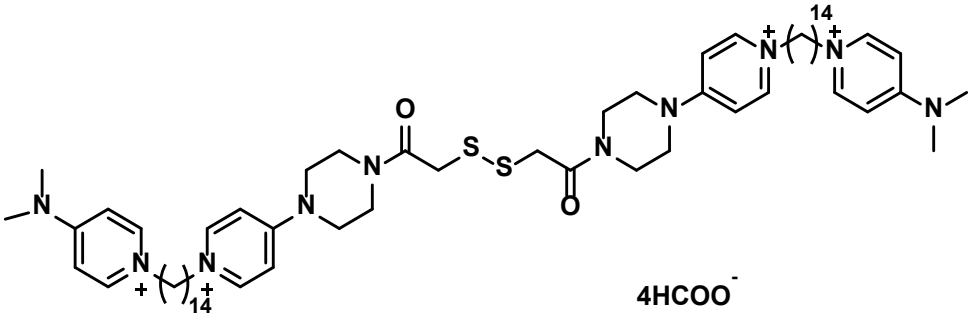
chloroform proved dried under sodium sulfate and was evaporated to dryness by smart evaporator. The product had a final wash with 1 mL ethanol and crystalised to give a white solid (287 mg, yield: 60%). ^{1}H NMR (400 MHz, $CDCl_3$) δ 2.42 (3H, s), 2.83 (2H, s), 3.98 (2H, s); ^{13}C NMR (101 MHz, $CDCl_3$) δ 25.69, 28.46, 30.12, 164.78, 168.69, 192.44.

Thioacetic acid S-[2-oxo-2-(4-pyridin-4-yl-piperazin-1-yl)-ethyl] ester (11)



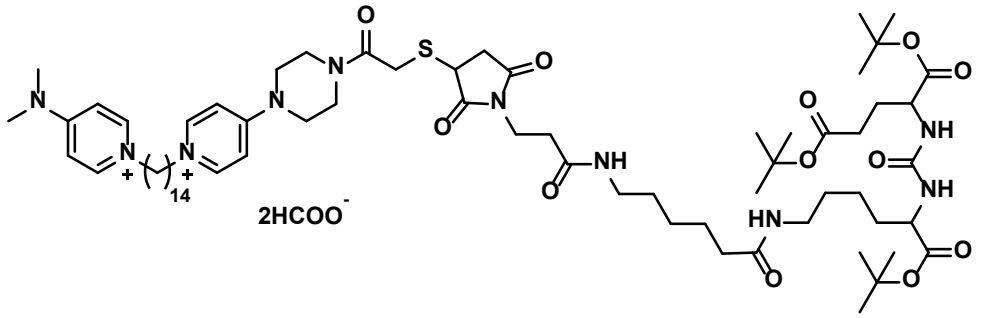
To a round bottom flask was added acetylsulfanyl-acetic acid 2,5-dioxo-pyrrolidin-1-yl ester (SATA) (**10**) (1 mmol, 250 mg) and 1-(Pyridin-4-yl)piperazine (0.72 mmol, 118 mg) in a mixed solution of anhydrous acetonitrile (13 mL) and triethylamine (1.4 mmol, 142 mg). The reaction was stirred at room temperature for 5 hours under nitrogen. After reaction, the mixture was concentrated *in vacuo* and firstly purified by flash chromatography (dichloromethane: methanol: TEA, 86:4:10, RF value: 0.25). Then the title compound was finally purified by recrystallisation with methanol and diethyl ether to give a white solid (30 mg, yield: 25%). ^{1}H NMR (400 MHz, $CDCl_3$) δH 2.35 (3H, s), 3.36 (4H, t, J = 4.0 Hz), 3.71 (4H, t, J = 4.0 Hz), 3.81 (2H,s), 6.63 (2H, d, J = 4.0 Hz), 8.26 (2H, d, J = 4.0 Hz); ^{13}C NMR (101 MHz, $CDCl_3$) δ 30.14, 31.34, 41.52, 45.63, 108.52, 150.29, 154.46, 166.39, 194.51; MS (ES-ToF) m/z: 280.1 $[M+H]^+$.

4,4'-((2,2'-disulfanediylbis(acetyl))bis(piperazine-4,1-diyl))bis(1-(14-(4-(dimethylamino)pyridin-1-ium-1-yl)tetradecyl)pyridin-1-ium) formate (14)



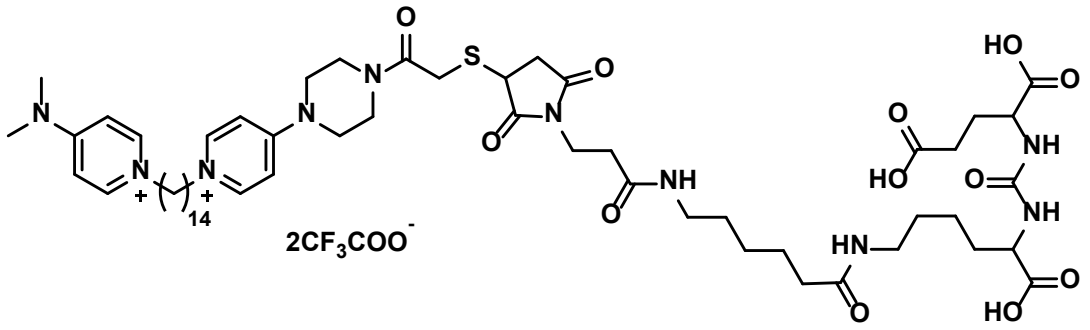
To a round bottom flask was added compound **6** (hydrochloride salt form, 0.27 mmol, 180 mg), dithiodiglycolic acid (0.133 mmol, 24 mg), EDC·HCl (0.27 mmol, 51 mg), HOBt (0.27 mmol, 36 mg), and DIPEA (0.27 mmol, 47 μL) in anhydrous DMF (6 mL) before being purged with nitrogen. The reaction was stirred at room temperature for 72 hours before being dried by smart evaporator. The title compound was purified by semi-preparative HPLC purification (See HPLC method A) to give a clear beige solid (70 mg, yield = 48%).^{1}H NMR (400 MHz, MeOD-d_4) δ 1.07 - 1.35 (40H, m), 1.7 - 1.87 (8H, m), 3.16 (12H, s), 3.41 - 3.99 (19H, m), 4.03 - 4.22 (9H, m), 6.91 (4H, d, *J* = 7 Hz), 7.11 (4H, s), 8.08 (4H, d, *J* = 7.1 Hz), 8.17 (4H, s); ^{13}C NMR (101 MHz, MeOD-d_4) δ 27.16, 30.15, 30.55, 30.63, 30.70, 31.89, 31.91, 42.29, 45.84, 46.41, 46.97, 58.93, 59.15, 108.88, 109.52, 142.99, 143.74, 157.49, 157.84, 166.74, 169.55. MS (ES-ToF) m/z ([M-$HCOO^-$]$^{4+}$): calcd: 277.1941, found 277.1960.

4-(4-(2-((1-(7,11-bis(tert-butoxycarbonyl)-2,2-dimethyl-4,9,17,24-tetraoxo-3-oxa-8,10,16,23-tetraazahexacosan-26-yl)-2,5-dioxopyrrolidin-3-yl)thio)acetyl)piperazin-1-yl)-1-(14-(4-(dimethylamino)pyridin-1-ium-1-yl)tetradecyl)pyridin-1-ium formate (CK148) (16)



To a round bottom flask was added compound **14** (0.054 mmol, 70 mg) and tris(2-carboxyethyl)phosphine (TCEP) hydrochloride (0.27 mmol, 78 mg) in 4 mL of degassed Tris-HCl buffer (pH = 7.3) before being purged with nitrogen. The pH of the reaction was adjusted to 7 using 1 M NaOH and stirred at room temperature for 2 hours. Then PSMA-Maleimide (Creative Chemistry, Hampton, UK) (0.14 mmol, 102 mg) was pre-dissolved in DMF and Tris-HCl buffer solution (4 mL) was dropwise added into the reaction mixture. The reaction was stirred at room temperature under nitrogen atmosphere for 16 h before being dried by smart evaporator. The title compound was purified by semi-preparative HPLC purification (See HPLC method A) to give a clear yellow solid (85 mg, yield = 56%). ^{1}H NMR (400 MHz, MeOD-d_4) δ 1.16 - 1.31 (20H, m), 1.31 - 1.37 (3H, m), 1.37 - 1.41 (27H, m), 1.43 - 2.06 (14H, m), 2.08 - 2.15 (2H, t, *J* = 7.4 Hz), 2.16 - 2.46 (4H, m), 2.56 - 2.67 (2H, m), 2.95 - 3.18 (4H, m), 3.19 (6H, s), 3.60 - 3.90 (12H, m), 3.93 - 4.21 (7H, m), 6.94 (2H, d, *J* = 7.4 Hz), 7.14 (2H, d, *J* = 6.5 Hz), 8.10 (2H, d, *J* = 7.4 Hz), 8.19 (2H, d, *J* = 6.6 Hz). ^{13}C NMR (101 MHz, MeOD-d_4) δ 23.99, 26.67, 27.18, 27.56, 28.99, 29.94, 29.99, 30.18, 30.58, 30.66, 30.73, 31.92, 32.48, 33.00, 33.14, 34.78, 36.05, 36.79, 36.99, 40.06, 40.27, 40.31, 41.05, 42.25, 45.79, 46.36, 46.83, 54.18, 54.90, 58.93, 59.15, 81.71, 82.52, 82.76, 108.89, 109.52, 143.01, 143.76, 157.52, 157.86, 159.92, 169.80, 172.70, 173.43, 173.70, 173.89, 175.95, 176.37, 177.76. MS (ES-ToF) m/z ($[M\text{-}HCOO^-]^{2+}$): calcd: 653.4169, found 653.4164.

4-(dimethylamino)-1-(14-(4-(4-(2-((2,5-dioxo-1-(1,3,7-tricarboxy-5,13,20-trioxo-4,6,12,19-tetraazadocosan-22-yl)pyrrolidin-3-yl)thio)acetyl)piperazin-1-yl)pyridin-1-ium-1-yl)tetradecyl)pyridin-1-ium 2,2,2-trifluoroacetate (CK147) (17)



To a round bottom flask was added compound **16** (0.0138 mmol, 18 mg) and TFA (1.32 mmol, 100 µL), in anhydrous DCM (500 µL) before being purged with nitrogen. The reaction was stirred at room temperature for 16 hours before being dried *in vacuo*. The title compound was used without further purification as a clear pale yellow solid (16 mg, yield = 25%). ^{1}H NMR (400 MHz, MeOD-d_4) δ 1.13 - 1.25 (20H, m), 1.27 - 1.84 (17H, m), 191 - 2.21 (4H, m), 2.24 - 2.39 (4H, m), 2.5 - 2.67 (2H, m), 2.95 - 3.10 (4H, m), 3.12 (6H, s), 3.55 - 3.82 (12H, m), 3.93 - 4.23 (7H, m), 6.86 (2H, d, *J* = 7.9 Hz), 7.06 (2H, d, *J* = 7.8 Hz), 8.02 (2H, d, *J* = 7.8 Hz), 8.11 (2H, d, *J* = 7.7 Hz).; ^{13}C NMR (101 MHz, MeOD-d_4) δ 23.97, 26.66, 27.21, 27.50, 28.88, 29.93, 30.21, 30.61, 30.69, 30.77, 31.95, 32.97, 33.16, 34.82, 35.99, 36.81, 36.96, 40.07, 40.25, 40.33, 41.06, 42.27, 45.79, 46.35, 46.82, 53.52, 54.00, 58.95, 59.17, 108.88, 109.51, 143.01, 143.75, 157.53, 157.88, 160.12, 169.86, 172.82, 175.80, 176.08, 176.36, 176.43, 177.79. MS (ES-ToF) m/z ($[M\text{-}CF_3COO^-]^{2+}$): calcd: 569.3230, found 569.3251.

8. References

1. Wang, N.; Brickute, D.; Braga, M.; Barnes, C.; Lu, H.; Allott, L.; Aboagye, E. O., Novel Non-Congeneric Derivatives of the Choline Kinase Alpha Inhibitor ICL-CCIC-0019. *Pharmaceutics* **2021,** *13* (7), 1078. https://doi.org/doi:10.3390/pharmaceutics13071078
2. Li, Y.; Inglese, M.; Dubash, S.; Barnes, C.; Brickute, D.; Braga, M. C.; Wang, N.; Beckley, A.; Heinzmann, K.; Allott, L.; Lu, H.; Chen, C.; Fu, R.; Carroll, L.; Aboagye, E. O., Consideration of Metabolite Efflux in Radiolabelled Choline Kinetics. *Pharmaceutics* **2021,** *13* (8), 1246. https://doi.org/doi:10.3390/pharmaceutics13081246
3. Allott, L.; Amgheib, A.; Barnes, C.; Braga, M.; Brickute, D.; Wang, N.; Fu, R.; Ghaem-Maghami, S.; Aboagye, E. O., Radiolabelling an 18F biologic via facile IEDDA "click" chemistry on the GE FASTLab™ platform. *Reaction Chemistry & Engineering* **2021,** *6* (6), 1070-1078. https://doi.org/10.1039/D1RE00117E
4. Allott, L.; Chen, C.; Braga, M.; Leung, S. F. J.; Wang, N.; Barnes, C.; Brickute, D.; Carroll, L.; Aboagye, E. O., Detecting hypoxia in vitro using 18F-pretargeted IEDDA "click" chemistry in live cells. *RSC Advances* **2021,** *11* (33), 20335-20341. https://doi.org/10.1039/D1RA02482E
5. Allott, L.; Brickute, D.; Chen, C.; Braga, M.; Barnes, C.; Wang, N.; Aboagye, E. O., Development of a fluorine-18 radiolabelled fluorescent chalcone: evaluated for detecting glycogen. *EJNMMI Radiopharmacy and Chemistry* **2020,** *5* (1), 17. https://doi.org/10.1186/s41181-020-00098-6
6. Berg, J. M.; Tymoczko, J. L.; Gatto, G. J.; Stryer, L., *Biochemistry*. Ninth edition. ed.; Macmillan International Higher Education: New York, 2019.
7. van Meer, G.; Voelker, D. R.; Feigenson, G. W., Membrane lipids: where they are and how they behave. *Nature Reviews Molecular Cell Biology* **2008,** *9* (2), 112-124. https://doi.org/10.1038/nrm2330
8. Zeisel, S. H., Choline: Critical Role During Fetal Development and Dietary Requirements in Adults. *Annual Review of Nutrition* **2006,** *26* (1), 229-250. https://doi.org/10.1146/annurev.nutr.26.061505.111156
9. Aoyama, C.; Liao, H.; Ishidate, K., Structure and function of choline kinase isoforms in mammalian cells. *Progress in Lipid Research* **2004,** *43* (3), 266-281. https://doi.org/https://doi.org/10.1016/j.plipres.2003.12.001
10. Walkey, C. J.; Yu, L.; Agellon, L. B.; Vance, D. E., Biochemical and Evolutionary Significance of Phospholipid Methylation⋆. *Journal of Biological Chemistry* **1998,** *273* (42), 27043-27046. https://doi.org/https://doi.org/10.1074/jbc.273.42.27043
11. Walkey, C. J.; Donohue, L. R.; Bronson, R.; Agellon, L. B.; Vance, D. E., Disruption of the murine gene encoding phosphatidylethanolamine N-methyltransferase. *Proc Natl Acad Sci U S A* **1997,** *94* (24), 12880-12885. https://doi.org/10.1073/pnas.94.24.12880
12. Kent, C., CTP:phosphocholine cytidylyltransferase. *Biochimica et Biophysica Acta (BBA) - Lipids and Lipid Metabolism* **1997,** *1348* (1), 79-90. https://doi.org/https://doi.org/10.1016/S0005-2760(97)00112-4
13. Kent, C., Regulation of phosphatidylcholine biosynthesis. *Progress in Lipid Research* **1990,** *29* (2), 87-105. https://doi.org/https://doi.org/10.1016/0163-7827(90)90010-I
14. da Costa, K.-A.; Badea, M.; Fischer, L. M.; Zeisel, S. H., Elevated serum creatine

phosphokinase in choline-deficient humans: mechanistic studies in C2C12 mouse myoblasts. *The American Journal of Clinical Nutrition* **2004,** *80* (1), 163-170. https://doi.org/10.1093/ajcn/80.1.163

15. Zeisel, S. H.; Da Costa, K.-A.; Franklin, P. D.; Alexander, E. A.; Lamont, J. T.; Sheard, N. F.; Beiser, A., Choline, an essential nutrient for humans. *The FASEB Journal* **1991,** *5* (7), 2093-2098. https://doi.org/https://doi.org/10.1096/fasebj.5.7.2010061

16. Guba, S. C.; Fink, L. M.; Fonseca, V., Hyperhomocysteinemia:An Emerging and Important Risk Factor for Thromboembolic and Cardiovascular Disease. *American Journal of Clinical Pathology* **1996,** *106* (6), 709-722. https://doi.org/10.1093/ajcp/106.6.709

17. da Costa, K.-A.; Gaffney, C. E.; Fischer, L. M.; Zeisel, S. H., Choline deficiency in mice and humans is associated with increased plasma homocysteine concentration after a methionine load. *The American journal of clinical nutrition* **2005,** *81* (2), 440-444. https://doi.org/10.1093/ajcn.81.2.440

18. Tiwari, P.; Dwivedi, S.; Singh, M. P.; Mishra, R.; Chandy, A., Basic and modern concepts on cholinergic receptor: A review. *Asian Pacific Journal of Tropical Disease* **2013,** *3* (5), 413-420. https://doi.org/https://doi.org/10.1016/S2222-1808(13)60094-8

19. Michel, V.; Yuan, Z.; Ramsubir, S.; Bakovic, M., Choline Transport for Phospholipid Synthesis. *Experimental Biology and Medicine* **2006,** *231* (5), 490-504. https://doi.org/10.1177/153537020623100503

20. Blusztajn, J. K., Choline, a Vital Amine. *Science* **1998,** *281* (5378), 794-795. https://doi.org/10.1126/science.281.5378.794

21. Zeisel, S. H.; Blusztajn, J. K., Choline and Human Nutrition. *Annual Review of Nutrition* **1994,** *14* (1), 269-296. https://doi.org/10.1146/annurev.nu.14.070194.001413

22. Simon, J. R.; Atweh, S.; Kuhar, M. J., Sodium-dependent high affinity choline uptake: a regulatory step in the synthesis of acetylcholine. *Journal of Neurochemistry* **1976,** *26* (5), 909-922. https://doi.org/https://doi.org/10.1111/j.1471-4159.1976.tb06472.x

23. Koepsell, H.; Endou, H., The SLC22 drug transporter family. *Pflügers Archiv* **2004,** *447* (5), 666-676. https://doi.org/10.1007/s00424-003-1089-9

24. Glunde, K.; Bhujwalla, Z. M.; Ronen, S. M., Choline metabolism in malignant transformation. *Nature Reviews Cancer* **2011,** *11* (12), 835-848. https://doi.org/10.1038/nrc3162

25. Griffiths, J. R.; Stevens, A. N.; Iles, R. A.; Gordon, R. E.; Shaw, D., 31P-NMR investigation of solid tumours in the living rat. *Bioscience Reports* **1981,** *1* (4), 319-325. https://doi.org/10.1007/bf01114871

26. Griffiths, J. R.; Cady, E.; Edwards, R. H. T.; McCready, V. R.; Wilkie, D. R.; Wiltshaw, E., 31P-NMR studies of a human tumour in situ. *The Lancet* **1983,** *321* (8339), 1435-1436. https://doi.org/10.1016/S0140-6736(83)92375-9

27. Glunde, K.; Bhujwalla, Z. M., Metabolic Tumor Imaging Using Magnetic Resonance Spectroscopy. *Seminars in Oncology* **2011,** *38* (1), 26-41. https://doi.org/https://doi.org/10.1053/j.seminoncol.2010.11.001

28. Schmidt, D. R.; Patel, R.; Kirsch, D. G.; Lewis, C. A.; Vander Heiden, M. G.; Locasale, J. W., Metabolomics in cancer research and emerging applications in clinical oncology. *CA: A Cancer Journal for Clinicians* **2021,** *71* (4), 333-358. https://doi.org/https://doi.org/10.3322/caac.21670

29. Ortmayr, K.; Dubuis, S.; Zampieri, M., Metabolic profiling of cancer cells reveals genome-wide crosstalk between transcriptional regulators and metabolism. *Nature Communications* **2019,**

10 (1), 1841. https://doi.org/10.1038/s41467-019-09695-9

30. Hu, J.; Locasale, J. W.; Bielas, J. H.; O'Sullivan, J.; Sheahan, K.; Cantley, L. C.; Heiden, M. G. V.; Vitkup, D., Heterogeneity of tumor-induced gene expression changes in the human metabolic network. *Nature Biotechnology* **2013,** *31* (6), 522-529. https://doi.org/10.1038/nbt.2530

31. Elia, I.; Haigis, M. C., Metabolites and the tumour microenvironment: from cellular mechanisms to systemic metabolism. *Nature Metabolism* **2021,** *3* (1), 21-32. https://doi.org/10.1038/s42255-020-00317-z

32. Weber, W. A.; Avril, N.; Schwaiger, M., Relevance of Positron Emission Tomography (PET) in Oncology. *Strahlentherapie und Onkologie* **1999,** *175* (8), 356-373. https://doi.org/10.1007/s000660050022

33. Been, L. B.; Suurmeijer, A. J. H.; Cobben, D. C. P.; Jager, P. L.; Hoekstra, H. J.; Elsinga, P. H., [18F]FLT-PET in oncology: current status and opportunities. *European Journal of Nuclear Medicine and Molecular Imaging* **2004,** *31* (12), 1659-1672. https://doi.org/10.1007/s00259-004-1687-6

34. Leyton, J.; Smith, G.; Zhao, Y.; Perumal, M.; Nguyen, Q.-D.; Robins, E.; Arstad, E.; Aboagye, E. O., [18F]fluoromethyl-[1,2-2H4]-choline: a novel radiotracer for imaging choline metabolism in tumors by positron emission tomography. *Cancer research* **2009,** *69* (19), 7721-7728. https://doi.org/10.1158/0008-5472.CAN-09-1419

35. Shetty, D.; Lee, Y.-S.; Jeong, J. M., (68)Ga-labeled radiopharmaceuticals for positron emission tomography. *Nucl Med Mol Imaging* **2010,** *44* (4), 233-240. https://doi.org/10.1007/s13139-010-0056-6

36. La, M. T.; Tran, V. H.; Kim, H.-K., Progress of Coordination and Utilization of Zirconium-89 for Positron Emission Tomography (PET) Studies. *Nucl Med Mol Imaging* **2019,** *53* (2), 115-124. https://doi.org/10.1007/s13139-019-00584-z

37. Vaquero, J. J.; Kinahan, P., Positron Emission Tomography: Current Challenges and Opportunities for Technological Advances in Clinical and Preclinical Imaging Systems. *Annual Review of Biomedical Engineering* **2015,** *17* (1), 385-414. https://doi.org/10.1146/annurev-bioeng-071114-040723

38. Witney, T. H.; Alam, I. S.; Turton, D. R.; Smith, G.; Carroll, L.; Brickute, D.; Twyman, F. J.; Nguyen, Q.-D.; Tomasi, G.; Awais, R. O.; Aboagye, E. O., Evaluation of deuterated 18F- and 11C-labeled choline analogs for cancer detection by positron emission tomography. *Clin Cancer Res* **2012,** *18* (4), 1063-1072. https://doi.org/10.1158/1078-0432.ccr-11-2462

39. Wittenberg, J.; Kornberg, A., CHOLINE PHOSPHOKINASE. *Journal of Biological Chemistry* **1953,** *202* (1), 431-444. https://doi.org/https://doi.org/10.1016/S0021-9258(19)57144-7

40. Ishidate K Fau - Nakagomi, K.; Nakagomi K Fau - Nakazawa, Y.; Nakazawa, Y., Complete purification of choline kinase from rat kidney and preparation of rabbit antibody against rat kidney choline kinase. (0021-9258 (Print)).

41. Hosaka, K.; Kodaki T Fau - Yamashita, S.; Yamashita, S., Cloning and characterization of the yeast CKI gene encoding choline kinase and its expression in Escherichia coli. (0021-9258 (Print)).

42. Hosaka, K.; Tanaka, S.; Nikawa, J.-i.; Yamashita, S., Cloning of a human choline kinase cDNA by complementation of the yeast cki mutation. *FEBS Letters* **1992,** *304* (2-3), 229-232. https://doi.org/https://doi.org/10.1016/0014-5793(92)80625-Q

43. Monks, D. E.; Goode, J. H.; Dewey, R. E., Characterization of Soybean Choline Kinase cDNAs

and Their Expression in Yeast and Escherichia coli. *Plant Physiology* **1996,** *110* (4), 1197-1205. https://doi.org/10.1104/pp.110.4.1197

44. Kim, K.-H.; Carman, G. M., Phosphorylation and Regulation of Choline Kinase from Saccharomyces cerevisiae by Protein Kinase A ⁎. *Journal of Biological Chemistry* **1999,** *274* (14), 9531-9538. https://doi.org/10.1074/jbc.274.14.9531

45. Wu, G.; Vance, D. E., Choline kinase and its function. (1208-6002 (Electronic)). https://doi.org/10.1139/O09-160

46. Aoyama, C.; Ohtani, A.; Ishidate, K., Expression and characterization of the active molecular forms of choline/ethanolamine kinase-α and -β in mouse tissues, including carbon tetrachloride-induced liver. *Biochemical Journal* **2002,** *363* (3), 777-784. https://doi.org/10.1042/bj3630777

47. Gallego-Ortega, D.; Ramirez de Molina, A.; Ramos, M. A.; Valdes-Mora, F.; Barderas, M. G.; Sarmentero-Estrada, J.; Lacal, J. C., Differential Role of Human Choline Kinase α and β Enzymes in Lipid Metabolism: Implications in Cancer Onset and Treatment. *PLOS ONE* **2009,** *4* (11), e7819. https://doi.org/10.1371/journal.pone.0007819

48. Contractor, K.; Challapalli, A.; Barwick, T.; Winkler, M.; Hellawell, G.; Hazell, S.; Tomasi, G.; Al-Nahhas, A.; Mapelli, P.; Kenny, L. M.; Tadrous, P.; Coombes, R. C.; Aboagye, E. O.; Mangar, S., Use of [11C]Choline PET-CT as a Noninvasive Method for Detecting Pelvic Lymph Node Status from Prostate Cancer and Relationship with Choline Kinase Expression. *Clinical Cancer Research* **2011,** *17* (24), 7673. https://doi.org/10.1158/1078-0432.CCR-11-2048

49. Wu, G.; Aoyama, C.; Young, S. G.; Vance, D. E., Early embryonic lethality caused by disruption of the gene for choline kinase alpha, the first enzyme in phosphatidylcholine biosynthesis. (0021-9258 (Print)).

50. Wu, G.; Sher, R. B.; Cox, G. A.; Vance, D. E., Understanding the muscular dystrophy caused by deletion of choline kinase beta in mice. *Biochimica et Biophysica Acta (BBA) - Molecular and Cell Biology of Lipids* **2009,** *1791* (5), 347-356. https://doi.org/https://doi.org/10.1016/j.bbalip.2009.02.006

51. Gruber, J.; See Too, W. C.; Wong, M. T.; Lavie, A.; McSorley, T.; Konrad, M., Balance of human choline kinase isoforms is critical for cell cycle regulation. *The FEBS Journal* **2012,** *279* (11), 1915-1928. https://doi.org/https://doi.org/10.1111/j.1742-4658.2012.08573.x

52. Ramírez de Molina, A.; Rodríguez-González, A.; Gutiérrez, R.; Martínez-Piñeiro, L.; Sánchez, J.; Bonilla, F.; Rosell, R.; Lacal, J., Overexpression of choline kinase is a frequent feature in human tumor-derived cell lines and in lung, prostate, and colorectal human cancers. *Biochem Biophys Res Commun* **2002,** *296* (3), 580-583. https://doi.org/10.1016/s0006-291x(02)00920-8

53. Glunde, K.; Raman, V.; Mori, N.; Bhujwalla, Z. M., RNA Interference–Mediated Choline Kinase Suppression in Breast Cancer Cells Induces Differentiation and Reduces Proliferation. *Cancer Research* **2005,** *65* (23), 11034-11043. https://doi.org/10.1158/0008-5472.Can-05-1807

54. Iorio, E.; Mezzanzanica, D.; Alberti, P.; Spadaro, F.; Ramoni, C.; D'Ascenzo, S.; Millimaggi, D.; Pavan, A.; Dolo, V.; Canevari, S.; Podo, F., Alterations of Choline Phospholipid Metabolism in Ovarian Tumor Progression. *Cancer Research* **2005,** *65* (20), 9369-9376. https://doi.org/10.1158/0008-5472.Can-05-1146

55. Ramírez de Molina, A.; Gutiérrez, R.; Ramos, M. A.; Silva, J. M.; Silva, J.; Bonilla, F.; Sánchez, J. J.; Lacal, J. C., Increased choline kinase activity in human breast carcinomas: clinical evidence for a potential novel antitumor strategy. *Oncogene* **2002,** *21* (27), 4317-4322.

https://doi.org/10.1038/sj.onc.1205556
56. Hernando, E.; Sarmentero-Estrada, J.; Koppie, T.; Belda-Iniesta, C.; Ramírez de Molina, V.; Cejas, P.; Ozu, C.; Le, C.; Sánchez, J. J.; González-Barón, M.; Koutcher, J.; Cordón-Cardó, C.; Bochner, B. H.; Lacal, J. C.; Ramírez de Molina, A., A critical role for choline kinase-α in the aggressiveness of bladder carcinomas. *Oncogene* **2009,** *28* (26), 2425-2435. https://doi.org/10.1038/onc.2009.91
57. Iorio, E.; Ricci, A.; Bagnoli, M.; Pisanu, M. E.; Castellano, G.; Di Vito, M.; Venturini, E.; Glunde, K.; Bhujwalla, Z. M.; Mezzanzanica, D.; Canevari, S.; Podo, F., Activation of Phosphatidylcholine Cycle Enzymes in Human Epithelial Ovarian Cancer Cells. *Cancer Research* **2010,** *70* (5), 2126-2135. https://doi.org/10.1158/0008-5472.Can-09-3833
58. Li, Z.; Wu, G.; van der Veen, J. N.; Hermansson, M.; Vance, D. E., Phosphatidylcholine metabolism and choline kinase in human osteoblasts. *Biochimica et Biophysica Acta (BBA) - Molecular and Cell Biology of Lipids* **2014,** *1841* (6), 859-867. https://doi.org/https://doi.org/10.1016/j.bbalip.2014.02.004
59. de Molina, A. R.; Sarmentero-Estrada, J.; Belda-Iniesta, C.; Tarón, M.; de Molina, V. R.; Cejas, P.; Skrzypski, M.; Gallego-Ortega, D.; de Castro, J.; Casado, E.; García-Cabezas, M. A.; Sánchez, J. J.; Nistal, M.; Rosell, R.; González-Barón, M.; Lacal, J. C., Expression of choline kinase alpha to predict outcome in patients with early-stage non-small-cell lung cancer: a retrospective study. *The Lancet Oncology* **2007,** *8* (10), 889-897. https://doi.org/10.1016/S1470-2045(07)70279-6
60. Asim, M.; Massie, C. E.; Orafidiya, F.; Pértega-Gomes, N.; Warren, A. Y.; Esmaeili, M.; Selth, L. A.; Zecchini, H. I.; Luko, K.; Qureshi, A.; Baridi, A.; Menon, S.; Madhu, B.; Escriu, C.; Lyons, S.; Vowler, S. L.; Zecchini, V. R.; Shaw, G.; Hessenkemper, W.; Russell, R.; Mohammed, H.; Stefanos, N.; Lynch, A. G.; Grigorenko, E.; D'Santos, C.; Taylor, C.; Lamb, A.; Sriranjan, R.; Yang, J.; Stark, R.; Dehm, S. M.; Rennie, P. S.; Carroll, J. S.; Griffiths, J. R.; Tavaré, S.; Mills, I. G.; McEwan, I. J.; Baniahmad, A.; Tilley, W. D.; Neal, D. E., Choline Kinase Alpha as an Androgen Receptor Chaperone and Prostate Cancer Therapeutic Target. *JNCI: Journal of the National Cancer Institute* **2015,** *108* (5). https://doi.org/10.1093/jnci/djv371
61. Ramírez de Molina, A.; Rodríguez-González, A.; Penalva, V.; Lucas, L.; Lacal, J. C., Inhibition of ChoK Is an Efficient Antitumor Strategy for Harvey-, Kirsten-, and N-ras-Transformed Cells. *Biochemical and Biophysical Research Communications* **2001,** *285* (4), 873-879. https://doi.org/https://doi.org/10.1006/bbrc.2001.5250
62. Ramírez de Molina, A.; Penalva, V.; Lucas, L.; Lacal, J. C., Regulation of choline kinase activity by Ras proteins involves Ral–GDS and PI3K. *Oncogene* **2002,** *21* (6), 937-946. https://doi.org/10.1038/sj.onc.1205144
63. Rami´rez de Molina, A.; Gallego-Ortega, D.; Sarmentero, J.; Ban˜ez-Coronel, M. n.; Marti´n-Cantalejo, Y.; Lacal, J. C., Choline Kinase Is a Novel Oncogene that Potentiates RhoA-Induced Carcinogenesis. *Cancer Research* **2005,** *65* (13), 5647-5653. https://doi.org/10.1158/0008-5472.Can-04-4416
64. Trousil, S.; Kaliszczak, M.; Schug, Z.; Nguyen, Q.-D.; Tomasi, G.; Favicchio, R.; Brickute, D.; Fortt, R.; Twyman, F. J.; Carroll, L.; Kalusa, A.; Navaratnam, N.; Adejumo, T.; Carling, D.; Gottlieb, E.; Aboagye, E. O., The novel choline kinase inhibitor ICL-CCIC-0019 reprograms cellular metabolism and inhibits cancer cell growth. *Oncotarget* **2016,** *7* (24). https://doi.org/https://doi.org/10.18632/oncotarget.9466

65. Chinchar, V. G., REPLICATION OF VIRUSES. In *Encyclopedia of Virology (Second Edition)*, Granoff, A.; Webster, R. G., Eds. Elsevier: Oxford, 1999; pp 1471-1478.
66. Fire, A.; Albertson, D.; Harrison, S. W.; Moerman, D. G., Production of antisense RNA leads to effective and specific inhibition of gene expression in C. elegans muscle. *Development* **1991,** *113* (2), 503-514. https://doi.org/10.1242/dev.113.2.503
67. Ray, S., The Cell: A Molecular Approach. *Yale J Biol Med* **2014,** *87* (4), 603-604.
68. Housden, B. E.; Muhar, M.; Gemberling, M.; Gersbach, C. A.; Stainier, D. Y. R.; Seydoux, G.; Mohr, S. E.; Zuber, J.; Perrimon, N., Loss-of-function genetic tools for animal models: cross-species and cross-platform differences. *Nature Reviews Genetics* **2017,** *18* (1), 24-40. https://doi.org/10.1038/nrg.2016.118
69. Alló, M.; Buggiano, V.; Fededa, J. P.; Petrillo, E.; Schor, I.; de la Mata, M.; Agirre, E.; Plass, M.; Eyras, E.; Elela, S. A.; Klinck, R.; Chabot, B.; Kornblihtt, A. R., Control of alternative splicing through siRNA-mediated transcriptional gene silencing. *Nature Structural & Molecular Biology* **2009,** *16* (7), 717-724. https://doi.org/10.1038/nsmb.1620
70. Iorns, E.; Lord, C. J.; Turner, N.; Ashworth, A., Utilizing RNA interference to enhance cancer drug discovery. *Nature Reviews Drug Discovery* **2007,** *6* (7), 556-568. https://doi.org/10.1038/nrd2355
71. Hannon, G. J.; Rossi, J. J., Unlocking the potential of the human genome with RNA interference. *Nature* **2004,** *431* (7006), 371-378. https://doi.org/10.1038/nature02870
72. Hannon, G. J., RNA interference. *Nature* **2002,** *418* (6894), 244-251. https://doi.org/10.1038/418244a
73. MacKeigan, J. P.; Murphy, L. O.; Blenis, J., Sensitized RNAi screen of human kinases and phosphatases identifies new regulators of apoptosis and chemoresistance. *Nature Cell Biology* **2005,** *7* (6), 591-600. https://doi.org/10.1038/ncb1258
74. Yalcin, A.; Clem, B.; Makoni, S.; Clem, A.; Nelson, K.; Thornburg, J.; Siow, D.; Lane, A. N.; Brock, S. E.; Goswami, U.; Eaton, J. W.; Telang, S.; Chesney, J., Selective inhibition of choline kinase simultaneously attenuates MAPK and PI3K/AKT signaling. *Oncogene* **2010,** *29* (1), 139-149. https://doi.org/10.1038/onc.2009.317
75. de Molina, A. R.; Báñez-Coronel, M.; Gutiérrez, R.; Rodríguez-González, A.; Olmeda, D.; Megías, D.; Lacal, J. C., Choline Kinase Activation Is a Critical Requirement for the Proliferation of Primary Human Mammary Epithelial Cells and Breast Tumor Progression. *Cancer Research* **2004,** *64* (18), 6732-6739. https://doi.org/10.1158/0008-5472.Can-04-0489
76. Krishnamachary, B.; Glunde, K.; Wildes, F.; Mori, N.; Takagi, T.; Raman, V.; Bhujwalla, Z. M., Noninvasive Detection of Lentiviral-Mediated Choline Kinase Targeting in a Human Breast Cancer Xenograft. *Cancer Research* **2009,** *69* (8), 3464-3471. https://doi.org/10.1158/0008-5472.Can-08-4120
77. Malito, E.; Sekulic, N.; Too, W. C. S.; Konrad, M.; Lavie, A., Elucidation of Human Choline Kinase Crystal Structures in Complex with the Products ADP or Phosphocholine. *Journal of Molecular Biology* **2006,** *364* (2), 136-151. https://doi.org/https://doi.org/10.1016/j.jmb.2006.08.084
78. Torretta, A.; Lopez-Cara, L. C.; Parisini, E., Crystal Structure of the Apo and the ADP-Bound Form of Choline Kinase from Plasmodium falciparum. *Crystals* **2020,** *10* (7), 613. https://doi.org/https://doi.org/10.3390/cryst10070613
79. Peisach, D.; Gee, P.; Kent, C.; Xu, Z., The Crystal Structure of Choline Kinase Reveals a

Eukaryotic Protein Kinase Fold. *Structure* **2003,** *11* (6), 703-713. https://doi.org/https://doi.org/10.1016/S0969-2126(03)00094-7

80. Scheeff, E. D.; Bourne, P. E., Structural evolution of the protein kinase-like superfamily. *PLoS Comput Biol* **2005,** *1* (5), e49. https://doi.org/10.1371/journal.pcbi.0010049

81. Brown, M.; Schumacher, M. A.; Wiens, G. D.; Brennan, R. G.; Rittenberg, M. B., The Structural Basis of Repertoire Shift in an Immune Response to Phosphocholine. *Journal of Experimental Medicine* **2000,** *191* (12), 2101-2112. https://doi.org/10.1084/jem.191.12.2101

82. Lacal, J. C., In vivo antitumor activity of choline kinase inhibitors: a novel target for anticancer drug discovery. *European Journal of Cancer* **1999,** *35*, S133. https://doi.org/10.1016/S0959-8049(99)80913-7

83. Cannon, J. G., Structure-activity aspects of hemicholinium-3 (HC-3) and its analogs and congeners. *Medicinal Research Reviews* **1994,** *14* (5), 505-531. https://doi.org/https://doi.org/10.1002/med.2610140503

84. Gómez-Pérez, V.; McSorley, T.; See Too, W. C.; Konrad, M.; Campos, J. M., Novel 4-Amino Bis-pyridinium and Bis-quinolinium Derivatives as Choline Kinase Inhibitors with Antiproliferative Activity against the Human Breast Cancer SKBR-3 Cell Line. *ChemMedChem* **2012,** *7* (4), 663-669. https://doi.org/https://doi.org/10.1002/cmdc.201100505

85. Campos, J.; Núñez, M. C.; Conejo-García, A.; Sánchez-Martín, R. M.; Hernández-Alcoceba, R.; Rodríguez-González, A.; Lacal, J. C.; Gallo, M. A.; Espinosa, A., QSAR-derived choline kinase inhibitors: how rational can antiproliferative drug design be? *Current medicinal chemistry* **2003,** *10* (13), 1095-1112. https://doi.org/10.2174/0929867033457539

86. Hernández-Alcoceba, R.; Saniger, L.; Campos, J.; Núñez, M. C.; Khaless, F.; Gallo, M. A.; Espinosa, A.; Lacal, J. C., Choline kinase inhibitors as a novel approach for antiproliferative drug design. *Oncogene* **1997,** *15* (19), 2289-2301. https://doi.org/10.1038/sj.onc.1201414

87. Ferguson, S. M.; Blakely, R. D., The choline transporter resurfaces: new roles for synaptic vesicles? *Mol Interv* **2004,** *4* (1), 22-37. https://doi.org/10.1124/mi.4.1.22

88. Campos, J. n.; Núñez, M. a. d. C.; Rodrı´guez, V.; Gallo, M. A.; Espinosa, A., QSAR of 1,1′-(1,2-ethylenebisbenzyl)bis(4-substitutedpyridinium) dibromides as choline kinase inhibitors: a different approach for antiproliferative drug design. *Bioorganic & Medicinal Chemistry Letters* **2000,** *10* (8), 767-770. https://doi.org/https://doi.org/10.1016/S0960-894X(00)00080-9

89. Rodríguez-González, A.; Ramirez de Molina, A.; Fernández, F.; Lacal, J. C., Choline kinase inhibition induces the increase in ceramides resulting in a highly specific and selective cytotoxic antitumoral strategy as a potential mechanism of action. *Oncogene* **2004,** *23* (50), 8247-8259. https://doi.org/10.1038/sj.onc.1208045

90. Sanchez-Lopez, E.; Zimmerman, T.; Gomez del Pulgar, T.; Moyer, M. P.; Lacal Sanjuan, J. C.; Cebrian, A., Choline kinase inhibition induces exacerbated endoplasmic reticulum stress and triggers apoptosis via CHOP in cancer cells. *Cell Death & Disease* **2013,** *4* (11), e933-e933. https://doi.org/10.1038/cddis.2013.453

91. Chua, B. T.; Gallego-Ortega, D.; de Molina, A. R.; Ullrich, A.; Lacal, J. C.; Downward, J., Regulation of Akt(ser473) phosphorylation by Choline kinase in breast carcinoma cells. *Molecular Cancer* **2009,** *8* (1), 131. https://doi.org/10.1186/1476-4598-8-131

92. Al-Saffar, N. M. S.; Troy, H.; de Molina, A. R.; Jackson, L. E.; Madhu, B.; Griffiths, J. R.; Leach, M. O.; Workman, P.; Lacal, J. C.; Judson, I. R.; Chung, Y.-L., Noninvasive Magnetic Resonance Spectroscopic Pharmacodynamic Markers of the Choline Kinase Inhibitor MN58b in

Human Carcinoma Models. *Cancer Research* **2006,** *66* (1), 427-434. https://doi.org/10.1158/0008-5472.Can-05-1338

93. Trousil, S.; Carroll, L.; Kalusa, A.; Aberg, O.; Kaliszczak, M.; Aboagye, E. O., Design of symmetrical and nonsymmetrical N,N-dimethylaminopyridine derivatives as highly potent choline kinase alpha inhibitors. *MedChemComm* **2013,** *4* (4), 693-696. https://doi.org/10.1039/C3MD00068K

94. Schiaffino-Ortega, S.; Baglioni, E.; Mariotto, E.; Bortolozzi, R.; Serrán-Aguilera, L.; Ríos-Marco, P.; Carrasco-Jimenez, M. P.; Gallo, M. A.; Hurtado-Guerrero, R.; Marco, C.; Basso, G.; Viola, G.; Entrena, A.; López-Cara, L. C., Design, synthesis, crystallization and biological evaluation of new symmetrical biscationic compounds as selective inhibitors of human Choline Kinase α1 (ChoKα1). *Scientific Reports* **2016,** *6* (1), 23793. https://doi.org/10.1038/srep23793

95. Mariotto, E.; Viola, G.; Ronca, R.; Persano, L.; Aveic, S.; Bhujwalla, Z. M.; Mori, N.; Accordi, B.; Serafin, V.; López-Cara, L. C.; Bortolozzi, R., Choline Kinase Alpha Inhibition by EB-3D Triggers Cellular Senescence, Reduces Tumor Growth and Metastatic Dissemination in Breast Cancer. *Cancers* **2018,** *10* (10), 391. https://doi.org/10.3390/cancers10100391

96. Mariotto, E.; Bortolozzi, R.; Volpin, I.; Carta, D.; Serafin, V.; Accordi, B.; Basso, G.; Navarro, P. L.; López-Cara, L. C.; Viola, G., EB-3D a novel choline kinase inhibitor induces deregulation of the AMPK-mTOR pathway and apoptosis in leukemia T-cells. *Biochemical Pharmacology* **2018,** *155*, 213-223. https://doi.org/https://doi.org/10.1016/j.bcp.2018.07.004

97. Sola-Leyva, A.; López-Cara, L. C.; Ríos-Marco, P.; Ríos, A.; Marco, C.; Carrasco-Jiménez, M. P., Choline kinase inhibitors EB-3D and EB-3P interferes with lipid homeostasis in HepG2 cells. *Scientific Reports* **2019,** *9* (1), 5109. https://doi.org/10.1038/s41598-019-40885-z

98. Lacal, J. C., Choline kinase: a novel target for antitumor drugs. *IDrugs* **2001,** *4* (4), 419-426.

99. Sánchez-Martín, R.; Campos, J. M.; Conejo-García, A.; Cruz-López, O.; Báñez-Coronel, M.; Rodríguez-González, A.; Gallo, M. A.; Lacal, J. C.; Espinosa, A., Symmetrical Bis-Quinolinium Compounds: New Human Choline Kinase Inhibitors with Antiproliferative Activity against the HT-29 Cell Line. *Journal of Medicinal Chemistry* **2005,** *48* (9), 3354-3363. https://doi.org/10.1021/jm049061o

100. Campos, J. M.; Sanchez-Martin, R. M.; Conejo-Garcia, A.; Entrena, A.; Gallo, M. A.; Espinosa, A., (Q)SAR Studies to Design New Human Choline Kinase Inhibitors as Antiproliferative Drugs. *Current Medicinal Chemistry* **2006,** *13* (11), 1231-1248. https://doi.org/http://dx.doi.org/10.2174/092986706776872961

101. Lacal, J. C.; Campos, J. M., Preclinical Characterization of RSM-932A, a Novel Anticancer Drug Targeting the Human Choline Kinase Alpha, an Enzyme Involved in Increased Lipid Metabolism of Cancer Cells. *Molecular Cancer Therapeutics* **2015,** *14* (1), 31-39. https://doi.org/10.1158/1535-7163.Mct-14-0531

102. de la Cueva, A.; Ramírez de Molina, A.; Álvarez-Ayerza, N.; Ramos, M. A.; Cebrián, A.; Pulgar, T. G. d.; Lacal, J. C., Combined 5-FU and ChoKα Inhibitors as a New Alternative Therapy of Colorectal Cancer: Evidence in Human Tumor-Derived Cell Lines and Mouse Xenografts. *PLOS ONE* **2013,** *8* (6), e64961. https://doi.org/10.1371/journal.pone.0064961

103. Arlauckas, S. P.; Popov, A. V.; Delikatny, E. J., Direct Inhibition of Choline Kinase by a Near-Infrared Fluorescent Carbocyanine. *Molecular Cancer Therapeutics* **2014,** *13* (9), 2149-2158. https://doi.org/10.1158/1535-7163.Mct-14-0085

104. Arlauckas, S. P.; Kumar, M.; Popov, A. V.; Poptani, H.; Delikatny, E. J., Near infrared

fluorescent imaging of choline kinase alpha expression and inhibition in breast tumors. *Oncotarget* **2017,** *8* (10). https://doi.org/10.18632/oncotarget.14965

105. Clem, B. F.; Clem, A. L.; Yalcin, A.; Goswami, U.; Arumugam, S.; Telang, S.; Trent, J. O.; Chesney, J., A novel small molecule antagonist of choline kinase-α that simultaneously suppresses MAPK and PI3K/AKT signaling. *Oncogene* **2011,** *30* (30), 3370-3380. https://doi.org/10.1038/onc.2011.51

106. Serrán-Aguilera, L.; Nuti, R.; López-Cara, L. C.; Mezo, M. Á. G.; Macchiarulo, A.; Entrena, A.; Hurtado-Guerrero, R., Pharmacophore-Based Virtual Screening to Discover New Active Compounds for Human Choline Kinase α1. *Molecular Informatics* **2015,** *34* (6-7), 458-466. https://doi.org/https://doi.org/10.1002/minf.201400140

107. Hudson, C. S.; Knegtel, R. M.; Brown, K.; Charlton, P. A.; Pollard, J. R., Kinetic and mechanistic characterisation of Choline Kinase-α. *Biochim Biophys Acta* **2013,** *1834* (6), 1107-1116. https://doi.org/10.1016/j.bbapap.2013.02.008

108. Falcon, S. C.; Hudson, C. S.; Huang, Y.; Mortimore, M.; Golec, J. M.; Charlton, P. A.; Weber, P.; Sundaram, H., A non-catalytic role of choline kinase alpha is important in promoting cancer cell survival. *Oncogenesis* **2013,** *2* (3), e38-e38. https://doi.org/10.1038/oncsis.2013.2

109. Arlauckas, S. P.; Popov, A. V.; Delikatny, E. J., Choline kinase alpha—Putting the ChoK-hold on tumor metabolism. *Progress in Lipid Research* **2016,** *63*, 28-40. https://doi.org/https://doi.org/10.1016/j.plipres.2016.03.005

110. Sheff, K. Y.; Tedford, C. E.; Flynn, J. R.; Yorek, M. A.; Cannon, J. G.; Long, J. P., Stereoisomers of quaternary and tertiary 4-methyl piperidine analogs of hemicholinium-3. *J Pharmacol Exp Ther* **1988,** *247* (2), 640-644.

111. Cannon, J. G.; Lee, T. M.; Chang, Y.; Nyanda, A. M.; Bhattacharyya, B.; Flynn, J. R.; Chatterjee, T.; Bhatnagar, R. K.; Long, J. P., Structure-activity relationship studies of hemicholinium (HC-3) congeners. *Pharm Res* **1988,** *5* (6), 359-364. https://doi.org/10.1023/a:1015955527100

112.Castro-Navas, F. F.; Schiaffino-Ortega, S.; Carrasco-Jimenez, M. P.; Ríos-Marco, P.; Marco, C.; Espinosa, A.; Gallo, M. A.; Mariotto, E.; Basso, G.; Viola, G.; Entrena-Guadix, A.; López-Cara, L. C., New more polar symmetrical bipyridinic compounds: new strategy for the inhibition of choline kinase α1. *Future Medicinal Chemistry* **2015,** *7* (4), 417-436. https://doi.org/10.4155/fmc.15.1

113. Campos, J. n. M.; Núñez, M. a. C.; Sánchez, R. M.; Gómez-Vidal, J. A.; Rodrı´guez-Gonzá lez, A. n.; Báñez, M.; Gallo, M. A.; Lacal, J. C.; Espinosa, A., Quantitative structure–activity relationships for a series of symmetrical bisquaternary anticancer compounds. *Bioorganic & Medicinal Chemistry* **2002,** *10* (7), 2215-2231. https://doi.org/https://doi.org/10.1016/S0968-0896(02)00054-8

114. Porporato, P. E.; Filigheddu, N.; Pedro, J. M. B.-S.; Kroemer, G.; Galluzzi, L., Mitochondrial metabolism and cancer. *Cell Research* **2018,** *28* (3), 265-280. https://doi.org/10.1038/cr.2017.155

115. Klein, K.; He, K.; Younes, A. I.; Barsoumian, H. B.; Chen, D.; Ozgen, T.; Mosaffa, S.; Patel, R. R.; Gu, M.; Novaes, J.; Narayanan, A.; Cortez, M. A.; Welsh, J. W., Role of Mitochondria in Cancer Immune Evasion and Potential Therapeutic Approaches. *Frontiers in Immunology* **2020,** *11*. https://doi.org/10.3389/fimmu.2020.573326

116. Wang, F.; Ogasawara, M. A.; Huang, P., Small mitochondria-targeting molecules as anti-

cancer agents. *Molecular Aspects of Medicine* **2010,** *31* (1), 75-92. https://doi.org/https://doi.org/10.1016/j.mam.2009.12.003

117. Modica-Napolitano, J. S.; Aprille, J. R., Delocalized lipophilic cations selectively target the mitochondria of carcinoma cells. *Advanced Drug Delivery Reviews* **2001,** *49* (1), 63-70. https://doi.org/https://doi.org/10.1016/S0169-409X(01)00125-9

118. Rodríguez-González, A.; Ramírez De Molina, A.; Bañez-Coronel, M.; Megias, D.; Lacal, J. C., Inhibition of choline kinase renders a highly selective cytotoxic effect in tumour cells through a mitochondrial independent mechanism. *Int J Oncol* **2005,** *26* (4), 999-1008. https://doi.org/10.3892/ijo.26.4.999

119. Rubio-Ruiz, B.; Serrán-Aguilera, L.; Hurtado-Guerrero, R.; Conejo-García, A., Recent advances in the design of choline kinase α inhibitors and the molecular basis of their inhibition. *Medicinal Research Reviews* **2021,** *41* (2), 902-927. https://doi.org/https://doi.org/10.1002/med.21746

120. Bernard, N. J., Choline kinase—more than a cancer therapy target? *Nature Reviews Rheumatology* **2014,** *10* (12), 699-699. https://doi.org/10.1038/nrrheum.2014.180

121. Guma, M.; Sanchez-Lopez, E.; Lodi, A.; Garcia-Carbonell, R.; Tiziani, S.; Karin, M.; Lacal, J. C.; Firestein, G. S., Choline kinase inhibition in rheumatoid arthritis. *Annals of the Rheumatic Diseases* **2015,** *74* (7), 1399-1407. https://doi.org/10.1136/annrheumdis-2014-205696

122. Zimmerman, T.; Lacal, J. C.; Ibrahim, S. A., Choline Kinase Emerges as a Promising Drug Target in Gram-Positive Bacteria. *Frontiers in Microbiology* **2019,** *10* (2146). https://doi.org/10.3389/fmicb.2019.02146

123. Zimmerman, T.; Moneriz, C.; Diez, A.; Bautista, J. M.; Pulgar, T. G. d.; Cebrián, A.; Lacal, J. C., Antiplasmodial Activity and Mechanism of Action of RSM-932A, a Promising Synergistic Inhibitor of Plasmodium falciparum Choline Kinase. *Antimicrobial Agents and Chemotherapy* **2013,** *57* (12), 5878-5888. https://doi.org/doi:10.1128/AAC.00920-13

124. Serrán-Aguilera, L.; Denton, H.; Rubio-Ruiz, B.; López-Gutiérrez, B.; Entrena, A.; Izquierdo, L.; Smith, T. K.; Conejo-García, A.; Hurtado-Guerrero, R., Plasmodium falciparum Choline Kinase Inhibition Leads to a Major Decrease in Phosphatidylethanolamine Causing Parasite Death. *Scientific Reports* **2016,** *6* (1), 33189. https://doi.org/10.1038/srep33189

125. Rubio-Ruiz, B.; Castillo-Acosta, V. M.; Pérez-Moreno, G.; Espinosa, A.; González-Pacanowska, D.; Ruiz-Pérez, L. M.; Entrena, A.; Conejo-García, A., In vitro antiplasmodial and cytotoxic activities of asymmetrical pyridinium derivatives. *European Journal of Medicinal Chemistry* **2014,** *85*, 289-292. https://doi.org/https://doi.org/10.1016/j.ejmech.2014.07.105

126. Lima, L. M.; Barreiro, E. J., Bioisosterism: A Useful Strategy for Molecular Modification and Drug Design. *Current Medicinal Chemistry* **2005,** *12* (1), 23-49. https://doi.org/10.2174/0929867053363540

127. Lima, L. M.; Alves, M. A.; do Amaral, D. N., Homologation: A Versatile Molecular Modification Strategy to Drug Discovery. *Current Topics in Medicinal Chemistry* **2019,** *19* (19), 1734-1750. https://doi.org/10.2174/1568026619666190808145235

128. Rafael, V. C. G.; Glaucius, O.; Adriano, D. A., Modern Drug Discovery Technologies: Opportunities and Challenges in Lead Discovery. *Combinatorial Chemistry & High Throughput Screening* **2011,** *14* (10), 830-839. https://doi.org/http://dx.doi.org/10.2174/138620711797537067

129. Rautio, J.; Kumpulainen, H.; Heimbach, T.; Oliyai, R.; Oh, D.; Järvinen, T.; Savolainen, J.,

Prodrugs: design and clinical applications. *Nature Reviews Drug Discovery* **2008,** *7* (3), 255-270. https://doi.org/10.1038/nrd2468

130. Rautio, J.; Meanwell, N. A.; Di, L.; Hageman, M. J., The expanding role of prodrugs in contemporary drug design and development. *Nature Reviews Drug Discovery* **2018,** *17* (8), 559-587. https://doi.org/10.1038/nrd.2018.46

131. Albert, A., Chemical Aspects of Selective Toxicity. *Nature* **1958,** *182* (4633), 421-423. https://doi.org/10.1038/182421a0

132. Najjar, A.; Najjar, A.; Karaman, R., Newly Developed Prodrugs and Prodrugs in Development; an Insight of the Recent Years. *Molecules* **2020,** *25* (4), 884.

133. Kevin, B.; Robert, W.; Iain, G.; Kevin, D., Design of Ester Prodrugs to Enhance Oral Absorption of Poorly Permeable Compounds: Challenges to the Discovery Scientist. *Current Drug Metabolism* **2003,** *4* (6), 461-485. https://doi.org/http://dx.doi.org/10.2174/1389200033489253

134. Ortiz de Montellano, P. R., Cytochrome P450-activated prodrugs. *Future Medicinal Chemistry* **2013,** *5* (2), 213-228. https://doi.org/10.4155/fmc.12.197

135. VanderMolen, K. M.; McCulloch, W.; Pearce, C. J.; Oberlies, N. H., Romidepsin (Istodax, NSC 630176, FR901228, FK228, depsipeptide): a natural product recently approved for cutaneous T-cell lymphoma. *The Journal of Antibiotics* **2011,** *64* (8), 525-531. https://doi.org/10.1038/ja.2011.35

136. Cundy, K. C.; Branch, R.; Chernov-Rogan, T.; Dias, T.; Estrada, T.; Hold, K.; Koller, K.; Liu, X.; Mann, A.; Panuwat, M.; Raillard, S. P.; Upadhyay, S.; Wu, Q. Q.; Xiang, J.-N.; Yan, H.; Zerangue, N.; Zhou, C. X.; Barrett, R. W.; Gallop, M. A., XP13512 [(±)-1-([(α-Isobutanoyloxyethoxy)carbonyl] aminomethyl)-1-cyclohexane Acetic Acid], A Novel Gabapentin Prodrug: I. Design, Synthesis, Enzymatic Conversion to Gabapentin, and Transport by Intestinal Solute Transporters. *Journal of Pharmacology and Experimental Therapeutics* **2004,** *311* (1), 315-323. https://doi.org/10.1124/jpet.104.067934

137. Cundy, K. C.; Annamalai, T.; Bu, L.; De Vera, J.; Estrela, J.; Luo, W.; Shirsat, P.; Torneros, A.; Yao, F.; Zou, J.; Barrett, R. W.; Gallop, M. A., XP13512 [(±)-1-([(α-Isobutanoyloxyethoxy)carbonyl] aminomethyl)-1-cyclohexane Acetic Acid], A Novel Gabapentin Prodrug: II. Improved Oral Bioavailability, Dose Proportionality, and Colonic Absorption Compared with Gabapentin in Rats and Monkeys. *Journal of Pharmacology and Experimental Therapeutics* **2004,** *311* (1), 324-333. https://doi.org/10.1124/jpet.104.067959

138. Ohwada, J.; Tsukazaki, M.; Hayase, T.; Oikawa, N.; Isshiki, Y.; Fukuda, H.; Mizuguchi, E.; Sakaitani, M.; Shiratori, Y.; Yamazaki, T.; Ichihara, S.; Umeda, I.; Shimma, N., Design, synthesis and antifungal activity of a novel water soluble prodrug of antifungal triazole. *Bioorganic & Medicinal Chemistry Letters* **2003,** *13* (2), 191-196. https://doi.org/https://doi.org/10.1016/S0960-894X(02)00892-2

139. Kratz, F.; Warnecke, A.; Scheuermann, K.; Stockmar, C.; Schwab, J.; Lazar, P.; Drückes, P.; Esser, N.; Drevs, J.; Rognan, D.; Bissantz, C.; Hinderling, C.; Folkers, G.; Fichtner, I.; Unger, C., Probing the Cysteine-34 Position of Endogenous Serum Albumin with Thiol-Binding Doxorubicin Derivatives. Improved Efficacy of an Acid-Sensitive Doxorubicin Derivative with Specific Albumin-Binding Properties Compared to That of the Parent Compound. *Journal of Medicinal Chemistry* **2002,** *45* (25), 5523-5533. https://doi.org/10.1021/jm020276c

140. Nakamura, A.; Yamada, T.; Asaki, T., Synthesis and evaluation of N-acylsulfonamide and N-

acylsulfonylurea prodrugs of a prostacyclin receptor agonist. *Bioorganic & Medicinal Chemistry* **2007,** *15* (24), 7720-7725. https://doi.org/https://doi.org/10.1016/j.bmc.2007.08.052

141. Asaki, T.; Kuwano, K.; Morrison, K.; Gatfield, J.; Hamamoto, T.; Clozel, M., Selexipag: An Oral and Selective IP Prostacyclin Receptor Agonist for the Treatment of Pulmonary Arterial Hypertension. *Journal of Medicinal Chemistry* **2015,** *58* (18), 7128-7137. https://doi.org/10.1021/acs.jmedchem.5b00698

142. Manzari, M. T.; Shamay, Y.; Kiguchi, H.; Rosen, N.; Scaltriti, M.; Heller, D. A., Targeted drug delivery strategies for precision medicines. *Nature Reviews Materials* **2021,** *6* (4), 351-370. https://doi.org/10.1038/s41578-020-00269-6

143. Vasir, J. K.; Labhasetwar, V., Targeted Drug Delivery in Cancer Therapy. *Technology in Cancer Research & Treatment* **2005,** *4* (4), 363-374. https://doi.org/10.1177/153303460500400405

144. Duncan, R.; Vicent, M. J., Polymer therapeutics-prospects for 21st century: The end of the beginning. *Advanced Drug Delivery Reviews* **2013,** *65* (1), 60-70. https://doi.org/https://doi.org/10.1016/j.addr.2012.08.012

145. Riber, C. F.; Zelikin, A. N., Recent advances in macromolecular prodrugs. *Current Opinion in Colloid & Interface Science* **2017,** *31*, 1-9. https://doi.org/https://doi.org/10.1016/j.cocis.2017.06.002

146. Duncan, R., Polymer conjugates as anticancer nanomedicines. *Nature Reviews Cancer* **2006,** *6* (9), 688-701. https://doi.org/10.1038/nrc1958

147. Duncan, R.; Gaspar, R., Nanomedicine(s) under the Microscope. *Molecular Pharmaceutics* **2011,** *8* (6), 2101-2141. https://doi.org/10.1021/mp200394t

148. Parslow, A. C.; Parakh, S.; Lee, F.-T.; Gan, H. K.; Scott, A. M., Antibody–Drug Conjugates for Cancer Therapy. *Biomedicines* **2016,** *4* (3), 14.

149. McCombs, J. R.; Owen, S. C., Antibody Drug Conjugates: Design and Selection of Linker, Payload and Conjugation Chemistry. *The AAPS Journal* **2015,** *17* (2), 339-351. https://doi.org/10.1208/s12248-014-9710-8

150. Casi, G.; Neri, D., Antibody–Drug Conjugates and Small Molecule–Drug Conjugates: Opportunities and Challenges for the Development of Selective Anticancer Cytotoxic Agents. *Journal of Medicinal Chemistry* **2015,** *58* (22), 8751-8761. https://doi.org/10.1021/acs.jmedchem.5b00457

151. Srinivasarao, M.; Galliford, C. V.; Low, P. S., Principles in the design of ligand-targeted cancer therapeutics and imaging agents. *Nature Reviews Drug Discovery* **2015,** *14* (3), 203-219. https://doi.org/10.1038/nrd4519

152. Shi, G.; Guo, W.; Stephenson, S. M.; Lee, R. J., Efficient intracellular drug and gene delivery using folate receptor-targeted pH-sensitive liposomes composed of cationic/anionic lipid combinations. *Journal of Controlled Release* **2002,** *80* (1), 309-319. https://doi.org/https://doi.org/10.1016/S0168-3659(02)00017-2

153. Lewis Phillips, G. D.; Li, G.; Dugger, D. L.; Crocker, L. M.; Parsons, K. L.; Mai, E.; Blättler, W. A.; Lambert, J. M.; Chari, R. V. J.; Lutz, R. J.; Wong, W. L. T.; Jacobson, F. S.; Koeppen, H.; Schwall, R. H.; Kenkare-Mitra, S. R.; Spencer, S. D.; Sliwkowski, M. X., Targeting HER2-Positive Breast Cancer with Trastuzumab-DM1, an Antibody–Cytotoxic Drug Conjugate. *Cancer Research* **2008,** *68* (22), 9280-9290. https://doi.org/10.1158/0008-5472.Can-08-1776

154. Chen, Y.; Kim, M. T.; Zheng, L.; Deperalta, G.; Jacobson, F., Structural Characterization of

Cross-Linked Species in Trastuzumab Emtansine (Kadcyla). *Bioconjugate Chemistry* **2016,** *27* (9), 2037-2047. https://doi.org/10.1021/acs.bioconjchem.6b00316
155. Verma, S.; Miles, D.; Gianni, L.; Krop, I. E.; Welslau, M.; Baselga, J.; Pegram, M.; Oh, D.-Y.; Diéras, V.; Guardino, E.; Fang, L.; Lu, M. W.; Olsen, S.; Blackwell, K., Trastuzumab Emtansine for HER2-Positive Advanced Breast Cancer. *New England Journal of Medicine* **2012,** *367* (19), 1783-1791. https://doi.org/10.1056/NEJMoa1209124
156. Teicher, B. A.; Doroshow, J. H., The Promise of Antibody–Drug Conjugates. *New England Journal of Medicine* **2012,** *367* (19), 1847-1848. https://doi.org/10.1056/NEJMe1211736
157. Chen, L.; Wang, L.; Shion, H.; Yu, C.; Yu, Y. Q.; Zhu, L.; Li, M.; Chen, W.; Gao, K., In-depth structural characterization of Kadcyla® (ado-trastuzumab emtansine) and its biosimilar candidate. *mAbs* **2016,** *8* (7), 1210-1223. https://doi.org/10.1080/19420862.2016.1204502
158. Low, P. S.; Henne, W. A.; Doorneweerd, D. D., Discovery and Development of Folic-Acid-Based Receptor Targeting for Imaging and Therapy of Cancer and Inflammatory Diseases. *Accounts of Chemical Research* **2008,** *41* (1), 120-129. https://doi.org/10.1021/ar7000815
159. Dosio, F.; Milla P Fau - Cattel, L.; Cattel, L., EC-145, a folate-targeted Vinca alkaloid conjugate for the potential treatment of folate receptor-expressing cancers. (2040-3429 (Electronic)).
160. Ghosh, A.; Heston, W. D. W., Tumor target prostate specific membrane antigen (PSMA) and its regulation in prostate cancer. *J Cell Biochem* **2004,** *91* (3), 528-539. https://doi.org/10.1002/jcb.10661
161. Holmes, E. H.; Greene, T. G.; Tino, W. T.; Boynton, A. L.; Aldape, H. C.; Misrock, S. L.; Murphy, G. P., Analysis of glycosylation of prostate-specific membrane antigen derived from LNCaP cells, prostatic carcinoma tumors, and serum from prostate cancer patients. *The Prostate* **1996,** *29* (S7), 25-29. https://doi.org/https://doi.org/10.1002/(SICI)1097-0045(1996)7+<25::AID-PROS3>3.0.CO;2-I
162. Pinto, J. T.; Suffoletto, B. P.; Berzin, T. M.; Qiao, C. H.; Lin, S.; Tong, W. P.; May, F.; Mukherjee, B.; Heston, W. D., Prostate-specific membrane antigen: a novel folate hydrolase in human prostatic carcinoma cells. *Clinical Cancer Research* **1996,** *2* (9), 1445-1451.
163. Carter, R. E.; Feldman, A. R.; Coyle, J. T., Prostate-specific membrane antigen is a hydrolase with substrate and pharmacologic characteristics of a neuropeptidase. *Proceedings of the National Academy of Sciences* **1996,** *93* (2), 749-753. https://doi.org/10.1073/pnas.93.2.749
164. Halsted, C. H.; Ling, E.-h.; Luthi-Carter, R.; Villanueva, J. A.; Gardner, J. M.; Coyle, J. T., Folylpoly-γ-glutamate Carboxypeptidase from Pig Jejunum: MOLECULAR CHARACTERIZATION AND RELATION TO GLUTAMATE CARBOXYPEPTIDASE II*. *Journal of Biological Chemistry* **1998,** *273* (32), 20417-20424. https://doi.org/https://doi.org/10.1074/jbc.273.32.20417
165. Bräuer, A.; Grubert, L. S.; Roll, W.; Schrader, A. J.; Schäfers, M.; Bögemann, M.; Rahbar, K., 177Lu-PSMA-617 radioligand therapy and outcome in patients with metastasized castration-resistant prostate cancer. *European Journal of Nuclear Medicine and Molecular Imaging* **2017,** *44* (10), 1663-1670. https://doi.org/10.1007/s00259-017-3751-z
166. Benešová, M.; Schäfer, M.; Bauder-Wüst, U.; Afshar-Oromieh, A.; Kratochwil, C.; Mier, W.; Haberkorn, U.; Kopka, K.; Eder, M., Preclinical Evaluation of a Tailor-Made DOTA-Conjugated PSMA Inhibitor with Optimized Linker Moiety for Imaging and Endoradiotherapy of Prostate Cancer. *Journal of Nuclear Medicine* **2015,** *56* (6), 914-920. https://doi.org/10.2967/jnumed.114.147413

167. Sartor, A. O.; Morris, M. J.; Krause, B. J., VISION: An international, prospective, open-label, multicenter, randomized phase 3 study of 177Lu-PSMA-617 in the treatment of patients with progressive PSMA-positive metastatic castration-resistant prostate cancer (mCRPC). *Journal of Clinical Oncology* **2019,** *37* (15_suppl), TPS5099-TPS5099. https://doi.org/10.1200/JCO.2019.37.15_suppl.TPS5099

168. Ueki, N.; Lee, S.; Sampson, N. S.; Hayman, M. J., Selective cancer targeting with prodrugs activated by histone deacetylases and a tumour-associated protease. *Nature Communications* **2013,** *4* (1), 2735. https://doi.org/10.1038/ncomms3735

169. Lee, J. B.; Zhang, K.; Tam, Y. Y. C.; Quick, J.; Tam, Y. K.; Lin, P. J. C.; Chen, S.; Liu, Y.; Nair, J. K.; Zlatev, I.; Rajeev, K. G.; Manoharan, M.; Rennie, P. S.; Cullis, P. R., A Glu-urea-Lys Ligand-conjugated Lipid Nanoparticle/siRNA System Inhibits Androgen Receptor Expression In Vivo. *Molecular Therapy - Nucleic Acids* **2016,** *5*. https://doi.org/10.1038/mtna.2016.43

170. Smith, G.; Zhao, Y.; Leyton, J.; Shan, B.; Nguyen, Q.-d.; Perumal, M.; Turton, D.; Årstad, E.; Luthra, S. K.; Robins, E. G.; Aboagye, E. O., Radiosynthesis and pre-clinical evaluation of [18F]fluoro-[1,2-2H4]choline. *Nuclear Medicine and Biology* **2011,** *38* (1), 39-51. https://doi.org/https://doi.org/10.1016/j.nucmedbio.2010.06.012

171. *IUPAC. Compendium of Chemical Terminology, 2nd ed. (the "Gold Book"). Online version (2019-) created by S. J. Chalk.* . Compiled by A. D. McNaught and A. Wilkinson. Blackwell Scientific Publications: Oxford, 1997.

172. Nyquist, M. D.; Li, Y.; Hwang, T. H.; Manlove, L. S.; Vessella, R. L.; Silverstein, K. A. T.; Voytas, D. F.; Dehm, S. M., TALEN-engineered AR gene rearrangements reveal endocrine uncoupling of androgen receptor in prostate cancer. *Proceedings of the National Academy of Sciences* **2013,** *110* (43), 17492-17497. https://doi.org/10.1073/pnas.1308587110

173. Vichai, V.; Kirtikara, K., Sulforhodamine B colorimetric assay for cytotoxicity screening. *Nature Protocols* **2006,** *1* (3), 1112-1116. https://doi.org/10.1038/nprot.2006.179

174. Seto, E.; Yoshida, M., Erasers of histone acetylation: the histone deacetylase enzymes. *Cold Spring Harb Perspect Biol* **2014,** *6* (4), a018713-a018713. https://doi.org/10.1101/cshperspect.a018713

175. Marks, P. A.; Xu, W.-S., Histone deacetylase inhibitors: Potential in cancer therapy. *J Cell Biochem* **2009,** *107* (4), 600-608. https://doi.org/https://doi.org/10.1002/jcb.22185

176. Glaser, K. B.; Li, J.; Staver, M. J.; Wei, R.-Q.; Albert, D. H.; Davidsen, S. K., Role of Class I and Class II histone deacetylases in carcinoma cells using siRNA. *Biochemical and Biophysical Research Communications* **2003,** *310* (2), 529-536. https://doi.org/https://doi.org/10.1016/j.bbrc.2003.09.043

177. Schwartz-Roberts, J. L.; Clarke, R., Chapter 7 - Blockage of Lysosomal Degradation Is Detrimental to Cancer Cell Survival: Role of Autophagy Activation. In *Autophagy: Cancer, Other Pathologies, Inflammation, Immunity, Infection, and Aging*, Hayat, M. A., Ed. Academic Press: Amsterdam, 2015; pp 121-133.

178. Joyce, J. A.; Baruch, A.; Chehade, K.; Meyer-Morse, N.; Giraudo, E.; Tsai, F.-Y.; Greenbaum, D. C.; Hager, J. H.; Bogyo, M.; Hanahan, D., Cathepsin cysteine proteases are effectors of invasive growth and angiogenesis during multistage tumorigenesis. *Cancer Cell* **2004,** *5* (5), 443-453. https://doi.org/10.1016/S1535-6108(04)00111-4

179. Jedeszko, C.; Sloane, B. F., Cysteine cathepsins in human cancer. **2004,** *385* (11), 1017-1027. https://doi.org/doi:10.1515/BC.2004.132

180. Gonzalez-Suarez, I.; Redwood, A. B.; Grotsky, D. A.; Neumann, M. A.; Cheng, E. H.-Y.; Stewart, C. L.; Dusso, A.; Gonzalo, S., A new pathway that regulates 53BP1 stability implicates Cathepsin L and vitamin D in DNA repair. *The EMBO Journal* **2011,** *30* (16), 3383-3396. https://doi.org/https://doi.org/10.1038/emboj.2011.225

181. Wegener, D.; Wirsching, F.; Riester, D.; Schwienhorst, A., A Fluorogenic Histone Deacetylase Assay Well Suited for High-Throughput Activity Screening. *Chemistry & Biology* **2003,** *10* (1), 61-68. https://doi.org/10.1016/S1074-5521(02)00305-8

182. Khan, N.; Jeffers, M.; Kumar, S.; Hackett, C.; Boldog, F.; Khramtsov, N.; Qian, X.; Mills, E.; Berghs, Stanny C.; Carey, N.; Finn, Paul W.; Collins, Laura S.; Tumber, A.; Ritchie, James W.; Jensen, Peter B.; Lichenstein, Henri S.; Sehested, M., Determination of the class and isoform selectivity of small-molecule histone deacetylase inhibitors. *Biochemical Journal* **2007,** *409* (2), 581-589. https://doi.org/10.1042/bj20070779

183. Arts, J.; King, P.; Mariën, A.; Floren, W.; Beliën, A.; Janssen, L.; Pilatte, I.; Roux, B.; Decrane, L.; Gilissen, R.; Hickson, I.; Vreys, V.; Cox, E.; Bol, K.; Talloen, W.; Goris, I.; Andries, L.; Du Jardin, M.; Janicot, M.; Page, M.; van Emelen, K.; Angibaud, P., JNJ-26481585, a Novel "Second-Generation" Oral Histone Deacetylase Inhibitor, Shows Broad-Spectrum Preclinical Antitumoral Activity. *Clinical Cancer Research* **2009,** *15* (22), 6841-6851. https://doi.org/10.1158/1078-0432.Ccr-09-0547

184. Vara, J. A.; Portela, A.; Ortìn, J.; Jimènez, A., Expression in mammalian cells of a gene from Streptomyces alboniger conferring puromycin resistance. *Nucleic Acids Research* **1986,** *14* (11), 4617-4624. https://doi.org/10.1093/nar/14.11.4617

185. Rubio-Ruiz, B.; Figuerola-Conchas, A.; Ramos-Torrecillas, J.; Capitán-Cañadas, F.; Ríos-Marco, P.; Carrasco, M. P.; Gallo, M. Á.; Espinosa, A.; Marco, C.; Ruiz, C.; Entrena, A.; Hurtado-Guerrero, R.; Conejo-García, A., Discovery of a New Binding Site on Human Choline Kinase α1: Design, Synthesis, Crystallographic Studies, and Biological Evaluation of Asymmetrical Bispyridinium Derivatives. *Journal of Medicinal Chemistry* **2014,** *57* (2), 507-515. https://doi.org/10.1021/jm401665x

186. Abou-Shehada, S.; Teasdale, M. C.; Bull, S. D.; Wade, C. E.; Williams, J. M. J., Lewis Acid Activation of Pyridines for Nucleophilic Aromatic Substitution and Conjugate Addition. *ChemSusChem* **2015,** *8* (6), 1083-1087. https://doi.org/https://doi.org/10.1002/cssc.201403154

187. John A. Joule, K. M., Heterocyclic Chemistry, 5th Edition. In *Heterocyclic Chemistry, 5th Edition*, 5th ed.; A John Wiley & Sons, Ltd., Publication: 2010; pp 19 - 33.

188. Silver, D. A.; Pellicer, I.; Fair, W. R.; Heston, W. D.; Cordon-Cardo, C., Prostate-specific membrane antigen expression in normal and malignant human tissues. *Clinical Cancer Research* **1997,** *3* (1), 81-85.

189. Mannweiler, S.; Amersdorfer, P.; Trajanoski, S.; Terrett, J. A.; King, D.; Mehes, G., Heterogeneity of Prostate-Specific Membrane Antigen (PSMA) Expression in Prostate Carcinoma with Distant Metastasis. *Pathology & Oncology Research* **2009,** *15* (2), 167-172. https://doi.org/10.1007/s12253-008-9104-2

190. Maurer, T.; Eiber, M.; Schwaiger, M.; Gschwend, J. E., Current use of PSMA–PET in prostate cancer management. *Nature Reviews Urology* **2016,** *13* (4), 226-235. https://doi.org/10.1038/nrurol.2016.26

191. Kularatne, S. A.; Wang, K.; Santhapuram, H.-K. R.; Low, P. S., Prostate-Specific Membrane Antigen Targeted Imaging and Therapy of Prostate Cancer Using a PSMA Inhibitor as a Homing

Ligand. *Molecular Pharmaceutics* **2009,** *6* (3), 780-789. https://doi.org/10.1021/mp900069d
192. Kularatne, S. A.; Venkatesh, C.; Santhapuram, H.-K. R.; Wang, K.; Vaitilingam, B.; Henne, W. A.; Low, P. S., Synthesis and Biological Analysis of Prostate-Specific Membrane Antigen-Targeted Anticancer Prodrugs. *Journal of Medicinal Chemistry* **2010,** *53* (21), 7767-7777. https://doi.org/10.1021/jm100729b
193. Thomas, M.; Kularatne, S. A.; Qi, L.; Kleindl, P.; Leamon, C. P.; Hansen, M. J.; Low, P. S., Ligand-Targeted Delivery of Small Interfering RNAs to Malignant Cells and Tissues. *Annals of the New York Academy of Sciences* **2009,** *1175* (1), 32-39. https://doi.org/https://doi.org/10.1111/j.1749-6632.2009.04977.x
194. Banerjee, S. R.; Foss, C. A.; Castanares, M.; Mease, R. C.; Byun, Y.; Fox, J. J.; Hilton, J.; Lupold, S. E.; Kozikowski, A. P.; Pomper, M. G., Synthesis and Evaluation of Technetium-99m- and Rhenium-Labeled Inhibitors of the Prostate-Specific Membrane Antigen (PSMA). *Journal of Medicinal Chemistry* **2008,** *51* (15), 4504-4517. https://doi.org/10.1021/jm800111u
195. Maresca, K. P.; Hillier, S. M.; Femia, F. J.; Keith, D.; Barone, C.; Joyal, J. L.; Zimmerman, C. N.; Kozikowski, A. P.; Barrett, J. A.; Eckelman, W. C.; Babich, J. W., A Series of Halogenated Heterodimeric Inhibitors of Prostate Specific Membrane Antigen (PSMA) as Radiolabeled Probes for Targeting Prostate Cancer. *Journal of Medicinal Chemistry* **2009,** *52* (2), 347-357. https://doi.org/10.1021/jm800994j
196. Murelli, R. P.; Zhang, A. X.; Michel, J.; Jorgensen, W. L.; Spiegel, D. A., Chemical Control over Immune Recognition: A Class of Antibody-Recruiting Small Molecules That Target Prostate Cancer. *Journal of the American Chemical Society* **2009,** *131* (47), 17090-17092. https://doi.org/10.1021/ja906844e
197. Zhang, A. X.; Murelli, R. P.; Barinka, C.; Michel, J.; Cocleaza, A.; Jorgensen, W. L.; Lubkowski, J.; Spiegel, D. A., A Remote Arene-Binding Site on Prostate Specific Membrane Antigen Revealed by Antibody-Recruiting Small Molecules. *Journal of the American Chemical Society* **2010,** *132* (36), 12711-12716. https://doi.org/10.1021/ja104591m
198. Archibald, S. J.; Allott, L., The aluminium-[18F]fluoride revolution: simple radiochemistry with a big impact for radiolabelled biomolecules. *EJNMMI Radiopharmacy and Chemistry* **2021,** *6* (1), 30. https://doi.org/10.1186/s41181-021-00141-0
199. Rajasekaran, S. A.; Anilkumar, G.; Oshima, E.; Bowie, J. U.; Liu, H.; Heston, W.; Bander, N. H.; Rajasekaran, A. K., A Novel Cytoplasmic Tail MXXXL Motif Mediates the Internalization of Prostate-specific Membrane Antigen. *Molecular Biology of the Cell* **2003,** *14* (12), 4835-4845. https://doi.org/10.1091/mbc.e02-11-0731
200. Erickson, H. K.; Park, P. U.; Widdison, W. C.; Kovtun, Y. V.; Garrett, L. M.; Hoffman, K.; Lutz, R. J.; Goldmacher, V. S.; Blättler, W. A., Antibody-Maytansinoid Conjugates Are Activated in Targeted Cancer Cells by Lysosomal Degradation and Linker-Dependent Intracellular Processing. *Cancer Research* **2006,** *66* (8), 4426-4433. https://doi.org/10.1158/0008-5472.Can-05-4489
201. Hu, X.; Zhao, X.; He, B.; Zhao, Z.; Zheng, Z.; Zhang, P.; Shi, X.; Kwok, R. T. K.; Lam, J. W. Y.; Qin, A.; Tang, B. Z., A Simple Approach to Bioconjugation at Diverse Levels: Metal-Free Click Reactions of Activated Alkynes with Native Groups of Biotargets without Prefunctionalization. *Research* **2018,** *2018*, 3152870. https://doi.org/10.1155/2018/3152870
202. Hermanson, G. T., *Bioconjugate Techniques, Elsevier Science & Technology*. 3rd edition ed.; Elsevier: UK, 2013.
203. Brewer, C. F.; Riehm, J. P., Evidence for possible nonspecific reactions between N-

ethylmaleimide and proteins. *Analytical Biochemistry* **1967,** *18* (2), 248-255. https://doi.org/https://doi.org/10.1016/0003-2697(67)90007-3
204. Rutkowska, E.; Pajak, K.; Jóźwiak, K., Lipophilicity--methods of determination and its role in medicinal chemistry. *Acta Pol Pharm* **2013,** *70* (1), 3-18.
205. Chmiel, T.; Mieszkowska, A.; Kempińska-Kupczyk, D.; Kot-Wasik, A.; Namieśnik, J.; Mazerska, Z., The impact of lipophilicity on environmental processes, drug delivery and bioavailability of food components. *Microchemical Journal* **2019,** *146*, 393-406. https://doi.org/https://doi.org/10.1016/j.microc.2019.01.030
206. Liu, X.; Testa, B.; Fahr, A., Lipophilicity and Its Relationship with Passive Drug Permeation. *Pharm Res* **2011,** *28* (5), 962-977. https://doi.org/10.1007/s11095-010-0303-7
207. Hansch, C.; Fujita, T., p-σ-π Analysis. A Method for the Correlation of Biological Activity and Chemical Structure. *Journal of the American Chemical Society* **1964,** *86* (8), 1616-1626. https://doi.org/10.1021/ja01062a035
208. Hansch, C., Quantitative approach to biochemical structure-activity relationships. *Accounts of Chemical Research* **1969,** *2* (8), 232-239. https://doi.org/10.1021/ar50020a002
209. Poole, S. K.; Poole, C. F., Separation methods for estimating octanol–water partition coefficients. *Journal of Chromatography B* **2003,** *797* (1), 3-19. https://doi.org/https://doi.org/10.1016/j.jchromb.2003.08.032
210. Sangster, J. M., *Octanol-Water Partition Coefficients: Fundamentals and Physical Chemistry*. Wiley: New York, 1997; p 184.
211. Lu, D.; Chambers, P.; Wipf, P.; Xie, X.-Q.; Englert, D.; Weber, S., Lipophilicity screening of novel drug-like compounds and comparison to clogP. *Journal of Chromatography A* **2012,** *1258*, 161-167. https://doi.org/https://doi.org/10.1016/j.chroma.2012.07.078
212. McGinity, J. W., Drug Stability: Principles and Practices. By Jens T. Carstensen. Marcel Dekker: New York. 1990. 520 pp. 16 ×23cm. ISBN 0–8247–8285–2. $99.75. *Journal of Pharmaceutical Sciences* **1991,** *80* (1), 98-98. https://doi.org/https://doi.org/10.1002/jps.2600800127
213. Ishiyama, M.; Tominaga, H.; Shiga, M.; Sasamoto, K.; Ohkura, Y.; Ueno, K., A Combined Assay of Cell Vability and in Vitro Cytotoxicity with a Highly Water-Soluble Tetrazolium Salt, Neutral Red and Crystal Violet. *Biological & Pharmaceutical Bulletin* **1996,** *19* (11), 1518-1520. https://doi.org/10.1248/bpb.19.1518
214. Aslantürk, Ö. S., In Vitro Cytotoxicity and Cell Viability Assays: Principles, Advantages, and Disadvantages, Genotoxicity - A Predictable Risk to Our Actual World. IntechOpen: 2017.
215. Skehan, P.; Storeng, R.; Scudiero, D.; Monks, A.; McMahon, J.; Vistica, D.; Warren, J. T.; Bokesch, H.; Kenney, S.; Boyd, M. R., New Colorimetric Cytotoxicity Assay for Anticancer-Drug Screening. *JNCI: Journal of the National Cancer Institute* **1990,** *82* (13), 1107-1112. https://doi.org/10.1093/jnci/82.13.1107
216. Watson, H., Biological membranes. *Essays in Biochemistry* **2015,** *59*, 43-69. https://doi.org/10.1042/bse0590043
217. Cell Membrane: Structure and Physical Properties. In *Integrated Molecular and Cellular Biophysics*, Springer Netherlands: Dordrecht, 2008; pp 73-99.
218. Yang, N. J.; Hinner, M. J., Getting Across the Cell Membrane: An Overview for Small Molecules, Peptides, and Proteins. In *Site-Specific Protein Labeling: Methods and Protocols*, Gautier, A.; Hinner, M. J., Eds. Springer New York: New York, NY, 2015; pp 29-53.
219. Pauls, R. E.; McCoy, R. W.; Ziegel, E. R.; Wolf, T.; Fritz, G. T.; Marmion, D. M., Results of a

Cooperative Study Comparing the Precision of Peak Height and Area Measurements in Liquid Chromatography. Part II*. *Journal of Chromatographic Science* **1986,** *24* (7), 273-277. https://doi.org/10.1093/chromsci/24.7.273

220. Manning, G.; Whyte, D. B.; Martinez, R.; Hunter, T.; Sudarsanam, S., The Protein Kinase Complement of the Human Genome. *Science* **2002,** *298* (5600), 1912-1934. https://doi.org/doi:10.1126/science.1075762

221. Kennedy, T., Managing the drug discovery/development interface. *Drug Discovery Today* **1997,** *2* (10), 436-444. https://doi.org/https://doi.org/10.1016/S1359-6446(97)01099-4

222. Pires, D. E. V.; Blundell, T. L.; Ascher, D. B., pkCSM: Predicting Small-Molecule Pharmacokinetic and Toxicity Properties Using Graph-Based Signatures. *Journal of Medicinal Chemistry* **2015,** *58* (9), 4066-4072. https://doi.org/10.1021/acs.jmedchem.5b00104

223. Song, N.-n.; Zhang, S.; Liu, C.-x. In *Overview of factors affecting oral drug absorption*, 2004.

224. Amidon, G. L.; Lennernäs, H.; Shah, V. P.; Crison, J. R., A Theoretical Basis for a Biopharmaceutic Drug Classification: The Correlation of in Vitro Drug Product Dissolution and in Vivo Bioavailability. *Pharm Res* **1995,** *12* (3), 413-420. https://doi.org/10.1023/A:1016212804288

225. Wu, C.-Y.; Benet, L. Z., Predicting Drug Disposition via Application of BCS: Transport/Absorption/Elimination Interplay and Development of a Biopharmaceutics DrugDisposition Classification System. *Pharm Res* **2005,** *22* (1), 11-23. https://doi.org/10.1007/s11095-004-9004-4

226. Saal, C.; Petereit, A. C., Optimizing solubility: Kinetic versus thermodynamic solubility temptations and risks. *European Journal of Pharmaceutical Sciences* **2012,** *47* (3), 589-595. https://doi.org/https://doi.org/10.1016/j.ejps.2012.07.019

227. Hubatsch, I.; Ragnarsson, E. G. E.; Artursson, P., Determination of drug permeability and prediction of drug absorption in Caco-2 monolayers. *Nature Protocols* **2007,** *2* (9), 2111-2119. https://doi.org/10.1038/nprot.2007.303

228. Krämer, S. D., Absorption prediction from physicochemical parameters. *Pharmaceutical Science & Technology Today* **1999,** *2* (9), 373-380. https://doi.org/https://doi.org/10.1016/S1461-5347(99)00188-1

229. Artursson, P.; Palm, K.; Luthman, K., Caco-2 monolayers in experimental and theoretical predictions of drug transport1PII of original article: S0169-409X(96)00415-2. The article was originally published in Advanced Drug Delivery Reviews 22 (1996) 67–84.1. *Advanced Drug Delivery Reviews* **2001,** *46* (1), 27-43. https://doi.org/https://doi.org/10.1016/S0169-409X(00)00128-9

230. Stenberg, P.; Norinder, U.; Luthman, K.; Artursson, P., Experimental and Computational Screening Models for the Prediction of Intestinal Drug Absorption. *Journal of Medicinal Chemistry* **2001,** *44* (12), 1927-1937. https://doi.org/10.1021/jm001101a

231. Ohura, K.; Nishiyama, H.; Saco, S.; Kurokawa, K.; Imai, T., Establishment and Characterization of a Novel Caco-2 Subclone with a Similar Low Expression Level of Human Carboxylesterase 1 to Human Small Intestine. *Drug Metabolism and Disposition* **2016,** *44* (12), 1890-1898. https://doi.org/10.1124/dmd.116.072736

232. Giacomini, K. M.; Huang, S.-M.; Tweedie, D. J.; Benet, L. Z.; Brouwer, K. L. R.; Chu, X.; Dahlin, A.; Evers, R.; Fischer, V.; Hillgren, K. M.; Hoffmaster, K. A.; Ishikawa, T.; Keppler, D.; Kim, R. B.; Lee, C. A.; Niemi, M.; Polli, J. W.; Sugiyama, Y.; Swaan, P. W.; Ware, J. A.; Wright, S. H.; Wah Yee, S.; Zamek-Gliszczynski, M. J.; Zhang, L.; The International Transporter, C., Membrane

transporters in drug development. *Nature Reviews Drug Discovery* **2010,** *9* (3), 215-236. https://doi.org/10.1038/nrd3028
233. Schmiedlin-Ren, P.; Thummel, K. E.; Fisher, J. M.; Paine, M. F.; Lown, K. S.; Watkins, P. B., Expression of Enzymatically Active CYP3A4 by Caco-2 Cells Grown on Extracellular Matrix-Coated Permeable Supports in the Presence of 1α,25-Dihydroxyvitamin D₃. *Molecular Pharmacology* **1997,** *51* (5), 741-754. https://doi.org/10.1124/mol.51.5.741
234. Klein, S., The Use of Biorelevant Dissolution Media to Forecast the In Vivo Performance of a Drug. *The AAPS Journal* **2010,** *12* (3), 397-406. https://doi.org/10.1208/s12248-010-9203-3
235. McGinnity, D. F.; Soars, M. G.; Urbanowicz, R. A.; Riley, R. J., EVALUATION OF FRESH AND CRYOPRESERVED HEPATOCYTES AS IN VITRO DRUG METABOLISM TOOLS FOR THE PREDICTION OF METABOLIC CLEARANCE. *Drug Metabolism and Disposition* **2004,** *32* (11), 1247-1253. https://doi.org/10.1124/dmd.104.000026
236. J. Richardson, S.; Bai, A.; A. Kulkarni, A.; F. Moghaddam, M., Efficiency in Drug Discovery: Liver S9 Fraction Assay As a Screen for Metabolic Stability. *Drug Metabolism Letters* **2016,** *10* (2), 83-90. https://doi.org/http://dx.doi.org/10.2174/1872312810666160223121836
237. Fisher, M. B.; Paine, M. F.; Strelevitz, T. J.; Wrighton, S. A., The role of hepatic and extrahepatic UDP-glucuronosyltransferases in human drug metabolism*†. *Drug Metabolism Reviews* **2001,** *33* (3-4), 273-297. https://doi.org/10.1081/DMR-120000653
238. Guengerich, F. P., Cytochrome P450s and other enzymes in drug metabolism and toxicity. *The AAPS Journal* **2006,** *8* (1), E101-E111. https://doi.org/10.1208/aapsj080112
239.Gombar, C. T.; Harrington, G. W.; Pylypiw, H. M.; Anderson, L. M.; Palmer, A. E.; Rice, J. M.; Magee, P. N.; Burak, E. S., Interspecies Scaling of the Pharmacokinetics of N-Nitrosodimethylamine. *Cancer Research* **1990,** *50* (14), 4366-4370.
240.Challapalli, A.; Sharma, R.; Hallett, W. A.; Kozlowski, K.; Carroll, L.; Brickute, D.; Twyman, F.; Al-Nahhas, A.; Aboagye, E. O., Biodistribution and Radiation Dosimetry of Deuterium-Substituted 18F-Fluoromethyl-[1, 2-2H4]Choline in Healthy Volunteers. *Journal of Nuclear Medicine* **2014,** *55* (2), 256-263. https://doi.org/10.2967/jnumed.113.129577
241. Hara, T.; Kosaka, N.; Shinoura, N.; Kondo, T., PET Imaging of Brain Tumor with [methyl-11C]Choline. *Journal of Nuclear Medicine* **1997,** *38* (6), 842-847.
242. Shinoura, N.; Nishijima, M.; Hara, T.; Haisa, T.; Yamamoto, H.; Fujii, K.; Mitsui, I.; Kosaka, N.; Kondo, T.; Hara, T., Brain tumors: detection with C-11 choline PET. *Radiology* **1997,** *202* (2), 497-503. https://doi.org/10.1148/radiology.202.2.9015080
243. Hara, T.; Kosaka, N.; Kishi, H., PET Imaging of Prostate Cancer Using Carbon-11-Choline. *Journal of Nuclear Medicine* **1998,** *39* (6), 990-995.
244. Marriott, C. J. C.; Thorstad, W.; Akabani, G.; Brown, M. T.; McLendon, R. E.; Hanson, M. W.; R.Edward, C., Locally Increased Uptake of Fluorine-18-Fluorodeoxyglucose After Intracavitary Administration of Iodine-131-Labeled Antibody for Primary Brain Tumors. *Journal of Nuclear Medicine* **1998,** *39* (8), 1376-1380.
245. Shreve, P. D.; Grossman, H. B.; Gross, M. D.; Wahl, R. L., Metastatic prostate cancer: initial findings of PET with 2-deoxy-2-[F-18]fluoro-D-glucose. *Radiology* **1996,** *199* (3), 751-756. https://doi.org/10.1148/radiology.199.3.8638000
246. DeGrado, T. R.; Coleman, R. E.; Wang, S.; Baldwin, S. W.; Orr, M. D.; Robertson, C. N.; Polascik, T. J.; Price, D. T., Synthesis and Evaluation of 18F-labeled Choline as an Oncologic Tracer for Positron Emission Tomography: Initial Findings in Prostate Cancer. *Cancer Research*

2001, *61* (1), 110-117.
247. Trousil, S. Choline Kinase Inhibition as a Treatment Strategy of Cancers with Deregulated Lipid Metabolism. Imperial College London, UK, Imperial College London, UK, 2014.
248. Barretina, J.; Caponigro, G.; Stransky, N.; Venkatesan, K.; Margolin, A. A.; Kim, S.; Wilson, C. J.; Lehár, J.; Kryukov, G. V.; Sonkin, D.; Reddy, A.; Liu, M.; Murray, L.; Berger, M. F.; Monahan, J. E.; Morais, P.; Meltzer, J.; Korejwa, A.; Jané-Valbuena, J.; Mapa, F. A.; Thibault, J.; Bric-Furlong, E.; Raman, P.; Shipway, A.; Engels, I. H.; Cheng, J.; Yu, G. K.; Yu, J.; Aspesi, P.; de Silva, M.; Jagtap, K.; Jones, M. D.; Wang, L.; Hatton, C.; Palescandolo, E.; Gupta, S.; Mahan, S.; Sougnez, C.; Onofrio, R. C.; Liefeld, T.; MacConaill, L.; Winckler, W.; Reich, M.; Li, N.; Mesirov, J. P.; Gabriel, S. B.; Getz, G.; Ardlie, K.; Chan, V.; Myer, V. E.; Weber, B. L.; Porter, J.; Warmuth, M.; Finan, P.; Harris, J. L.; Meyerson, M.; Golub, T. R.; Morrissey, M. P.; Sellers, W. R.; Schlegel, R.; Garraway, L. A., The Cancer Cell Line Encyclopedia enables predictive modelling of anticancer drug sensitivity. *Nature* **2012,** *483* (7391), 603-607. https://doi.org/10.1038/nature11003
249. Jochems, P. G. M.; Garssen, J.; Van Keulen, A. M.; Masereeuw, R.; Jeurink, P. V., Evaluating Human Intestinal Cell Lines for Studying Dietary Protein Absorption. *Nutrients* **2018,** *10* (3), 322.
250. McNamara, C. W.; Lee, M. C. S.; Lim, C. S.; Lim, S. H.; Roland, J.; Nagle, A.; Simon, O.; Yeung, B. K. S.; Chatterjee, A. K.; McCormack, S. L.; Manary, M. J.; Zeeman, A.-M.; Dechering, K. J.; Kumar, T. R. S.; Henrich, P. P.; Gagaring, K.; Ibanez, M.; Kato, N.; Kuhen, K. L.; Fischli, C.; Rottmann, M.; Plouffe, D. M.; Bursulaya, B.; Meister, S.; Rameh, L.; Trappe, J.; Haasen, D.; Timmerman, M.; Sauerwein, R. W.; Suwanarusk, R.; Russell, B.; Renia, L.; Nosten, F.; Tully, D. C.; Kocken, C. H. M.; Glynne, R. J.; Bodenreider, C.; Fidock, D. A.; Diagana, T. T.; Winzeler, E. A., Targeting Plasmodium PI(4)K to eliminate malaria. *Nature* **2013,** *504* (7479), 248-253. https://doi.org/10.1038/nature12782
251. Borawski, J.; Troke, P.; Puyang, X.; Gibaja, V.; Zhao, S.; Mickanin, C.; Leighton-Davies, J.; Wilson, C. J.; Myer, V.; CornellaTaracido, I.; Baryza, J.; Tallarico, J.; Joberty, G.; Bantscheff, M.; Schirle, M.; Bouwmeester, T.; Mathy, J. E.; Lin, K.; Compton, T.; Labow, M.; Wiedmann, B.; Gaither, L. A., Class III Phosphatidylinositol 4-Kinase Alpha and Beta Are Novel Host Factor Regulators of Hepatitis C Virus Replication. *Journal of Virology* **2009,** *83* (19), 10058-10074. https://doi.org/doi:10.1128/JVI.02418-08
252. Umbricht, C. A.; Benešová, M.; Schibli, R.; Müller, C., Preclinical Development of Novel PSMA-Targeting Radioligands: Modulation of Albumin-Binding Properties To Improve Prostate Cancer Therapy. *Molecular Pharmaceutics* **2018,** *15* (6), 2297-2306. https://doi.org/10.1021/acs.molpharmaceut.8b00152
253. Benešová, M.; Umbricht, C. A.; Schibli, R.; Müller, C., Albumin-Binding PSMA Ligands: Optimization of the Tissue Distribution Profile. *Molecular Pharmaceutics* **2018,** *15* (3), 934-946. https://doi.org/10.1021/acs.molpharmaceut.7b00877
254. Vraneš, M.; Panić, J.; Tot, A.; Popsavin, M.; Jocić, A.; Gadžurić, S., Physicochemical characterization of choline based ionic liquids with chelating anions. *The Journal of Chemical Thermodynamics* **2019,** *131*, 80-87. https://doi.org/https://doi.org/10.1016/j.jct.2018.10.026
255. Mitsuhashi, S.; Hatakeyama, H.; Karahashi, M.; Koumura, T.; Nonaka, I.; Hayashi, Y. K.; Noguchi, S.; Sher, R. B.; Nakagawa, Y.; Manfredi, G.; Goto, Y.-i.; Cox, G. A.; Nishino, I., Muscle choline kinase beta defect causes mitochondrial dysfunction and increased mitophagy. *Human Molecular Genetics* **2011,** *20* (19), 3841-3851. https://doi.org/10.1093/hmg/ddr305
256. Neel, B. A.; Lin, Y.; Pessin, J. E., Skeletal muscle autophagy: a new metabolic regulator.

Trends in Endocrinology & Metabolism **2013,** *24* (12), 635-643. https://doi.org/https://doi.org/10.1016/j.tem.2013.09.004

9. HPLC chromatograms

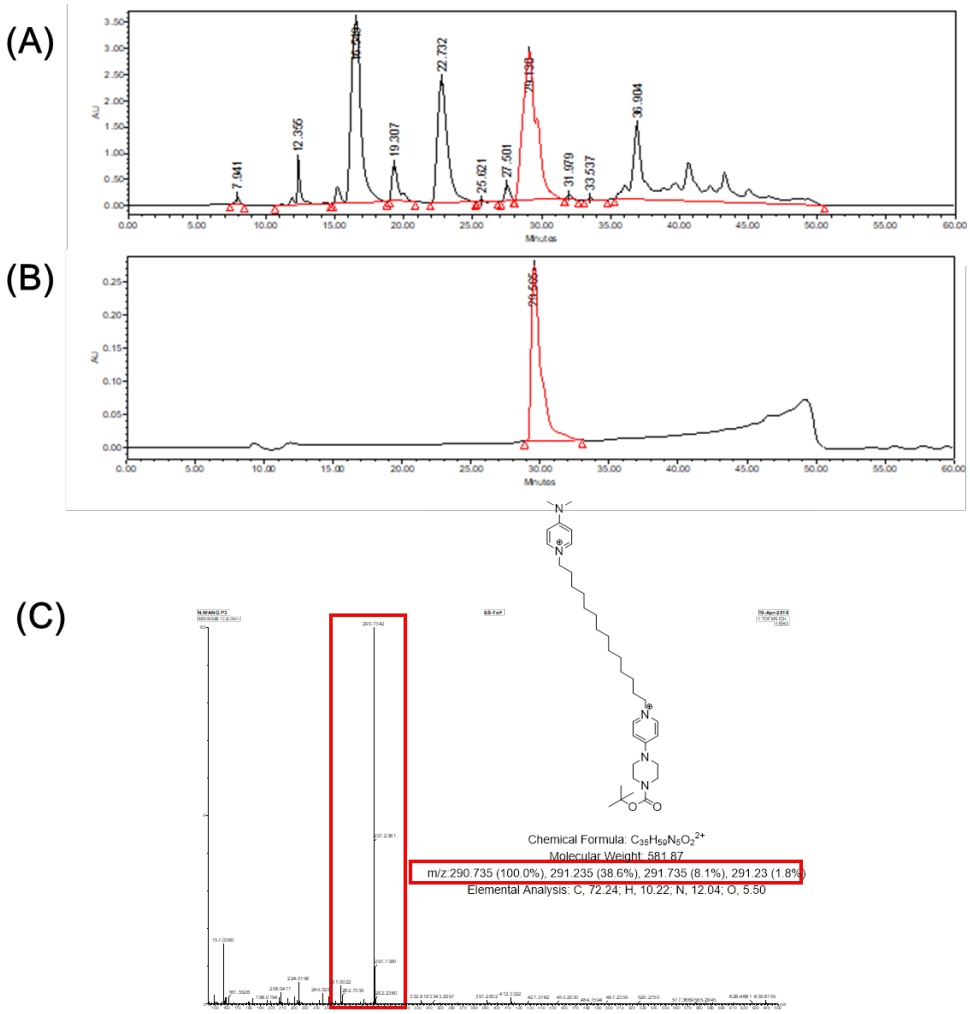


Figure 9. 1: Purification and chemical identity confirmation of compound 5; HPLC method used: A. (A) HPLC chromatogram of the reaction crude containing compound **5**; the peak of compound **5** was coloured in red with a t_R of 29.1 min:sec; (B) HPLC chromatogram of the diluted combined fractions; the peak of compound **5** was coloured in red with a t_R of 29.5 min:sec; (C) MS analysis of the sample corresponding to the peak at 29.3 min:sec.

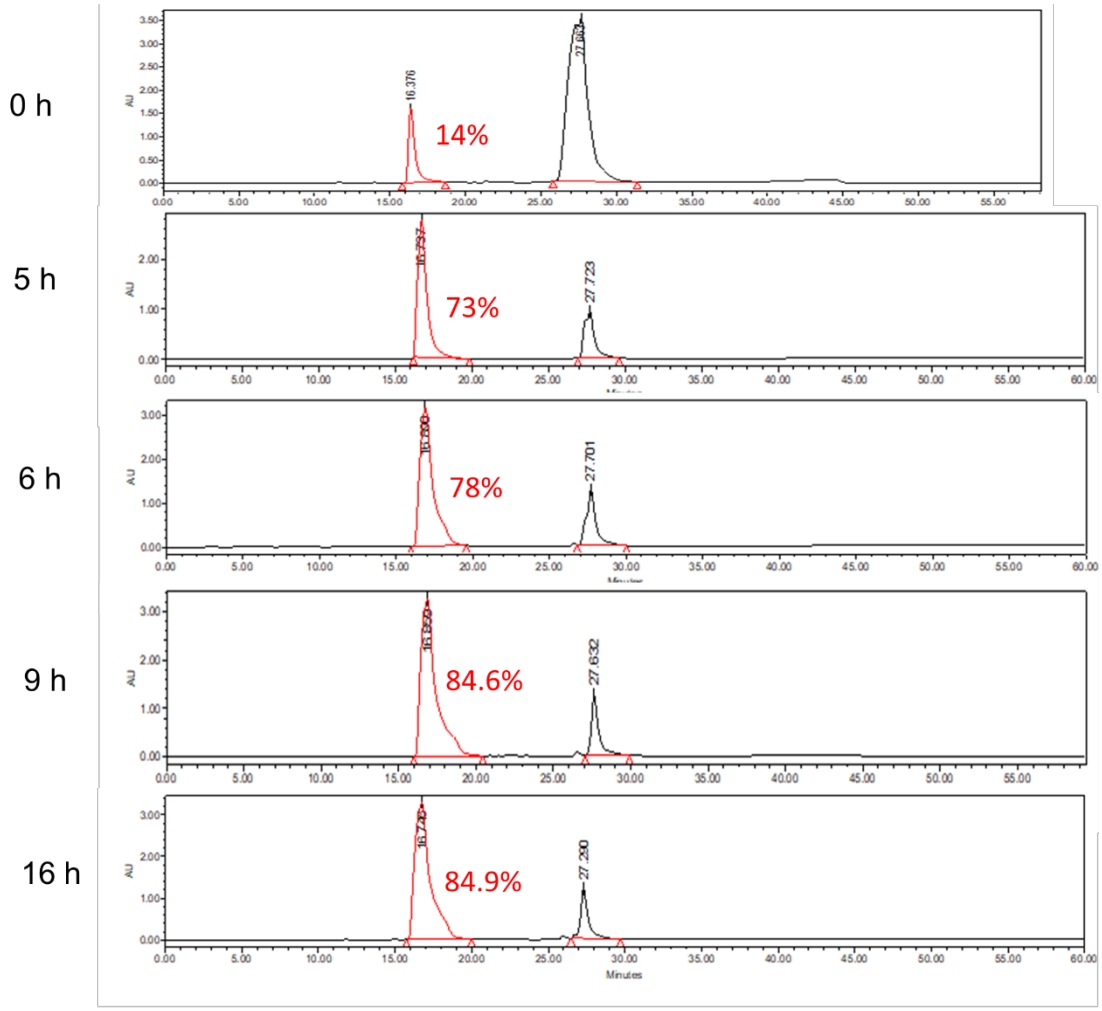


Figure 9. 2: HPLC monitoring of compound 5 Boc deprotection (HPLC method used: A). At five different time points (0-hour, 5 h-hour, 6-hour, 9-hour and 16-hour), the Boc deprotection progress of compound **5** using 15X TFA in acetonitrile at room temperature. The target peak corresponding to compound **6** (highlighted in red) appeared at 16.8 min:sec, while the unreacted compound **5** was at 27.7 min:sec. In 24 hours, the signal representing compound **6** increased to 85% and stayed constant.

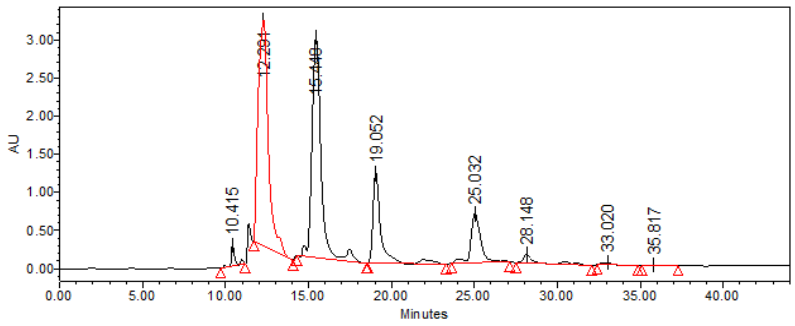


Figure 9. 3: The HPLC chromatogram of CK144 purification by semi-preparative HPLC using HPLC method A; the peak representing CK144 highlighted in red has a t_R at 12.3 min:sec.

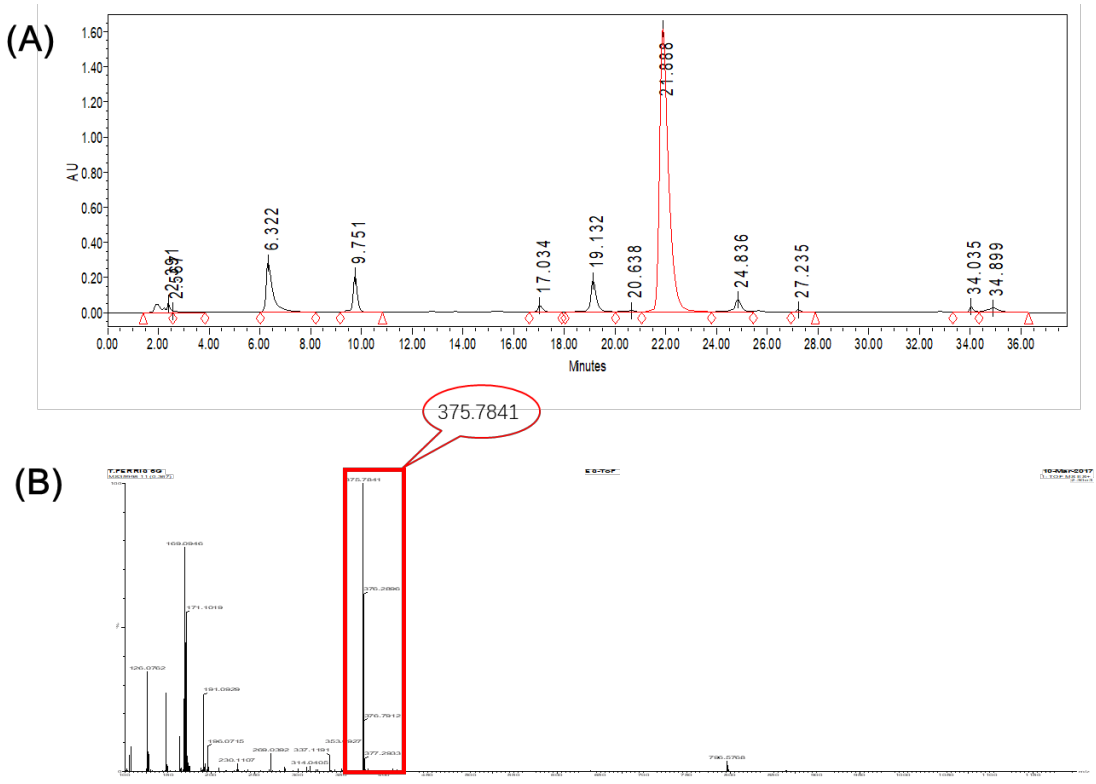


Figure 9. 4: HPLC analysis of the crude containing CK145 which was provided by Creative Chemistry Ltd. (A) The analytical HPLC chromatogram using HPLC method B; the peak of CK145 is highlighted in red; (B) MS analysis; the mass of CK145 (375.7841) detected is boxed in red.

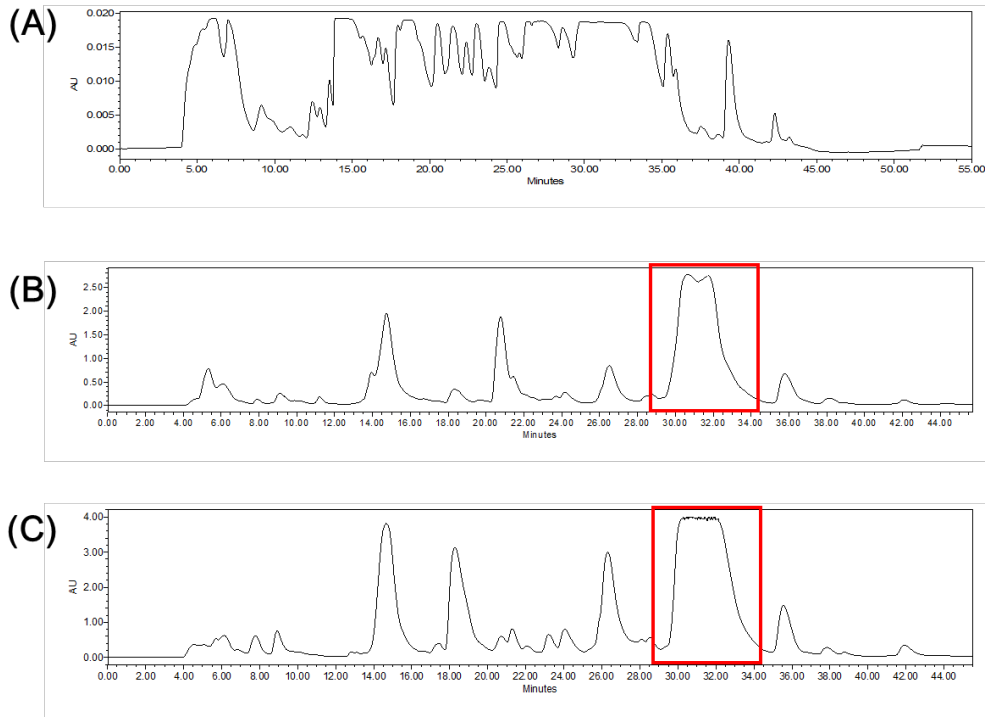


Figure 9. 5: HPLC chromatograms of CK145 purification. (A) The analytical HPLC chromatogram of CK145 with the concentration over the loading limit (HPLC method B); (B) The semi-preparative HPLC chromatogram of CK145 (30 mg/mL) at 254 nm (HPLC method C); (C) The semi-preparative HPLC chromatogram of CK145 (30 mg/mL) at 318 nm (HPLC method C). The peaks (44 %) of CK145 were boxed in red.

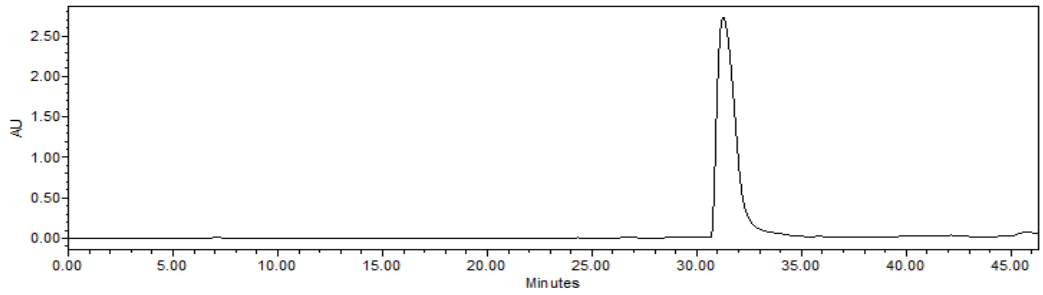


Figure 9. 6: The HPLC chromatogram of purified CK145 (254 nm; HPLC method C).

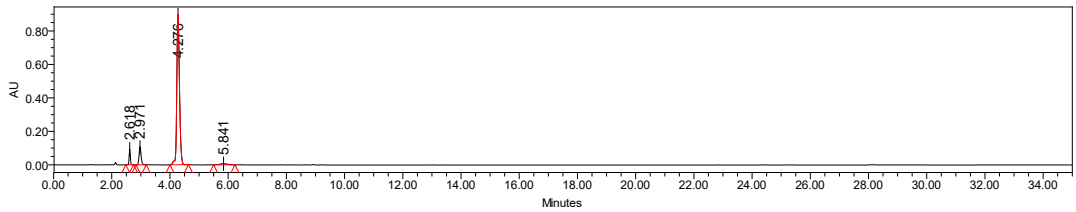


Figure 9. 7: The HPLC chromatogram of the crude containing compound 11 (HPLC method used: E). The purity of **11** (the peak labelled in red; t_R: 4.276 min) was integrated as 90%.

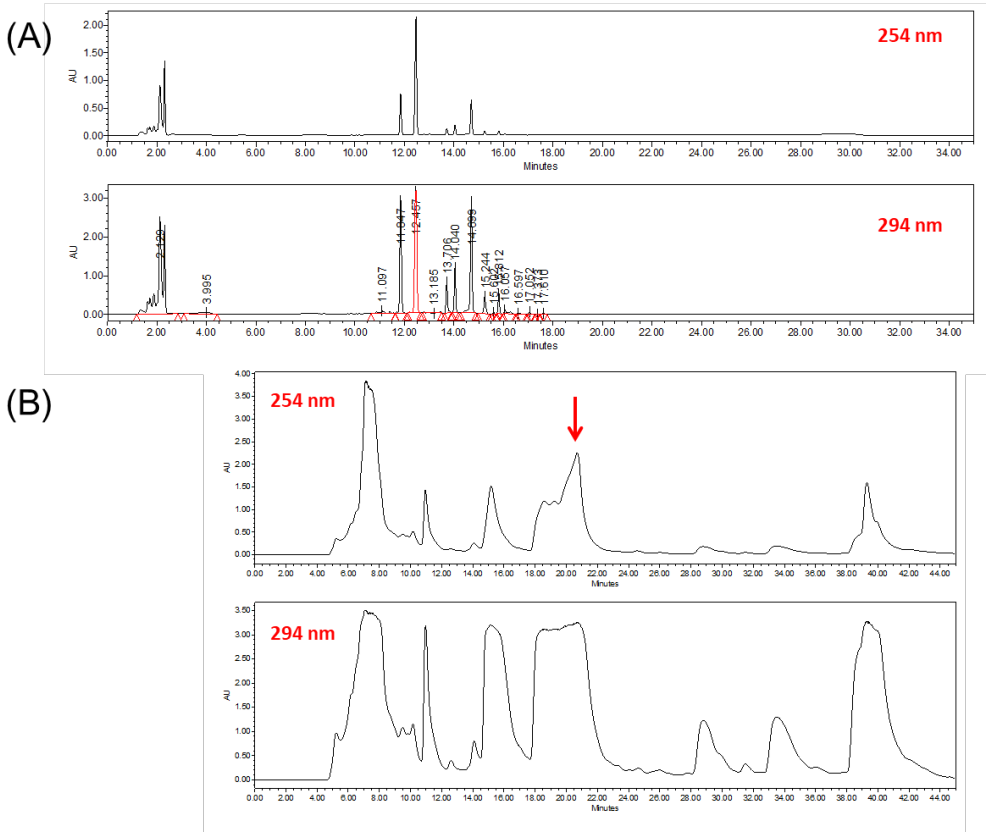


Figure 9. 8: Optimisation of semi-preparative HPLC methods using dual wavelengths (254 nm and 294 nm). (A) analytical HPLC chromatograms of crude analysis after the coupling reaction yielding compound **12**; HPLC method used: E; According to the MS analysis, the possible peak of interest (in red) has a retention time of 12.46 min:sec; (B) Semi-preparative HPLC chromatograms for the purification of compound **12**; the HPLC method used: E; The peak of interest is labelled with a red arrow.

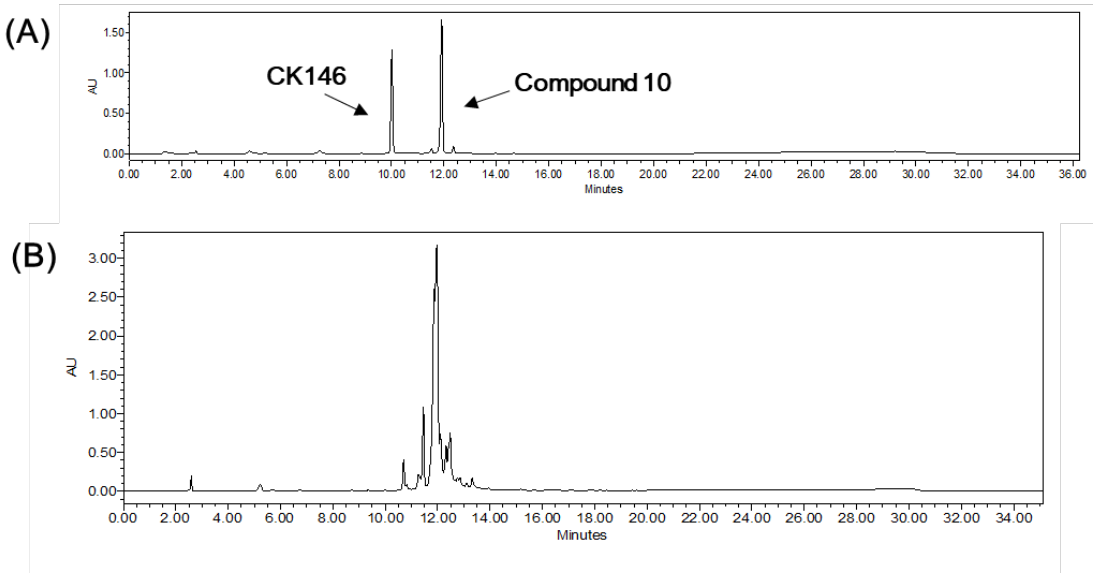


Figure 9. 9: The NHS ester crosslinking of CK146 and compound 10 (HPLC method used: F). (A) the HPLC analysis of the reaction without TEA; (B) the HPLC analysis of the reaction with 4 equiv. TEA overnight.

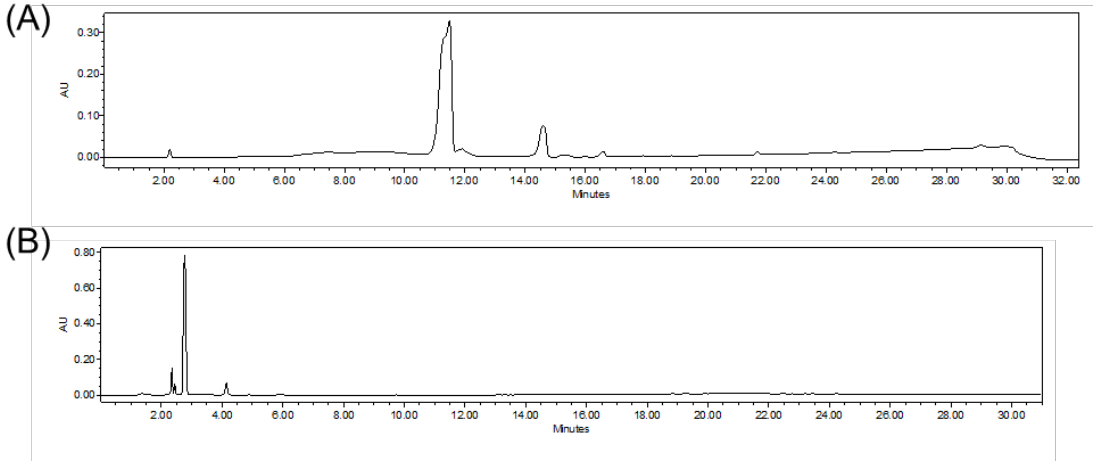
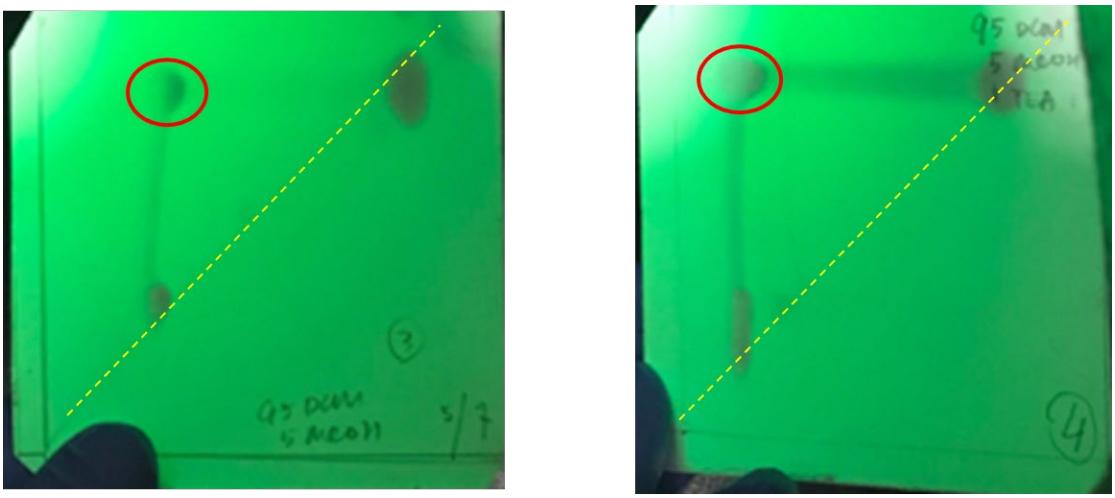


Figure 9. 10: The stability investigations of compound 10 using TEA (HPLC method used: F). (A) the analytical HPLC characterisation of compound **10** without TEA; (B) The HPLC analysis on compound **10** with TEA.

10. Supplementary information



(A) (B)

Figure S10. 1: Decomposition check of compound 11 by two-dimensional thin-layer chromatography (TLC) plates, in which case the spot representing compound **11** will run diagonally across the square plate (labelled with yellow dash lines) if there is no decomposition occurring. The off-diagonal spots circled in red show the decomposition product. (a) TLC conditions (v/v): DCM: methanol 95:5; (b) TLC conditions (v/v): DCM: Methanol 95:5, 1% TEA was added to neutralise the acidic sites of silica.

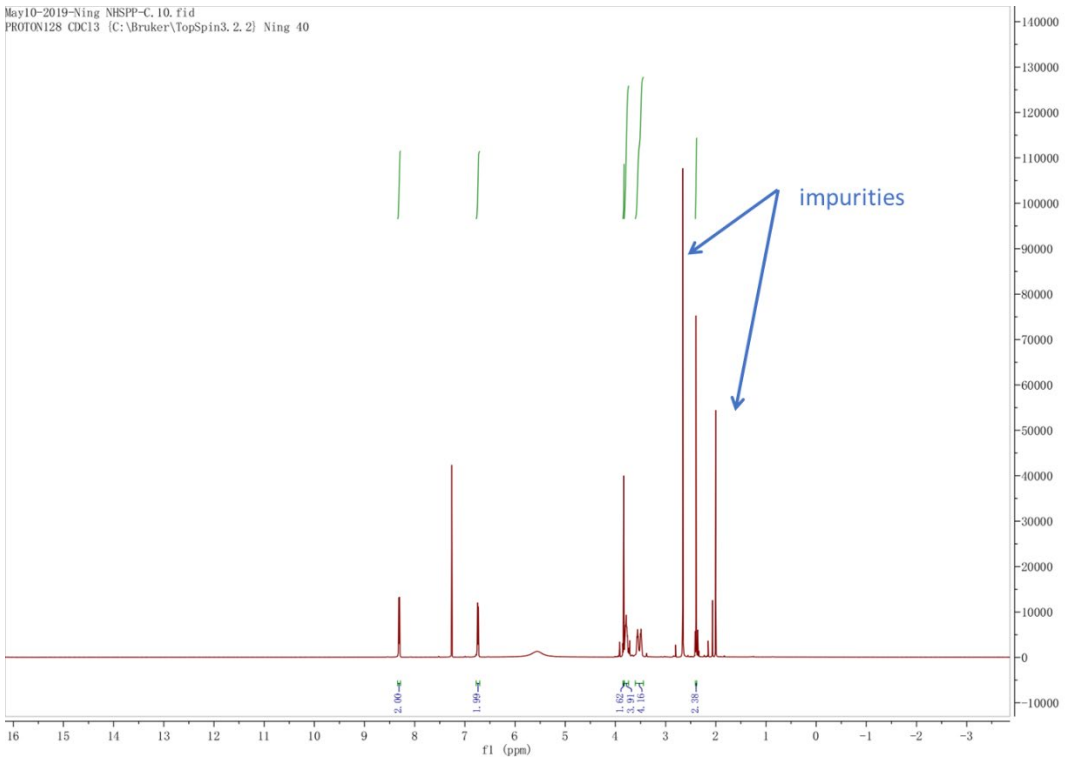


Figure S10. 2: ^{1}H NMR characterisation of the crude containing compound 11. The main peaks from impurities are demonstrated with arrows.

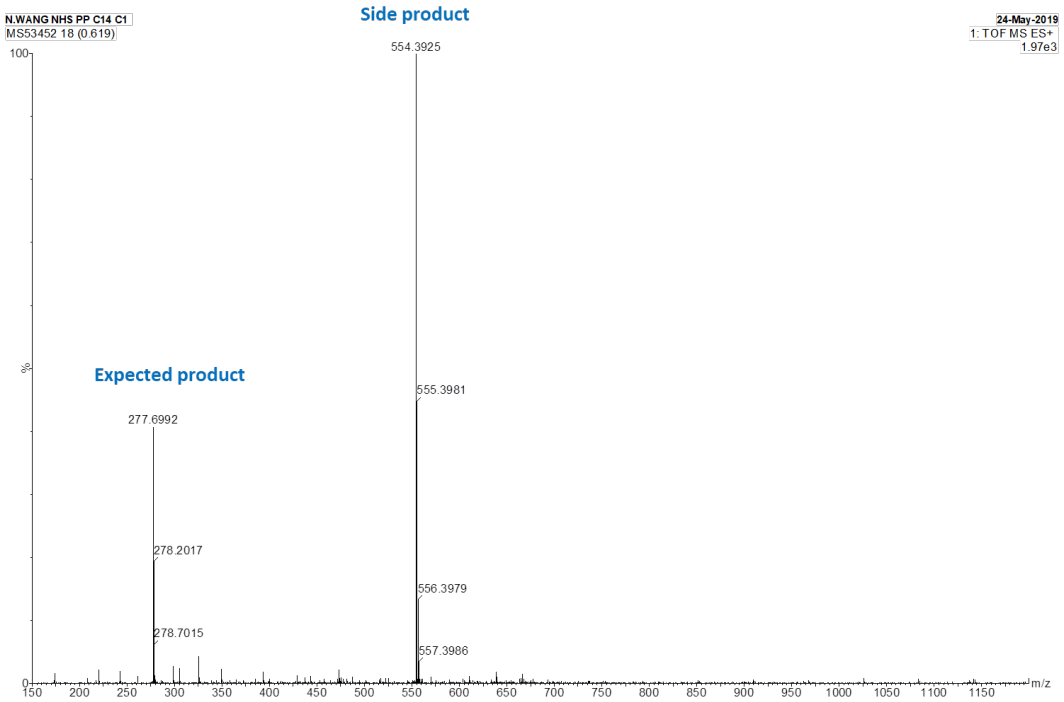


Figure S10. 3: MS analysis of the component collected from semi-prep HPLC purification. The two main peaks labelled represent the expected compound **12** and side products

respectively. It is shown that the side product accounts for the majority and these two compounds could not be separated under the current HPLC conditions we had.

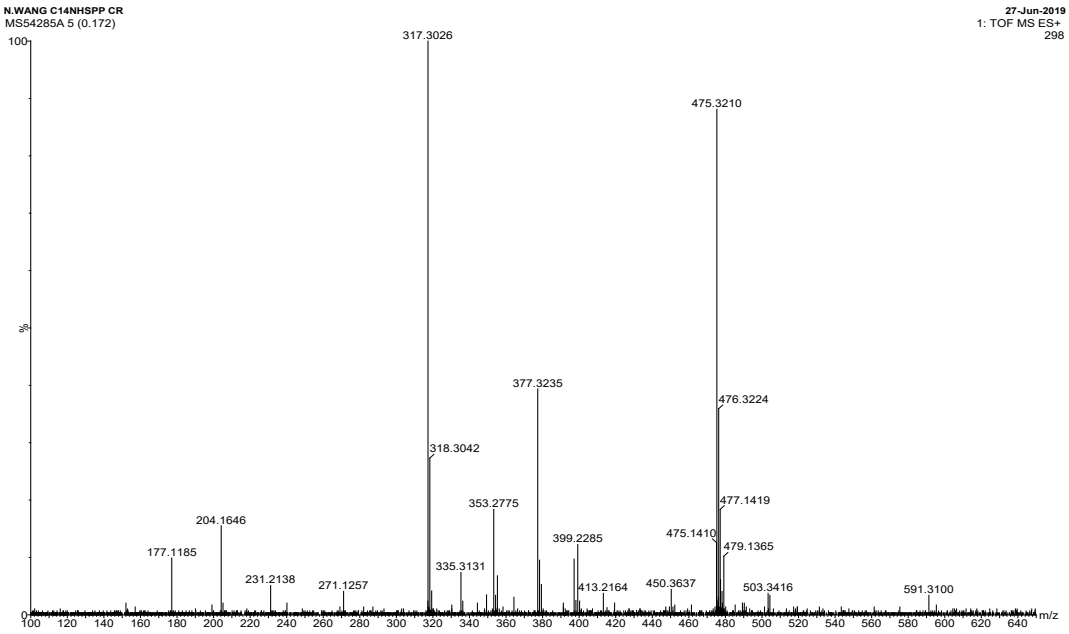


Figure S10. 4: MS analysis of the coupling between CK146 and compound 10: only singly charged ions were detected.

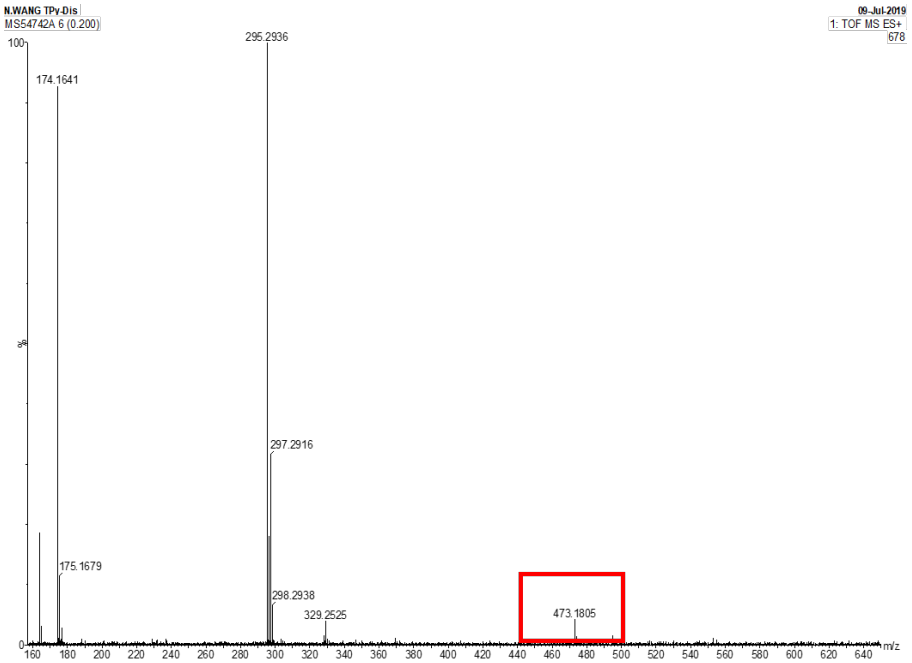


Figure S10. 5: MS check of the mock EDC coupling using 1-(4-Pyridyl)piperazine hydrochloride. The mass of interest is boxed in red.

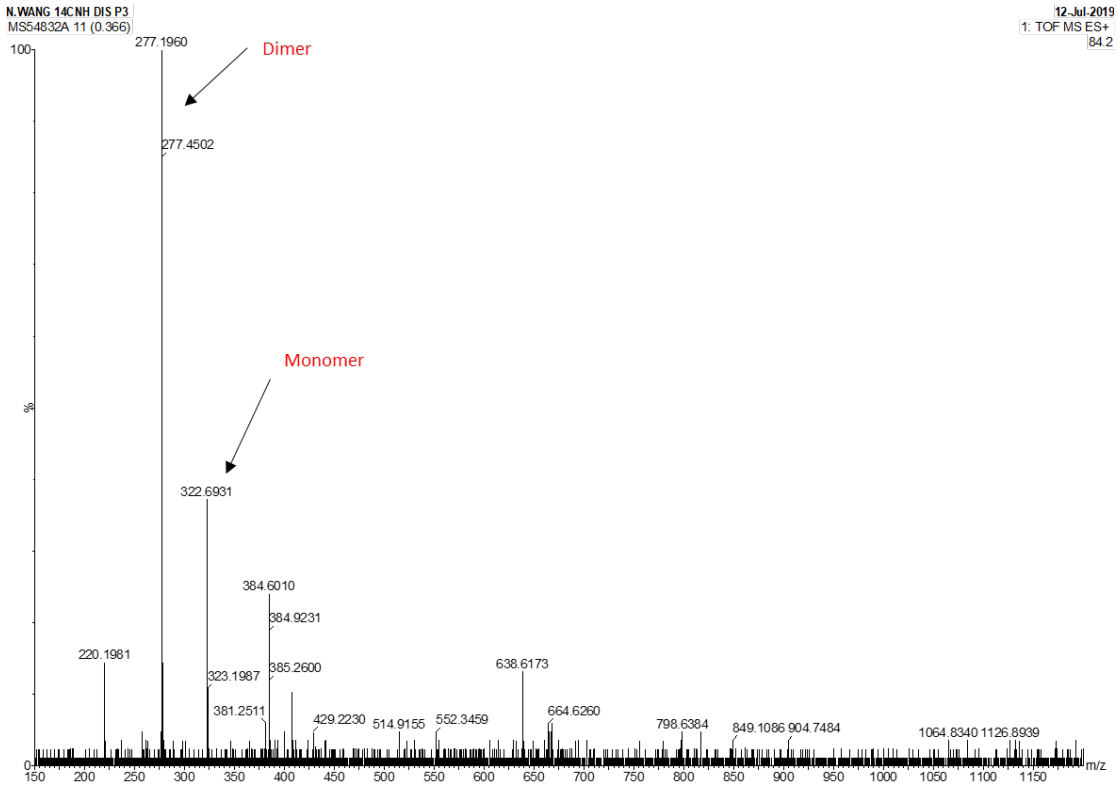


Figure S10. 6: MS analysis of EDC coupling between CK146 and dithiodiglycolic acid.

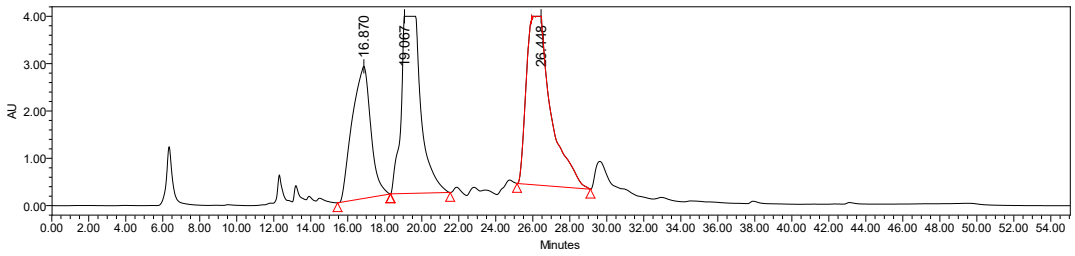


Figure S10. 7: The semi-preparative HPLC chromatogram of the coupling between dithiodiglycolic acid and CK146. According to MS analysis, the monomer and dimer conjugative products had the same retention time (t_R: 26.448 min:sec, coloured in red) using this HPLC method (See HPLC Method D).

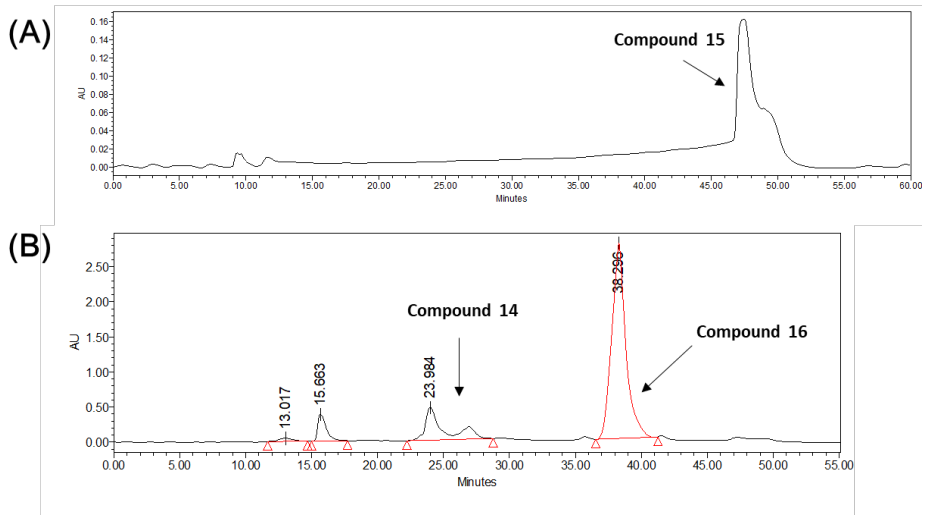


Figure S10. 8: HPLC analysis of the thiol-maleimide conjugation yielding compound 16 (HPLC method C). (A) the HPLC chromatogram of compound **15** (t_R: 47.5 min:sec); (B) the HPLC chromatogram of the reaction crude where compound **16** had been consumed and the desired compound **17** (t_R: 38 min:sec) was produced (yield: 85%).

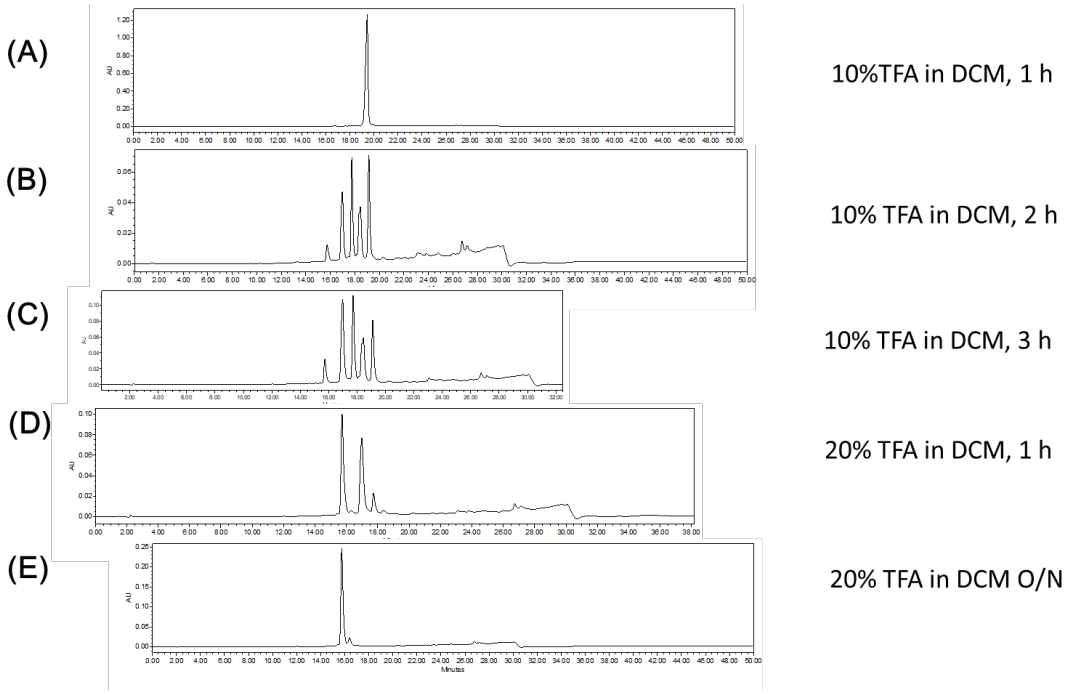


Figure S10. 9: Condition investigations and monitoring of compound 16 deprotection using analytical HPLC (HPLC method F). (A) The analytical HPLC chromatogram of compound **16** deprotection using 10% TFA in DCM for 1 hour (Deprotection did not occur); (B) The analytical HPLC chromatogram of compound **16** deprotection using 10% TFA in DCM for 2

hours (Deprotection started); (C) The analytical HPLC chromatogram of compound **16** deprotection using 10% TFA in DCM for 3 hours (Deprotection slowed down); (D) The analytical HPLC chromatogram of compound **16** deprotection using 20% TFA in DCM for 1 hour (Deprotection was accelerated); (E) The analytical HPLC chromatogram of compound **16** deprotection using 20% TFA in DCM overnight (Deprotection completed; the purity of compound **17**: 95%).

Table S10. 1: Growth inhibitory activities (GI_{50}) of ICL-CCIC-0019, CK146 and CK145 after 120-hour treatment in HCT-116 and Caco-2 cells. The data were obtained by SRB assay; n= 6, mean ± SD.

Drug	HCT-116 $GI_{50} \pm$ SD (μM)	Caco-2 $GI_{50} \pm$ SD (μM)
ICL-CCIC-0019	0.40 ± 0.04	1.20 ± 0.04
CK146	3.30 ± 0.38	3.10 ± 0.14
CK145	6.15 ± 0.13	10.80 ± 1.10

Table S10. 2: Growth inhibitory activities (GI_{50}) of ICL-CCIC-0019, CK146 and CK147 in 22Rv1, C4-2B, LNCap, R1AD1, R1-D567, PC3, PNT1A and HCT-116 cells. The data were obtained by SRB assay; n= 6, mean ± SD.

		GI_{50} (μM) ± SD		
PSMA	Cell line	ICL-CCIC-0019	CK146	CK147
+	22Rv1	0.91 ± 0.13	4.98 ± 1.50	45.64 ± 6.40
+	C4-2B	1.20 ± 0.31	4.22 ± 0.43	63.00 ± 12.12
+	LNCap	0.30 ± 0.06	1.92 ± 0.99	39.03 ± 8.56
−	R1AD1	0.40 ± 0.01	5.67± 2.33	53.40 ± 2.27
−	R1-D567	0.32 ± 0.00	0.87 ± 0.03	40.43 ± 4.56
−	PC3	0.79 ± 0.03	4.73 ± 0.81	84.92 ± 7.03
−	PNT1A	0.47 ± 0.08	3.00 ± 0.26	63.64 ±10.38
−	HCT-116	0.42 ± 0.03	4.76 ± 0.8	103.49 ± 6.27

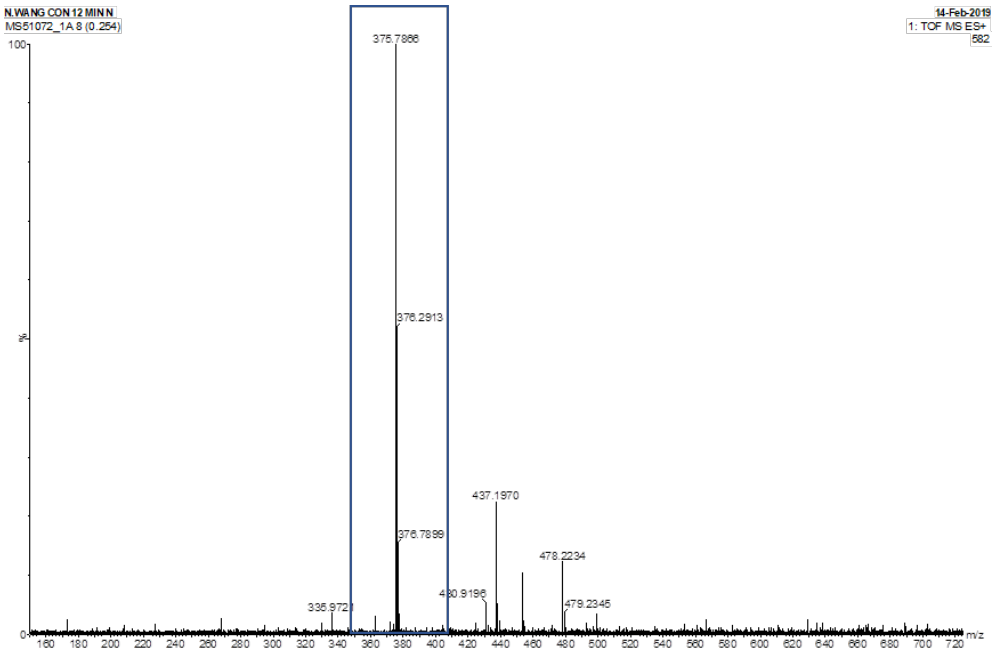


Figure S10. 10: MS analysis of the compound collected at 12.5 min:sec on HPLC (HPLC method F). The compound detected by HPLC was confirmed to be CK145 (boxed in blue).

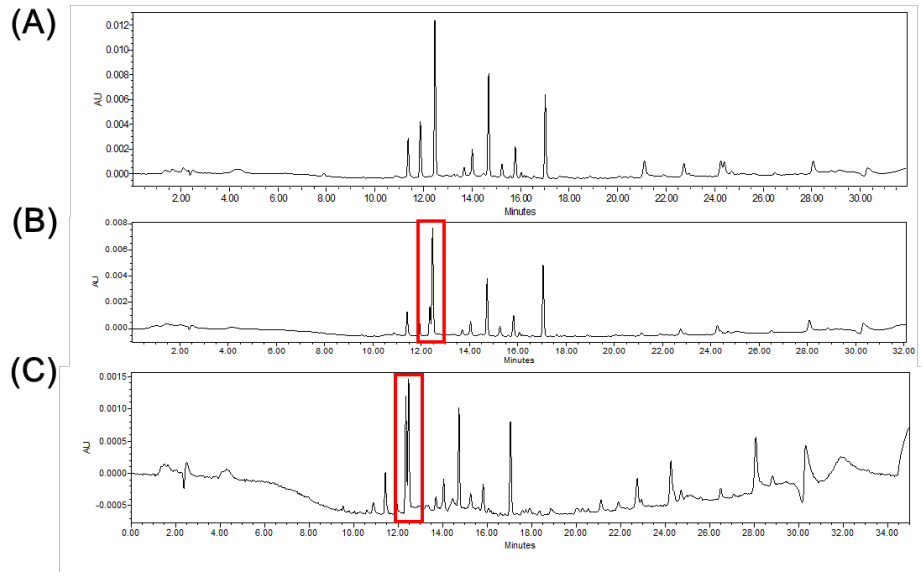


Figure S10. 11: The HPLC chromatograms of CK146 detection in media with or without CK145 treatment (HPLC method F); wavelength: 294 nm. (A) the vehicle group after 2-hour incubation without CK145; (B) 1-hour incubation with CK145; (C) 2-hour incubation with CK145. The signals representing CK145 (t_R: 12.5 min:sec) were highlighted in red rectangles. CK146 (t_R: 9.8 min:sec) was not detected in medium (LOD value: 1.382 μg/L).

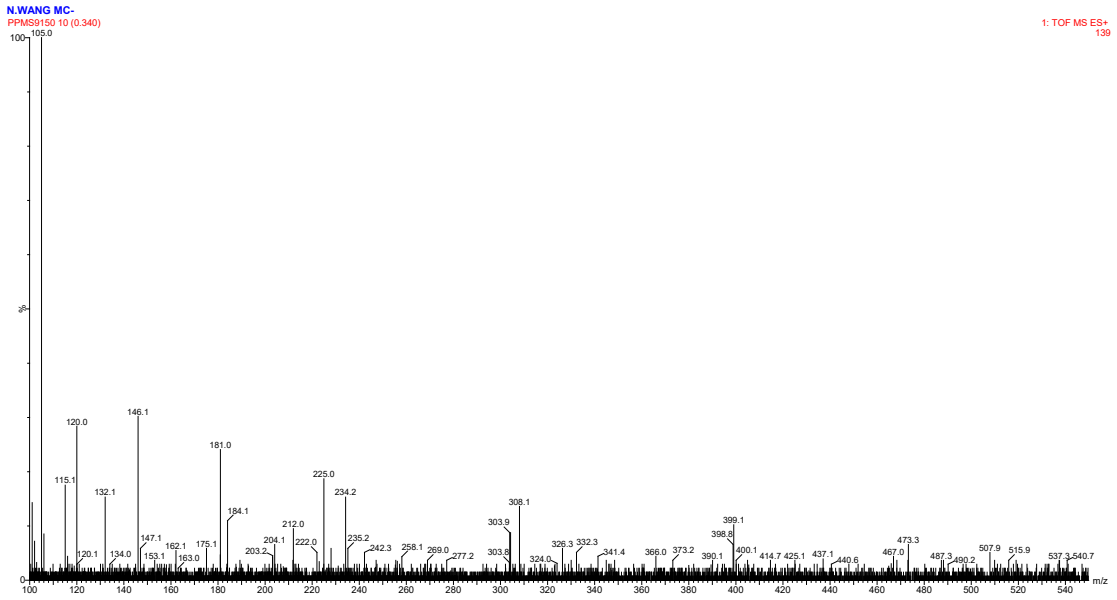


Figure S10. 12: MS analysis of the FCS-free medium without drug treatment.

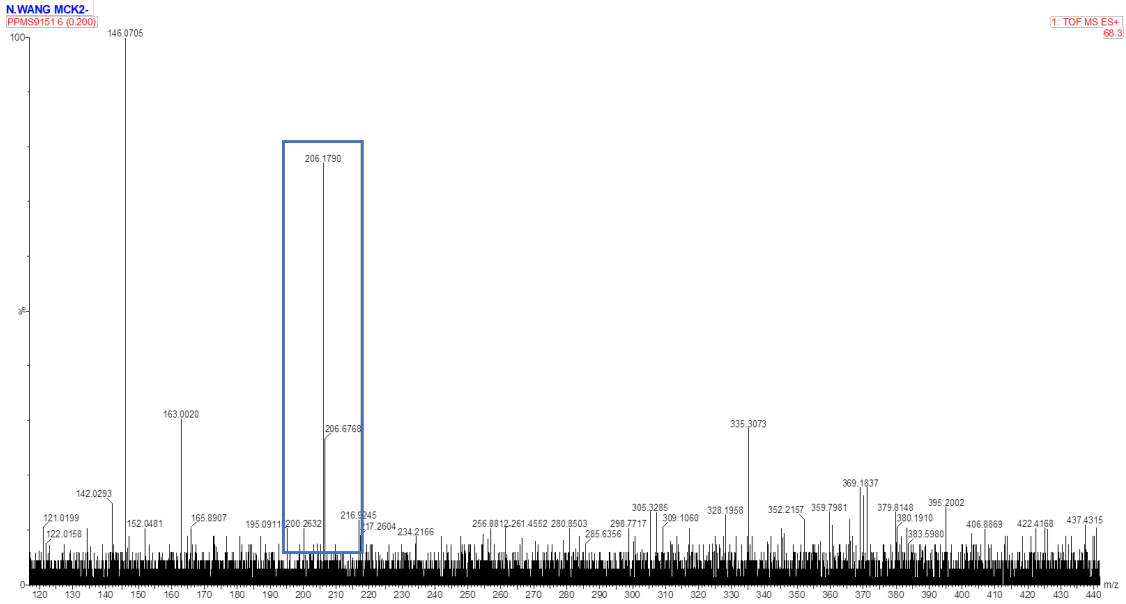


Figure S10. 13: MS analysis of the FCS-free medium incubated with ICL-CCIC-0019 for 4 hours. The mass of ICL-CCIC-0019 was highlighted. No metabolites from ICL-CCIC-0019 were detected.

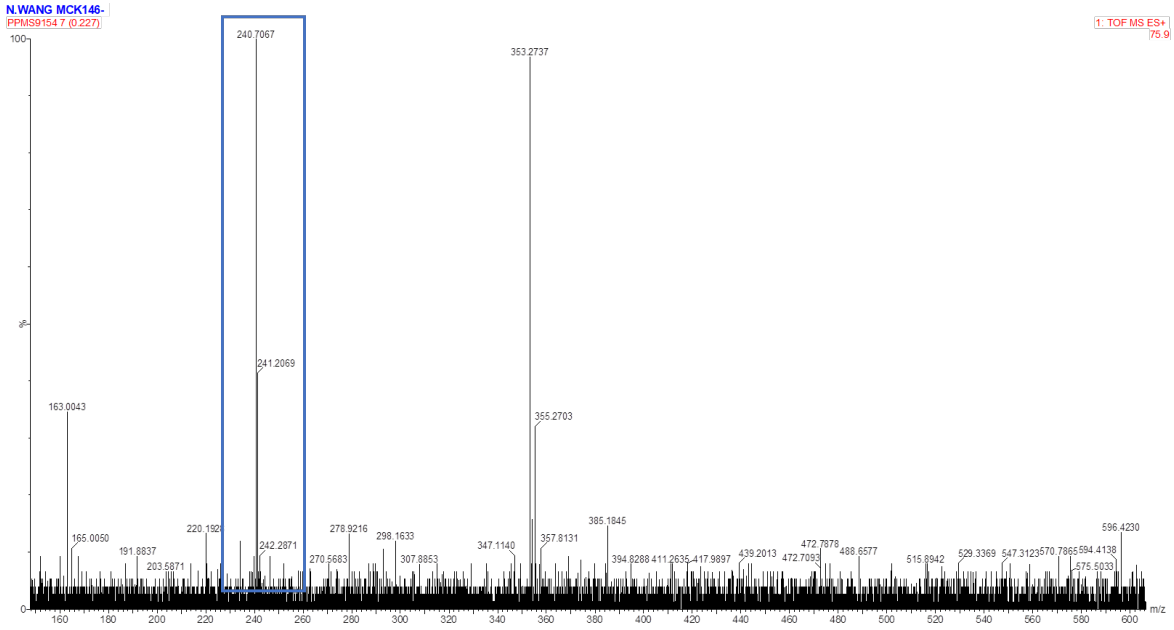


Figure S10. 14: MS analysis of the FCS-free medium incubated with CK146 for 4 hours. The mass of CK146 was highlighted. No metabolites from CK146 were detected.

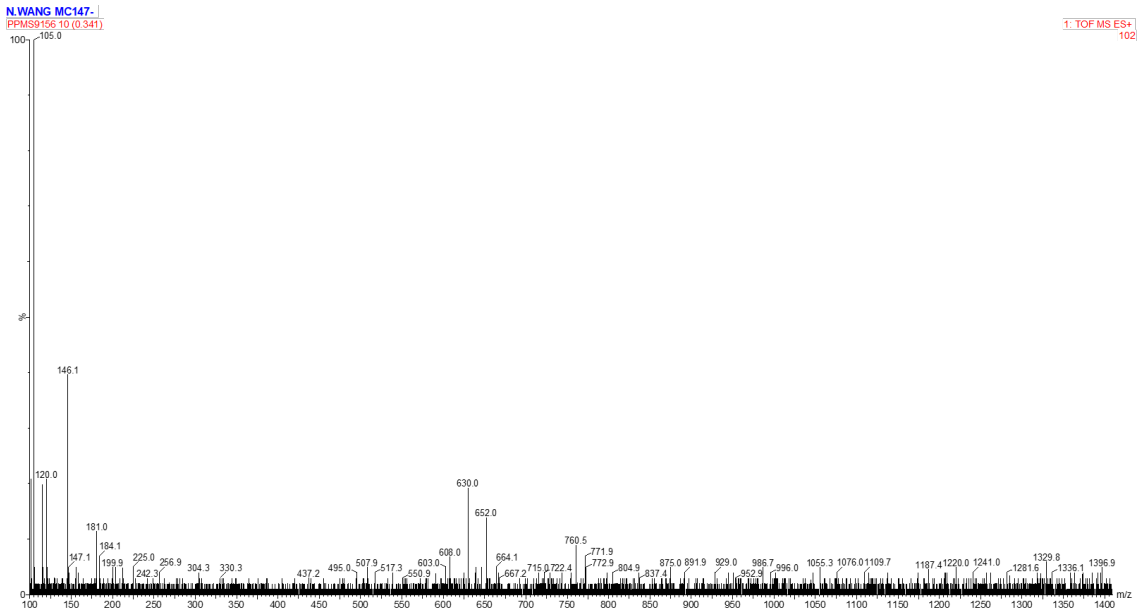


Figure S10. 15: MS analysis of the FCS-free medium incubated with CK147 for 4 hours. CK147 and any metabolites from CK147 were not detected.

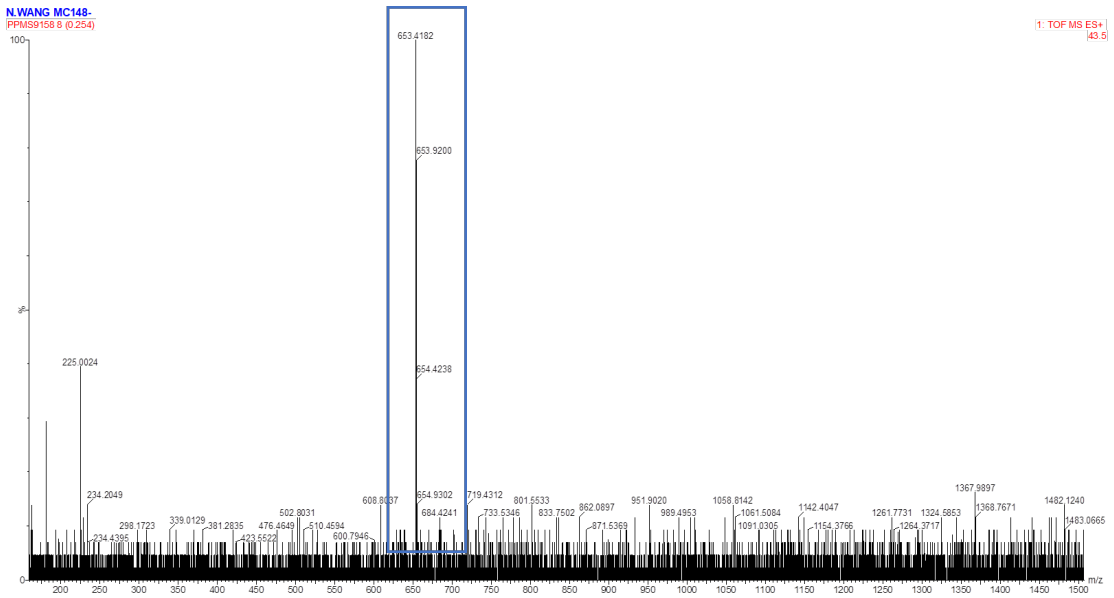


Figure S10. 16: MS analysis of the FCS-free medium incubated with CK148 for 4 hours. The mass of CK148 was highlighted. No metabolites from CK148 were detected.

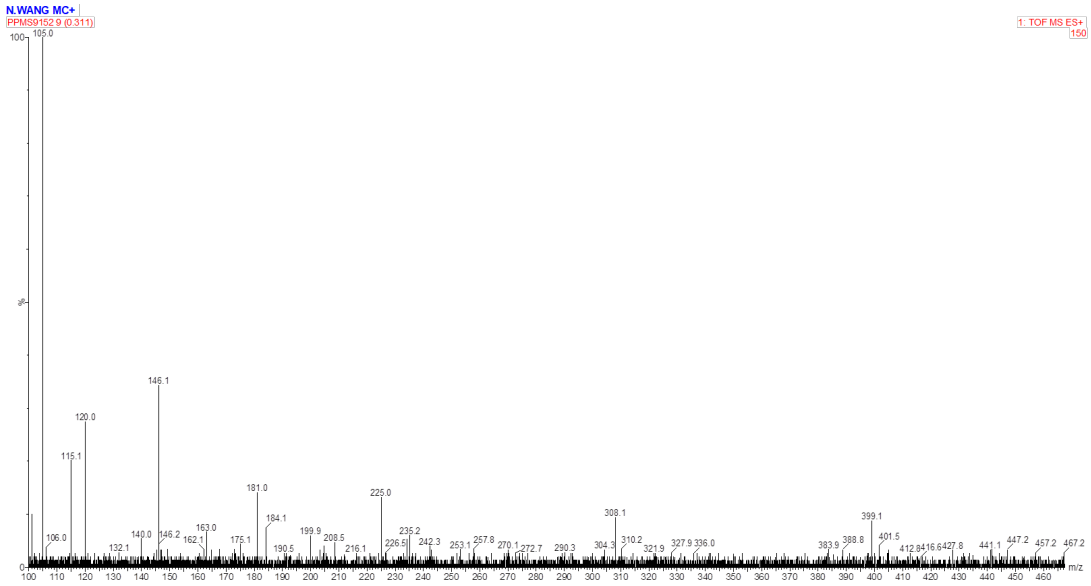


Figure S10. 17: MS analysis of the FCS supplemented medium without drug treatment.

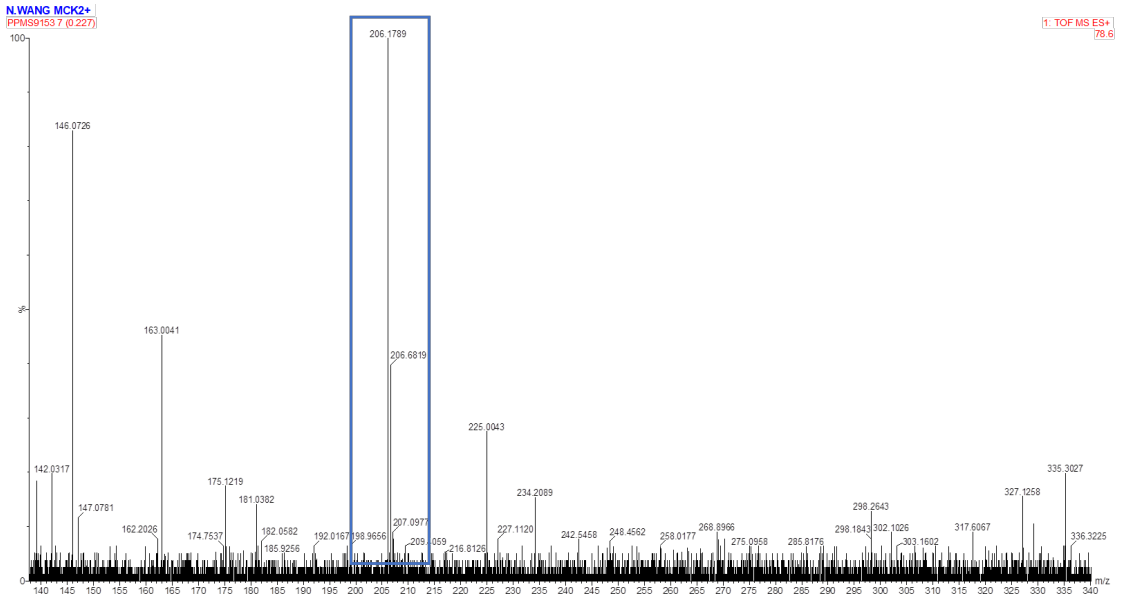


Figure S10. 18: MS analysis of the FCS supplemented medium incubated with ICL-CCIC-0019 for 4 hours. The mass of ICL-CCIC-0019 was highlighted. No metabolites from ICL-CCIC-0019 were detected.

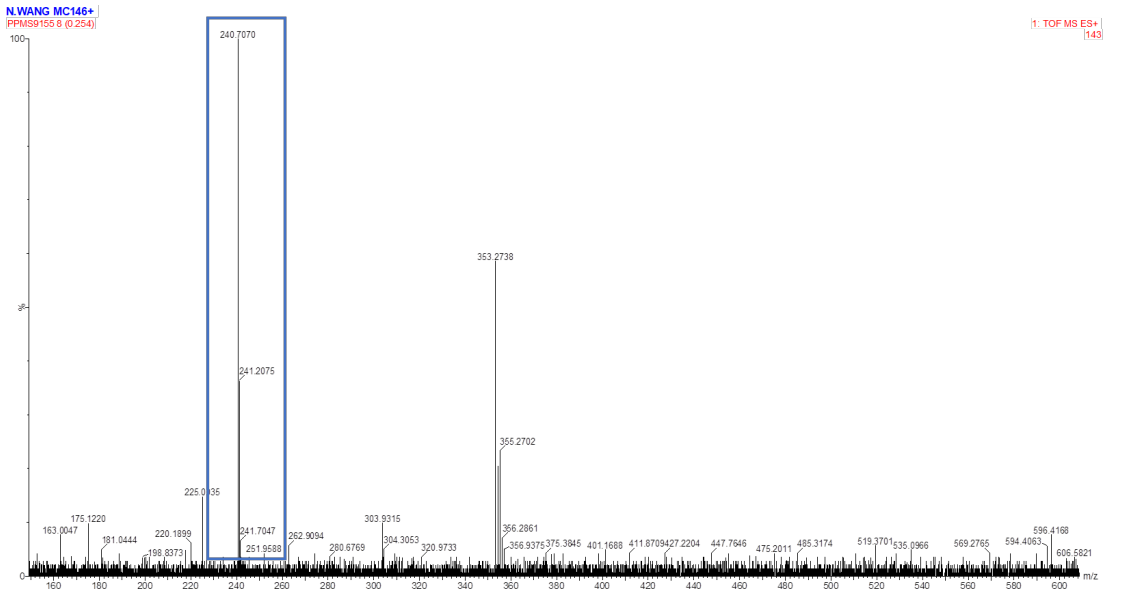


Figure S10. 19: MS analysis of the FCS supplemented medium incubated with CK146 for 4 hours. The mass of CK146 was highlighted. No metabolites from CK146 were detected.

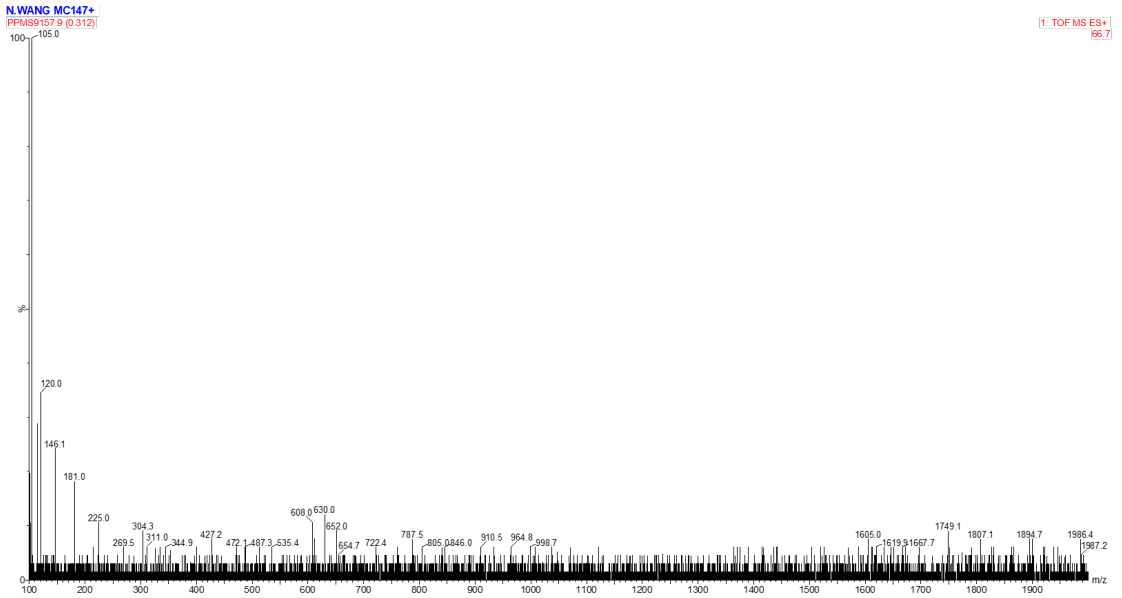


Figure S10. 20: MS analysis of the FCS supplemented medium incubated with CK147 for 4 hours. CK147 and any metabolites from CK147 were not detected.

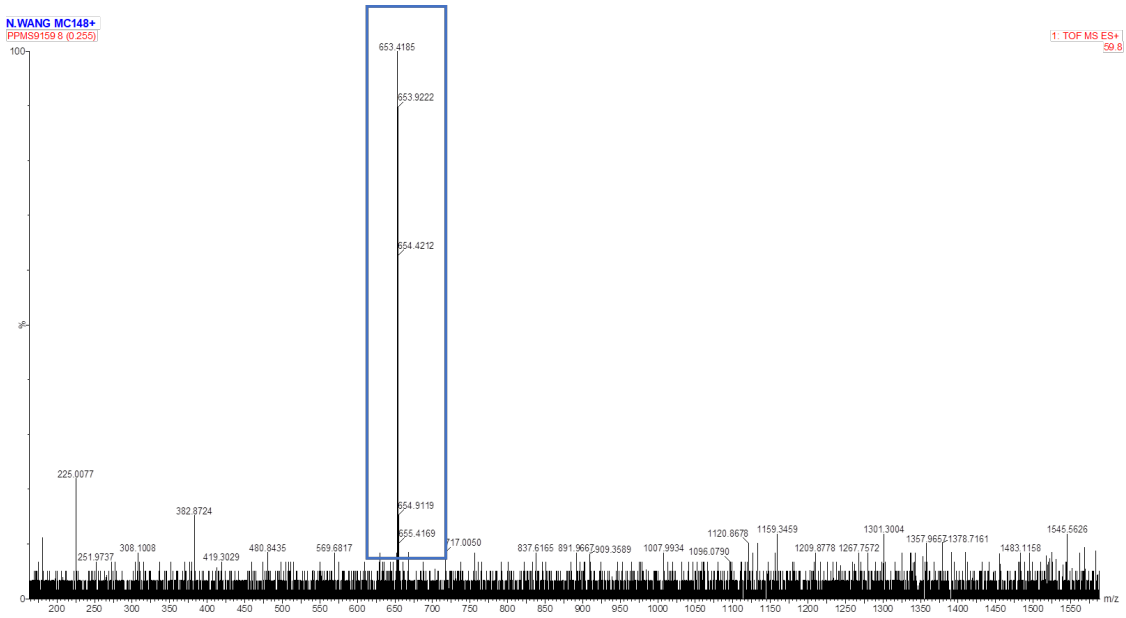


Figure S10. 21: MS analysis of the FCS supplemented medium incubated with CK148 for 4 hours. The mass of CK148 was highlighted. No metabolites from CK148 were detected.

11. Appendix

Appendix A: ^{1}H NMR, ^{13}C NMR, MS spectra

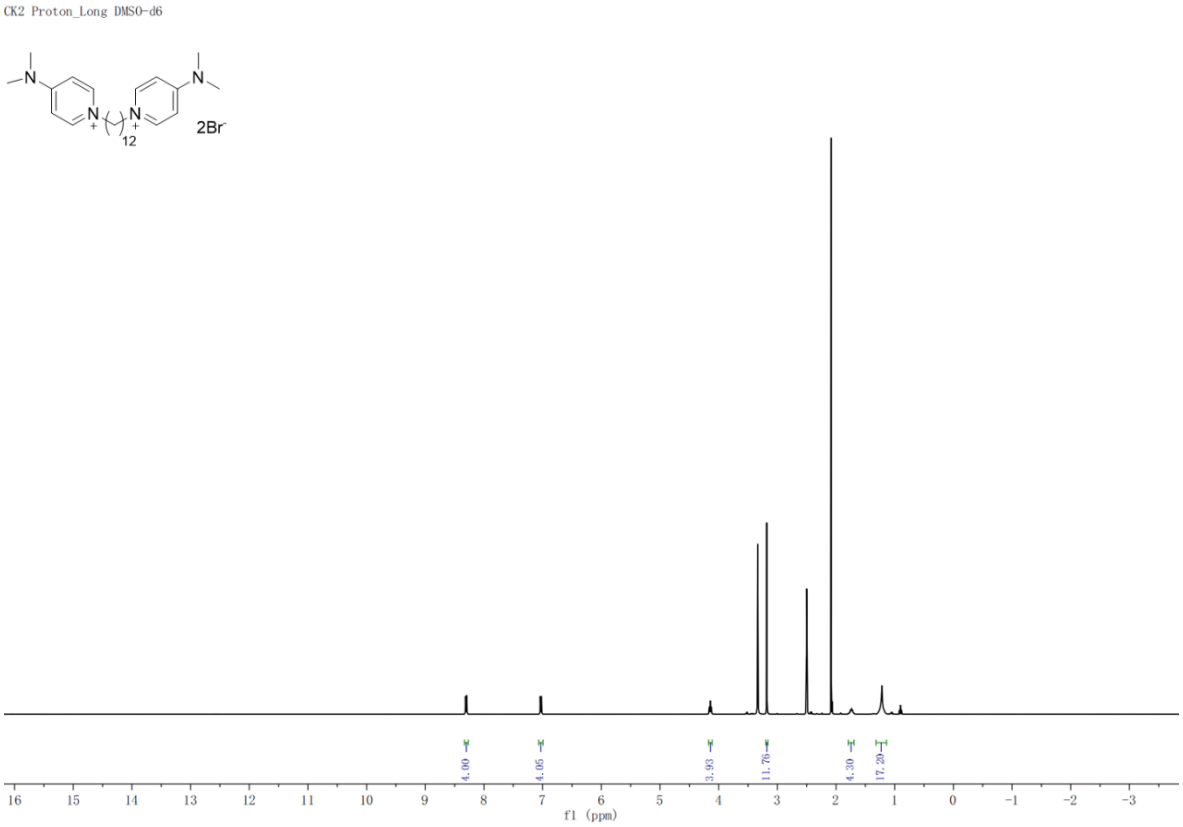


Figure 11. 1: ^{1}H NMR of ICL-CCIC-0019.

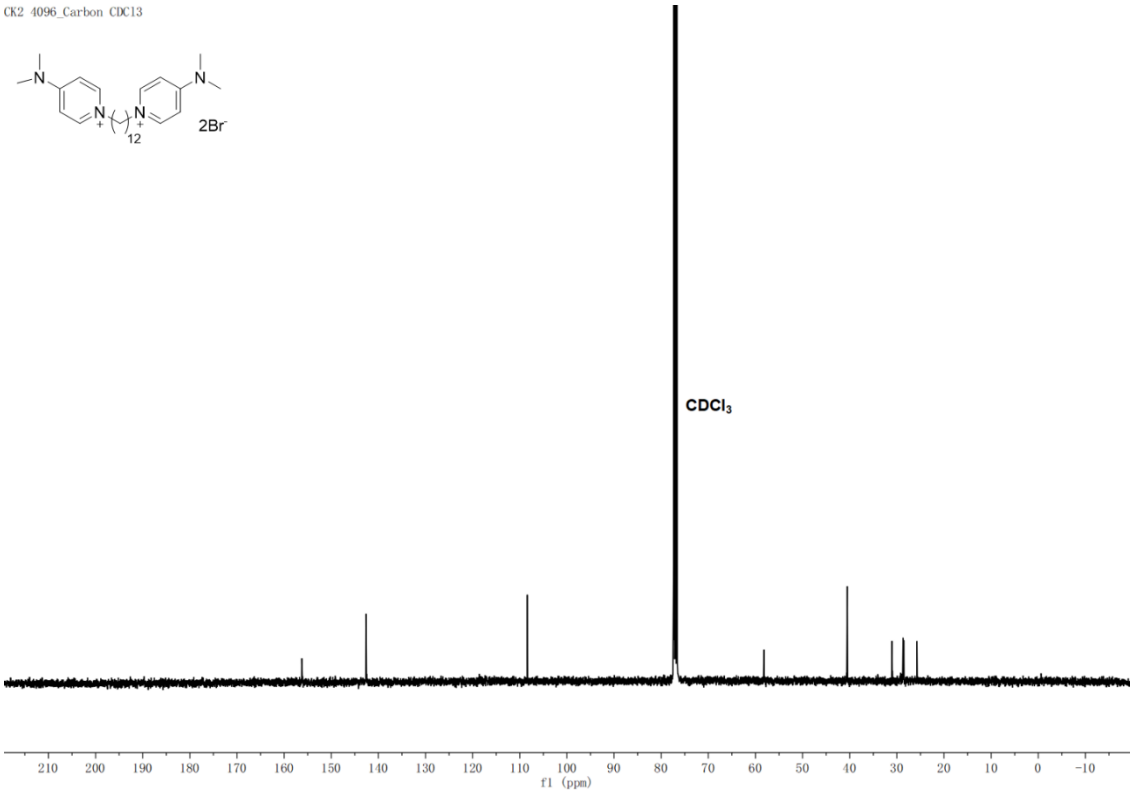


Figure 11. 2: ^{13}C NMR of ICL-CCIC-0019.

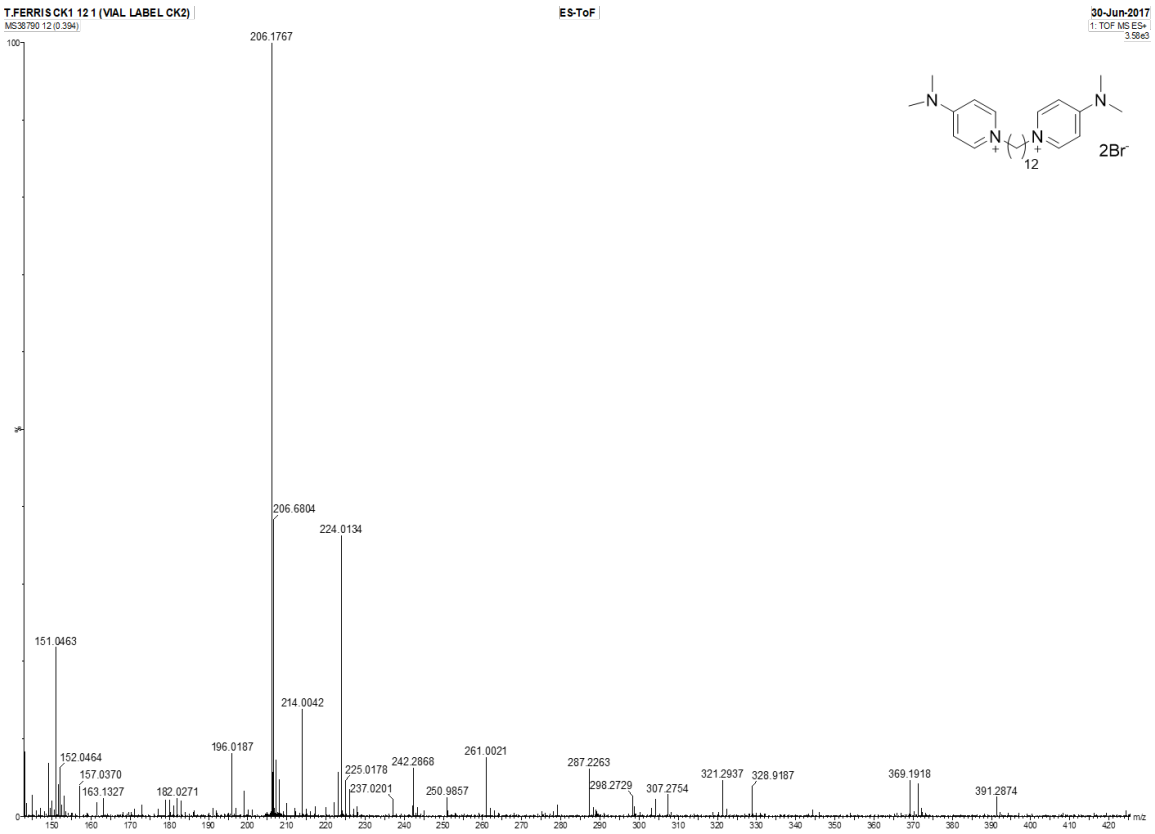


Figure 11. 3: MS analysis of ICL-CCIC-0019.

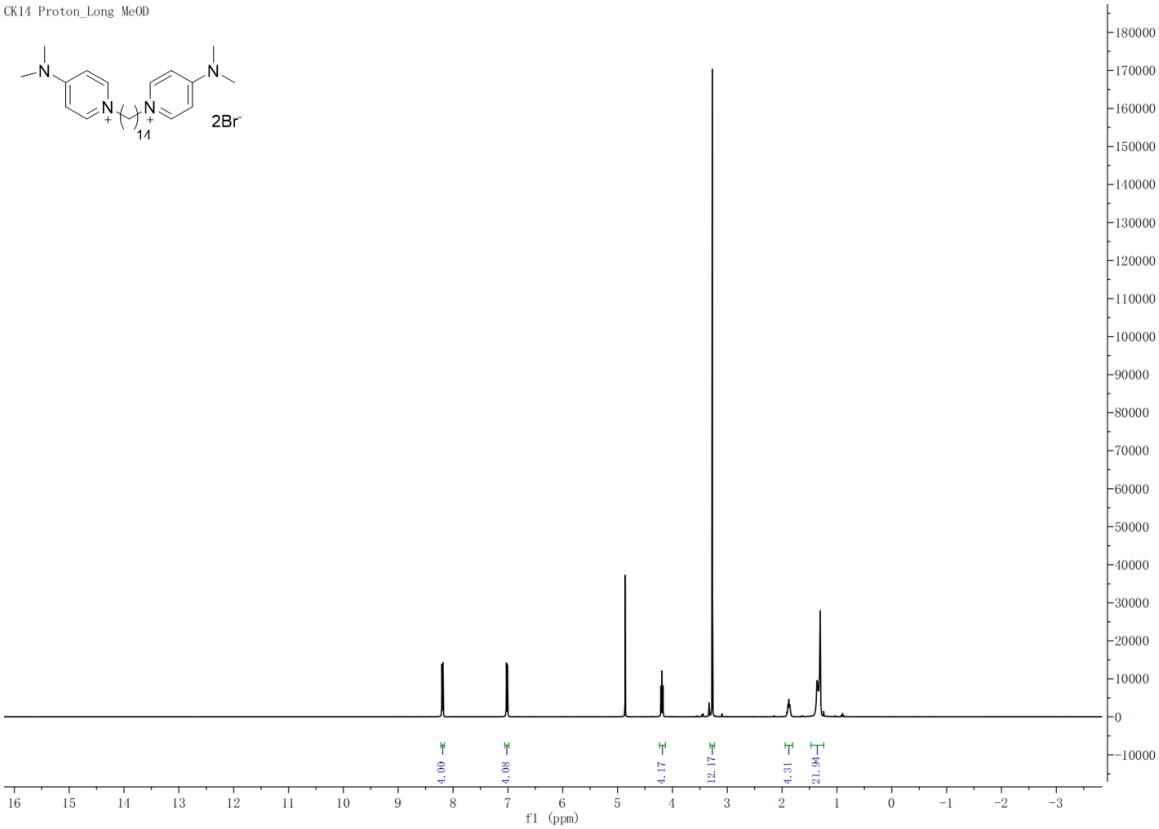


Figure 11. 4: ^{1}H NMR of CK14.

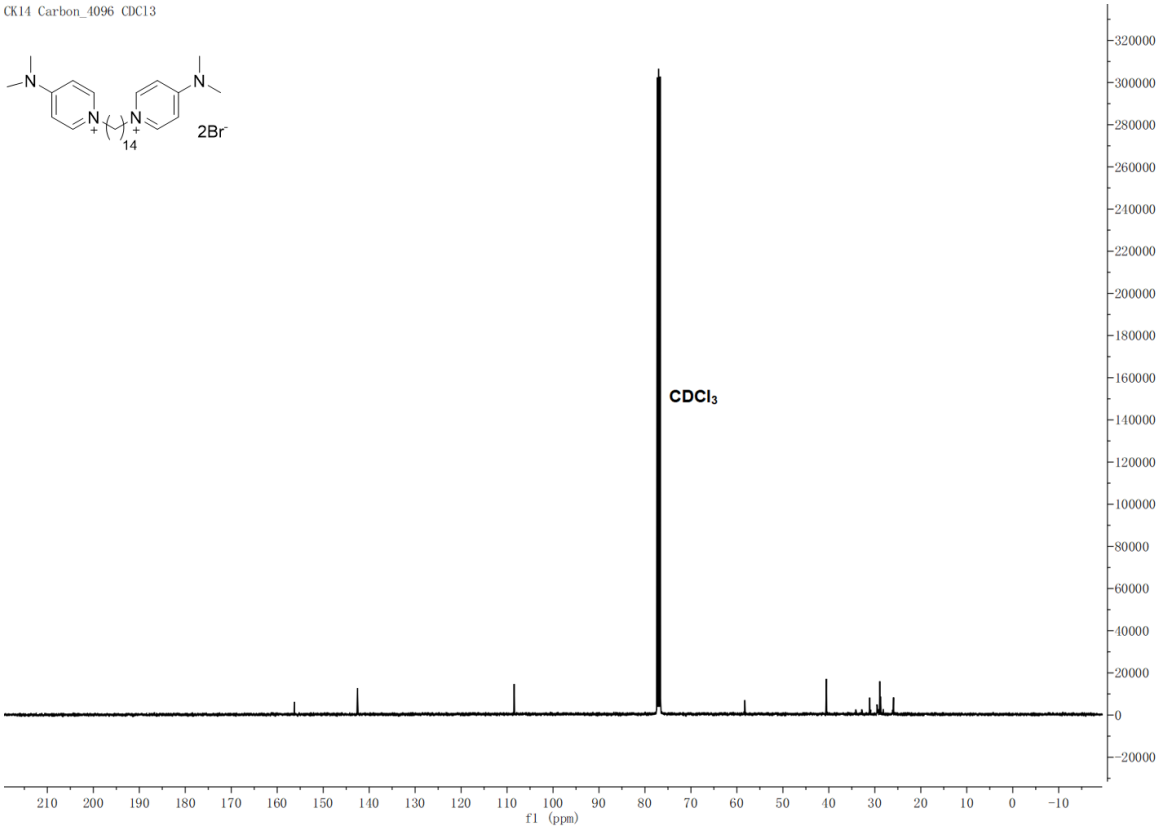


Figure 11. 5: ^{13}C NMR of CK14.

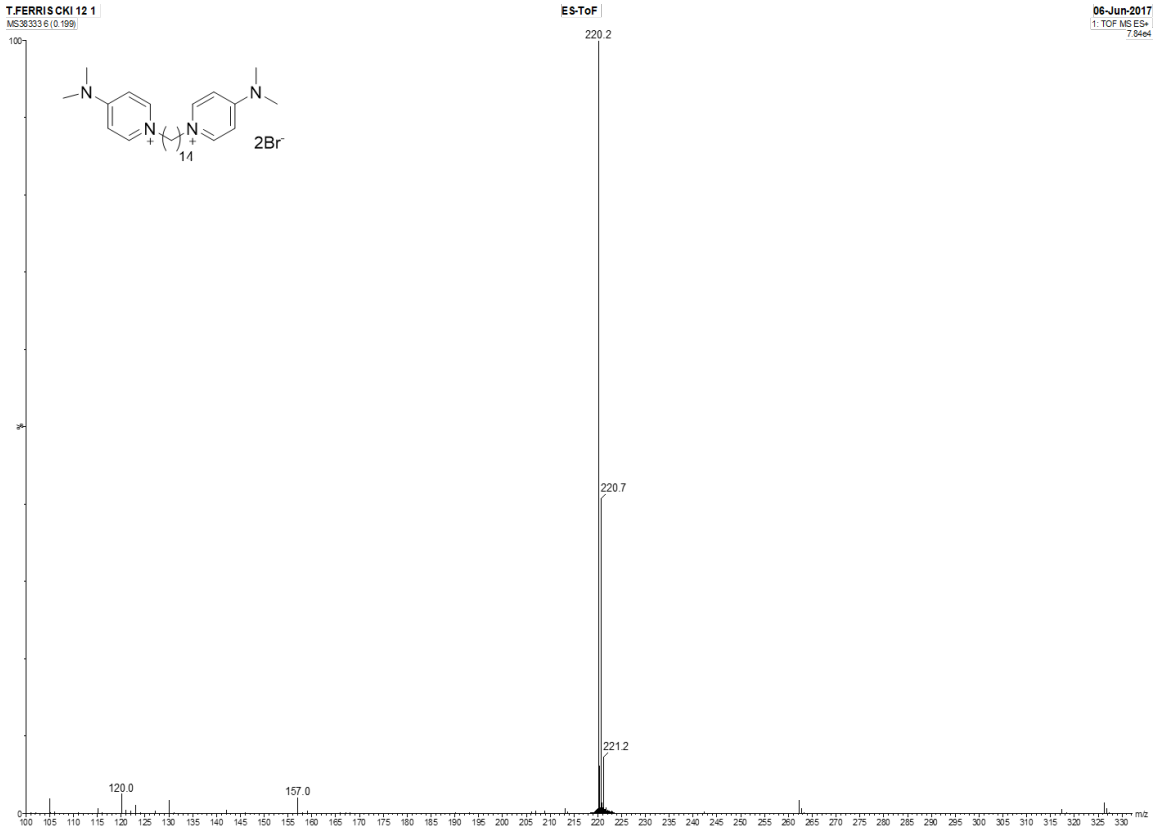


Figure 11. 6: MS analysis of CK14.

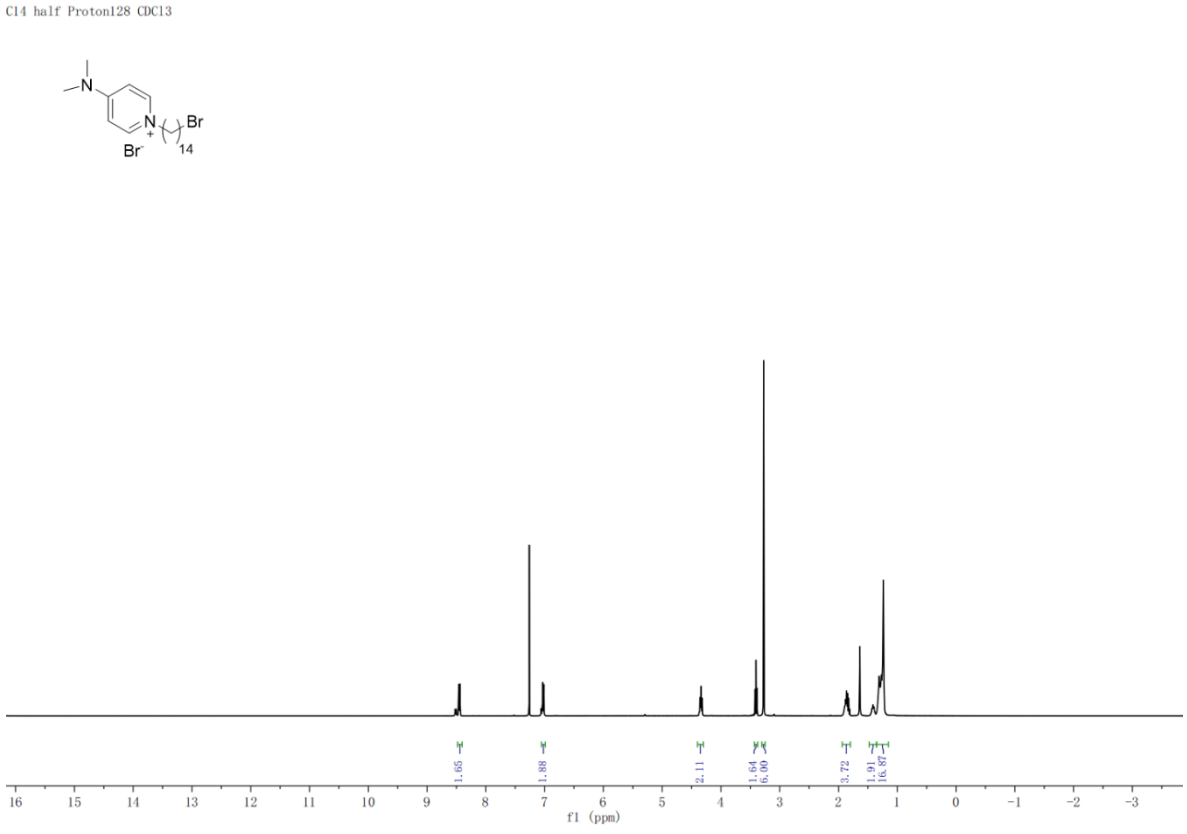


Figure 11. 7: ^{1}H NMR of compound 3.

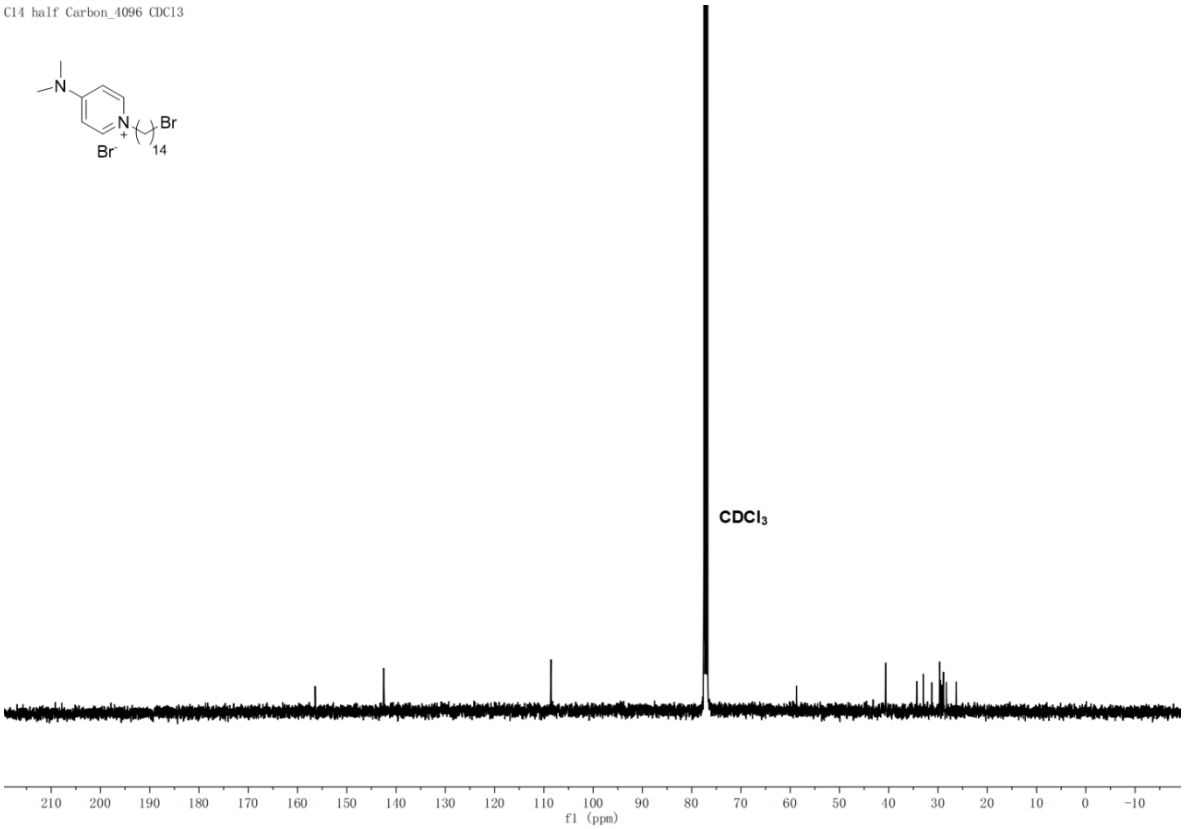


Figure 11. 8: ^{13}C NMR of compound 3.

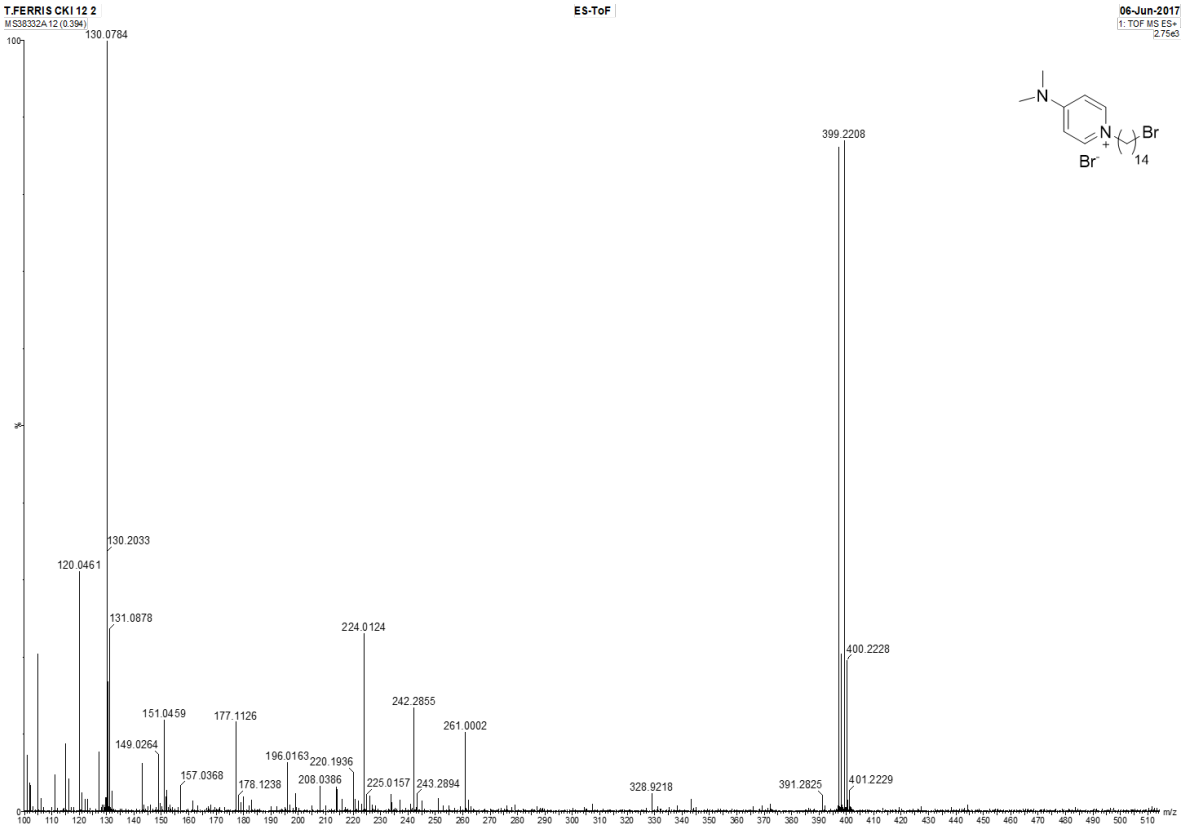


Figure 11. 9: MS analysis of compound 3.

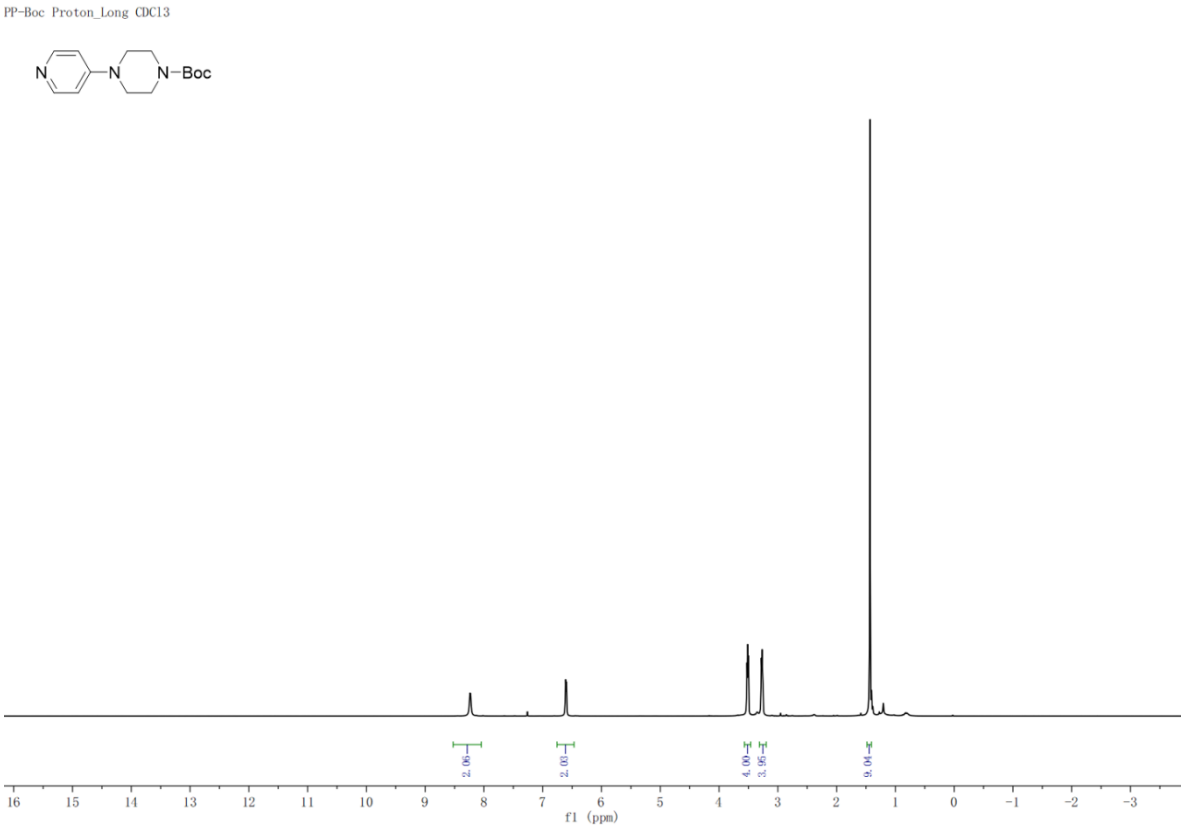


Figure 11. 10: ^{1}H NMR of compound 4.

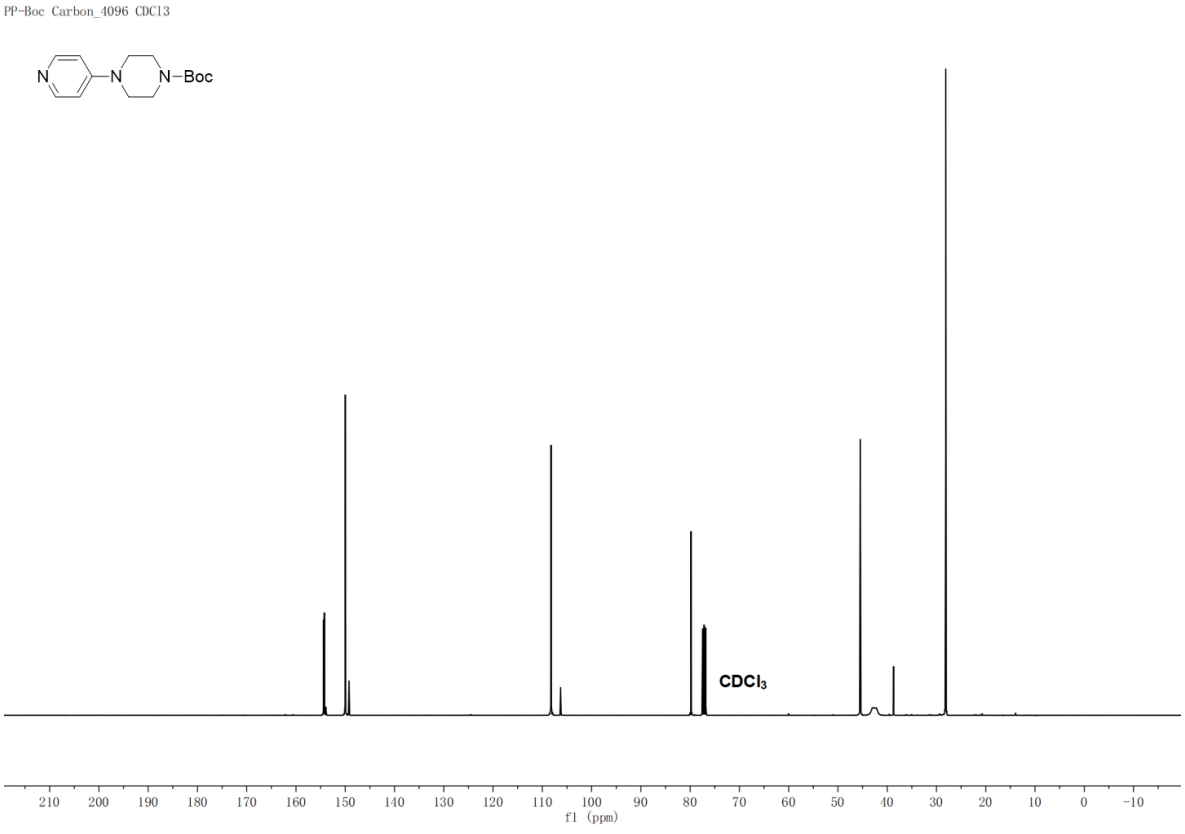


Figure 11. 11: ^{13}C NMR of compound 4.

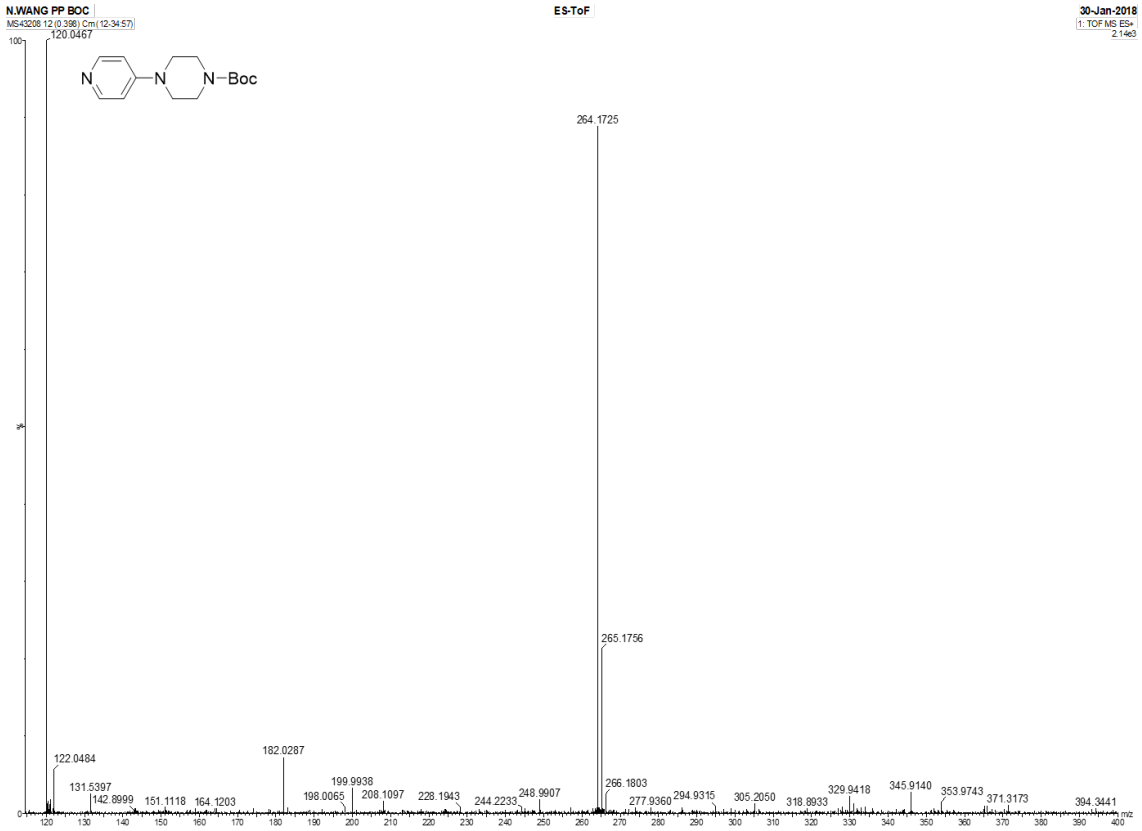


Figure 11. 12: MS analysis of compound 4.

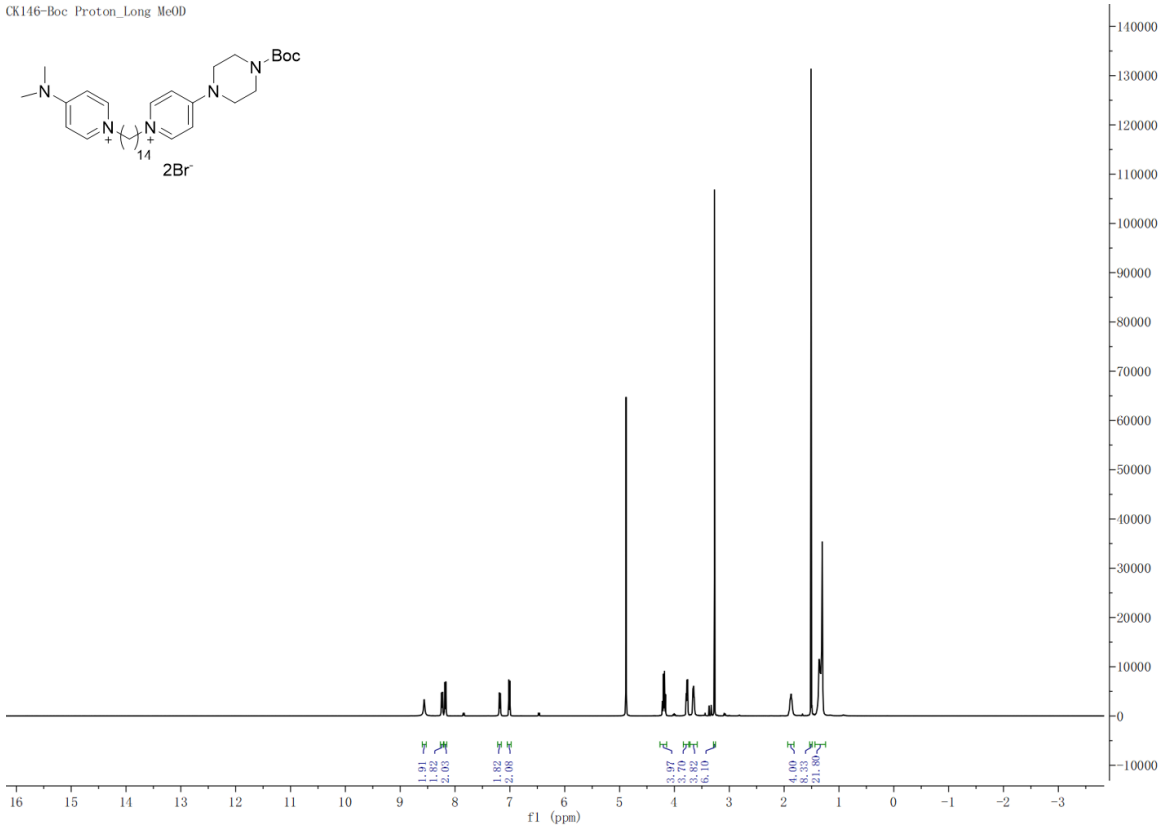


Figure 11. 13: ^{1}H NMR of compound 5.

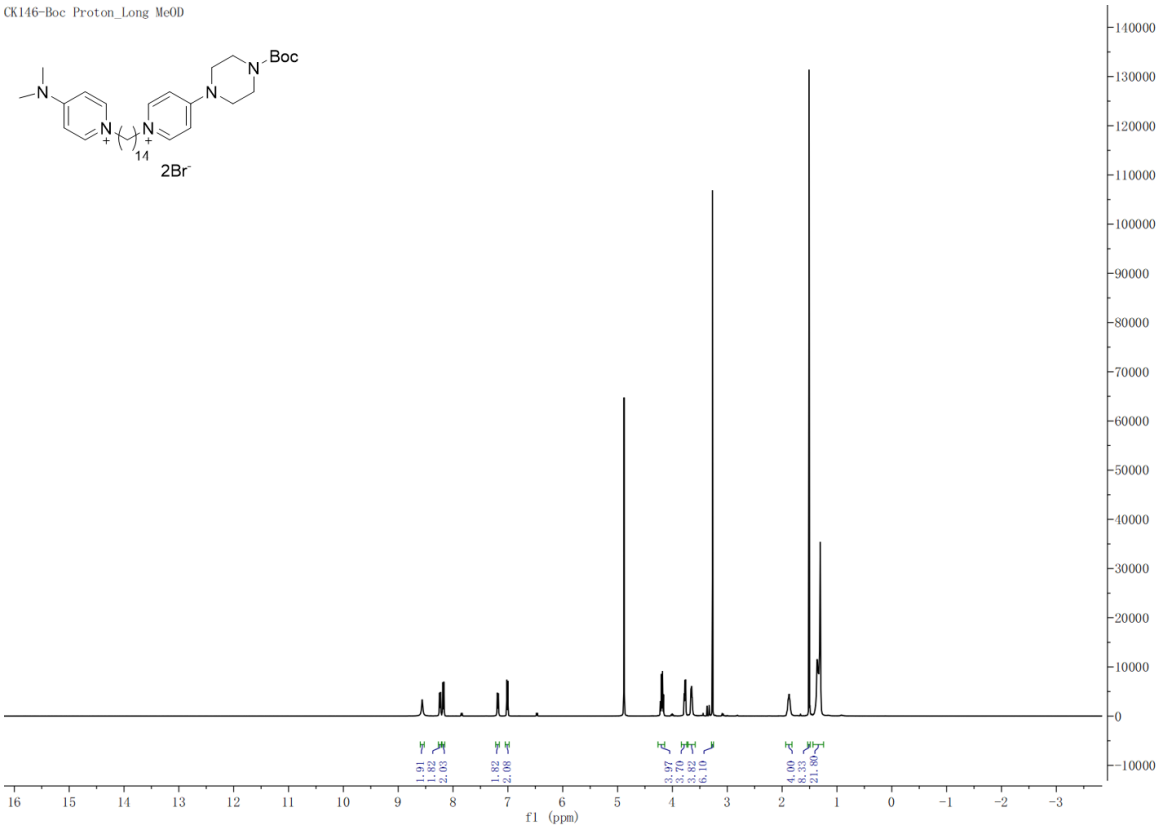


Figure 11. 14: ^{13}C NMR of compound 5.

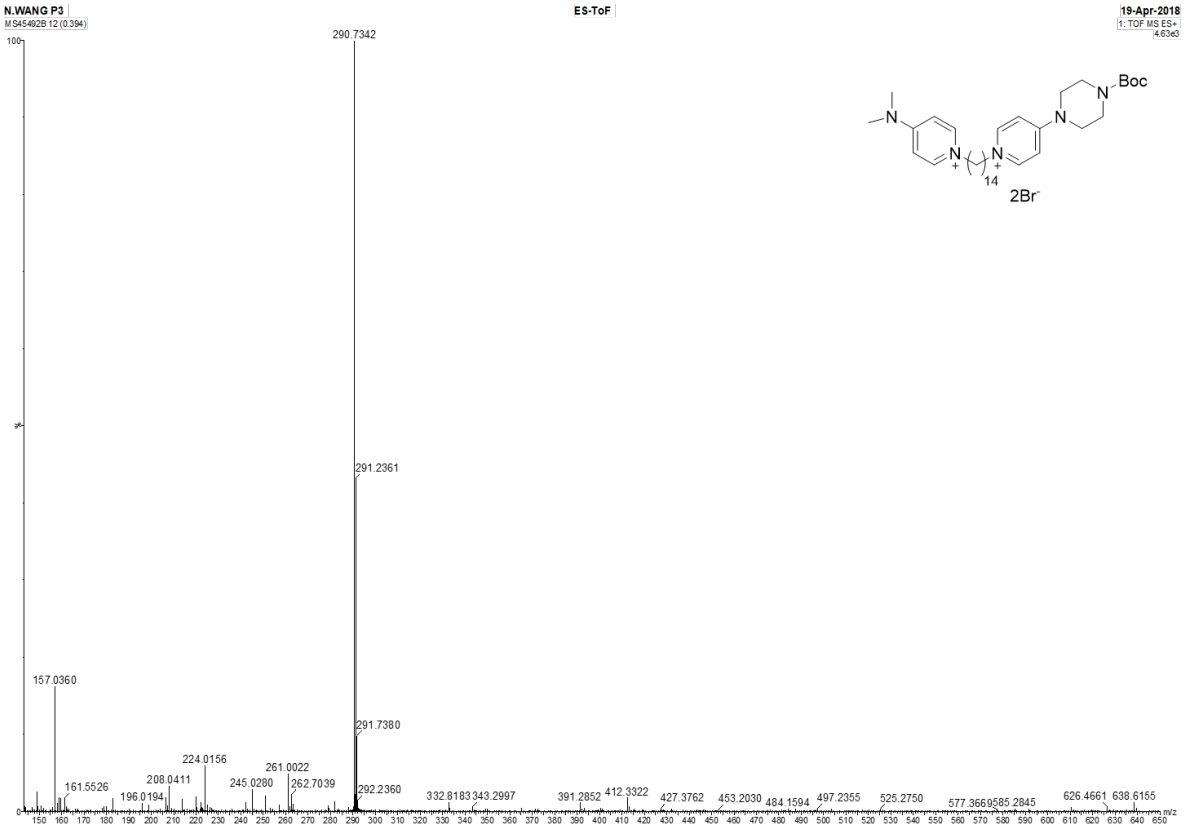


Figure 11. 15: MS analysis of compound 5.

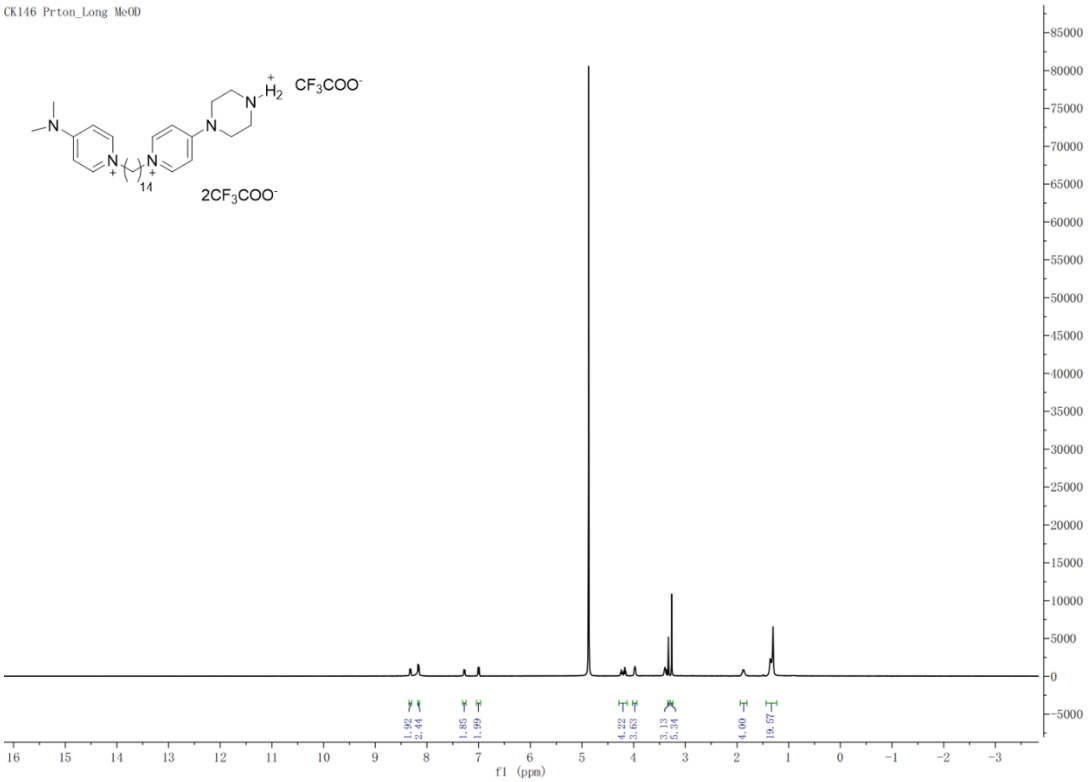


Figure 11. 16: ^{1}H NMR of compound 6.

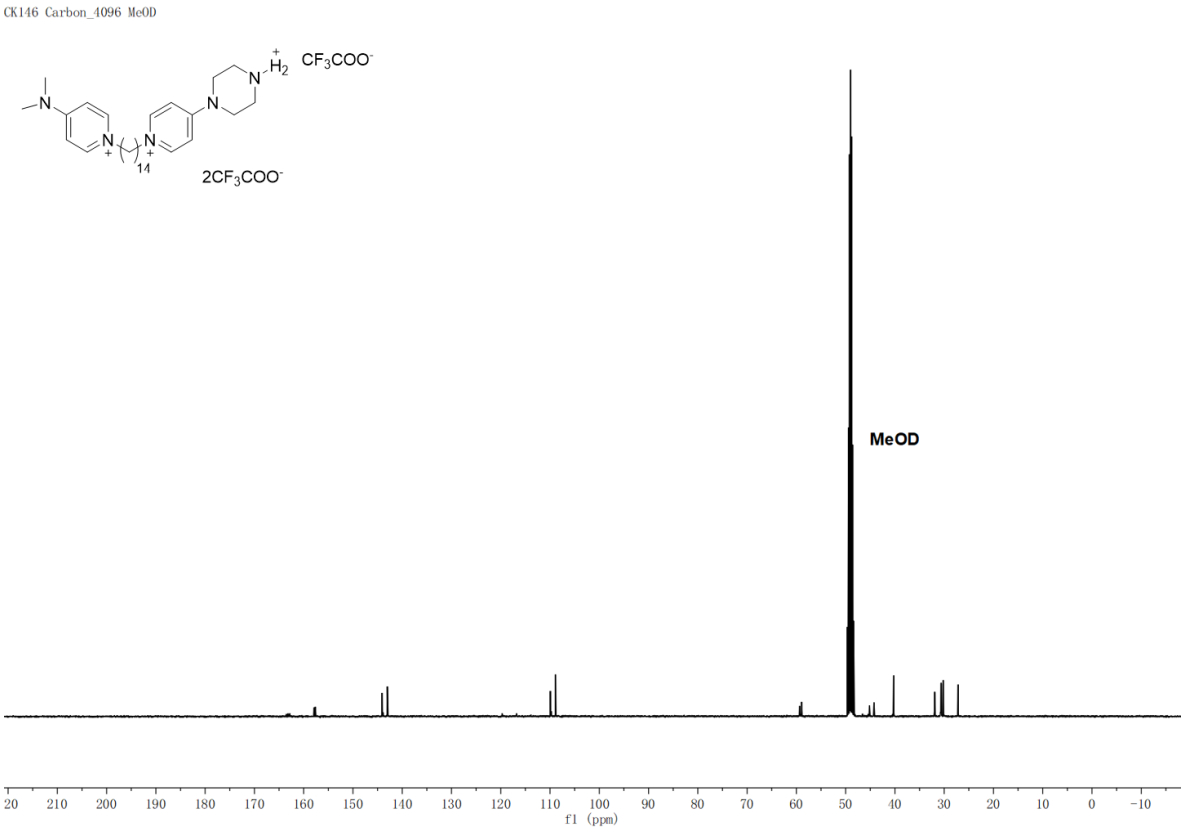


Figure 11. 17: ^{13}C NMR of compound 6.

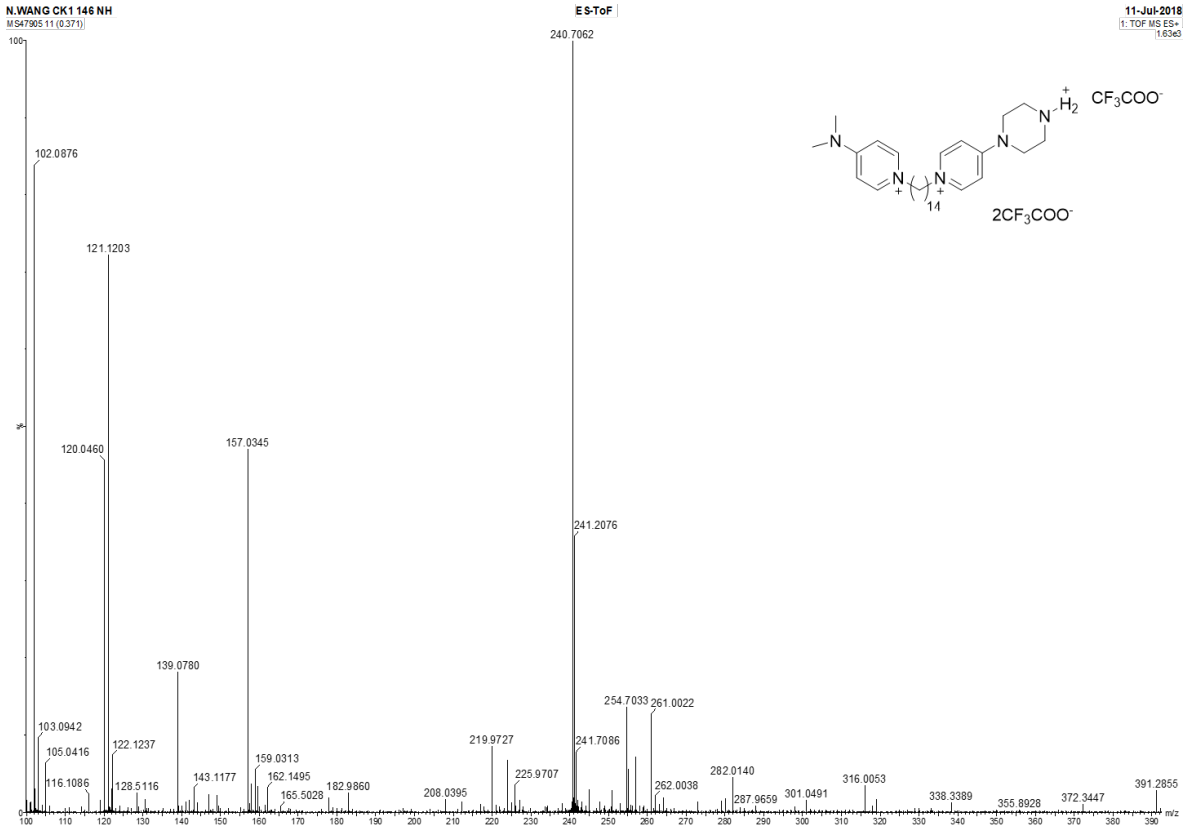


Figure 11. 18: MS analysis of compound 6.

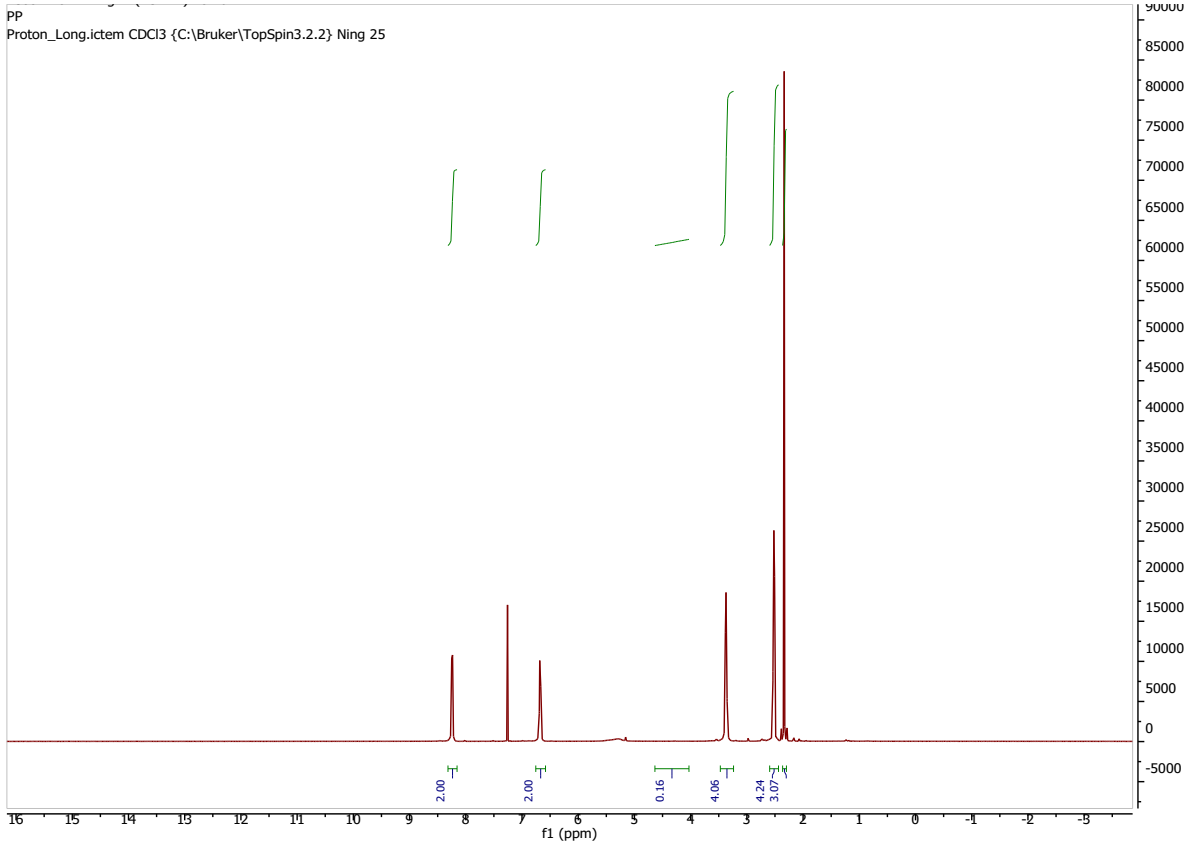


Figure 11. 19: ^{1}H NMR of compound 7.

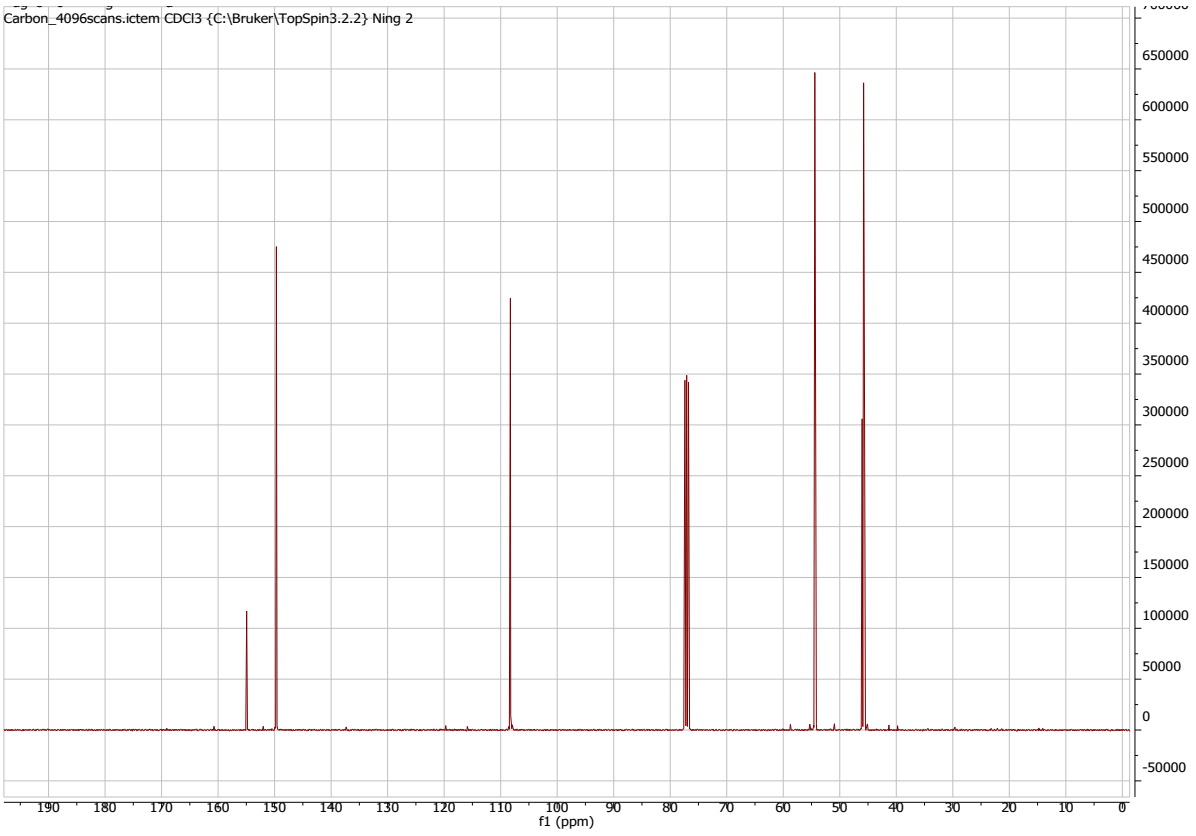


Figure 11. 20: ^{13}C NMR of compound 7.

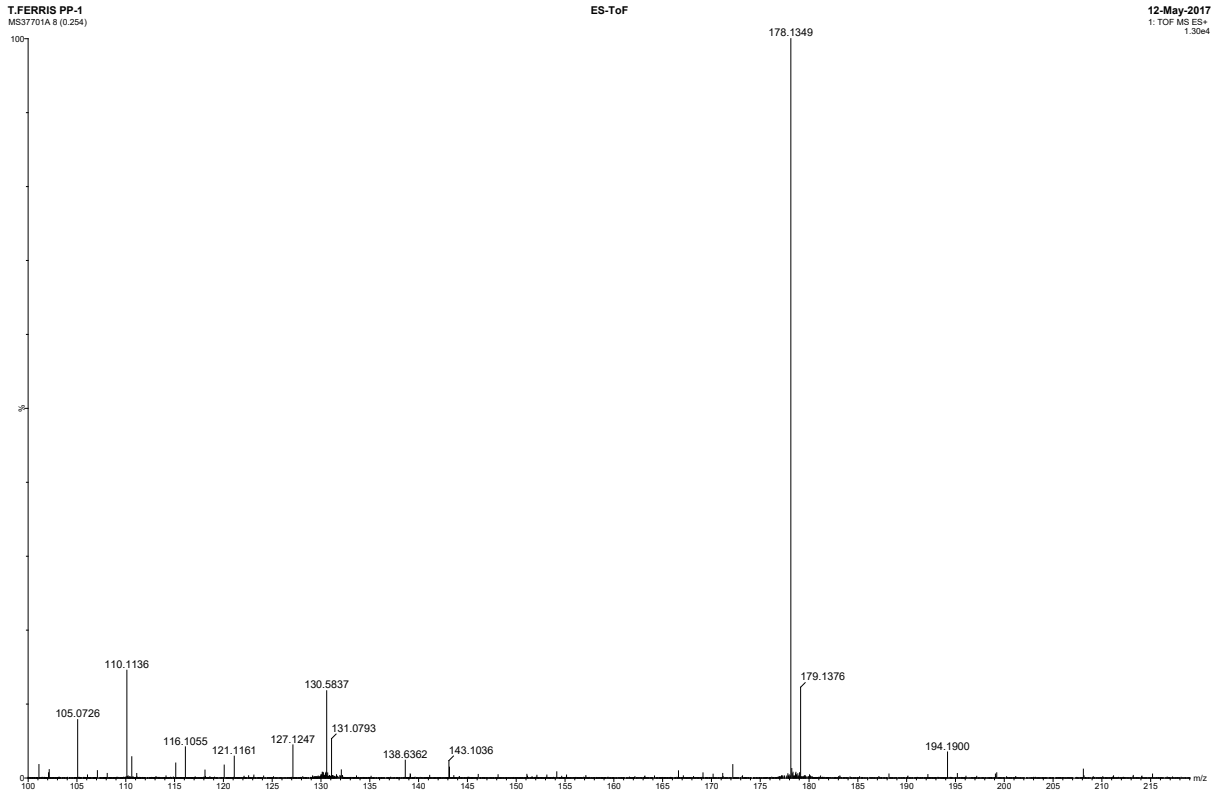


Figure 11. 21: MS analysis of compound 7.

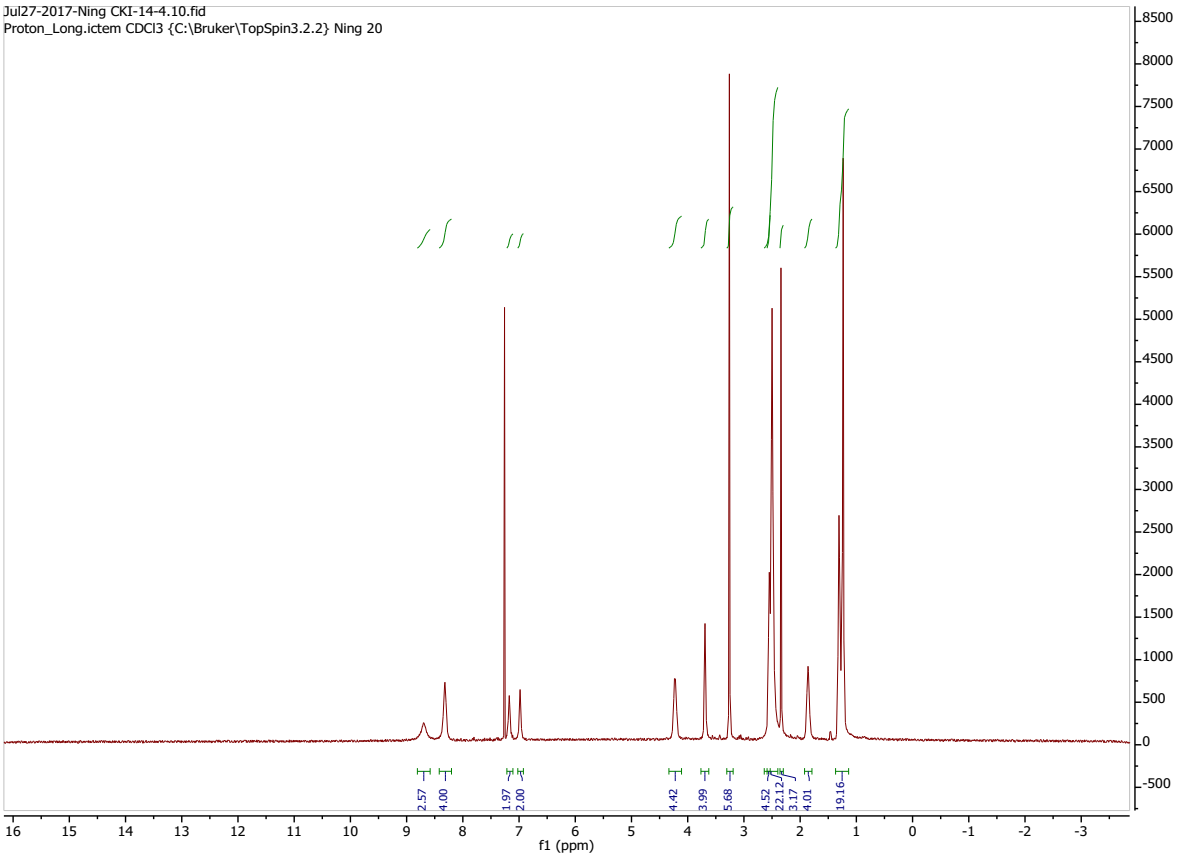


Figure 11. 22: ^{1}H NMR of compound 8.

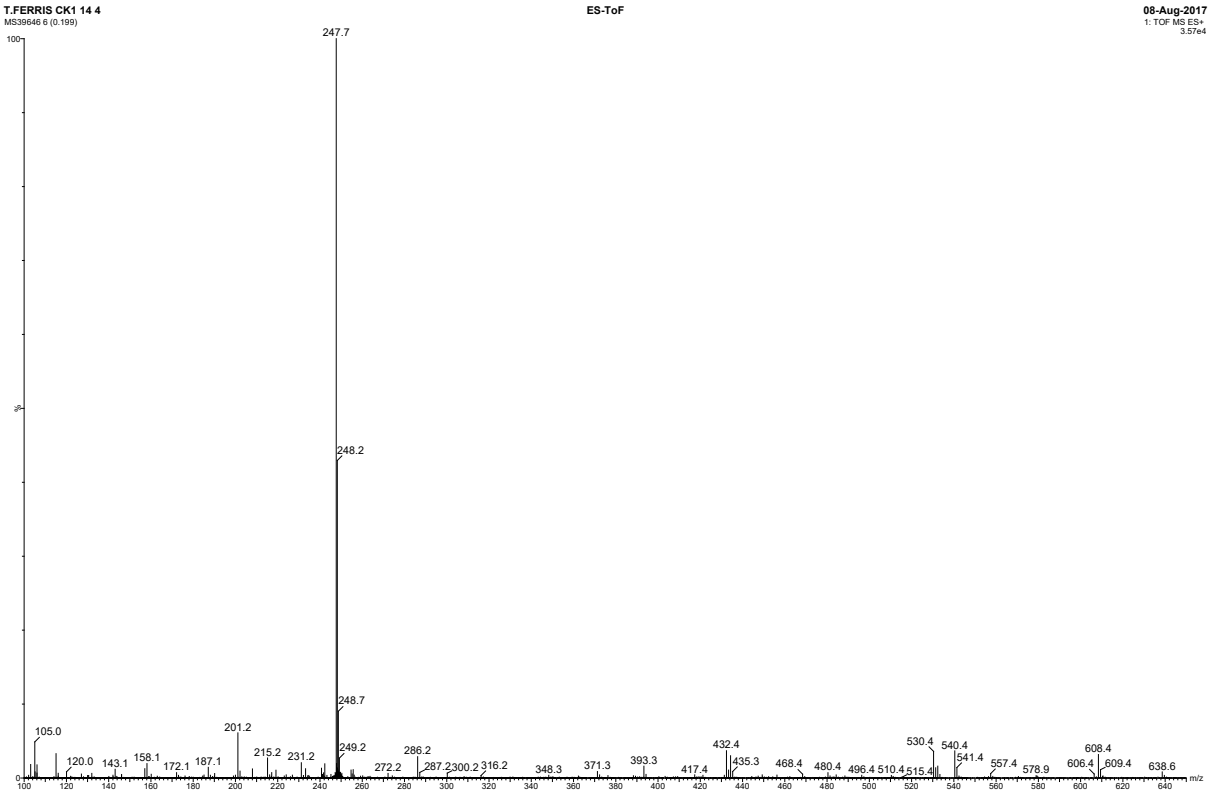


Figure 11. 23: MS analysis of compound 8.

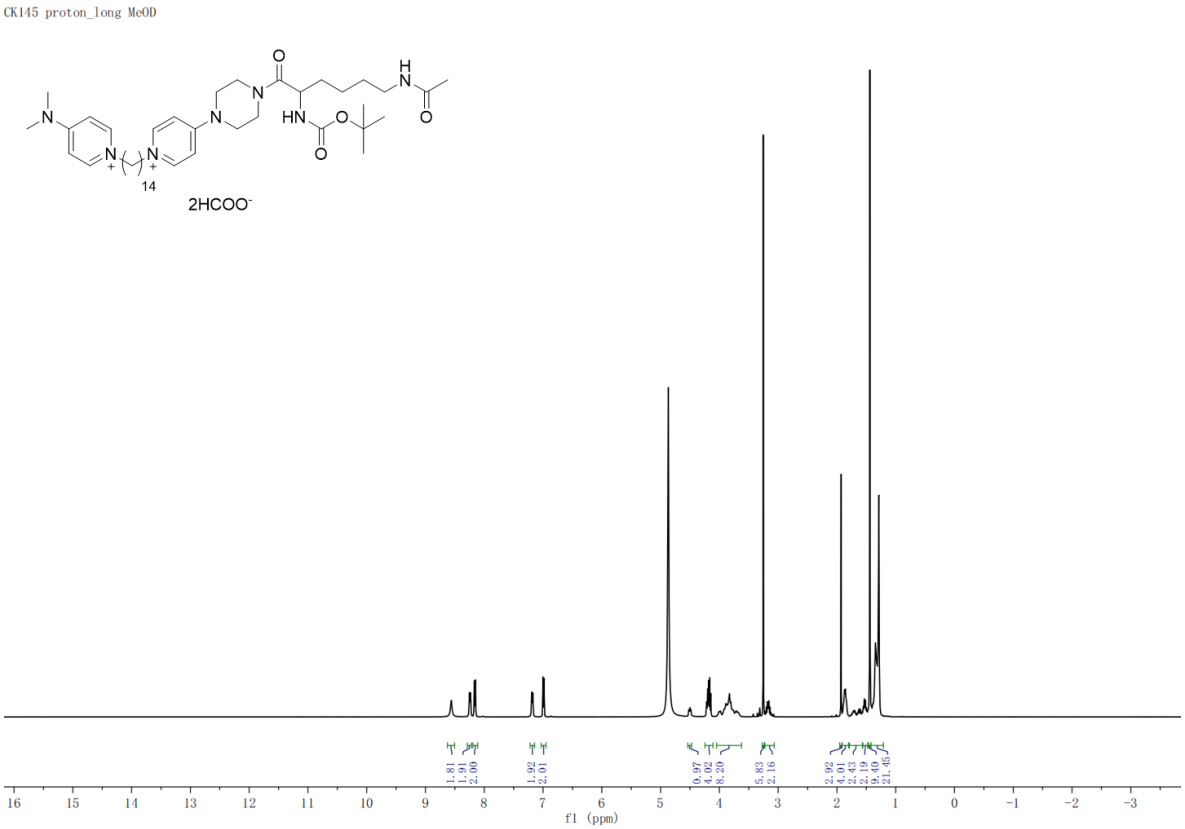


Figure 11. 24: ^{1}H NMR of compound 9.

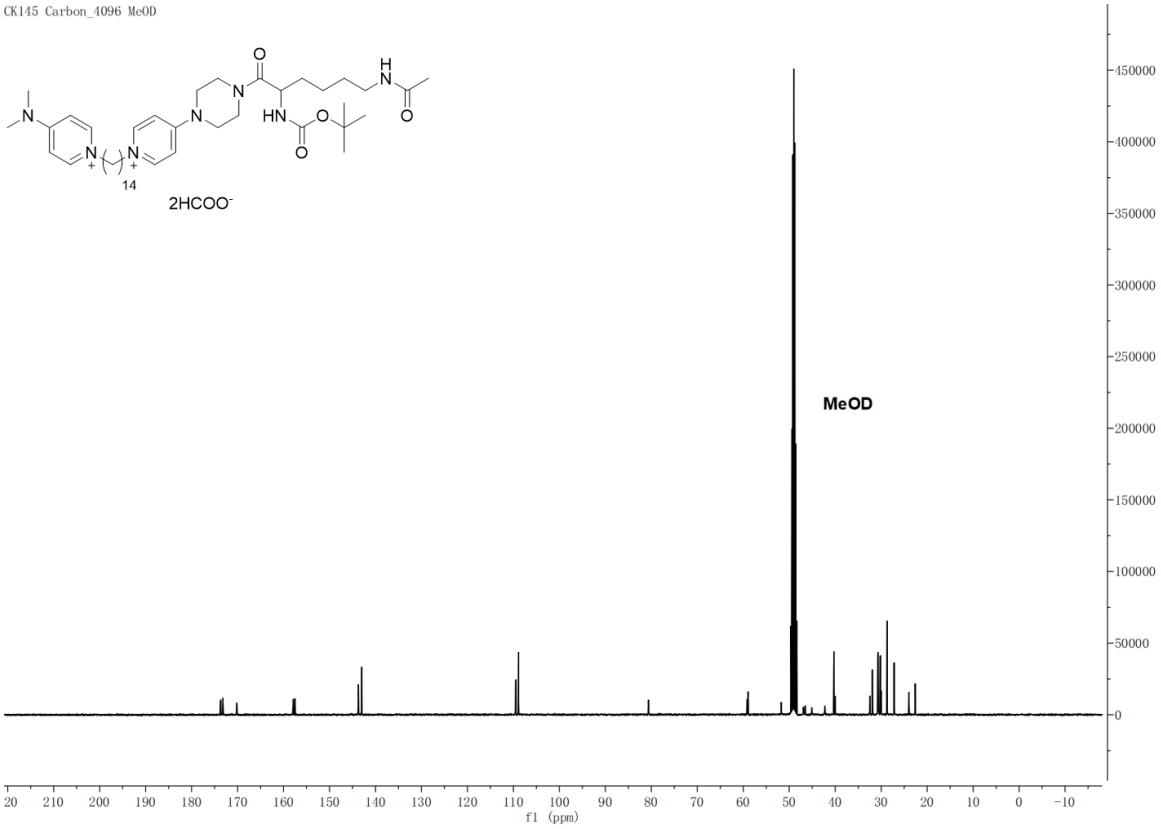


Figure 11. 25: ^{13}C NMR of compound 9.

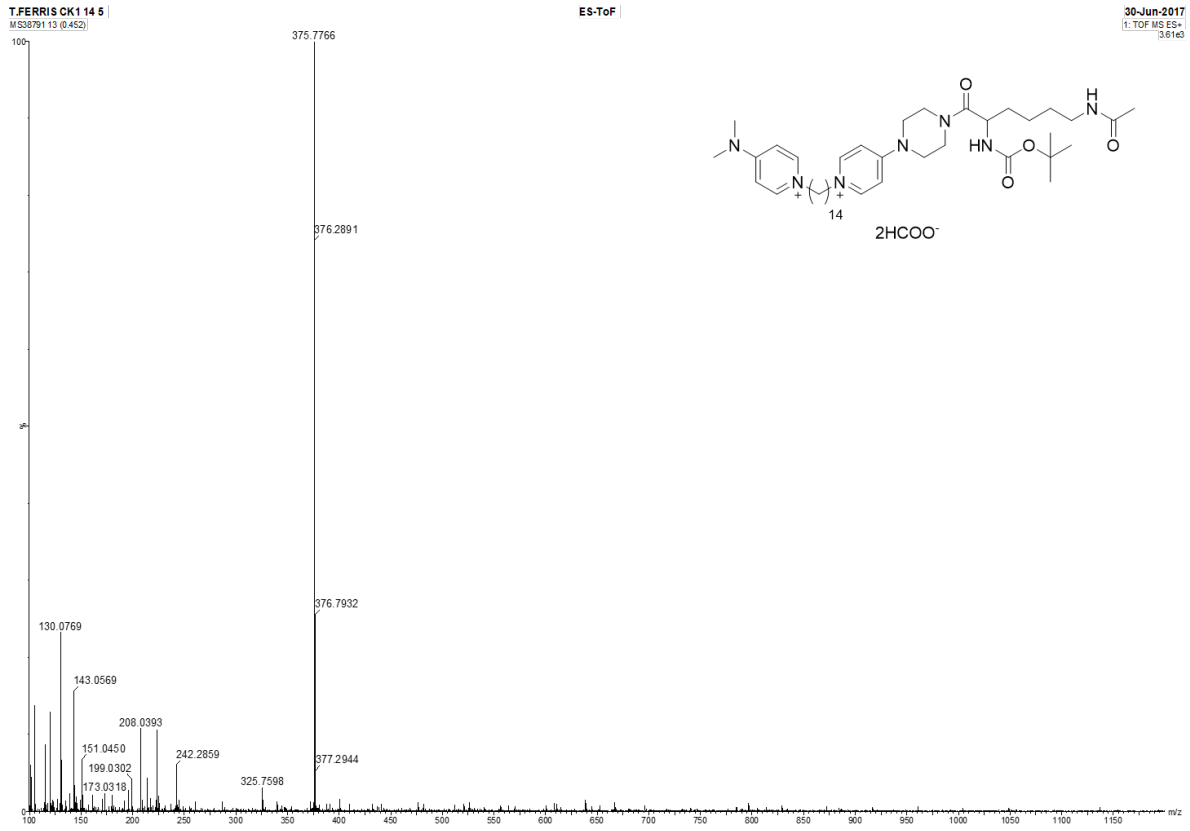


Figure 11. 26: MS analysis of compound 9.

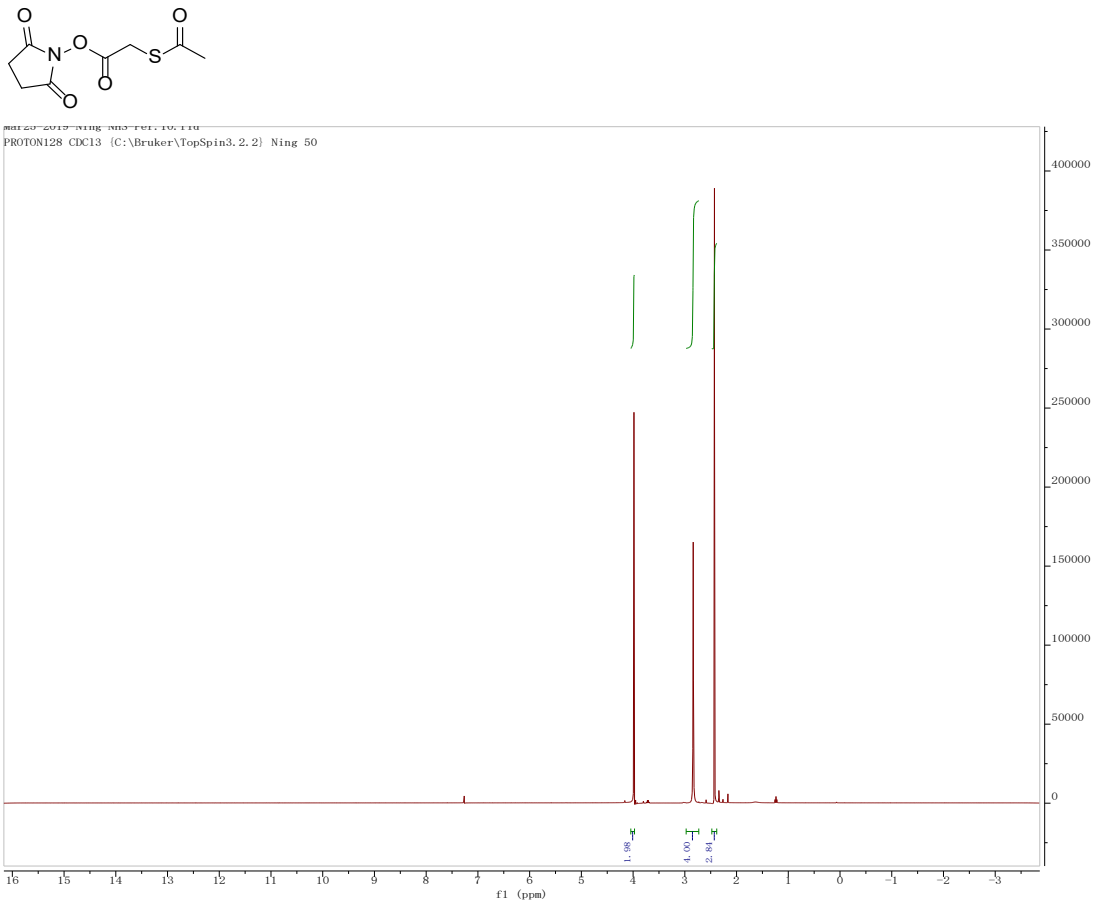


Figure 11. 27: ^{1}H NMR of compound 10.

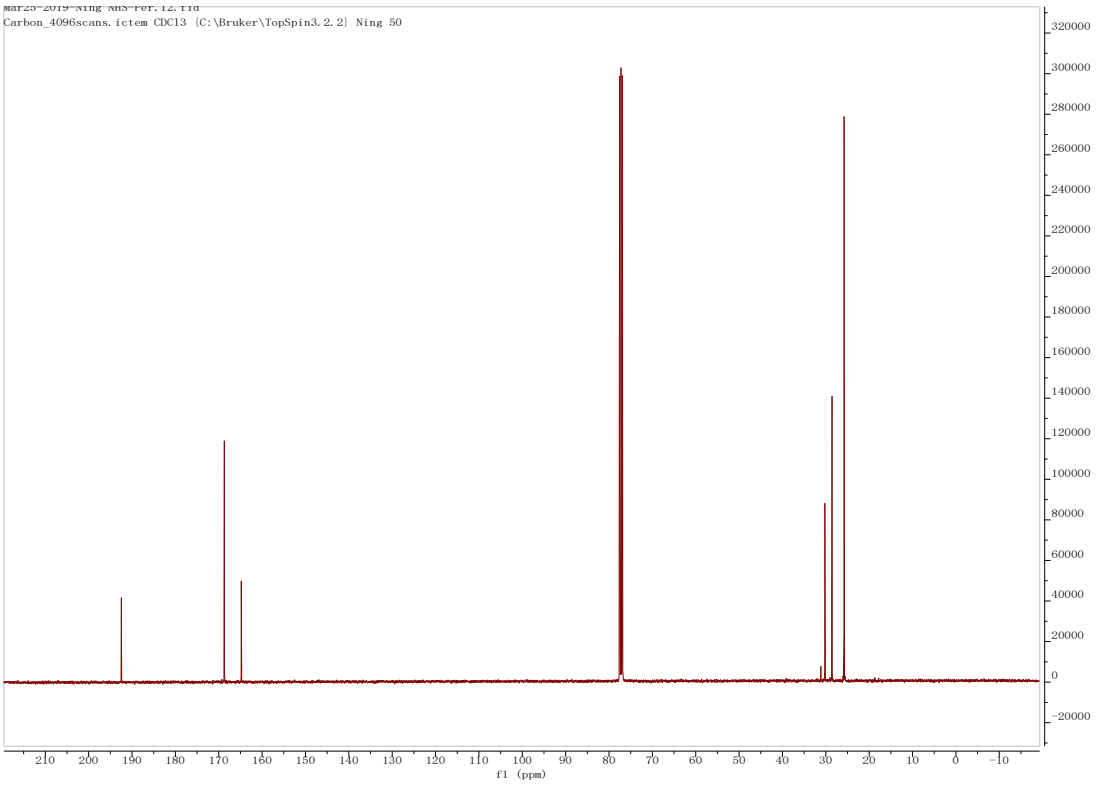


Figure 11. 28: ^{13}C NMR of compound 10.

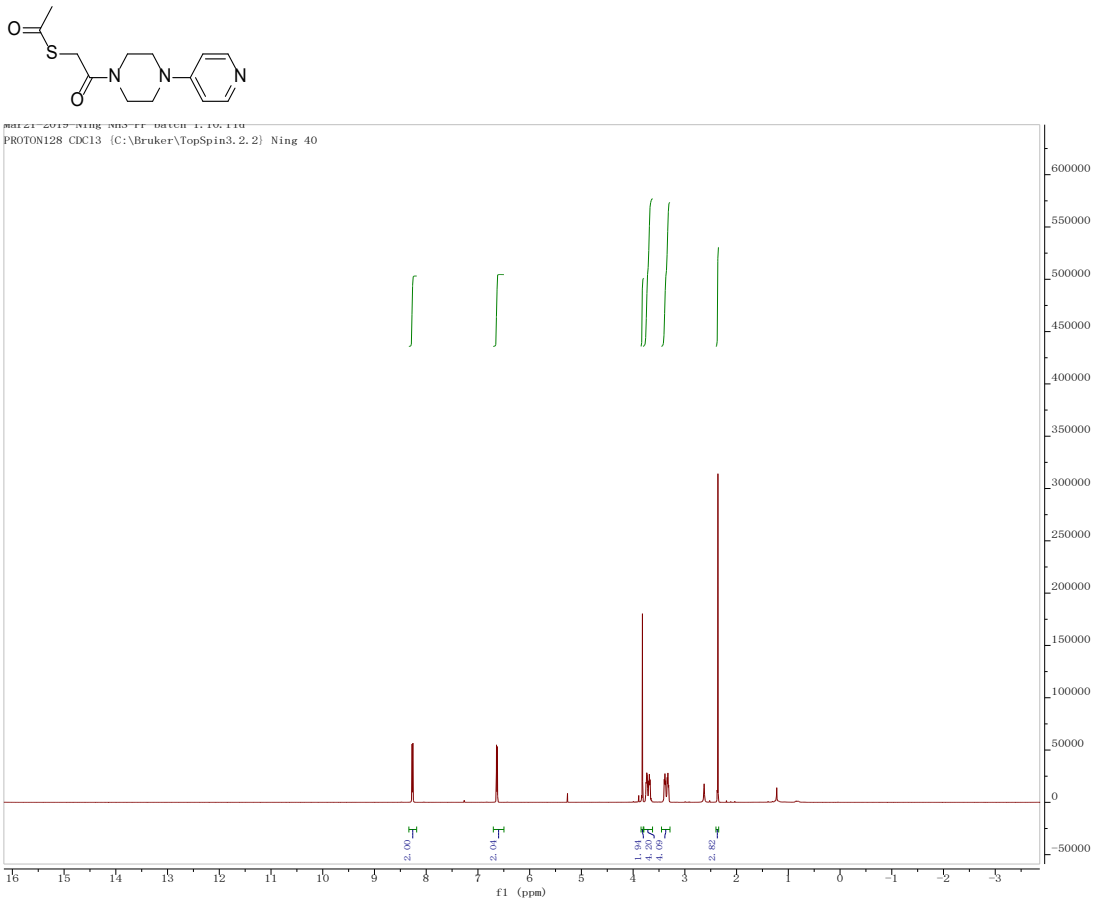


Figure 11. 29: ^{1}H NMR of compound 11.

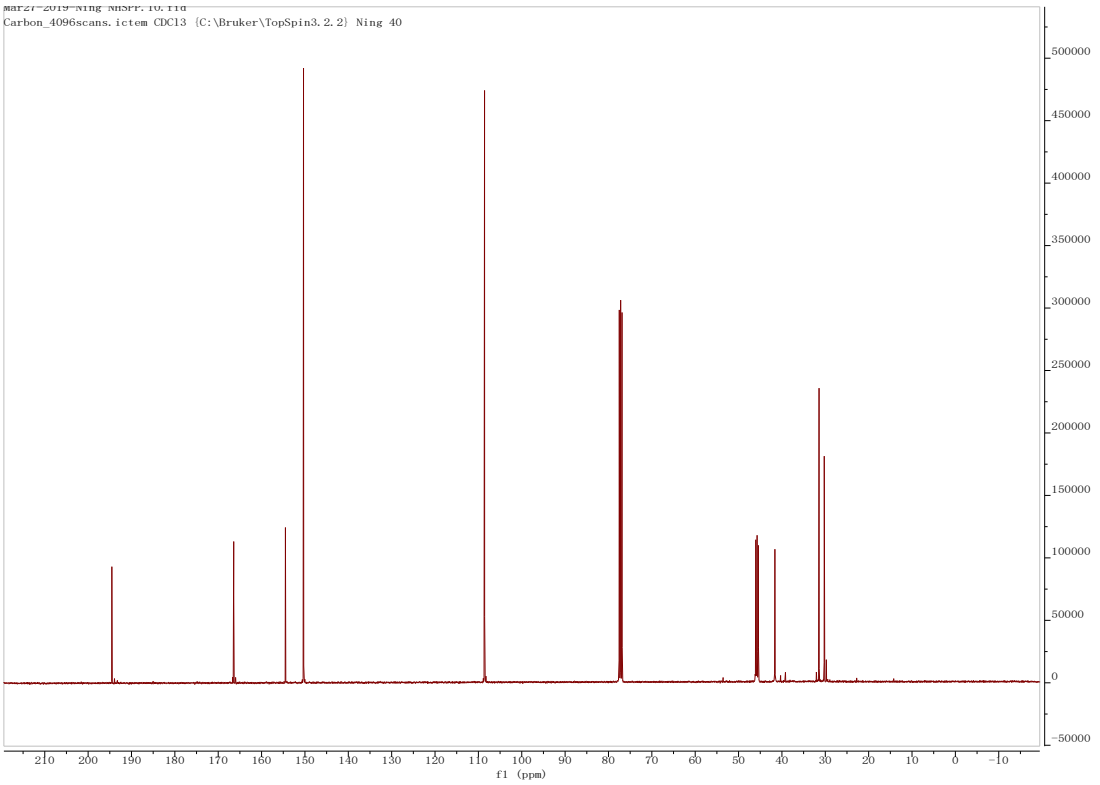


Figure 11. 30: ^{13}C NMR of compound 11.

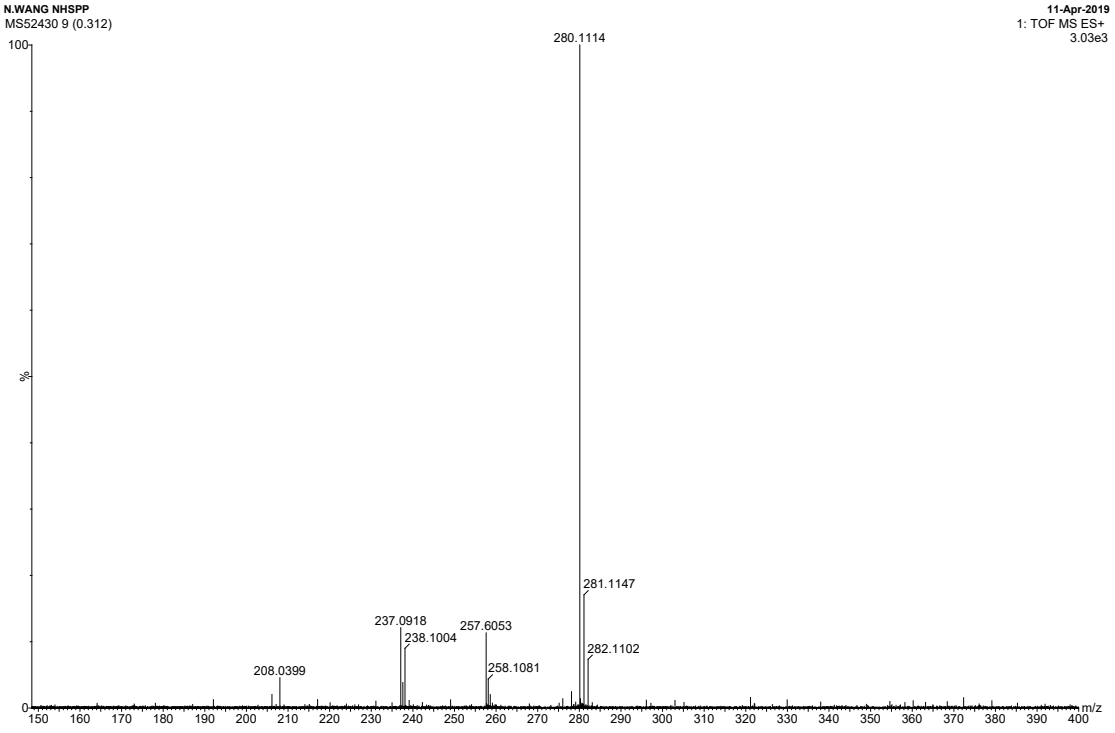


Figure 11. 31: MS analysis of compound 11.

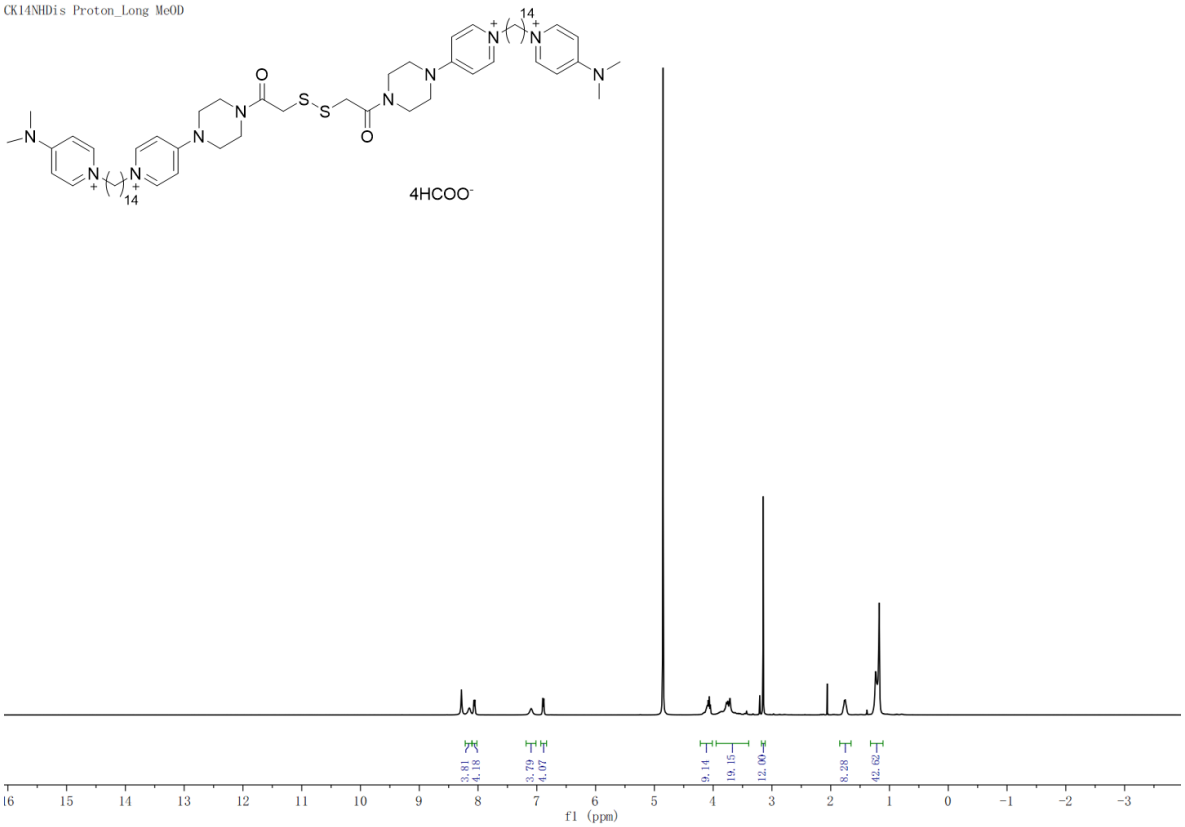


Figure 11. 32: ^{1}H NMR of compound 14.

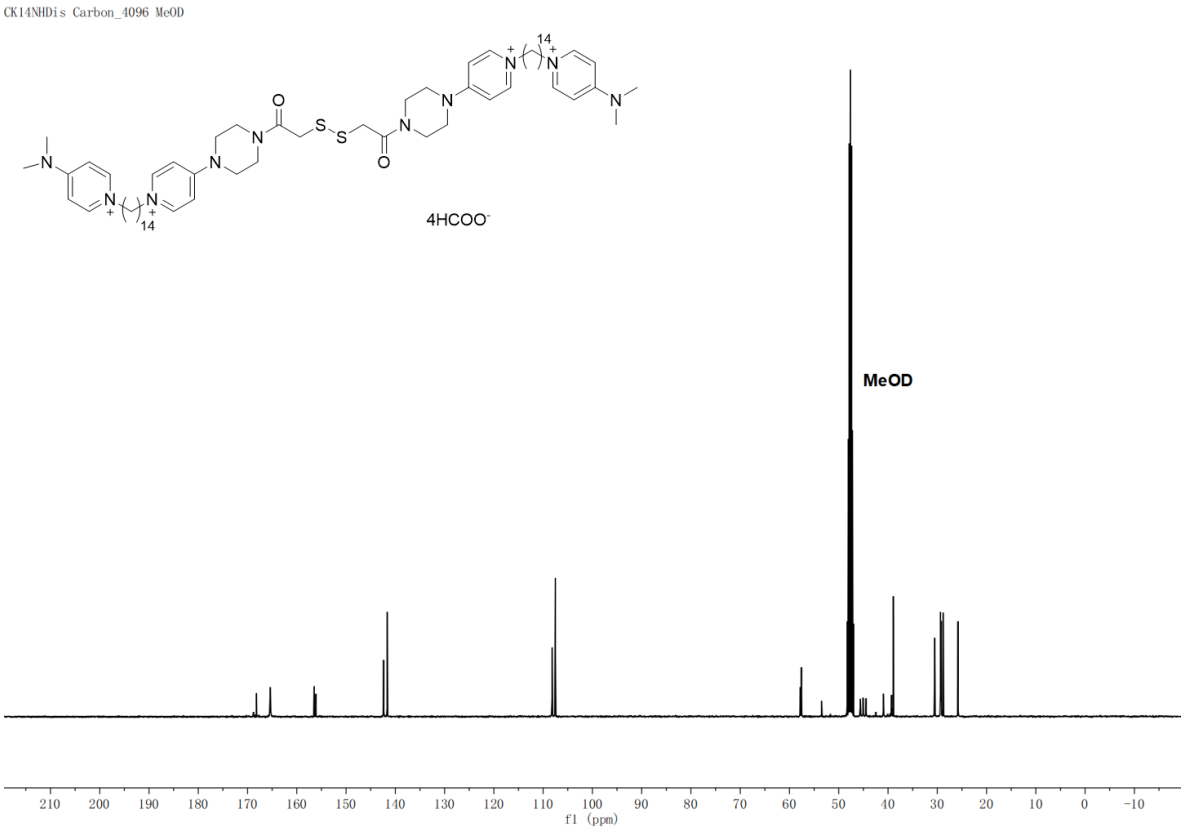


Figure 11. 33: ^{13}C NMR of compound 14.

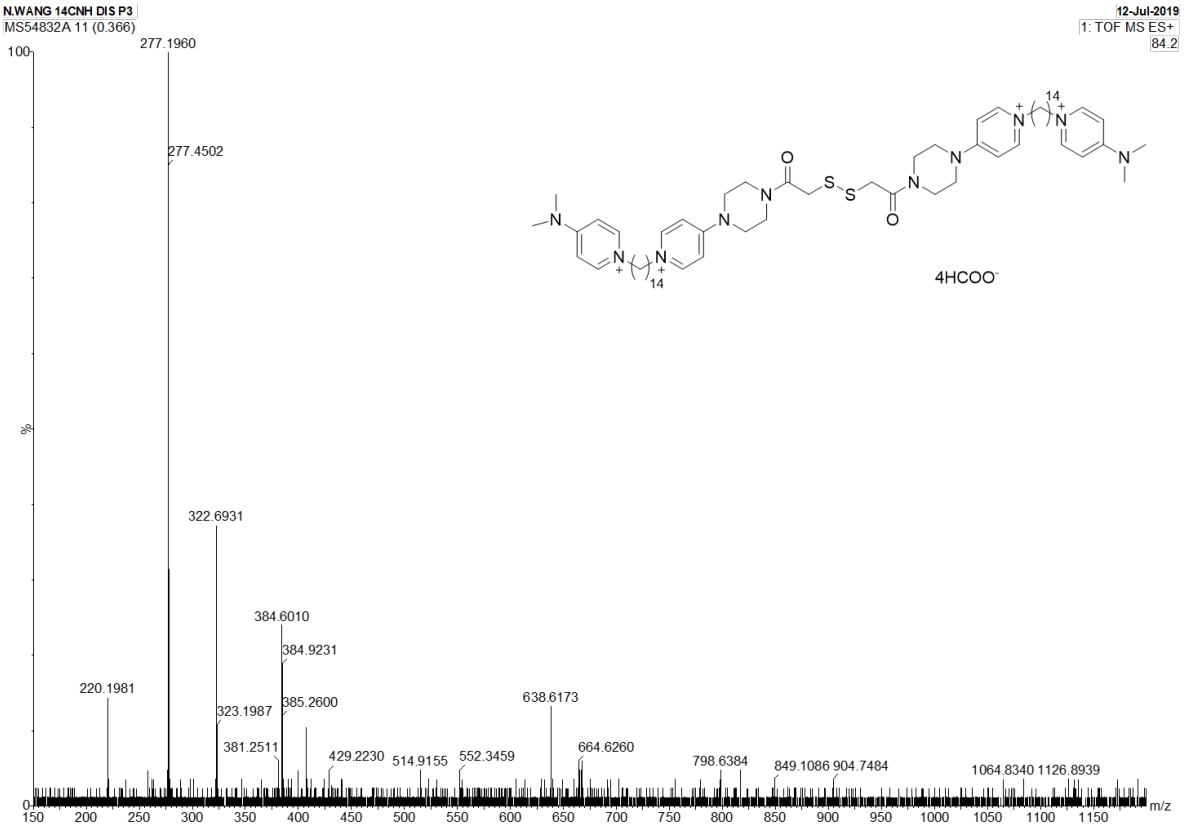


Figure 11. 34: MS analysis of compound 14.

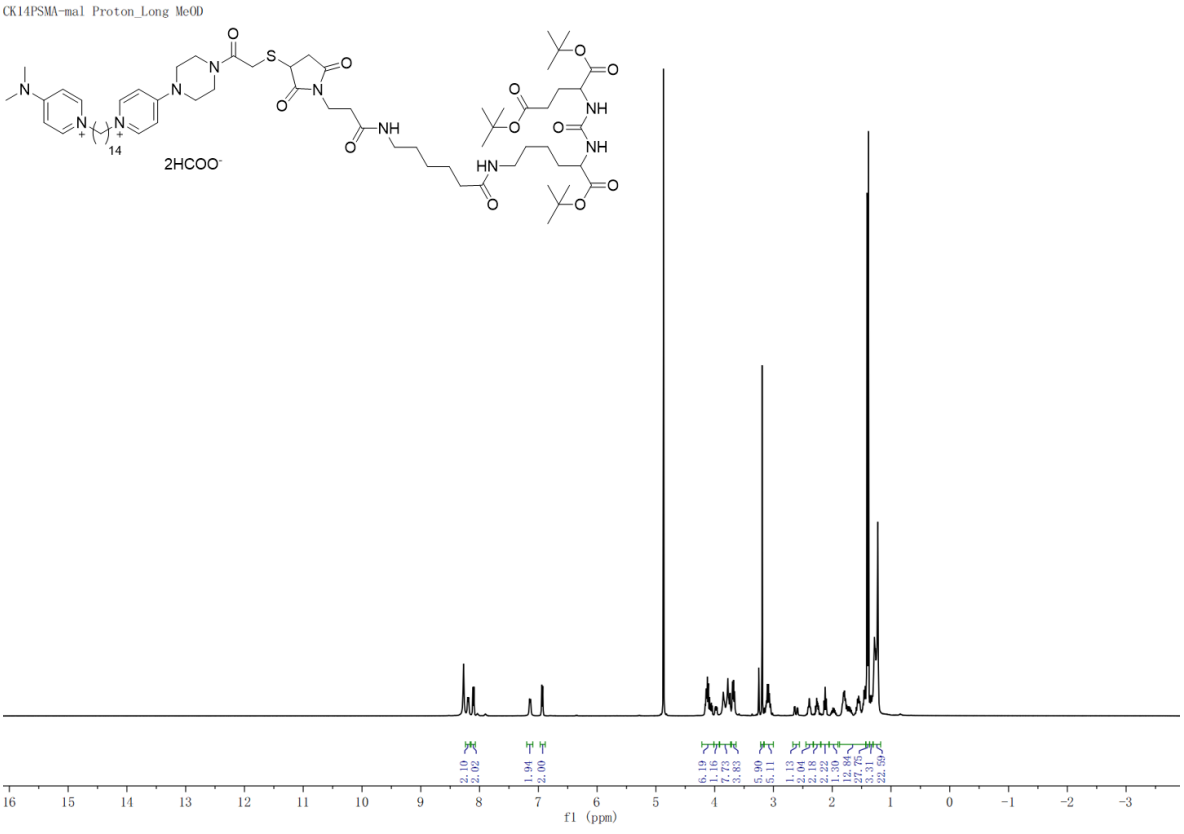


Figure 11. 35: ^{1}H NMR of compound 16.

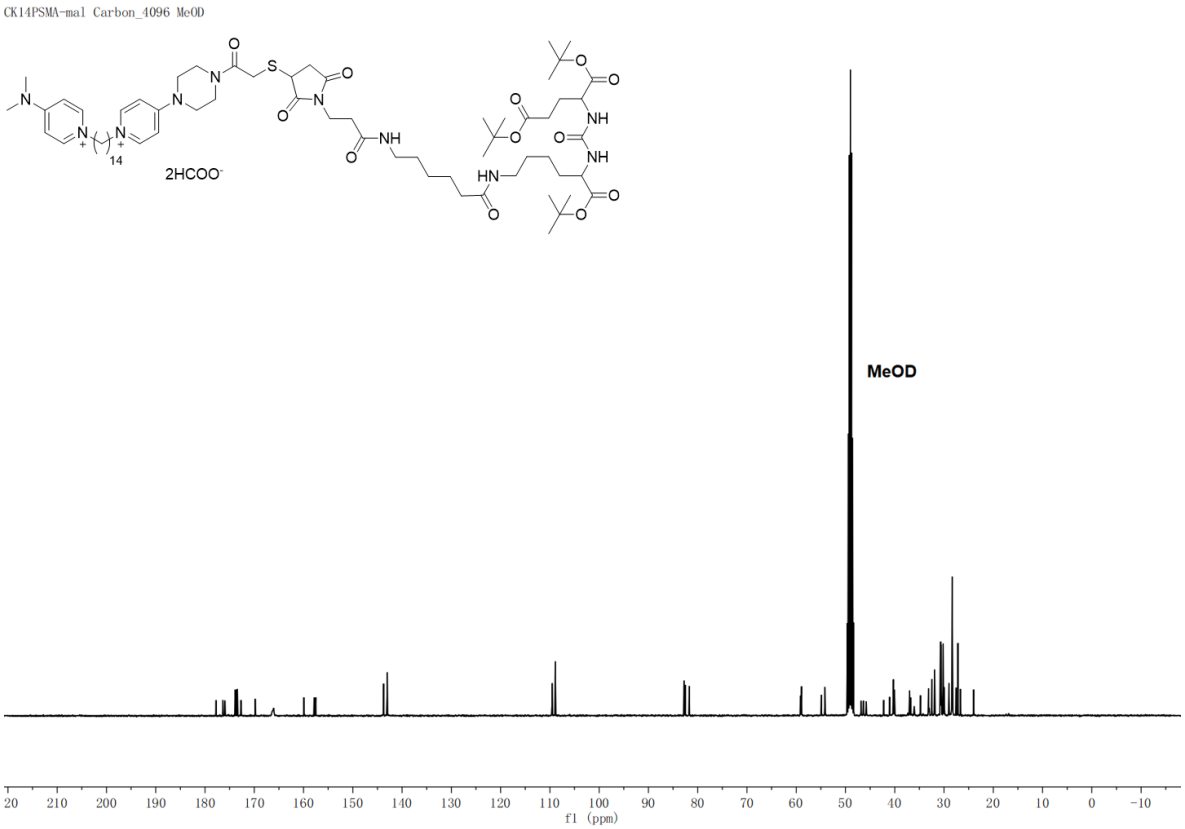


Figure 11. 36: ^{13}C NMR of compound 16.

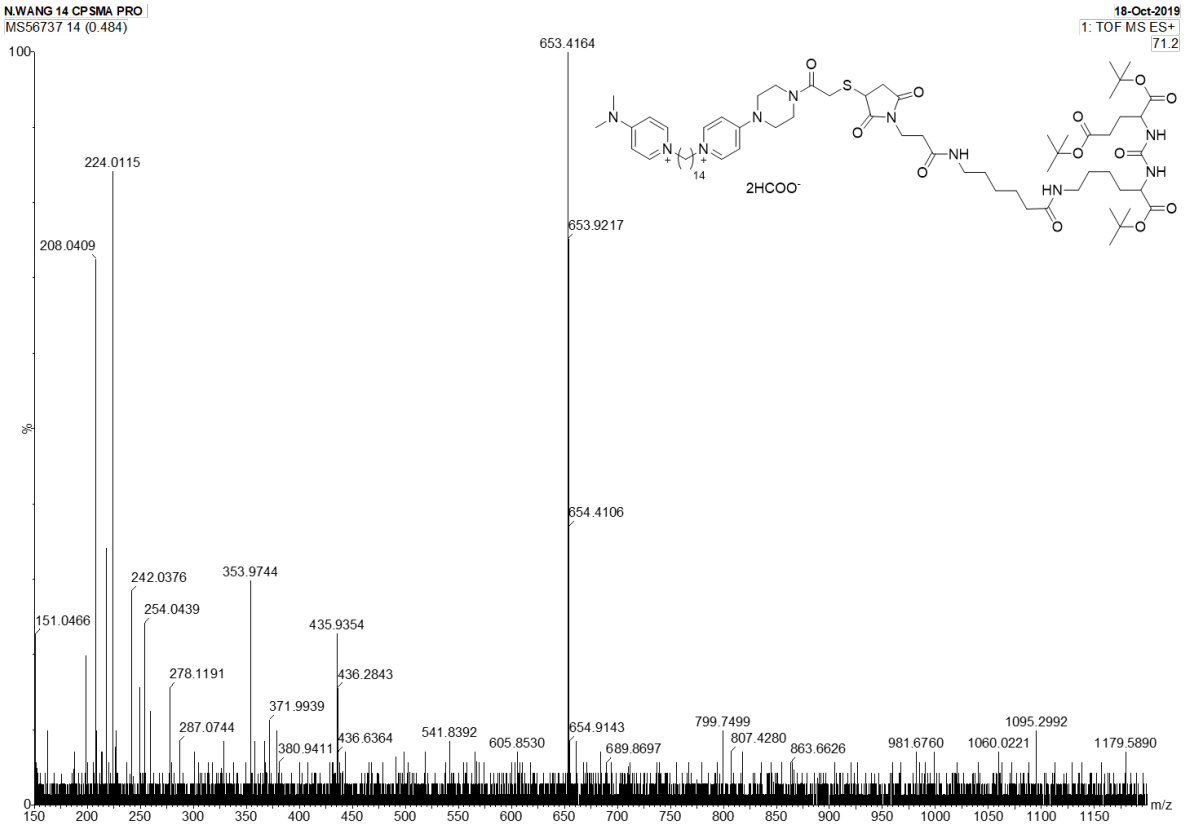


Figure 11. 37: MS analysis of compound 16.

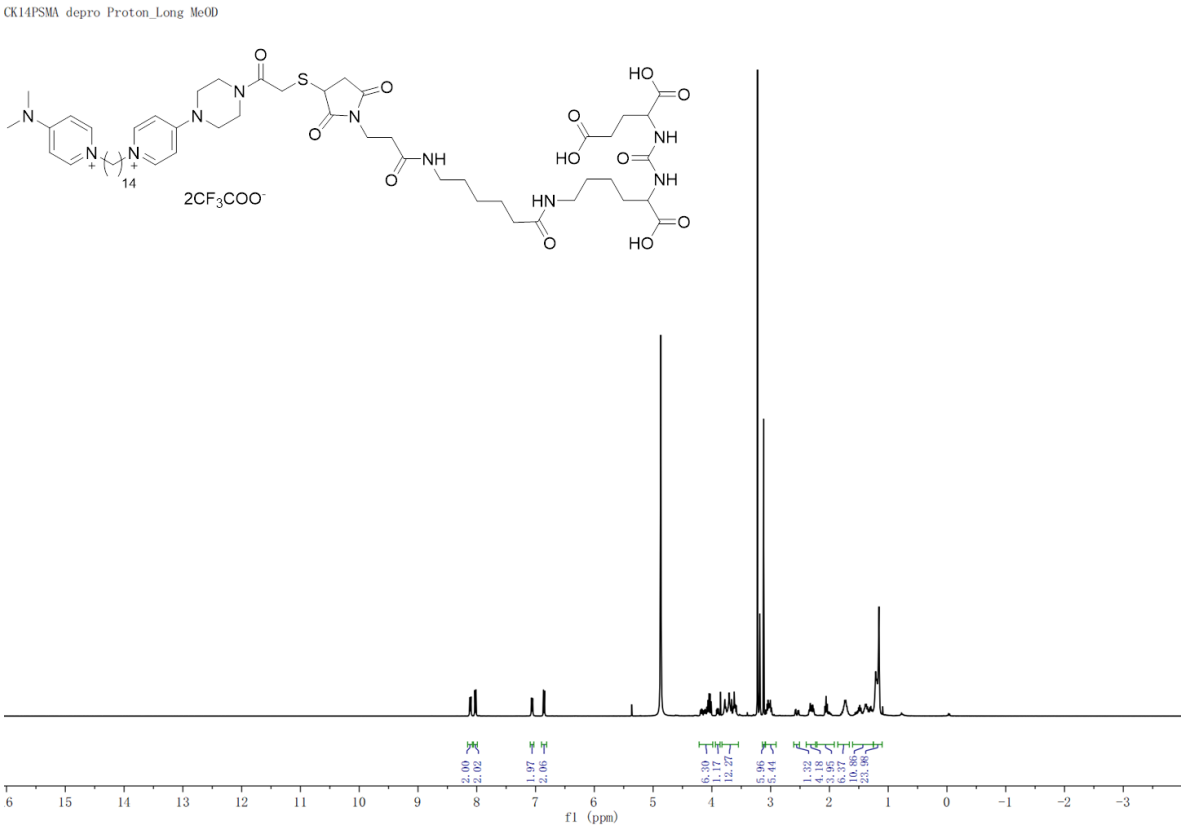


Figure 11. 38: ^{1}H NMR of compound 17.

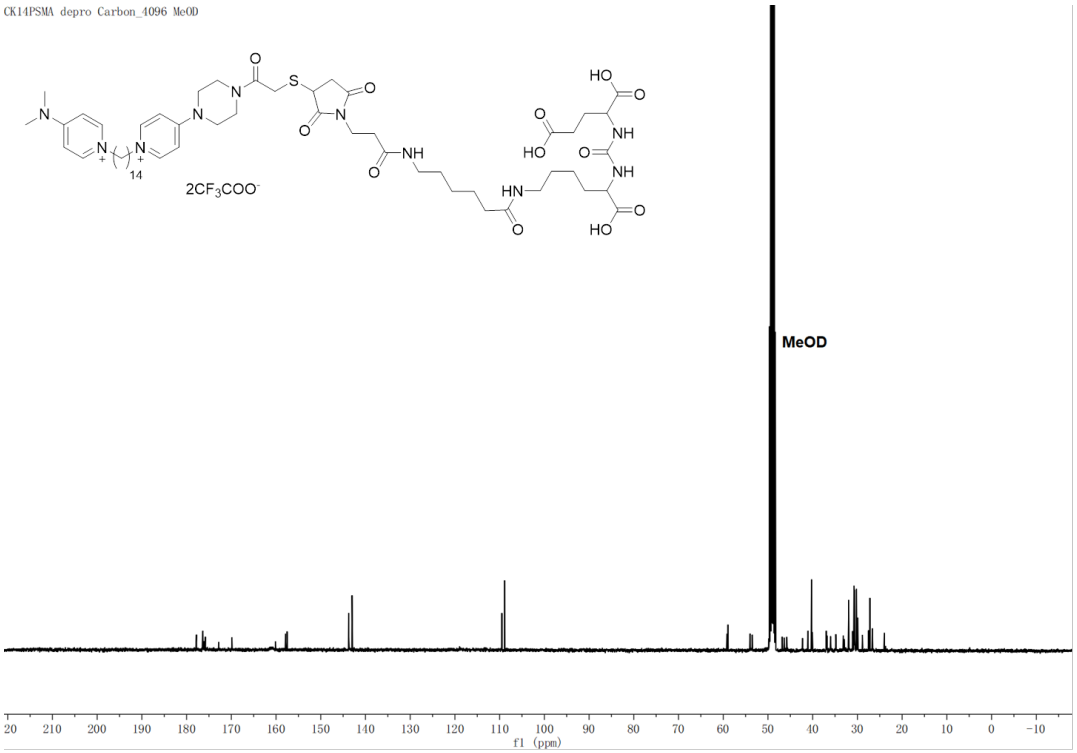


Figure 11. 39: ^{13}C NMR of compound 17.

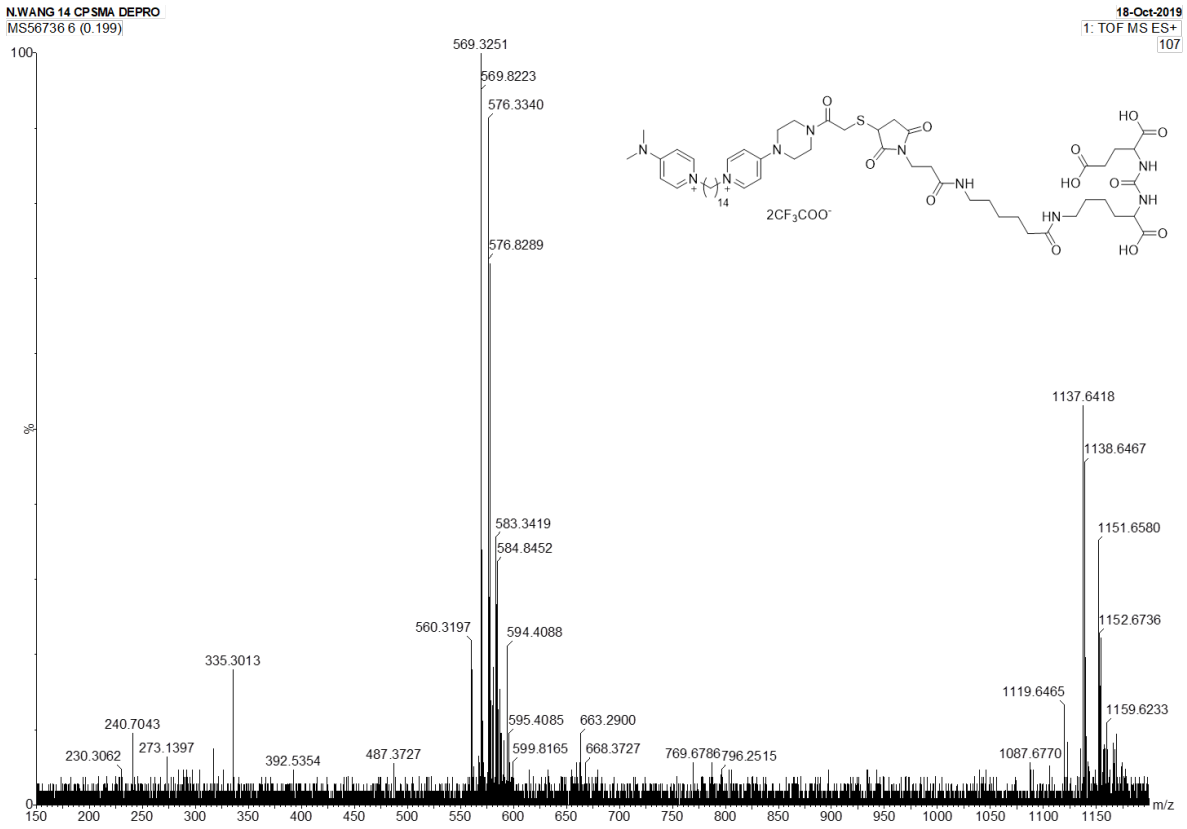


Figure 11. 40: MS analysis of compound 17.

Appendix B: Kinase Screen

(For the method, see Chapter 2.7)

	ICL-CCIC-0019		CK14	
Lipid Kinase	**% activity remaining**	**SD**	**% activity remaining**	**SD**
PI3K a	99.04	4.9	101.9	3.3
PI3K b	139.6	11.2	136.2	12.5
PI3K g	95.1	10.9	83.6	1.2
PI3Ka E545K + p85	106.1	2.4	115.2	7.5
PI3Ka E524K + p85	98.4	1.0	98.4	0.2
PIP5K2A	116.1	10.9	102.7	2.8
SPHK1	103.6	9.7	110.1	6.9
SPHK2	77.6	20.0	84.0	14.0
CHK a	46.6	2.4	23.0	10.2
DGK b	91.4	8.9	88.1	3.4
PIK4CB	124.1	6.9	104.1	1.7
DGK g	92.2	12.7	87.2	3.9
DGK z	92.5	0.5	95.3	6.7
PI4K2a	113.9	4.6	148.8	25.3
CHK b	128.6	5.9	133.7	8.8

	CK144		CK145	
Lipid Kinase	**% activity remaining**	**SD**	**% activity remaining**	**SD**
PI3K a	103.2	3.0	101.0	6.9
PI3K b	122.3	4.9	115.8	14.9
PI3K g	93.1	1.9	97.1	3.3
PI3Ka E545K + p85	105.1	3.5	101.8	1.2
PI3Ka E524K + p85	91.6	4.9	100.1	6.3
PIP5K2A	99.6	0.6	99.6	0.7
SPHK1	105.3	0.4	99.4	1.6
SPHK2	85.9	1.2	86.8	3.2
CHK a	40.8	0.7	37.1	3.6
DGK b	105.9	24.2	92.0	7.1
PIK4CB	56.3	1.9	49.4	4.5
DGK g	88.8	1.5	86.8	2.3
DGK z	98.6	0.2	88.4	2.5
PI4K2a	109.9	6.0	111.4	5.6
CHK b	129.1	5.9	118.1	0.2

	CK146		CK147	
Lipid Kinase	**% activity remaining**	**SD**	**% activity remaining**	**SD**
PI3K a	105.4	13.2	102.6	4.1
PI3K b	145.9	27.2	100.2	3.2
PI3K g	93.3	8.7	97.9	1.3
PI3Ka E545K + p85	101.0	1.4	77.2	0.2
PI3Ka E524K + p85	106.5	9.6	80.8	1.6
PIP5K2A	98.6	2.1	101.6	0.5
SPHK1	97.9	8.7	101.0	0.1
SPHK2	90.0	3.5	103.8	7.9
CHK a	30.9	11.2	86.9	6.0
DGK b	98.9	3.3	104.9	11.5
PIK4CB	53.0	0.6	99.5	2.5
DGK g	89.3	1.9	106.5	1.8
DGK z	91.4	2.2	95.3	13.5
PI4K2a	113.4	4.8	89.5	13.2
CHK b	149.0	0.8	96.8	1.0

Page No.	Type of work:	Name of work	Source of work	Copyright holder and contact	permission requested on	I have permission yes /no	Permission note
26	figure	Figure 1. 4: Choline metabolite analysis by ^{1}H and ^{31}P MRS	Glunde, K.; Bhujwalla, Z. M.; Ronen, S. M., Choline metabolism in malignant transformation. Nature Reviews Cancer 2011, 11 (12), 835-848. https://doi.org/10.1038/nrc3162	Springer Nature	13.07.21	yes	Reproduce permission
34	figure	Figure 1. 6: The structures of CHKA2 monomer in ribbon diagram, with ADP and PCho molecules concomitantly present.	Malito, E.; Sekulic, N.; Too, W. C. S.; Konrad, M.; Lavie, A., Elucidation of Human Choline Kinase Crystal Structures in Complex with the Products ADP or Phosphocholine. Journal of Molecular Biology 2006, 364 (2), 136-151. https://doi.org/https://doi.org/10.1016/j.jmb.2006.08.084	Elsevier	13.07.21	yes	Reproduce permission
35	figure	Figure 1. 8: The interactions of choline with CHKA2 at the choline-binding site.	Malito, E.; Sekulic, N.; Too, W. C. S.; Konrad, M.; Lavie, A., Elucidation of Human Choline Kinase Crystal Structures in Complex with the Products ADP or Phosphocholine. Journal of Molecular Biology 2006, 364 (2), 136-151. https://doi.org/https://doi.org/10.1016/j.jmb.2006.08.084	Elsevier	13.07.21	yes	Reproduce permission
36	figure	Figure 1. 1: The interactions of ADP with CHKA2 at the ATP-binding site.	Malito, E.; Sekulic, N.; Too, W. C. S.; Konrad, M.; Lavie, A., Elucidation of Human Choline Kinase Crystal Structures in Complex with the Products ADP	Elsevier	14.07.21	yes	Reproduce permission

			or Phosphocholine. Journal of Molecular Biology 2006, 364 (2), 136-151. https://doi.org/https://doi.org/10.1016/j.jmb.2006.08.084				

SPRINGER NATURE LICENSE
TERMS AND CONDITIONS

Jul 13, 2021

This Agreement between Miss. Ning Wang ("You") and Springer Nature ("Springer Nature") consists of your license details and the terms and conditions provided by Springer Nature and Copyright Clearance Center.

License Number	5107090489360
License date	Jul 13, 2021
Licensed Content Publisher	Springer Nature
Licensed Content Publication	Nature Reviews Cancer
Licensed Content Title	Choline metabolism in malignant transformation
Licensed Content Author	Kristine Glunde et al
Licensed Content Date	Nov 17, 2011
Type of Use	Thesis/Dissertation
Requestor type	non-commercial (non-profit)
Format	electronic
Portion	figures/tables/illustrations
Number of figures/tables/illustrations	1

High-res required	no
Will you be translating?	no
Circulation/distribution	1 - 29
Author of this Springer Nature content	no
Title	Design, synthesis and characterisation of next-generation choline kinase inhibitors
Institution name	Imperial College London
Expected presentation date	Mar 2022
Portions	Box 1 on Page 838
Requestor Location	Miss. Ning Wang Flat C404, 80 Wood Lane, White City London, W12 0BZ United Kingdom Attn: Miss. Ning Wang
Total	0.00 USD

Terms and Conditions

Springer Nature Customer Service Centre GmbH
Terms and Conditions

This agreement sets out the terms and conditions of the licence (the **Licence**) between you and **Springer Nature Customer Service Centre GmbH** (the **Licensor**). By clicking 'accept' and completing the transaction for the material (**Licensed Material**), you also confirm your acceptance of these terms and conditions.

1. Grant of License

1. 1. The Licensor grants you a personal, non-exclusive, non-transferable, world-wide licence to reproduce the Licensed Material for the purpose specified in your order only. Licences are granted for the specific use requested in the order and for no other use, subject to the conditions below.

1. 2. The Licensor warrants that it has, to the best of its knowledge, the rights to license reuse of the Licensed Material. However, you should ensure that the material you are requesting is original to the Licensor and does not carry the copyright of another entity (as credited in the published version).

1. 3. If the credit line on any part of the material you have requested indicates that it was reprinted or adapted with permission from another source, then you should also seek permission from that source to reuse the material.

2. Scope of Licence

2. 1. You may only use the Licensed Content in the manner and to the extent permitted by these Ts&Cs and any applicable laws.

2. 2. A separate licence may be required for any additional use of the Licensed Material, e.g. where a licence has been purchased for print only use, separate permission must be obtained for electronic re-use. Similarly, a licence is only valid in the language selected and does not apply for editions in other languages unless additional translation rights have been granted separately in the licence. Any content owned by third parties are expressly excluded from the licence.

2. 3. Similarly, rights for additional components such as custom editions and derivatives require additional permission and may be subject to an additional fee. Please apply to Journalpermissions@springernature.com/bookpermissions@springernature.com for these rights.

2. 4. Where permission has been granted **free of charge** for material in print, permission may also be granted for any electronic version of that work, provided that the material is incidental to your work as a whole and that the electronic version is essentially equivalent to, or substitutes for, the print version.

2. 5. An alternative scope of licence may apply to signatories of the STM Permissions Guidelines, as amended from time to time.

3. Duration of Licence

3. 1. A licence for is valid from the date of purchase ('Licence Date') at the end of the relevant period in the below table:

Scope of Licence	Duration of Licence

Post on a website	12 months
Presentations	12 months
Books and journals	Lifetime of the edition in the language purchased

4. Acknowledgement

4. 1. The Licensor's permission must be acknowledged next to the Licenced Material in print. In electronic form, this acknowledgement must be visible at the same time as the figures/tables/illustrations or abstract, and must be hyperlinked to the journal/book's homepage. Our required acknowledgement format is in the Appendix below.

5. Restrictions on use

5. 1. Use of the Licensed Material may be permitted for incidental promotional use and minor editing privileges e.g. minor adaptations of single figures, changes of format, colour and/or style where the adaptation is credited as set out in Appendix 1 below. Any other changes including but not limited to, cropping, adapting, omitting material that affect the meaning, intention or moral rights of the author are strictly prohibited.

5. 2. You must not use any Licensed Material as part of any design or trademark.

5. 3. Licensed Material may be used in Open Access Publications (OAP) before publication by Springer Nature, but any Licensed Material must be removed from OAP sites prior to final publication.

6. Ownership of Rights

6. 1. Licensed Material remains the property of either Licensor or the relevant third party and any rights not explicitly granted herein are expressly reserved.

7. Warranty

IN NO EVENT SHALL LICENSOR BE LIABLE TO YOU OR ANY OTHER PARTY OR ANY OTHER PERSON OR FOR ANY SPECIAL, CONSEQUENTIAL, INCIDENTAL OR INDIRECT DAMAGES, HOWEVER CAUSED, ARISING OUT OF OR IN CONNECTION WITH THE DOWNLOADING, VIEWING OR USE OF THE MATERIALS REGARDLESS OF THE FORM OF ACTION, WHETHER FOR BREACH OF CONTRACT, BREACH OF WARRANTY, TORT, NEGLIGENCE, INFRINGEMENT OR OTHERWISE (INCLUDING, WITHOUT LIMITATION, DAMAGES BASED ON LOSS OF PROFITS, DATA, FILES, USE, BUSINESS OPPORTUNITY OR CLAIMS OF THIRD PARTIES), AND

WHETHER OR NOT THE PARTY HAS BEEN ADVISED OF THE POSSIBILITY OF SUCH DAMAGES. THIS LIMITATION SHALL APPLY NOTWITHSTANDING ANY FAILURE OF ESSENTIAL PURPOSE OF ANY LIMITED REMEDY PROVIDED HEREIN.

8. Limitations

8. 1. ***BOOKS ONLY:*** Where **'reuse in a dissertation/thesis'** has been selected the following terms apply: Print rights of the final author's accepted manuscript (for clarity, NOT the published version) for up to 100 copies, electronic rights for use only on a personal website or institutional repository as defined by the Sherpa guideline (www.sherpa.ac.uk/romeo/).

8. 2. For content reuse requests that qualify for permission under the STM Permissions Guidelines, which may be updated from time to time, the STM Permissions Guidelines supersede the terms and conditions contained in this licence.

9. Termination and Cancellation

9. 1. Licences will expire after the period shown in Clause 3 (above).

9. 2. Licensee reserves the right to terminate the Licence in the event that payment is not received in full or if there has been a breach of this agreement by you.

Appendix 1 — Acknowledgements:

For Journal Content:
Reprinted by permission from [**the Licensor**]: [**Journal Publisher** (e.g. Nature/Springer/Palgrave)] [**JOURNAL NAME**] [**REFERENCE CITATION** (Article name, Author(s) Name), [**COPYRIGHT**] (year of publication)

For **Advance Online Publication papers:**
Reprinted by permission from [**the Licensor**]: [**Journal Publisher** (e.g. Nature/Springer/Palgrave)] [**JOURNAL NAME**] [**REFERENCE CITATION** (Article name, Author(s) Name), [**COPYRIGHT**] (year of publication), advance online publication, day month year (doi: 10.1038/sj.[JOURNAL ACRONYM].)

For Adaptations/Translations:
Adapted/Translated by permission from [**the Licensor**]: [**Journal Publisher** (e.g. Nature/Springer/Palgrave)] [**JOURNAL NAME**] [**REFERENCE CITATION** (Article name, Author(s) Name), [**COPYRIGHT**] (year of publication)

Note: For any republication from the British Journal of Cancer, the following credit line style applies:

Reprinted/adapted/translated by permission from [**the Licensor**]: on behalf of Cancer Research UK: : [**Journal Publisher** (e.g. Nature/Springer/Palgrave)] [**JOURNAL NAME**] [**REFERENCE CITATION** (Article name, Author(s) Name), [**COPYRIGHT]** (year of publication)

For **Advance Online Publication** papers:
Reprinted by permission from The [**the Licensor**]: on behalf of Cancer Research UK: [**Journal Publisher** (e.g. Nature/Springer/Palgrave)] [**JOURNAL NAME**] [**REFERENCE CITATION** (Article name, Author(s) Name), [**COPYRIGHT**] (year of publication), advance online publication, day month year (doi: 10.1038/sj. [JOURNAL ACRONYM])

For Book content:
Reprinted/adapted by permission from [**the Licensor**]: [**Book Publisher** (e.g. Palgrave Macmillan, Springer etc) [**Book Title**] by [**Book author**(s)] [**COPYRIGHT**] (year of publication)

Other Conditions:

Version 1.3

Questions? customercare@copyright.com or +1-855-239-3415 (toll free in the US) or +1-978-646-2777.

ELSEVIER LICENSE
TERMS AND CONDITIONS

Jul 13, 2021

This Agreement between Miss. Ning Wang ("You") and Elsevier ("Elsevier") consists of your license details and the terms and conditions provided by Elsevier and Copyright Clearance Center.

License Number	5107081433988
License date	Jul 13, 2021
Licensed Content Publisher	Elsevier
Licensed Content Publication	Journal of Molecular Biology
Licensed Content Title	Elucidation of Human Choline Kinase Crystal Structures in Complex with the Products ADP or Phosphocholine
Licensed Content Author	Enrico Malito,Nikolina Sekulic,Wei Cun See Too,Manfred Konrad,Arnon Lavie
Licensed Content Date	Nov 24, 2006
Licensed Content Volume	364
Licensed Content Issue	2
Licensed Content Pages	16
Start Page	136

End Page	151
Type of Use	reuse in a thesis/dissertation
Portion	figures/tables/illustrations
Number of figures/tables/illustrations	2
Format	electronic
Are you the author of this Elsevier article?	No
Will you be translating?	No
Title	Design, synthesis and characterisation of next-generation choline kinase inhibitors
Institution name	Imperial College London
Expected presentation date	Mar 2022
Portions	Figure 1 on page 138, Figure 5 on page 145
Requestor Location	Miss. Ning Wang Flat C404, 80 Wood Lane, White City London, W12 0BZ United Kingdom Attn: Miss. Ning Wang
Publisher Tax ID	GB 494 6272 12
Total	0.00 USD

Terms and Conditions

INTRODUCTION

1. The publisher for this copyrighted material is Elsevier. By clicking "accept" in connection with completing this licensing transaction, you agree that the following terms and conditions apply to this transaction (along with the Billing and Payment terms and conditions established by Copyright Clearance Center, Inc. ("CCC"), at the time that you opened your Rightslink account and that are available at any time at http://myaccount.copyright.com).

GENERAL TERMS

2. Elsevier hereby grants you permission to reproduce the aforementioned material subject to the terms and conditions indicated.

3. Acknowledgement: If any part of the material to be used (for example, figures) has appeared in our publication with credit or acknowledgement to another source, permission must also be sought from that source. If such permission is not obtained then that material may not be included in your publication/copies. Suitable acknowledgement to the source must be made, either as a footnote or in a reference list at the end of your publication, as follows:

"Reprinted from Publication title, Vol /edition number, Author(s), Title of article / title of chapter, Pages No., Copyright (Year), with permission from Elsevier [OR APPLICABLE SOCIETY COPYRIGHT OWNER]." Also Lancet special credit - "Reprinted from The Lancet, Vol. number, Author(s), Title of article, Pages No., Copyright (Year), with permission from Elsevier."

4. Reproduction of this material is confined to the purpose and/or media for which permission is hereby given.

5. Altering/Modifying Material: Not Permitted. However figures and illustrations may be altered/adapted minimally to serve your work. Any other abbreviations, additions, deletions and/or any other alterations shall be made only with prior written authorization of Elsevier Ltd. (Please contact Elsevier' s permissions helpdesk here). No modifications can be made to any Lancet figures/tables and they must be reproduced in full.

6. If the permission fee for the requested use of our material is waived in this instance, please be advised that your future requests for Elsevier materials may attract a fee.

7. Reservation of Rights: Publisher reserves all rights not specifically granted in the combination of (i) the license details provided by you and accepted in the course of this licensing transaction, (ii) these terms and conditions and (iii) CCC's Billing and Payment terms and conditions.

8. License Contingent Upon Payment: While you may exercise the rights licensed immediately upon issuance of the license at the end of the licensing process for the transaction, provided that you have disclosed complete and accurate details of your proposed use, no license is finally effective unless

and until full payment is received from you (either by publisher or by CCC) as provided in CCC's Billing and Payment terms and conditions. If full payment is not received on a timely basis, then any license preliminarily granted shall be deemed automatically revoked and shall be void as if never granted. Further, in the event that you breach any of these terms and conditions or any of CCC's Billing and Payment terms and conditions, the license is automatically revoked and shall be void as if never granted. Use of materials as described in a revoked license, as well as any use of the materials beyond the scope of an unrevoked license, may constitute copyright infringement and publisher reserves the right to take any and all action to protect its copyright in the materials.

9. Warranties: Publisher makes no representations or warranties with respect to the licensed material.

10. Indemnity: You hereby indemnify and agree to hold harmless publisher and CCC, and their respective officers, directors, employees and agents, from and against any and all claims arising out of your use of the licensed material other than as specifically authorized pursuant to this license.

11. No Transfer of License: This license is personal to you and may not be sublicensed, assigned, or transferred by you to any other person without publisher's written permission.

12. No Amendment Except in Writing: This license may not be amended except in a writing signed by both parties (or, in the case of publisher, by CCC on publisher's behalf).

13. Objection to Contrary Terms: Publisher hereby objects to any terms contained in any purchase order, acknowledgment, check endorsement or other writing prepared by you, which terms are inconsistent with these terms and conditions or CCC's Billing and Payment terms and conditions. These terms and conditions, together with CCC's Billing and Payment terms and conditions (which are incorporated herein), comprise the entire agreement between you and publisher (and CCC) concerning this licensing transaction. In the event of any conflict between your obligations established by these terms and conditions and those established by CCC's Billing and Payment terms and conditions, these terms and conditions shall control.

14. Revocation: Elsevier or Copyright Clearance Center may deny the permissions described in this License at their sole discretion, for any reason or no reason, with a full refund payable to you. Notice of such denial will be made using the contact information provided by you. Failure to receive such notice will not alter or invalidate the denial. In no event will Elsevier or Copyright Clearance Center be responsible or liable for any costs, expenses or damage incurred by you as a result of a denial of your permission request, other than a refund of the amount(s) paid by you to Elsevier and/or Copyright Clearance Center for denied permissions.

LIMITED LICENSE

The following terms and conditions apply only to specific license types:

15. **Translation**: This permission is granted for non-exclusive world **English** rights only unless your license was granted for translation rights. If you licensed translation rights you may only translate this content into the languages you requested. A professional translator must perform all translations and reproduce the content word for word preserving the integrity of the article.

16. **Posting licensed content on any Website**: The following terms and conditions apply as follows: Licensing material from an Elsevier journal: All content posted to the web site must maintain the copyright information line on the bottom of each image; A hyper-text must be included to the Homepage of the journal from which you are licensing at http://www.sciencedirect.com/science/journal/xxxxx or the Elsevier homepage for books at http://www.elsevier.com; Central Storage: This license does not include permission for a scanned version of the material to be stored in a central repository such as that provided by Heron/XanEdu.

Licensing material from an Elsevier book: A hyper-text link must be included to the Elsevier homepage at http://www.elsevier.com . All content posted to the web site must maintain the copyright information line on the bottom of each image.

Posting licensed content on Electronic reserve: In addition to the above the following clauses are applicable: The web site must be password-protected and made available only to bona fide students registered on a relevant course. This permission is granted for 1 year only. You may obtain a new license for future website posting.

17. **For journal authors:** the following clauses are applicable in addition to the above:

Preprints:

A preprint is an author's own write-up of research results and analysis, it has not been peer-reviewed, nor has it had any other value added to it by a publisher (such as formatting, copyright, technical enhancement etc.).

Authors can share their preprints anywhere at any time. Preprints should not be added to or enhanced in any way in order to appear more like, or to substitute for, the final versions of articles however authors can update their preprints on arXiv or RePEc with their Accepted Author Manuscript (see below).

If accepted for publication, we encourage authors to link from the preprint to their formal publication via its DOI. Millions of researchers have access to the formal publications on ScienceDirect, and so links will help users to find, access, cite and use the best available version. Please note that Cell Press, The

Lancet and some society-owned have different preprint policies. Information on these policies is available on the journal homepage.

Accepted Author Manuscripts: An accepted author manuscript is the manuscript of an article that has been accepted for publication and which typically includes author-incorporated changes suggested during submission, peer review and editor-author communications.

Authors can share their accepted author manuscript:

- immediately
  - via their non-commercial person homepage or blog
  - by updating a preprint in arXiv or RePEc with the accepted manuscript
  - via their research institute or institutional repository for internal institutional uses or as part of an invitation-only research collaboration work-group
  - directly by providing copies to their students or to research collaborators for their personal use
  - for private scholarly sharing as part of an invitation-only work group on commercial sites with which Elsevier has an agreement
- After the embargo period
  - via non-commercial hosting platforms such as their institutional repository
  - via commercial sites with which Elsevier has an agreement

In all cases accepted manuscripts should:

- link to the formal publication via its DOI
- bear a CC-BY-NC-ND license - this is easy to do
- if aggregated with other manuscripts, for example in a repository or other site, be shared in alignment with our hosting policy not be added to or enhanced in any way to appear more like, or to substitute for, the published journal article.

Published journal article (JPA): A published journal article (PJA) is the definitive final record of published research that appears or will appear in the journal and embodies all value-adding publishing activities including peer review co-ordination, copy-editing, formatting, (if relevant) pagination and online enrichment.

Policies for sharing publishing journal articles differ for subscription and gold open access articles:

Subscription Articles: If you are an author, please share a link to your article rather than the full-text. Millions of researchers have access to the formal publications on ScienceDirect, and so links will help your users to find, access, cite, and use the best available version.

Theses and dissertations which contain embedded PJAs as part of the formal submission can be posted publicly by the awarding institution with DOI links

back to the formal publications on ScienceDirect.

If you are affiliated with a library that subscribes to ScienceDirect you have additional private sharing rights for others' research accessed under that agreement. This includes use for classroom teaching and internal training at the institution (including use in course packs and courseware programs), and inclusion of the article for grant funding purposes.

Gold Open Access Articles: May be shared according to the author-selected end-user license and should contain a CrossMark logo, the end user license, and a DOI link to the formal publication on ScienceDirect.

Please refer to Elsevier's posting policy for further information.

18. **For book authors** the following clauses are applicable in addition to the above: Authors are permitted to place a brief summary of their work online only. You are not allowed to download and post the published electronic version of your chapter, nor may you scan the printed edition to create an electronic version. **Posting to a repository:** Authors are permitted to post a summary of their chapter only in their institution's repository.

19. **Thesis/Dissertation**: If your license is for use in a thesis/dissertation your thesis may be submitted to your institution in either print or electronic form. Should your thesis be published commercially, please reapply for permission. These requirements include permission for the Library and Archives of Canada to supply single copies, on demand, of the complete thesis and include permission for Proquest/UMI to supply single copies, on demand, of the complete thesis. Should your thesis be published commercially, please reapply for permission. Theses and dissertations which contain embedded PJAs as part of the formal submission can be posted publicly by the awarding institution with DOI links back to the formal publications on ScienceDirect.

Elsevier Open Access Terms and Conditions

You can publish open access with Elsevier in hundreds of open access journals or in nearly 2000 established subscription journals that support open access publishing. Permitted third party re-use of these open access articles is defined by the author's choice of Creative Commons user license. See our open access license policy for more information.

Terms & Conditions applicable to all Open Access articles published with Elsevier:

Any reuse of the article must not represent the author as endorsing the adaptation of the article nor should the article be modified in such a way as to damage the author's honour or reputation. If any changes have been made, such changes must be clearly indicated.

The author(s) must be appropriately credited and we ask that you include the end user license and a DOI link to the formal publication on ScienceDirect.

If any part of the material to be used (for example, figures) has appeared in our publication with credit or acknowledgement to another source it is the responsibility of the user to ensure their reuse complies with the terms and conditions determined by the rights holder.

Additional Terms & Conditions applicable to each Creative Commons user license:

CC BY: The CC-BY license allows users to copy, to create extracts, abstracts and new works from the Article, to alter and revise the Article and to make commercial use of the Article (including reuse and/or resale of the Article by commercial entities), provided the user gives appropriate credit (with a link to the formal publication through the relevant DOI), provides a link to the license, indicates if changes were made and the licensor is not represented as endorsing the use made of the work. The full details of the license are available at http://creativecommons.org/licenses/by/4.0.

CC BY NC SA: The CC BY-NC-SA license allows users to copy, to create extracts, abstracts and new works from the Article, to alter and revise the Article, provided this is not done for commercial purposes, and that the user gives appropriate credit (with a link to the formal publication through the relevant DOI), provides a link to the license, indicates if changes were made and the licensor is not represented as endorsing the use made of the work. Further, any new works must be made available on the same conditions. The full details of the license are available at http://creativecommons.org/licenses/by-nc-sa/4.0.

CC BY NC ND: The CC BY-NC-ND license allows users to copy and distribute the Article, provided this is not done for commercial purposes and further does not permit distribution of the Article if it is changed or edited in any way, and provided the user gives appropriate credit (with a link to the formal publication through the relevant DOI), provides a link to the license, and that the licensor is not represented as endorsing the use made of the work. The full details of the license are available at http://creativecommons.org/licenses/by-nc-nd/4.0. Any commercial reuse of Open Access articles published with a CC BY NC SA or CC BY NC ND license requires permission from Elsevier and will be subject to a fee.

Commercial reuse includes:

- Associating advertising with the full text of the Article
- Charging fees for document delivery or access
- Article aggregation
- Systematic distribution via e-mail lists or share buttons

Posting or linking by commercial companies for use by customers of those companies.

20. **Other Conditions**:

v1.10

Questions? customercare@copyright.com or +1-855-239-3415 (toll free in the US) or +1-978-646-2777.

ELSEVIER LICENSE
TERMS AND CONDITIONS

Jul 14, 2021

This Agreement between Miss. Ning Wang ("You") and Elsevier ("Elsevier") consists of your license details and the terms and conditions provided by Elsevier and Copyright Clearance Center.

License Number	5107600018312
License date	Jul 14, 2021
Licensed Content Publisher	Elsevier
Licensed Content Publication	Journal of Molecular Biology
Licensed Content Title	Elucidation of Human Choline Kinase Crystal Structures in Complex with the Products ADP or Phosphocholine
Licensed Content Author	Enrico Malito,Nikolina Sekulic,Wei Cun See Too,Manfred Konrad,Arnon Lavie
Licensed Content Date	Nov 24, 2006
Licensed Content Volume	364
Licensed Content Issue	2
Licensed Content Pages	16
Start Page	136

End Page	151
Type of Use	reuse in a thesis/dissertation
Portion	figures/tables/illustrations
Number of figures/tables/illustrations	1
Format	electronic
Are you the author of this Elsevier article?	No
Will you be translating?	No
Title	Design, synthesis and characterisation of next-generation choline kinase inhibitors
Institution name	Imperial College London
Expected presentation date	Mar 2022
Portions	Figure 3 on Page 142
Requestor Location	Miss. Ning Wang Flat C404, 80 Wood Lane, White City London, W12 0BZ United Kingdom Attn: Miss. Ning Wang
Publisher Tax ID	GB 494 6272 12
Total	0.00 USD

Terms and Conditions

INTRODUCTION

1. The publisher for this copyrighted material is Elsevier. By clicking "accept" in connection with completing this licensing transaction, you agree that the following terms and conditions apply to this transaction (along with the Billing and Payment terms and conditions established by Copyright Clearance Center, Inc. ("CCC"), at the time that you opened your Rightslink account and that are available at any time at http://myaccount.copyright.com).

GENERAL TERMS

2. Elsevier hereby grants you permission to reproduce the aforementioned material subject to the terms and conditions indicated.

3. Acknowledgement: If any part of the material to be used (for example, figures) has appeared in our publication with credit or acknowledgement to another source, permission must also be sought from that source. If such permission is not obtained then that material may not be included in your publication/copies. Suitable acknowledgement to the source must be made, either as a footnote or in a reference list at the end of your publication, as follows:

"Reprinted from Publication title, Vol /edition number, Author(s), Title of article / title of chapter, Pages No., Copyright (Year), with permission from Elsevier [OR APPLICABLE SOCIETY COPYRIGHT OWNER]." Also Lancet special credit - "Reprinted from The Lancet, Vol. number, Author(s), Title of article, Pages No., Copyright (Year), with permission from Elsevier."

4. Reproduction of this material is confined to the purpose and/or media for which permission is hereby given.

5. Altering/Modifying Material: Not Permitted. However figures and illustrations may be altered/adapted minimally to serve your work. Any other abbreviations, additions, deletions and/or any other alterations shall be made only with prior written authorization of Elsevier Ltd. (Please contact Elsevier' s permissions helpdesk here). No modifications can be made to any Lancet figures/tables and they must be reproduced in full.

6. If the permission fee for the requested use of our material is waived in this instance, please be advised that your future requests for Elsevier materials may attract a fee.

7. Reservation of Rights: Publisher reserves all rights not specifically granted in the combination of (i) the license details provided by you and accepted in the course of this licensing transaction, (ii) these terms and conditions and (iii) CCC's Billing and Payment terms and conditions.

8. License Contingent Upon Payment: While you may exercise the rights licensed immediately upon issuance of the license at the end of the licensing process for the transaction, provided that you have disclosed complete and accurate details of your proposed use, no license is finally effective unless

and until full payment is received from you (either by publisher or by CCC) as provided in CCC's Billing and Payment terms and conditions. If full payment is not received on a timely basis, then any license preliminarily granted shall be deemed automatically revoked and shall be void as if never granted. Further, in the event that you breach any of these terms and conditions or any of CCC's Billing and Payment terms and conditions, the license is automatically revoked and shall be void as if never granted. Use of materials as described in a revoked license, as well as any use of the materials beyond the scope of an unrevoked license, may constitute copyright infringement and publisher reserves the right to take any and all action to protect its copyright in the materials.

9. Warranties: Publisher makes no representations or warranties with respect to the licensed material.

10. Indemnity: You hereby indemnify and agree to hold harmless publisher and CCC, and their respective officers, directors, employees and agents, from and against any and all claims arising out of your use of the licensed material other than as specifically authorized pursuant to this license.

11. No Transfer of License: This license is personal to you and may not be sublicensed, assigned, or transferred by you to any other person without publisher's written permission.

12. No Amendment Except in Writing: This license may not be amended except in a writing signed by both parties (or, in the case of publisher, by CCC on publisher's behalf).

13. Objection to Contrary Terms: Publisher hereby objects to any terms contained in any purchase order, acknowledgment, check endorsement or other writing prepared by you, which terms are inconsistent with these terms and conditions or CCC's Billing and Payment terms and conditions. These terms and conditions, together with CCC's Billing and Payment terms and conditions (which are incorporated herein), comprise the entire agreement between you and publisher (and CCC) concerning this licensing transaction. In the event of any conflict between your obligations established by these terms and conditions and those established by CCC's Billing and Payment terms and conditions, these terms and conditions shall control.

14. Revocation: Elsevier or Copyright Clearance Center may deny the permissions described in this License at their sole discretion, for any reason or no reason, with a full refund payable to you. Notice of such denial will be made using the contact information provided by you. Failure to receive such notice will not alter or invalidate the denial. In no event will Elsevier or Copyright Clearance Center be responsible or liable for any costs, expenses or damage incurred by you as a result of a denial of your permission request, other than a refund of the amount(s) paid by you to Elsevier and/or Copyright Clearance Center for denied permissions.

LIMITED LICENSE

The following terms and conditions apply only to specific license types:

15. **Translation**: This permission is granted for non-exclusive world **English** rights only unless your license was granted for translation rights. If you licensed translation rights you may only translate this content into the languages you requested. A professional translator must perform all translations and reproduce the content word for word preserving the integrity of the article.

16. **Posting licensed content on any Website**: The following terms and conditions apply as follows: Licensing material from an Elsevier journal: All content posted to the web site must maintain the copyright information line on the bottom of each image; A hyper-text must be included to the Homepage of the journal from which you are licensing at http://www.sciencedirect.com/science/journal/xxxxx or the Elsevier homepage for books at http://www.elsevier.com; Central Storage: This license does not include permission for a scanned version of the material to be stored in a central repository such as that provided by Heron/XanEdu.

Licensing material from an Elsevier book: A hyper-text link must be included to the Elsevier homepage at http://www.elsevier.com . All content posted to the web site must maintain the copyright information line on the bottom of each image.

Posting licensed content on Electronic reserve: In addition to the above the following clauses are applicable: The web site must be password-protected and made available only to bona fide students registered on a relevant course. This permission is granted for 1 year only. You may obtain a new license for future website posting.

17. **For journal authors:** the following clauses are applicable in addition to the above:

Preprints:

A preprint is an author's own write-up of research results and analysis, it has not been peer-reviewed, nor has it had any other value added to it by a publisher (such as formatting, copyright, technical enhancement etc.).

Authors can share their preprints anywhere at any time. Preprints should not be added to or enhanced in any way in order to appear more like, or to substitute for, the final versions of articles however authors can update their preprints on arXiv or RePEc with their Accepted Author Manuscript (see below).

If accepted for publication, we encourage authors to link from the preprint to their formal publication via its DOI. Millions of researchers have access to the formal publications on ScienceDirect, and so links will help users to find, access, cite and use the best available version. Please note that Cell Press, The

Lancet and some society-owned have different preprint policies. Information on these policies is available on the journal homepage.

Accepted Author Manuscripts: An accepted author manuscript is the manuscript of an article that has been accepted for publication and which typically includes author-incorporated changes suggested during submission, peer review and editor-author communications.

Authors can share their accepted author manuscript:

- immediately
  - via their non-commercial person homepage or blog
  - by updating a preprint in arXiv or RePEc with the accepted manuscript
  - via their research institute or institutional repository for internal institutional uses or as part of an invitation-only research collaboration work-group
  - directly by providing copies to their students or to research collaborators for their personal use
  - for private scholarly sharing as part of an invitation-only work group on commercial sites with which Elsevier has an agreement
- After the embargo period
  - via non-commercial hosting platforms such as their institutional repository
  - via commercial sites with which Elsevier has an agreement

In all cases accepted manuscripts should:

- link to the formal publication via its DOI
- bear a CC-BY-NC-ND license - this is easy to do
- if aggregated with other manuscripts, for example in a repository or other site, be shared in alignment with our hosting policy not be added to or enhanced in any way to appear more like, or to substitute for, the published journal article.

Published journal article (JPA): A published journal article (PJA) is the definitive final record of published research that appears or will appear in the journal and embodies all value-adding publishing activities including peer review co-ordination, copy-editing, formatting, (if relevant) pagination and online enrichment.

Policies for sharing publishing journal articles differ for subscription and gold open access articles:

Subscription Articles: If you are an author, please share a link to your article rather than the full-text. Millions of researchers have access to the formal publications on ScienceDirect, and so links will help your users to find, access, cite, and use the best available version.

Theses and dissertations which contain embedded PJAs as part of the formal submission can be posted publicly by the awarding institution with DOI links

back to the formal publications on ScienceDirect.

If you are affiliated with a library that subscribes to ScienceDirect you have additional private sharing rights for others' research accessed under that agreement. This includes use for classroom teaching and internal training at the institution (including use in course packs and courseware programs), and inclusion of the article for grant funding purposes.

Gold Open Access Articles: May be shared according to the author-selected end-user license and should contain a CrossMark logo, the end user license, and a DOI link to the formal publication on ScienceDirect.

Please refer to Elsevier's posting policy for further information.

18. **For book authors** the following clauses are applicable in addition to the above: Authors are permitted to place a brief summary of their work online only. You are not allowed to download and post the published electronic version of your chapter, nor may you scan the printed edition to create an electronic version. **Posting to a repository:** Authors are permitted to post a summary of their chapter only in their institution's repository.

19. **Thesis/Dissertation**: If your license is for use in a thesis/dissertation your thesis may be submitted to your institution in either print or electronic form. Should your thesis be published commercially, please reapply for permission. These requirements include permission for the Library and Archives of Canada to supply single copies, on demand, of the complete thesis and include permission for Proquest/UMI to supply single copies, on demand, of the complete thesis. Should your thesis be published commercially, please reapply for permission. Theses and dissertations which contain embedded PJAs as part of the formal submission can be posted publicly by the awarding institution with DOI links back to the formal publications on ScienceDirect.

Elsevier Open Access Terms and Conditions

You can publish open access with Elsevier in hundreds of open access journals or in nearly 2000 established subscription journals that support open access publishing. Permitted third party re-use of these open access articles is defined by the author's choice of Creative Commons user license. See our open access license policy for more information.

Terms & Conditions applicable to all Open Access articles published with Elsevier:

Any reuse of the article must not represent the author as endorsing the adaptation of the article nor should the article be modified in such a way as to damage the author's honour or reputation. If any changes have been made, such changes must be clearly indicated.

The author(s) must be appropriately credited and we ask that you include the end user license and a DOI link to the formal publication on ScienceDirect.

If any part of the material to be used (for example, figures) has appeared in our publication with credit or acknowledgement to another source it is the responsibility of the user to ensure their reuse complies with the terms and conditions determined by the rights holder.

Additional Terms & Conditions applicable to each Creative Commons user license:

CC BY: The CC-BY license allows users to copy, to create extracts, abstracts and new works from the Article, to alter and revise the Article and to make commercial use of the Article (including reuse and/or resale of the Article by commercial entities), provided the user gives appropriate credit (with a link to the formal publication through the relevant DOI), provides a link to the license, indicates if changes were made and the licensor is not represented as endorsing the use made of the work. The full details of the license are available at http://creativecommons.org/licenses/by/4.0.

CC BY NC SA: The CC BY-NC-SA license allows users to copy, to create extracts, abstracts and new works from the Article, to alter and revise the Article, provided this is not done for commercial purposes, and that the user gives appropriate credit (with a link to the formal publication through the relevant DOI), provides a link to the license, indicates if changes were made and the licensor is not represented as endorsing the use made of the work. Further, any new works must be made available on the same conditions. The full details of the license are available at http://creativecommons.org/licenses/by-nc-sa/4.0.

CC BY NC ND: The CC BY-NC-ND license allows users to copy and distribute the Article, provided this is not done for commercial purposes and further does not permit distribution of the Article if it is changed or edited in any way, and provided the user gives appropriate credit (with a link to the formal publication through the relevant DOI), provides a link to the license, and that the licensor is not represented as endorsing the use made of the work. The full details of the license are available at http://creativecommons.org/licenses/by-nc-nd/4.0. Any commercial reuse of Open Access articles published with a CC BY NC SA or CC BY NC ND license requires permission from Elsevier and will be subject to a fee.

Commercial reuse includes:

- Associating advertising with the full text of the Article
- Charging fees for document delivery or access
- Article aggregation
- Systematic distribution via e-mail lists or share buttons

Posting or linking by commercial companies for use by customers of those companies.

20. **Other Conditions**:

v1.10

Questions? customercare@copyright.com or +1-855-239-3415 (toll free in the US) or +1-978-646-2777.